Doctoral Dissertations   Graduate School

12-2017

An Exploration of Basic Processes for Aqueous Electrochemical Production of Hydrogen from Biomass Derived Molecules

Brian Fane
University of Tennessee, Knoxville, bfane@vols.utk.edu

Recommended Citation

To the Graduate Council:

I am submitting herewith a dissertation written by Brian Fane entitled "An Exploration of Basic Processes for Aqueous Electrochemical Production of Hydrogen from Biomass Derived Molecules." I have examined the final electronic copy of this dissertation for form and content and recommend that it be accepted in partial fulfillment of the requirements for the degree of Doctor of Philosophy, with a major in Chemical Engineering.

Thomas Zawodzinski, Major Professor

We have read this dissertation and recommend its acceptance:

Paul D. Frymier, Robert M. Counce, Nicole Labbé

Accepted for the Council:

Dixie L. Thompson

Vice Provost and Dean of the Graduate School

(Original signatures are on file with official student records.)

An Exploration of Basic Processes for Aqueous Electrochemical Production of Hydrogen from Biomass Derived Molecules

A Dissertation Presented for the

Doctor of Philosophy

Degree

The University of Tennessee, Knoxville

Brian Fane

December 2017

DEDICATION

I would like to thank my family for all their love and support. To my mother and father, who always looked out for me and encouraged me to continue my education. To my little sister, who beat me to being a doctor and has always been the best sibling I could ask for. I would like to acknowledge all the great friends I have made here in the Knoxville outdoors community, you have made this a great place to live. I wish to thank my best friends, Joshua Williams and Andrew Schmalzer, who have always been, and will always be there. No matter what happens in life, I'll see you both in the mountains.

ACKNOWLEDGEMENTS

ABSTRACT

Polymer electrolyte membrane fuel cells(PEMFCs) are energy conversion devices with significant potential. The factors preventing them from becoming widespread concern production and distribution of hydrogen. Developing an efficient hydrogen infrastructure with an approachable rollout plan is an essential step towards the future of fuel cells. Water electrolysis is limited by the thermodynamics of the process, which leads to high electrical consumption and significant materials challenges. Alternative methods for cleanly generating hydrogen while using a lower cell voltage are required. PEM based electrolyzers can operate with a "depolarized anode", whereby they become significantly less power hungry.

This thesis explores two techniques for chemically depolarized electrolyzer anodes. These include a methanol anode and a phosphomolybdic acid anode. To improve the phosphomolybdic acid anode we have characterized the basic electrochemical behavior of phosphomolybdic acid, the anode behavior in a zero-gap electrochemical cell, and the biomass oxidation characteristics of several Keggin ions and potential oxidation promoters.

The methanol cathode was evaluated using a dynamic hydrogen electrode and shown to be significantly more sensitive to crossover induced voltage losses than was previously reported.

Phosphomolybdic acid oxidation kinetics were examined and found to be facile, despite a change in mechanism which occurs after bulk reduction. The temperature dependent diffusion coefficient was found to be on the same order as other likely small, redox active molecules. A previously unreported crossover phenomena was noted and the diffusion coefficient through NAFION was calculated as on the same order as vanadium.

The whole cell performance of the phosphomolybdic acid mediated electrolyzer was examined and found to be highly dependent on supporting electrolyte, temperature, and electrode materials. The optimized condition of 5 M HCl and 80 Celsius showed significant improvement in exchange current density, versus the standard conditions of room temperature and no supporting acid, used in the literature. The electrode kinetics have now been removed as a major problem in the system design.

While the electrochemical performance of the POM mediated electrolyzer was sufficient, the glycerol oxidation rates were found to be lacking. Vanadium, iron, and hydrochloric acid were the most effective additives; while sulfuric acid decreased reaction rates.

TABLE OF CONTENTS

s

LIST OF TABLES

LIST OF FIGURES

CHAPTER 1

Introduction

Scale of the challenge

In recent years, the world has begun to awaken to the challenges posed by carbon emissions from burning fossil fuels. The likely hazards of our massive carbon dioxide emissions include ocean acidification, sea level rise, desertification, increasing storm intensity, loss of sea ice, receding glaciers, and changing precipitation patterns.[1] In addition to the challenges posed by climate change, extractive resources such as fossil fuels are not evenly distributed throughout the world. Many countries have insufficient resources to meet their peacetime or potential wartime energy needs. This creates a strategic liability for places like the United States and her allies. This weakness has always been exploited by producer states. For example, during the Arab oil embargo of the 1970s and recently Russia threatened to cutoff natural gas supplies to Europe during their invasions of Crimea and Georgia.

To address these liabilities, we are pursuing a variety of domestic, low carbon emissions energy resources. These include:

- Geothermal power

- Hydroelectric power

- Nuclear power

- Wind power

- Solar power

- Biomass

Each of these power sources has significant limitations. Besides biomass they are all either largely tapped out or unable to load follow in any significant way. Wind and solar power are particularly notorious for their intermittent nature. This is problematic since the electric grid has almost no ability to store energy.

Energy Storage

Energy storage could provide the electric grid with decreased need for additional infrastructure, improved resiliency, better tolerance of renewable energy, and decreased need to run excess capacity.[2] As of 2013, over 95% of grid level storage was pumped hydropower; the remainder was split between flywheels, batteries, compressed air, and thermal storage.

A largely undeveloped but promising energy storage methodology is hydrogen. Electrolysis can be used to produce hydrogen when electricity is in excess, the hydrogen can be stored, and then recombined with oxygen from the air as necessary to produce electricity. Importantly, this is not how hydrogen is mass produced currently. A hydrogen based energy storage system has the advantage of potentially limitless capacity. If considered as a battery it has decoupled charge power, discharge power, and capacity. Capacity is increased by building more pressure vessels to store hydrogen. It is also convenient to use the stored hydrogen to fuel vehicles and to move energy using hydrogen pipelines instead of electrical wires. Such a system would likely require a single unit electrolyzer and

fuel cell to control capital cost, this device has not yet been commercialized. Discharge power can be increased by adding fuel cells or potentially using hydrogen distribution and grid connected fuel cell vehicles.

Fuel Cell Status

Polymer electrolyte membrane fuel cells(PEMFC's) are often considered to be ideal energy conversion devices. This is because they have the potential for high efficiency, fast refuel times, quiet and scalable electrical energy generation.[3] Hydrogen is an ideal fuel for PEMFC's because of its high reactivity and negligible pollution concerns, but production, storage and transport still pose issues.[3] Hydrogen is currently used as an important feedstock for the production of chemicals and fertilizer. Hydrogen production worldwide is already significant at over 50 million tons produced annually, the majority coming from the steam reforming of natural gas.[4]

Progress is being made, the estimated cost of hydrogen fuel cells has decreased by a factor of 6 since 2002, down to 49$/kW and hydrogen storage capacity has increased by 50% since 2007.[4] This has led many to believe that the hydrogen economy is close fruition, auto manufacturers are even releasing hydrogen powered cars in limited cases.[5] Hydrogen fuel cells are also gaining prominence in large warehouses for their fast refuel times and zero emissions operation.[6]

Hydrogen Production

Progress in hydrogen production has not kept pace with these advances on the use side. The production of hydrogen is currently accomplished via steam reforming of natural gas. The steam reforming reaction is a two stage reaction performed on two catalysts at two different temperatures. Equation 1 shows the higher temperature, endothermic $((\Delta H = 206 \frac{kJ}{mol})$, first stage which takes place on a nickel catalyst. Equation 2 shows the lower temperature, exothermic $((\Delta H = -41 \frac{kJ}{mol})$, second stage, for which a on a copper catalyst is often used.

1    $CH_4 + H_2O \leftrightarrow CO + 3H_2$

2    $CO + H_2O \leftrightarrow CO_2 + H_2$
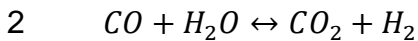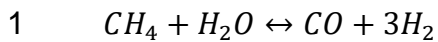
This system uses large, centralized plants and necessarily emits a minimum of 5.5 tons of CO_2 per ton of H_2 produced, not including the energy used for reforming or compression of the hydrogen gas.

The resulting hydrogen gas must be purified or the anode catalysts will be poisoned by carbon monoxide. This purification is generally accomplished using pressure swing absorption. Even moderate amounts of CO can be problematic for a low temperature PEM fuel cell. An 85% voltage loss has been reported at only 6 hours of exposure to 70 ppm CO feed, using pure Pt catalyst at $80° C$ [7]. This is because CO adsorbs on the platinum catalyst and requires several hundred mV of additional voltage to oxidize to CO_2.

These production facilities must then ship the hydrogen out to fueling stations using either a hydrogen pipeline network or tanker trucks. Estimates of the cost of a national hydrogen pipeline network are on the order of tens or hundreds of billions of dollars. This extreme cost is based on the analysts assumption of the creation of a hydrogen pipeline system similar to the natural gas pipeline system.[8] Delivery by tanker trucks is also cost prohibitive. Due to the volume constrains, a tanker truck deliver system would almost certainly require the use of liquefied hydrogen rather than compressed hydrogen. Nearly half the delivered cost of hydrogen obtained steam reforming and liquefied delivery comes from the liquefaction process.[9]

It has been shown that the use of distributed, small scale hydrogen production has the potential to significantly lower the rollout cost and cost per vehicle, especially in the early stages.[8] It is widely believed that the best way to achieve distributed production of hydrogen is either from electrolysis or steam/catalytic reforming of hydrocarbons.

On-board reforming was initially the preferred choice of automakers.[9] They believed that hydrogen production on the vehicle would help eliminate complications arising from the storage of hydrogen. Hydrogen has a low volumetric energy and a tendency to leak. Compression or cryogenic storage consume a significant portion of the energy used to make the hydrogen. Unfortunately, on-board reforming is costly in terms of energy, weight, and money.

An econometric study done by Thomas et al. suggests that on-board reforming does not make economic sense.[9] They show that the total costs of a distributed hydrogen infrastructure per vehicle will be significantly lower than the costs of adding reforming capability to each vehicle. These savings come primarily from scale, durability, and utilization. The reformer lifespan can be adversely affected by vibration, startup/shutdown, temperature extremes, load changes and other characteristics common to a moving vehicle. The capital cost per unit hydrogen produced by a stationary, multi-user system will be significantly lower than an on-board reformer. This is due to the increased load factor. While an on-board reformer might have a load factor of only 0.6%, a stationary reformer can be appropriately sized to run at nearly 100% load factor.[9] This will have a significant effect on cost since a much lower capacity reformer can be specified for the same output over a given timeframe.

On-board reforming could take place using steam reforming of nearly any hydrocarbon fuel. It can also be direct electrochemical reforming of hydrocarbon fuels. Many small molecules have been explored as direct electrochemical hydrogen sources including methanol, ethanol and dimethyl ether but only methanol has been shown to be feasible.[3] The other, larger molecules have suffered from incomplete combustion, excessive overpotential requirements and catalyst poisoning in low temperature fuel cells.

While steam reforming is a well-established technology currently used to generate hydrogen all over the world, it has important drawbacks. In addition to its inability

to directly produce pure hydrogen, steam reforming does not change the dependence on fossil fuels or prevent the emission of carbon dioxide. Steam reforming also requires longer startup times than a low temperature electrolyzer due to its high temperature nature. Electrolysis or electrochemical reforming is perhaps the most obvious solution to the problem of creating pure hydrogen while maintaining the potential for zero emissions. The electricity could potentially be supplied by renewable generation such as wind, solar, or hydroelectric. Production can be ramped up during times of excess production and decreased during times of high electricity demand to help stabilize the power grid.

Water Electrolysis

Water electrolysis is a process in which electrodes are submerged in an aqueous solution and current is run between them. If the applied potential is wider than the solvent window, then the water will be split into hydrogen and oxygen. Although different reactions hold in acidic versus aqueous media, they both require a minimum or thermodynamic potential of 1.23V vs SHE at standard conditions. The use of a separator is also required to prevent the mixing of hydrogen and oxygen, both for safety and efficiency.

The following equations describe water electrolysis in acidic media:

Anode: $2H_2O \rightarrow 4H^+ + O_2 + 4e^-$

 3   E=1.23V vs SHE

Cathode: $4H^+ + 4e^+ \rightarrow 2H_2$

4   E=0.00V vs SHE

Whole cell reaction: $2H_2O \rightarrow 2H_2 + O_2$
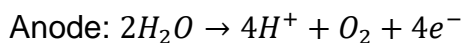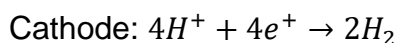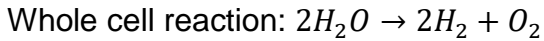
5   E=1.23V vs SHE

The following reactions describe water electrolysis in alkaline media:

6   Anode: $4OH^- \rightarrow O_2 + 2H_2O + 4e^-$

7   Cathode: $4H_2O + 4e^- \rightarrow 2H_2 + 4OH^-$

8   Whole cell reaction: $2H_2O \rightarrow 2H_2 + O_2$
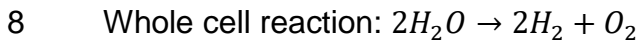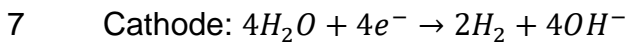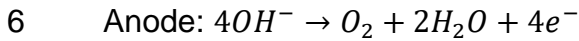
The following equation 9 can be used to calculate the actual voltage in any electrochemical cells. The voltages given above are the $V_{thermal}$.

9       $V_{actual} = V_{thermal} + V_{kinetic} + V_{ohmic} + V_{Mass\ Transfer}$

Electrolysis Efficiency

The efficiency of any process is essential to understanding its viability. The efficiency of electrochemical processes is described in terms of voltage and current efficiency. They are functions of device architecture, reaction fundamentals, materials selection, catalyst choice, and operating parameters.

Current efficiency is defined as the proportion of the current which goes into making the desired product. Current efficiency can be decreased by side reactions or through crossover of the active species. For example, in an electrolyzer hydrogen could back diffuse to the water/oxygen side (anode) and then have to be

pumped to the cathode again. It can also react with oxygen to form water while it's there, requiring the water to be split again. Current efficiency of electrolyzers can be decreased at extremely low current densities. This is primarily a function of permeability of the membrane.

Voltage efficiency relates directly to the overpotential of a given electrochemical process. Voltage efficiency of an electrochemical device is given by equation 10. The V_{actual} is calculated per equation 9. The $V_{kinetic}$ depends on reaction choice, pH, and catalyst choice. V_{ohmic} is primarily a function of the electrolyte resistance and the distance between the electrodes. $V_{mass\ transport}$ is controlled by the ability to supply reactants to the electrode. Concentration overpotential results when the reactant at the electrode becomes depleted and the reaction becomes unfavorable.

10 $\quad V_{efficiency} = 100 * \frac{V_{thermal} - V_{actual}}{V_{thermal}}$

A key performance metric for electrical energy time shifting is roundtrip combined efficiency of about 80%. Some secondary battery systems are already achieving this benchmark. Reaching it in either flow batteries or a combined electrolyzer/fuel cell will require overpotentials within 10% of theoretical voltage in each direction. Assuming a current density of 50 mA/cm^2 and a roughness factor of 10, exchange current density must be greater than 0.3 mA/cm^2 and a standard rate constant K^0 greater than 10^{-5} cm/s.[10]

Unitized PEM hydrogen electrolyzers/fuel cells achieved 85% efficiency electrolysis and 37% efficiency for fuel cell mode, a round trip efficiency of just 31.5%. They reported cell voltages of 1.74 V and 0.55 V at 0.5 A/cm^2. The utilized unsupported Pt-Ir catalysts for water oxidation and oxygen reduction. The fuel cell ran on pure hydrogen and oxygen to further improve efficiency.[11] Researchers at NASA developed a similar closed cycle regenerative fuel cell. They saw round trip efficiency below 50%.[12,13]

More recent work has shown that low temperature PEM regenerative fuel cells can achieve round trip efficiencies between 40-50%. Some of this efficiency may have been gained by decreasing operating current densities. Alkaline systems are slightly less efficient at 30-40%. The relatively low   efficiency is caused by sluggishness of the oxygen reactions(both reduction and oxidation).[14] This kind of efficiency comparison is important to understanding the viability of the system but it's also fraught with questions. The efficiency numbers are highly dependent on the current density chosen by the author and are therefore highly variable.

Alkaline Electrolysis

Historically, alkaline water electrolysis became common even before the invention of ion exchange membranes. Mass production of over 400 units was achieved by 1902.[15] Early designs utilized an asbestos diaphragm submerged in a solution of 20-30% KOH. Common catalysts include nickel, cobalt, iron, and platinum. The use of nonprecious metal catalysts, a common separator material, and high purity products were all drivers of its growth. The alkaline environment is less corrosive

than the acidic system allowing for the use of stainless steel bipolar plates, lowering cost relative to the acidic system.

Its use is limited by low partial load range, limited current densities, and low operating pressure. The tendency of products to back diffuse causes the issues with low load range and low operating pressures. When oxygen diffuses to the cathode compartment it causes safety concerns and must be catalytically recombined with hydrogen, reducing efficiency. Hydrogen also diffuses to the anode compartment creating similar safety issues. Hydrogen is particularly problematic due to its wide explosive window, from 4% to 75% by volume.[16] The problem becomes more pronounced at low loads since the electrochemical driving force keeping products on their respective sides of the diaphragm disappears. In larger systems, the marginal cost of increasing capacity scales linearly with surface area. Relatively low current density of .2-.4 A/cm^2 necessitates a large surface area and contributes to increased system cost.[17]

There have been significant recent advances in two main areas; efficiency and current density. Operational costs are almost entirely dependent on overpotential (efficiency), so the best way to improve these devices has been to decrease the resistances that cause increased overpotential. Capital costs can also be quite significant, therefore increasing current density will help to decrease cost. These advances were achieved using several techniques:

- Decreased distance between electrodes: One of the major sources of resistance is V_{ohmic}. Since $V_{ohmic} = IR$ and current is directly proportional to

12

hydrogen production, decreasing resistance is a major goal. The area specific resistance is defined as $ASR = \rho L$. Decreasing the distance (L) between electrodes under one millimeter is now standard and some manufacturers use a zero-gap architecture where the electrodes are pressed right up against the separator.

- Development of new separators: New separator technologies have reduced the resistivity (ρ) of the separator. This has been achieved by replacing asbestos diaphragms with inorganic ion exchange membranes.

- Development of high temperature alkaline electrolyzers: Operating at $150°$ C, these increase electrolyte conductivity (decreasing V_{ohmic}), improve catalytic activity (decreasing $V_{kinetic}$), and supply some of the required energy as heat instead of electricity. Since heat is generally cheaper than electricity this also lowers cost.

- Development of new electrocatalysts: Ni, Co, and Fe catalysts can be used to decrease the $V_{kinetic}$

Proton Exchange Membrane Electrolysis

Proton exchange membrane (PEM) electrolysis overcomes many of the issues associated with alkaline water electrolysis but introduces its own difficulties. The PEM based electrolyzer was first commercialized by General Electric in 1966.[18] The initial use of sulfonated polystyrene membranes as an electrolyte has been superseded by NAFION, a sulfonated tetrafluoroethylene based fluoropolymer

membrane (PFSA). The PFSA membranes have the advantages of high proton conductivity, low gas crossover, high pressure tolerance, and mature fabrication methods resulting in extremely thin membranes.

PEM electrolyzers have all the same components as fuel cells and alkaline electrolyzers but most of the components require different materials. Gas diffusion layers(GDL), flow-fields, catalysts, and methods of catalyst application all vary. Components of both electrolyzers and fuel cells are described in Table 1

Table 1: Components of Fuel Cells and Electrolyzers

Major Components	PEM Fuel Cell	PEM Electrolyzer[17]
Membrane	NAFION	NAFION
Anode Catalyst	Pt	IrO_2
Cathode Catalyst	Pt	Pt
GDL	Carbon paper/cloth	Sintered Ti
Bipolar plate (cathode)	Graphite	Ti, gold plated(Cathode)
Bipolar Plates(anode)	Graphite	Ti, Coated Stainless Steel

PEM electrolyzers can operate at much higher current densities than alkaline electrolyzers while still maintaining high voltage efficiency. They reached 1 A/cm^2 @ 1.88V and 2A/cm^2 @ 2.14V by the early 1970's.[18] The use of PSFA type membranes also enables both high pressure and high differential pressure. High

system pressure improves anode kinetics. High differential pressure enables electrochemical compression of product gas instead of mechanical compression.[19] The relevant form of the Nernst equation across a membrane is as follows:

11      $E = E^0 + \frac{RT}{nF} \ln \frac{P^{II}}{P^I}$

This leads to the conclusion that it is possible to increase pressure to 10,000 psi using 1/3 of the energy of 3 stage mechanical compression.[20] In practice this degree of compression, requires multiple stages although it is still likely be cheaper and simpler than mechanical compression.

Fast ionic transport across NAFION membranes allows quick response to changes in input power while alkaline systems have a somewhat delayed response due to the inertia of moving products across the liquid electrolyte.[17] PEM based systems also have lower gas crossover than traditional alkaline electrolyzers, improving partial load range. The solid electrolyte enables compact system design.

PEM electrolyzers are not without their drawbacks which include expensive components and durability issues. The choice of an acid environment means that the inexpensive catalysts used in alkaline fuel cells are not electrocatalytically active. Many of the catalysts that do show sufficient activity are not stable in the acid environment. This leads to the use of significant quantities of precious metals, including platinum, ruthenium, and iridium. The use of precious metals is an important cost driver in PEM electrolyzers.

Figure 1 shows the performance of a PEM water electrolysis cell with several advanced anodes. While the performance is considered to be quite efficient, the current does not even begin to flow until nearly 1.4 V. Operating at about 1.55 V and 0.5 A/cm^2 is roughly 75% efficient.

Iridium dioxide (IrO_2) is generally recognized to be the state of the art anode electrocatalyst for water electrolysis. Ruthenium dioxide has been shown to require a lower overpotential than Ir but it experiences extreme corrosion issues.[17] Iridium is one of the rarest metals on earth and the worldwide usage was only 5500 kg in 2012. [22,23] This means that there would likely be a large increase in the price of iridium if it were to be widely deployed in electrolysis.

For the case of cation exchange membrane with platinum electrocatalysts, the hydrogen reduction reaction is highly reversible. The current state of the art cathode catalysts are therefore based on high surface area platinum on carbon. Current loadings range between 0.5-1.0 mg/cm^2. While the reaction is electrochemically facile, there is still a strong overpotential dependence on Pt loading at high current densities.[17]

PEM water electrolysis is already highly mature but still has issues with durability, the overpotential required for water electrolysis and the low partial load range problems of alkaline water electrolysis.

Reducing the potential required is an essential component of increasing efficiency. One solution for reducing the electrochemical potential is to chemically depolarize

the anode. This involves replacing water electrolysis at the anode with a more electrochemically favorable reaction. A great variety of reactions have been explored as anode depolarizers including methanol, ethanol, glucose, Keggin ions, SO_2, and nearly every other reaction that can be used to run a fuel cell.

PEM Methanol Electrolysis

Direct electrochemical oxidation of liquid fuels has always been the ideal solution for increasing the market viability of fuel cells. The option of an easily transportable, energy dense, liquid fuel would solve the issues that surround production, transportation, and storage of hydrogen.

Methanol is the most feasible of the small organic molecules for electrochemical oxidation. This is due to the lack of a carbon-carbon(C-C) bond. The C-C bond is much stronger than carbon-hydrogen bonds, so methanol is easier to oxidize than other candidate fuels like ethanol and ethylene glycol. [3,24] Additionally the lower carbon to hydrogen ratio means less CO_2 is generated per unit energy. Methanol is a liquid at room temperature/pressure and is only slightly toxic, which makes it easy to store and transport.[3] While the bulk of methanol today is made from reforming of natural gas, it can be obtained from a variety of sources including renewables.[25]

Much progress has been made in the design of direct methanol fuel cells over the years. The major scientific discovery that increased their viability was the discovery of the Pt-Ru anode catalyst.

Early methanol electro-oxidation experiments used platinum electrodes but Pt is poisoned by adsorption products. On pure platinum, it was determined that the initial rate limiting step was the removal of the first hydrogen from the methanol. After a short time, on the order of milliseconds, the rate limiting step would then shift to the removal of adsorbed products.[26,27]

The Pt surface is covered with carbon monoxide and the reaction cannot be sustained at a high rate until the potential is raised by several hundred millivolts. To counter these effects, binary and ternary catalyst promoters have been used, the most effective of which has been mixtures of roughly 1:1 Pt:Ru. This is due to the bi-functional mechanism whereby Pt adsorbs and disassociates methanol (12). The CO binds strongly to the Pt surface and cannot be removed or further oxidized at modest over potentials.[26] The Ru reactively adsorbs a water molecule (13) to form surface hydroxyls. The adsorbed oxygen species diffuses to the Pt to further oxidize the CO to CO_2 (14).

12    $Pt + CH_3OH \rightarrow Pt - CO(ads) + \ 4H^+ + 4e^-$

13    $Ru + \ H_2O \rightarrow Ru - OH(ads) + \ H^+ + e^-$

14    $Pt - CO(ads) + Ru - OH(ads) \rightarrow \ CO_2 + H^+ + e^-$
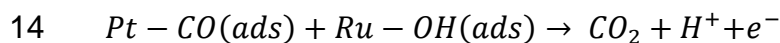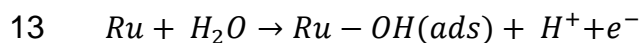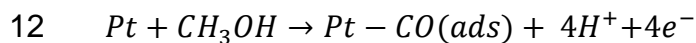
The two main obstacles to the implementation of the direct methanol fuel cells(DMFC) are the high precious metal loadings required and crossover of methanol from the anode to the cathode. The state of the art anode for a DMFC contains 2-4 mg/cm^2 of unsupported Pt-Ru and the cathode must contain

additional Pt catalyst to help deal with crossover oxidation, this results in 10 times the loadings required for a H_2 PEMFC.[3] Crossover of methanol from the anode to the cathode results in poor cell performance due to the formation of a mixed potential, poisoning of the cathode catalyst and fuel waste.[3] Limiting crossover requires the use of a thick membrane such as NAFION 117 (0.007 in) rather than a thinner NAFION 211 (0.001 in). This thicker membrane is both more expensive and induces a higher cell resistance than a thinner membrane would. Platinum catalysts at the cathode can be poisoned by the buildup of CO from methanol partial oxidation on their surface which requires increased voltage to remove.[7] A mixed potential is when multiple reactions are happening at a single electrode. In this case the undesired reaction would lower the overall cell potential and power. These effects limit the concentration of methanol which can be used, requiring additional storage space and complexity for dilution of the methanol[3]. in spite of these issues, DMFC's are a mature technology with products offered for sale. They are particularly gaining traction in the operation of forklift trucks and military applications.[28–30]

It is possible to physically separate the steps of electrochemical oxidation of methanol and the reduction of oxygen. With this physical separation, a temporal separation also becomes possible. A separate electrochemical reformer could be used to oxidize the methanol and pipe the hydrogen to the fuel cell. Some of the power from the fuel cell can be used to operate the electrolyzer, while the remainder provides power. The electrochemical reformer could also operate to fill

a hydrogen tank when plugged into the wall. The hydrogen produced in methanol electrolyzers has been shown to be of sufficient quality for direct use in fuel cells.[31,32]

This design has certain advantages over a DMFC. Crossover does not decrease, but its significance may, due to the potentials and chemicals present at the cathode of an electrolysis cell versus a DMFC. The methanol that crosses over will have no oxygen to react with and will not oxidize at the reductive potentials present. It can then be recycled with a mechanical trap, solving both the mixed potential and fuel loss issues. Studies have indicated that there is improved tolerance to high concentration methanol feeds relative to DMFCs.[31,32]

If the cost, weight, volume, or energy requirements of separate electrolyzers on-board vehicles proves prohibitive there is another option: Utilizing electrochemical reforming of the methanol to hydrogen in distributed sites. By concentrating methanol reforming at the gas station level, the increased load factor would decrease capital costs.[9] The distributed reforming approach is expected to be far cheaper than on-board reforming or the buildout of a nationwide hydrogen infrastructure.[8,9] The grid connected nature of these hydrogen supply nodes will also enable them to take advantage of dispatchable demand in a demand response market. That means purchasing power when there is an excess of (hopefully renewable) electricity supply.

While much of the design knowledge will be shared with a direct methanol fuel cell, an appropriate benchmark technology is water electrolysis. Relative to water

electrolysis, methanol electrolysis has the main advantage of reducing the theoretical potential from 1.23V to 0.016V.[32] It has been estimated that hydrogen production by methanol electrolysis has the potential to cost 50% less than water electrolysis, including the cost of methanol.[33] In acid, the following equations describe hydrogen production from methanol:

15   Anode: $H_3OH + H_2O \rightarrow 6H^+ + CO_2 + 6e^-$

      E=0.016 V vs SHE[32]

16   Cathode: $6H^+ + 6e^+ \rightarrow 3H_2$

      E=0.0V vs SHE

17   Whole cell reaction: $CH_3OH + H_2O \rightarrow 3H_2 + CO_2$
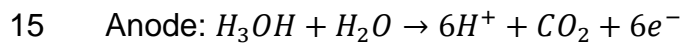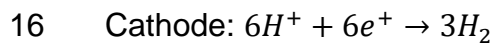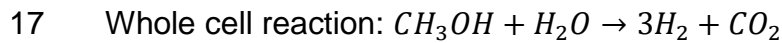
      E=0.016V vs SHE[32]

The presence of free oxygen and a strongly oxidizing environment at the anode of a PEM electrolyzer necessitates the use of expensive titanium bipolar plates, especially at the anode. DMFC anode current collectors are frequently stainless steel. This can result in a significant cost savings as bipolar plates are nearly 40% of capital cost in a PEM electrolyzer.[34]

Polyoxometalates

The overarching goal of this work is to develop clean and affordable methods of generating hydrogen from renewable feedstocks. The direct(heterogeneous) oxidation of methanol and other organics is slow and fraught with potential fouling

of the electrodes. In this case the electrode reaction occurs only at high overpotential or with large quantities of electrocatalysts.

An indirect approach may therefore be a useful way to circumvent these issues. In indirect electrochemistry, a mediator reacts heterogeneously at an electrode surface to become activated and then flows into a solution to undergo redox reactions with a substrate. The mediator carries electrons and other ions between the substrate and the electrode. This moves the catalytically slow step away from the electrode to the following effect:

- enabling increased current density

- decreasing or eliminating heterogeneous catalyst loading

- preventing passivation of the electrode

We have chosen the Keggin ion phosphomolybdic acid ($PMo_{12}O_{40}^{3-}$) as our homogenous catalyst. Keggin ions are polyoxometalates(POM) of the general form $XY_ZM_{(12-Z)}{}^{n-}$, where X is the hetero atom, M and Y are addenda atoms. M and Y are transition metal atoms. POMs tend to exhibit stronger acidity than typical mineral acids and the properties can be tuned by changing the hetero and addenda atoms. This tunability and acidity combine to create a set of highly attractive acid and oxidation catalysts. Figure 2 is a ball and stick representation of a Keggin ion. For phosphomolybdic acid, the orange center is phosphorus, the blue molecules are molybdenum, and the red molecules are oxygen.

Higher redox potential POM's are expected to more rapidly oxidize substrates but will require more energy to reoxidize. Therefore we must choose a POM that optimizes both of these requirements.[35] It has been shown in that polyoxometalates can convert cellulose to glucose and 5-hydroxymethlfurfual(HMF) at significantly higher rates than equivalent concentrations of mineral acids.[36] Solar and thermal oxidation of starch, cellulose, raw poplar and lignin were demonstrated to operate a fuel cell using Keggin ions.[37,38] Glucose and cellulose oxidation to produce hydrogen and syngas has also been confirmed and patented using Keggin ions.[39,40]

$PMo_{12}O_{40}{}^{3-}$ also written $H_3PMo_{12}O_{40}$, can undergo four reversible reductions of two, two, two, and four electrons followed by an irreversible reduction of two electrons.[41] The reduction potentials depend on pH as the electron transfer is coupled with protonation as shown in the following equations.[41] The stability is also a function of pH and solvent choice.

18    $H_3PMo_{12}O_{40} + 2e^- + 2H^+ = H_5PMo_{12}O_{40}$

19    $H_5PMo_{12}O_{40} + 2e^- + 2H^+ = H_7PMo_{12}O_{40}$

20    $H_7PMo_{12}O_{40} + 2e^- + 2H^+ = H_9PMo_{12}O_{40}{}^{3-}$
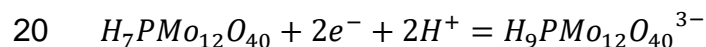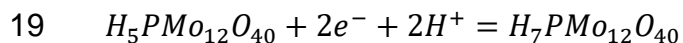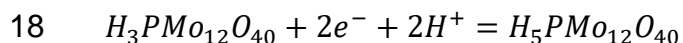
At a concentration of 0.5 M in deionized water, the first redox step occurs at 0.65 V vs NHE as shown in Figure 3. The dashed red line shows CV of 1 M phosphoric acid as a background. The CVs were performed under air with a Pt counter electrode, Ag/AgCl reference, and a 100 mV/Sec scan rate. Significantly the plot

of peak current vs square root of scan rate is linear, indicating that the reaction may be electrochemically reversible. Phosphomolybdic acid can be readily oxidized on multiple media including high surface area carbon paper.[38,42] $PMo_{12}O_{40}^{3-}$ is a large ion of molar mass 1822 kg/mol and a 3$^-$ charge, making it extremely resistant to crossing over cation exchange membranes. An experiment on using phosphomolybdic acid for time shifted water electrolysis showed no noticeable crossover with NAFION or neutral benzoylated cellulose dialysis membranes.[42] This lack of crossover suggests that the use of traditional PEM electrolysis cathodes for the production of hydrogen will be successful.

The use of a hydrogen on platinum cathode provides an additional benefit; it enables the cathode to perform as a dynamic hydrogen electrode (DHE). A DHE is a form of reference electrode based on the reversibility of the hydrogen on platinum reaction in acid. The use of an in-situ reference electrode allows for the examination of anode kinetics in a way that has not been done before with this system. Previous authors have either focused on fundamentals of POM behavior or the operation of biomass based fuel cells.

Liu et al. showed the creation of a "solar induced direct biomass to electricity" fuel cell.[38] The authors showed the photocatalytic activity of phosphomolybdic acid was sufficient to oxidize starch, cellulose, lignin, and poplar. They also showed a significant increase in catalytic effect from elevated temperature. When the two effects were isolated, the thermal effect was greater than the solar effect. They only presented results which allow inferences from the operation of the cell. They

24

show the comparison of fuel cell polarization curves using different biomass substrates and promoter ions. Their cell had poor power output and they did not attempt to decouple the anode and cathode losses. We are left to make inferences about the oxidation of the biomass based upon how the cell operates. This is inappropriate because polarization curves can be affected by the complex behavior of the POM anode and the ORR cathode. They use peak power as a surrogate for degree of reduction. This also leaves the question of anode performance untouched.

Bloor and Cronin have demonstrated solar driven water oxidation with decoupled hydrogen production using phosphomolybdic acid and a tungsten oxide photoanode.[43] This cell oxidized water at $1\frac{mA}{cm^2}$ under sunlight, storing the produced hydrogen in phosphomolybdic acid. Their designed system is shown in figure Figure 4. Their work showed the ability to completely reoxidize this mediator on carbon felt at 0.75 V vs Ag/AgCl, a voltage well below that required for water oxidation. They were only making a proof of concept and did not explain the anode performance on reoxidation of the biomass.

Several authors have shown the creation of a homogenous POM-TiO_2 co-catalyst system for enhancement of the photo catalytic ability of the system.[44,45] All authors used TiO_2 nanoparticles with Keggin type polyoxometalates and showed significant increases in reaction rates. The substrates used were methanol and 1,2-dichlorobenzene (DCB). The work by Gu showed a 4-fold increase in reaction rates compared to POM alone. This work was done at low concentrations of POM

to reduce the quantity of substrate oxidized by the POM rather than by TiO_2, despite increasing photocurrent with increasing POM concentration. It is possible that the addition of significant quantities of POM would reduce the effectiveness of the TiO_2 by acting as a local UV filter.

Dumesic et al.showed the creation of a polyoxometalate based fuel cell which ran on CO.[46] This is a particularly promising concept because the water-gas shift reaction is more efficient at low temperature.[39] The authors used gold nanoparticles in solution with $H_3PMo_{12}O_{40}$ to oxidize CO at room temperature. They achieved a maximum transfer of nearly 5 electrons per Keggin unit. The authors also showed 20-50% higher performance for anodes containing precious metals versus their unspecified carbon cloth anode. They found the rate of POM reduction to be first order with respect to CO partial pressure. They also achieved 5 electrons per Keggin unit reduction. As with the others, they are again only showing full cell polarization curves. They did not isolate the operation of the anode.

Roger Carson and Bruce Bremer have filed patent applications on a variety of waste oxidation methodologies, including one entitled "Mediated electrochemical oxidation processes used as a hydrogen fuel generator".[47] In this application they explain nearly every possible way such a mediated biomass to hydrogen generator could work. The authors explain how polyoxometalates interact with the solvent and other ions which may be present to synergistically increase the substrate destruction rate. They introduce the concept of superoxidizers, secondary oxidizer

free radicals such as O_2H, OH, SO_4, etc. The patent claims acid, alkaline, or neutral solutions with nearly every combination of simple anion mediators or heteropoly or isopoly anion mediators.

Mediator Cost

Cost is of great importance in the design of a system intended for widespread deployment. Many competing solutions require the extensive use of precious metals, which are both expensive and exhibit great price volatility.

The key components of phosphomolybdic acid, phosphorous and molybdenum are both abundant and widely used materials. 5.4 million tons of molybdenum are considered identified resources in the US alone, and 266,000 metric tons were mined in 2014.[48] Molybdenum oxide is a commodity chemical used in metal refining while phosphorus is used in the production of fertilizer. Their status as commodity chemicals will help to prevent massive price increases should this system become widespread.

Phosphomolybdic acid is currently a specialty chemical, priced on the order of $1 per gram. This need not be the case if mass production were to begin. As of June, 2017, the molybdenum spot price is $15 per kg.[49] Phosphorus can be purchased for as little as $0.55 per kg.[50] The metal content of phosphomolybdic acid is not the only price driver, synthesis and refining will also play a significant role in setting the cost. Phosphomolybdic acid is synthesized by mixing phosphoric acid with molybdenum trioxide and strong acid. The Keggin ion is

then extracted with ether and crystallized.[51] While not particularly complicated, this process does require several steps and results in significant waste, although most of the waste can likely be recovered.

Mechanisms for Polyoxometalate Mediated Oxidation of Organics

Two mechanisms have been proposed for the oxidation of biomass by Keggin ions. First is the proton coupled electron transfer (PC-ET). Using the notation of Neumann, the reaction is shown in equations 21 and 22.

21 $\quad SH_2 + PMo_{12}O_{40}{}^{3-} \rightarrow S + 2H^+ + PMo_{12}O_{40}{}^{5-}$

22 $\quad 2H^+ + PMo_{12}O_{40}{}^{5-} + \frac{1}{2}O_2 \rightarrow PMo_{12}O_{40}{}^{3-} + H_2O$
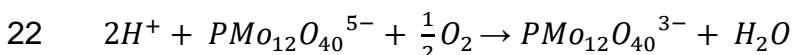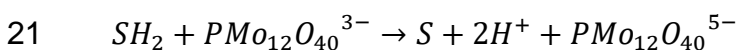
Neumann's work also posits an electron transfer-oxygen transfer (ET-OT) mechanism, summarized below where S is once again the substrate. [52]

23 $\quad S + H_3PMo_{12}O_{40} \rightarrow S - O + H_3PMo_{12}O_{39}$

24 $\quad H_2O + H_3PMo_{12}O_{39} \rightarrow H_5PMo_{12}O_{40}$

25 $\quad H_5PMo_{12}O_{40} + 2e^- \rightarrow H_3PMo_{12}O_{40} + H_2$
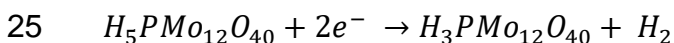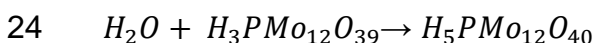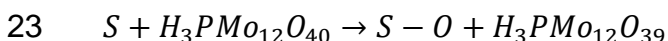
The authors state that the phosphomolybdovanadate anion $PV_2Mo_{10}O_{40}{}^{5-}$ is more reactive than $PVMo_{11}O_{40}{}^{4-}$, which is more reactive than $PMo_{12}O_{40}{}^{3-}$. The stability trend runs the opposite direction, while the redox potentials and acidity of all of three species are roughly the same. This increased reactivity is believed to be due

to faster re-oxidation by molecular oxygen. Our proposed process would take place in the absence of molecular oxygen so this may be an unimportant or even counterproductive characteristic. In the proposed systems, re-oxidation by oxygen is a competing reaction which would produce water instead of hydrogen.

In the presence of strong acids, Keggin ions have been found to catalyze the oxidation of vicinal diols via the ET-OT(electron transfer-oxygen transfer) mechanism and insertion of oxygen into the C-C bond.[53] Neumann's group has also developed and patented a phosphomolybdovanadate based system to oxidize cellulose and hemicellulose to carbon monoxide and hydrogen gas.[39,40,52,53] They found that the presence of strong acid shifts the reaction from PC-ET to ET-OT. This should enable a more complete oxidation reaction.

Locations of Common Mediator Redox Potentials

Figure 5, shows the redox potentials of many common redox couples used for batteries and mediated electrochemistry. Phosphomolybdic acid redox potential is dependent upon pH but the first two, two electron redox couples are located at 0.64 V and 0.43 V respectively. That places them between the iron and vanadium redox couples shown in Figure 5. The first 2 electron redox couple is shown on the figure below.

Glycerol

One of the most important choices for any proposed biofuels program is the question of substrates. An appropriate starting material for a biofuel will be

inexpensive, carbon neutral, and available in sufficient quantities. One trap to avoid is the use of a starting material that is currently cheap but will become expensive as the scale of the operation grows. According to a study done by the US EPA, the growth of corn based biofuels is believed to have increased corn prices 2-3% for each billion gallons of fuel produced.[55] For reference the US consumed about 140 billion gallons of gasoline in 2015.[56] The authors at the EPA also claim that increased use of biofuels will significantly increase the cost of food and raise the number of people at risk for poverty and starvation worldwide. We are driven to find waste streams available in sufficient quantity to serve as resources worth exploiting commercially.

Glycerol is the main component of triglycerides, found in animal fat and vegetable oils. It has been in continuous production for nearly 5000 years.[57] It was once a valuable commodity chemical but it is now available in large excess due to the production of biodiesel. Glycerol is produced as a byproduct of biodiesel at a rate of roughly 10% by weight.[58,59] Biodiesel has been in production in the EU commercially since 1992 but its production and adoption have grown worldwide.[57]

Glycerol is produced from a process known as saponification. Triglycerides are reacted with sodium or potassium salts in strong base to yield glycerol and soaps the reaction shown in Figure 6.[57] Increasing the concentration of NaOH will eventually cause a phase separation between the glycerol and the soap.

The biodiesel production process shown in Figure 6 is similar to the soap production process. It uses the same reagents as saponification but with the

addition of alcohol. This process is known as transesterification. The most common choice of alcohols for biodiesel production is methanol.[57]

From the 1970s until about 2004, the price of glycerol was stable between $1200 and $1800 per ton. Starting in 2004, the price of crude glycerol began to crash. This is attributed to the introduction of biodiesel mandates, subsidies, and vehicles. Crude glycerol prices reached between $0 and $70 per ton in 2007.[57] The market is fully saturated with glycerol and that is unlikely to change as biodiesel production is expected to increase.

Raw (unrefined or crude) glycerol contains 62-68% glycerol, 23-38% methanol, and the balance salts, water, and other free fatty acids. The exact composition of the raw glycerol depends primarily on the source of triglycerides for biodiesel production. It is nontoxic, not flammable, noncorrosive and nonvolatile liquid making it easy to handle. There are two primary handling concerns, high viscosity and susceptibility to oxidation.

Glycerol is stable against atmospheric oxidation although it is relatively easy to oxidize. Ferrous and copper materials must be kept away from glycerol due to their propensity to catalyze the oxidation of glycerol. This process is especially rapid at elevated temperatures.[60]

The simplest method of using glycerol for energy would seem to be combustion. Combustion occurs when a reductant(glycerol) is combined with an oxidant(oxygen) to release heat, forming CO_2 and water. The combustion of crude

glycerol is a more complicated proposition than might be expected for the following reasons:

- Glycerol has a low caloric energy density of 16 MJ/kg which makes it difficult to maintain a stable flame.

- It is hygroscopic and crude glycerol contains significant amounts of water. This high water content further decreases the energy density

- Its self-ignition temperature is relatively high at 370 ℃, compared to 210℃ for kerosene.

- It is highly viscous which makes it hard to atomize

- Presence of sufficient quantities of salt to clog atomizers without additional purification.

For an ideal combustion reaction, a spray of the fluid should be ignited from a single spark to yield a sustained flame. Due to the low energy density and high self-ignition temperature, even passing a glycerol spray over a flame is insufficient and will extinguish the flame. Glycerol must therefore be co-burned with other fuels in specialized setup.[57]

When used in an electrochemical reactor, crude glycerol must have some impurities removed. Crude glycerol can contain significant quantities of salt. These salts must be removed before the solution reaches an electrochemical reactor, as they will tend to clog the fragile gas diffusion layer. Indeed, fuel cells exposed to

vapor laden with salt from sea water will form a salt crust. The other major impurity in crude glycerol is methanol. Methanol is traditionally recovered for use as a reagent in the saponification process. The excess methanol in the presence of strong acid can cause an etherification reaction instead of the desired oxidation reaction. Full removal of the methanol is likely unnecessary because the presence of oxygen containing organics is known to stabilize Keggin ions in their reduced form.

One of the biggest potential hazards of glycerol oxidation is the byproduct acrolein. Acrolein is a toxic chemical formed by the dehydration of glycerol at high temperatures(equation 26). Occupational exposure is regulated by OSHA. Acrolein can also undergo polymerization reactions which might render it inaccessible to the polyoxometalate. The production of acrolein can be minimized by either preventing formation or consuming the acrolein. The formation of acrolein generally requires elevated temperatures so strategies to minimize the temperature make the formation of acrolein less likely. The other possibility is to consume the produced acrolein in the reactor where it is generated. In an ideal system, acrolein can be overoxidized to acrylic acid and then all the way to carbon dioxide.

26 $\quad (CH_2OH)_2CHOH) \rightarrow CH_2 = CHCHO + 2H_2O$
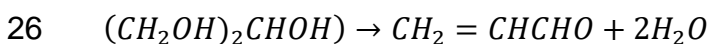
Glycerol Thermodynamics

One of the advantages of glycerol oxidation versus glucose or cellulose oxidation is the ratio of hydrogen to carbon dioxide released. Complete oxidation of glycerol (equation 29) yields 10 H_2 molecules per 3 molecules of carbon dioxide or a $\frac{H_2}{CO_2}$ ratio of 3.33. Glucose oxidation (equation 27) only yields 12 molecules of H_2 per 6 moles of carbon dioxide or a $\frac{H_2}{CO_2}$ ratio of 2. This will either lead to lower carbon emissions or less stress on any carbon capture system employed.

Glucose oxidation to carbon dioxide and hydrogen.

27 $\quad C_6H_{12}O_6 + H_2O \rightarrow 6CO_2 + 12H_2$
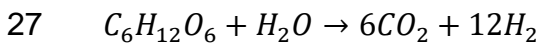
Glycerol partial oxidation to CO and H2 is given by 28. This mixture is known as syngas. The production of syngas may be economically valuable in certain conditions. It is used for producing methanol, ammonia, and synthetic hydrocarbons for fuel or lubricant.

28 $\quad C_3O_3H_8(l) \rightarrow 3CO(g) + 4H_2(g)$
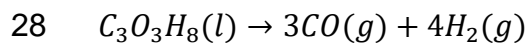
	Glycerol	Carbon Monoxide	Hydrogen
$\Delta_f H^\theta$	-669 kJ/mol	-110.5 kJ/mol	0 kJ/mol

$\Delta H_{RXN} = 337.5 \frac{kJ}{mol}$ is required for the partial oxidation of glycerol.

Glycerol complete oxidation to carbon dioxide and hydrogen is given by equation 29.

29    $C_3O_3H_8(l) + 3H_2O\ (l) \rightarrow 3CO_2(g) + 10H_2(g)$
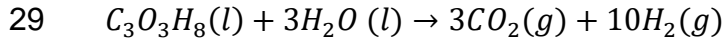
	Glycerol	Water	Carbon Dioxide	Hydrogen
$\Delta_f H^\theta$	-669 kJ/mol	-286 kJ/mol	-393.15 kJ/mol	0 kJ/mol

$\Delta H_{RXN} = 348\frac{kJ}{mol}$ is required for the complete oxidation of glycerol in the absence of molecular oxygen. The oxidation of glycerol to hydrogen and CO or CO_2 is endothermic. Some of this energy will be supplied by waste heat but some will be required as electrical energy to accomplish the final oxidation.

An alternative oxidation system would be the operation of a glycerol fuel cell as described by equation 30).

30    $C_3O_3H_8(l) + O_2(g) \rightarrow 3CO_2(g) + 4H_2O(l)$
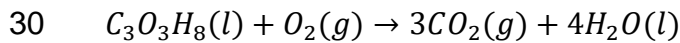
	Glycerol	Water	Carbon Dioxide	Oxygen
$\Delta_f H^\theta$	-669 kJ/mol	-286 kJ/mol	-393.15 kJ/mol	0 kJ/mol

$\Delta H_{RXN} = -393.15 * 3 - 286 * 4 + 669 = -1654\frac{kJ}{mol}$ could be obtained from the operation of a glycerol fuel cell if all of the heat were converted to electricity. The choice between the two modes of operation would depend of the economics of electricity and hydrogen at the time of implementation.

The Goal and Scope of This Dissertation

The goal of a vibrant, carbon free hydrogen economy will require the electrolytic production of hydrogen in the most efficient way possible. Current systems of water electrolysis are attractive but require large overpotentials and expensive materials. These two drawbacks speak to the operating cost and capital cost respectively.

Since nearly 80% of the cost of electrolytically produced hydrogen is electricity, most plans for addressing the operating cost of the stack revolve around reducing the potential. The three options for decreasing the overpotential mirror the sources of loss in an electrochemical cell. The goal is to decrease kinetic, ohmic, or mass transfer losses. Decreasing the kinetic potential requires advances in catalysis but will never advance beyond the thermodynamic voltage of 1.23 V. The ohmic potential is already quite low in zero gap flow cells. Advances traditionally come from thinner membranes, thinner electrodes, and improved contact between the cell components. The titanium surfaces required in PEM electrolysis present special challenges here because the titanium forms a passivating layer which both protects it and hinders electrical contacts. Improving the mass transport characteristics here tends to come from a better understanding of bubble formation, critically PEM electrolyzers tend to have less significant mass transport concerns since the pure reactant(water) is supplied in great excess.

Catalysts make up about 6% of total cost and flow-fields/separators make up a further 20% of installed cost.[34,61,62] Attempts to decrease the capital cost of the stack (40-50% of total cost) generally focus on three areas, the current, the

catalysts and the bipolar plates. The elimination or reduction of precious metals in all electrochemical devices is a longstanding goal. The advanced catalysts can decrease the precious metal loadings. Stack cost scales almost linearly with stack size, so decreased stack size is an important goal. Towards decreasing stack size the most important goal is increased current density.

These proposals are all fundamentally limited by the thermodynamics and the environment of water oxidation. An innovative approach will be required to circumvent many of these issues.

To further the goal of clean, abundant, and inexpensive hydrogen, we have explored the process of electrolytic hydrogen production from organic materials. The two systems used were direct methanol oxidation in an electrolyzer and indirect glycerol oxidation using polyoxometalates. The central points of this thesis are understanding ways to use electrochemical systems to harvest the energy content of biomass and increase the efficiency of hydrogen production processes. In this work we have shown that an aqueous system with a phosphomolybdic acid based anode is feasible using a carbon electrode. Despite this, substantial challenges remain in increasing the reaction rate of the biomass substrates.

In chapter 3 we constructed a direct methanol electrolysis cell. We utilized a dynamic hydrogen electrode to isolate the performance of the anode and cathode. We confirmed the expected decreases in cell potential with temperature. Overall cell performance and cathode performance were more negatively impacted by increasing methanol concentration than was expected.

37

To our knowledge, no group has performed kinetic studies of POMs in a zero gap electrochemical cell. Much work has been done to examine the electrochemistry of polyoxometalates in general and phosphomolybdic acid in particular, but only at low surface area electrodes.

To begin to solidify our understanding of the electrochemistry of phosphomolybdates, chapter 4 begins to characterize the electrochemistry of phosphomolybdic acid using cyclic voltammetry and rotating disk voltammetry. We find only some of the characteristics of electrochemical reversibility are met. We also find unexpected differences in the voltammetry based on state of charge. Finally kinetics and diffusion are examined using rotating disk voltammetry.

Chapter 5 is written with the goal of understanding the properties of the system in an operational configuration. The idea is to use polarization curves and cycling measurements to determine if operation in a PEM electrolyzer is a feasible proposition. By varying state of charge, temperature, electrode material, concentration, and pump speed we can understand what proportion of the loss comes from mass transfer, kinetics, and ohmic losses. This will direct future research towards how best to decreases these losses.

Chapter 6 begins to examine the chemical reduction of polyoxometalates by glycerol. We begin screening a variety of polyoxometalates, additives, and supporting acids to find sufficient reactivity with the glycerol.

CHAPTER 2

Materials and Methods

Cyclic Voltammetry at the Macroelectrode Theory

Cyclic voltammetry (CV) is a versatile electrochemical technique well suited to both rapid initial examination of systems and semi-quantitative kinetic analysis.

The CV experiment is an extension of linear scan voltammetry. A potential is applied, that cycles linearly up and down with time (Figure 7); the current response is recorded. The experimental results depend on the potential ranges scanned, the scan rate, diffusion coefficients, and the electrochemical rate constant k^0. Large current peaks which do not decrease at either end of a scan indicate electrolyte breakdown. The transport equations for the concentration profiles are not easily solved analytically for cyclic voltammetry experiments.[63] The key measured parameters for CV are shown in Figure 8. Initial analysis of the waveform reveals the formal potential $E^{0\prime}$ (Equation 31) and the locations of E_{pa} and E_{pc}. 31 $\boldsymbol{E^{0\prime}} = \frac{\boldsymbol{E_{pa} + E_{pc}}}{\boldsymbol{2}}$

Scans can immediately reveal the limits of the solvent electrochemical window and the locations of redox peaks. CV also allows a certain degree of analysis in aid of determining the mechanism of electrochemical reactions. By judicious choice of parameters such as scan rate and reversal potentials, the interconnections between peaks and the relation between electron transfer and homogenous processes can be revealed. Further analysis and planned experiments are required to determine kinetic parameters of the electron transfer reaction assuming the mechanism is known. This analysis, however, is rather difficult to perform to

high levels of accuracy unless a variety of aspects, notably solution IR and current distribution, are carefully controlled. CV can also be used in conjunction with modeling to confirm mechanistic information concerning the electron transfer reaction or to understand the kinetics of pure chemical reactions.

One of the important uses of CV is to determine reversibility of the electrode reaction. Electrochemical reactions can be reversible, quasi-reversible, or irreversible, while still maintaining chemical reversibility. This is because electrochemical reversibility is a kinetic condition rather than a thermodynamic one. Three characteristics must be met to determine reversibility from CV: $\Delta E_p < \frac{59}{n} mV$ (independent of scan rate), $i_{pa} = i_{pc}$, and a linear relationship between peak height and square root of scan rate. In reversible reactions, the following condition holds(equation 32). The determination of peak heights is often not a straightforward affair. It can require the use of potential hold experiments where on the second cycle the potential is held just before the start of the peak and the current at the time which would correspond to the peak is sampled. The recorded peak height minus the current sampled at that time is the peak height to be used in the experiment.[63]

32      $i_p = 2.69\text{x}10^5 AD^{\frac{1}{2}}[C_{Bulk]} v^{\frac{1}{2}}]$

In quasi-reversible and irreversible reactions, additional mechanistic information can be gained although the use of simulation is required. However, any residual

IR loss between the working and reference electrode as well as maldistribution of the current flow can have a significant impact on peak separation and morphology.

To maximize the utility of CV, it is recommended to perform an experiment across a wide range of scan rates. An initial scan at a high scan rate is often performed to determine the electrochemical window (the range of voltages where solvent breakdown begins). Additionally, the bounds of the scan must be selected such that they are far enough away from the target reaction to prevent interference. The conditions in this section apply to the first scan, if multiple scans are used then these diagnostics do not necessarily apply. This is because the environment around the electrode changes locally from the bulk during a scan.[63]

Scan rates are limited by capacitive charging on the high end and diffusion/convection at the low end. Capacitive charging introduces an additional contribution to the current that is linearly dependent on scan rate. This can make peaks difficult to resolve. CV relies on the assumption that all mass transport to the electrode is controlled by semi-infinite linear diffusion. If this assumption breaks down due to convection, then the results will be incorrect. This is most likely to happen in slow scan experiments since convection due to vibrations of the cell apparatus are most significant. The value P defined in chapter 4 describes the relationship between scan rate and the diffusion assumption in quiescent solutions.

CV For Analysis of Solution Reactions

CV can be used to determine the existence and kinetics of solution reactions coupled to electrochemical reactions. The coupled solution reaction will cause either an abundance or disappearance of one of the electrochemical reactants. The voltammogram will additionally depend on the solution reaction kinetics, concentration, and scan rate. This technique is described in chapter 6 where it is used.

Square Wave Voltammetry

Square wave voltammetry (SWV) is a type of potential step experiment useful for analytical studies due to its sensitivity. The name derives from the potential waveform shown in Figure 9. The current is sampled at the end of each step as is shown in the figure. The $i_{Forward}$ (i_1) and $i_{Reverse}$ (i_2) curves each will approximate a standard cyclic voltammetry sweep. The value i_Δ derived by subtracting forward and reverse scans, subtracting capacitive current while increasing faradaic response. This enables extremely high effective scan rates with high sensitivity. Effective scan rate is given as equation 34. SWV is most commonly used for concentration analysis where it is used with a calibration curve. While detailed mechanistic analysis is possible using SWV even for solutions of very low concentration, the analysis is strongly dependent on modeling of the results. [65]

$$33 \quad i_\Delta = i_{Forward} - i_{Reverse}$$

$$34 \quad Scan\ Rate = \frac{E_{Step}}{\tau}$$

Thin Layer Voltammetry

Thin layer voltammetry is a cross between cyclic voltammetry and bulk electrolysis techniques. A cell is constructed with a separation between electrodes on the order of the thickness of the diffusion layer. Thus, an appropriately slow scan will completely convert the material in the gap. It is useful because it is the most convenient technique to conduct rapid and complete bulk electrolysis. The major difference is that the system does not depend on semi-infinite diffusion, it is a complete electrolysis process. The potential waveform again follows Figure 7. Peaks should be stacked one atop the other, any differentiation from this condition is known as hysteresis. Hysteresis can be used to analyze the kinetics of the reaction (described in chapter 4).

Rotating Disk Electrode Theory

Rotating disk electrode (RDE) experiments employ a disk of electrode material placed within an insulating plane and mounted in a rotator which spins at high speed. The spinning electrode draws fresh solution to the center of the electrode and then spins it out to the edges. This controls the solution hydrodynamics and diffusion layer thickness in a well understood manner. Relatively high convective transport leads to a decreased diffusion layer thickness, yielding a steady state current-voltage response with increased currents and low sensitivity to extraneous

convection, relative to quiescent solution methods. The steady state curves quickly produced in RDE experiments enable rapid interpretation of data relative to CV. More detail is provided where this method is used in chapter 4.

Polarization Curves

Polarization curves are a common methodology for analysis of flowing electrochemical systems. Curves are generally taken as a series or potential or current steps, the dependent variable is then allowed to decay to a steady state before being sampled. Different portions of the curve correspond the three dominating sources of loss(Figure 10). The advantage of this methodology is that it can quickly distinguish between these sources of loss while also providing realistic information about different operating regimes. Polarization curves can be obtained under either potential or current control.

Potential Step Polarization Curves

In a potential step experiment the potential is stepped to a new potential and held for a time t; current will spike initially and decay to a steady state value. Performing the polarization curve in a potential step mode has the advantage of controlling the potential. This means that side reactions can be minimized, as can damage to the electrodes from potential excursions. For example, a vanadium battery operating on current control may become electrolyte starved; if this happens the potential will increase until something provides that current, either solvent breakdown or carbon corrosion. Electrolyte starvation in the case of potential control will simply result in no additional current rather than damage. Achieving the desired potentials for

analysis can require the use of active IR correction between each step. This experiment is used in chapter 3.

Current Step Polarization Curves

In a current step experiment the current is stepped to a new value and held for a time t; potential will tend to decay to a steady state value. If the system is mass transport limited and the demanded current is unachievable, the potential will continue to increase until other reactions meet the current demand. Despite this danger, current step experiments enable precise control of state of charge in batteries by allowing rapid alternation between reduction and oxidation. Furthermore, most power-generating electrochemical devices are operated under current control in real applications since some total current is typically demanded from a system. This experiment is used in chapter 5.

Reasons for Choosing the PEMFC-Based Flow-Battery Architecture

In chapters 4, 5, and 6 of this work we have used the PEMFC based flow battery architecture manufactured by Fuel Cell Technologies LLC. This cell design consists of two brass end plates, gold current collector, and serpentine flow-fields engraved in POCO graphite blocks. To this we added Teflon gaskets, carbon GDLs(gas diffusion layers), and Nafion 117 membranes.

Nafion 117 was chosen as the membrane for its ion selective properties, high conductivity, and mechanical properties. This is the thickest Nafion membrane sold

and accordingly is mechanically robust. It is capable of withstanding significant differential pressures and will not crack during assembly. As a perfluorosulfonated membrane, Nafion is ion selective for cations while maintaining high degrees of resistance to chemical attack. This is accomplished by binding sulfonate groups within the polymer which allows cations to transport across the membrane though acid sites. The resistance to chemical attack comes from the presence of fluorine within the polymer. The thickness of the membrane adds to the ohmic resistance of the cell; therefore a thinner membrane could be used in a production cell. The relative importance of the membrane thickness and concomitant resistance depends on the operating current density. Membrane thickness also represents a trade-off between the resistance and any unwanted transport through the membrane, generally referred to as 'cross-over.'

The cell components are pressed together to improve electrical and ohmic contact, this design feature minimizes resistance. The presence of flow-fields can help to mitigate mass transport issues, resulting in high current densities.

A major downside of this design is high cost. Nafion membranes are expensive and cost scales linearly with area. Accordingly, the increased current densities of this design can be useful to mitigate this issue. It is important to note that the price of Nafion and similar products is somewhat artificial; competition from other membrane types and increased production scale expected as large-scale users come on line will drive this price down.[67] Cells must be constructed to high precision and therefore construction is labor intensive and costly.

Resistance Measurements

In the ohmic region of the polarization curve shown in Figure 10, internal losses within the cell are nearly linear with current density and are caused primarily by internal resistance within the cell. The ohmic losses are caused by the sum of the cell resistances as shown in equation 35. R_j denotes the areal specific resistance of each of the cell components including electrolyte, bipolar plates, electrodes, current collectors, contact resistances, and electrical contacts.

35 $\quad \eta_\Omega = iA(\sum R_j)$

Well-built fuel cells will have an ohmic polarization dominated by ionic resistance, both within the separator and within the electrodes.[3] Other sources of ionic resistance could include contact resistances due to corrosion or insufficient compression. Tracking the areal specific resistance over time and current/potential space gives the opportunity to examine the performance state of the cell. Changes with time can indicate corrosion, formation of passivating layers, or other types of degradation. Changes with current, potential, or temperature tend to indicate fluctuation of the hydration state of the membrane.[3]

An electrochemical cell can be modeled as a series of resistors and capacitors. The capacitors represent double layer capacitance while charge and mass transfer are typically treated as resistances or possibly networks of resistors and capacitors.

It is possible to determine these cell resistances using a technique based upon alternating current called electrochemical impedance spectroscopy (EIS). One (physically questionable) method of analyzing the electrochemical circuit entails fitting the measured impedance to 'equivalent circuits' representing the various elements of the electrochemical response. Building a full equivalent circuit model requires knowledge of the physical processes within the cell and therefore should be approached with caution. At high frequency, capacitive elements will be shorted out and the remaining resistance is referred to as the high-frequency resistance (HFR). A Nyquist plot shows the real vs imaginary components of the impedance. An example is given in Figure 11 The zero intercept of the Nyquist plot shows the HFR, which contains all the ohmic 'DC' series resistance losses within the cell. The HFR must then be corrected to the ASR by multiplying by the geometric surface area. The HFR shown in Figure 11 is 0.042 Ohm and the surface area is 5 cm^2 so the ASR is 0.21 Ohm-cm^2.

Chemical Methods

All gasses used were ultra-high purity and supplied by AIRGAS. Millipore 18 MΩ water was used in all experiments.

Nafion membranes were cleaned and converted to proton form by boiling in 3% hydrogen peroxide for one hour, boiling in deionized water for 1 hr, 0.5 molar H_2SO_4 for one hour and then deionized water for one hour.[68]

The hydrogen evolution cathode in the phosphomolybdic acid system served as a pseudo-reference electrode in addition to its role as a cathode. This methodology was pioneered in understanding the direct methanol fuel cell anode and PEM fuel cell cathode.[69] The phosphomolybdic acid cathode catalyst was 20% Pt on Hi-Spec 3000 carbon. A representative preparation contained 1080 mg Pt/C, 2 grams water, 1 gram isopropanol, 600 mg 5% NAFION, and 56 mg 35% PTFE. The dry percentages are therefore 20% Pt, 2.7% ionomer, and 1.7% PTFE. The solution was sonicated for a minimum of 30 minutes, then sprayed onto a Teflon coated Sigracet 25 BC GDL with a dry weight catalyst loading of 3 mg/cm^2. Cathodes were hot pressed onto a NAFION 117 membrane except where otherwise specified. Except in chapter 6, humidified hydrogen flowed across the cathode at all times.

The phosphomolybdic acid anodes were not hot pressed onto the membrane.

Phosphomolybdic acid polarization curves were acquired using the Biologic VMP3-B potentiostat with 20A booster. The curves were taken under current control. The current was cycled from reduction to oxidation on each potential step to keep the overall state of charge constant. The potential was sampled at the end of each voltage step. The resistance was measured at the start of each polarization curve using galvanostatic electrochemical impedance spectroscopy. The membrane resistance to be corrected was taken to be the zero intercept of the Nyquist plot.

In Situ cyclic voltammetry experiments were conducted by flowing hydrogen gas over the cathode of the battery hardware and turning off the peristaltic pump supplying phosphomolybdic acid solution.

CHAPTER 3

Direct Electrochemical Oxidation of Methanol Coupled to

Hydrogen Evolution

Chapter Goals

In this chapter, we seek to use the relatively well-understood methanol oxidation reaction as a source of protons for hydrogen evolution. We initially regarded this as a model implementation of our eventual target, which is the ability to strip 'H' from organics by an oxidation (or partial oxidation) process to couple to the hydrogen evolution reaction on the cathode. The methanol oxidation anode is a mature technology. We therefore seek to understand the performance of the hydrogen reduction cathode in the environment arising from a methanol fed cell. Hydrogen reduction in an acidic environment is the prototypically reversible process and we thought it would be instructive to see any alteration in this reaction driven by the cross-over of methanol through the electrode. In general, sluggish reactions(DMFC anode or PEMFC cathode) are often examined by using a reversible hydrogen electrode as a counter electrode in a two-electrode system. Maintaining the conditions for reversibility requires high flow-rates of hydrogen across the counter electrode.

In a direct methanol fuel cell, crossover of methanol fuel from the anode to the cathode is a major source of both current and voltage (coulombic and voltage efficiency) loss. Current loss occurs because the fuel is no longer where it is needed. The crossover methanol either evaporates or is oxidized at the cathode but both options provide no energy to the device. In short, our fuel efficiency declines because it is not utilized at the reactive anode. Voltage loss occurs because the cathode catalyst is poisoned by adsorbed methanol oxidation

products, mostly carbon monoxide or because a 'mixed' potential occurs. To minimize the effect of crossover DMFC, designers have settled on the use of low methanol concentrations, which results in correspondingly lowered power and system energy densities.

Again, we want to probe whether such effects have a major impact on the hydrogen evolution reaction. The presence of methanol and hydrogen together at the *anode* has little effect on the hydrogen oxidation reaction and simultaneous anode feed is often used to probe the rate of cross-over.

The intention here is to use a reference electrode called a dynamic hydrogen electrode (DHE) to track the potential/current response of the hydrogen evolution cathode. Hydration of the membrane is rarely a concern in liquid feed DMFC's due to the presence of liquid water at one side of the membrane and the generation of water at the other. Considering the absence of water generation at the cathode, we investigated whether membrane hydration would become a concern. We also examined the effects of temperature, and feed concentration on the cathode and whole cell overpotential.

The crossover issue combined with the inherent catalytic difficulties of the oxygen reduction reaction make the DMFC cathode highly sensitive to these parameters. It is expected that the reversibility of hydrogen reduction on platinum should make the hydrogen evolution cathode relatively impervious to changes in the specified parameters. The electrode should be insensitive to changes in methanol feed

concentration and therefore crossover because the methanol will not be oxidized at these cathode potentials in the absence of oxygen.

Materials and Methods

Methanol electrode preparation: 5 cm^2 Electrodes were fabricated by painting a catalyst ink directly on the Sigracet 25 BC gas diffusion layer. The painted gas diffusion layers were then dried in an oven at 140 ^{o}C for 1 hour between layers and then for 12 hours after reaching the desired loading. Catalyst loading was calculated from before and after weights of the GDL and the ratio of metal to nonvolatile components in the ink.

Methanol electrolysis: Anode and cathode inks were glycerol based as described previously, employing 50/50 Pt/Ru black (Alfa Aesar) for the anode and Pt black for the cathode (Alfa Aesar). PTFE was added to the cathode ink to prevent flooding.[70] Inks were stirred for a minimum of 48 hours and sonicated before painting to improve dispersion. Nafion 117 membranes were used in all methanol tests. The catalyst coated GDL's were hot pressed onto the membranes with a pressure of 200 kg/cm^2 at 140 ^{o}C for 10 minutes.

Methanol cell testing was performed using a Fuel Cell Technology test stand and Fuel Cell Technology 5 cm^2 direct methanol fuel cell hardware. The endplates had heated flow channels for the methanol. The hardware included gold plated current collectors and POCO graphite flow-fields. Electrochemical tests were performed

using a Biologic VMP 3-B potentiostat with a 20A booster. A back pressure of 15 psi was placed on both anode and cathode streams.

The cell was allowed to equilibrate to temperature, pressure, and humidity settings at OCV for a minimum of 15 minutes. Potential steps of 0.05 V were held for 120 seconds and the recorded current was averaged across the final 10 seconds. Argon or nitrogen flowed over the cathode. The presence of flowing, inert gas allows control over humidity, backpressure and removes the produced hydrogen. If hydrogen were flowed over the cathode it could affect the measured cathode polarization. The hydrogen production rate alone was insufficient to attain the desired backpressure. The system was evaluated under potential control and the resistance was evaluated as high frequency intercept of the Nyquist Plot.

Reference Electrode: A dynamic hydrogen electrode (DHE) was constructed based on the design described previously.[71] The reason for including a reference electrode is to provide a stable voltage against which to compare the working and counter electrode potentials. The DHE was constructed using 2, 0.1 mm Pt wires, a 1.5 MOhm resistor, and a 9 Volt battery, connected to form a circuit. The wires were sandwiched between the NAFION membrane and the Teflon gasket, approximately 1mm apart and 1mm from the edge of the cathode GDL. This placed them in ionic contact with each other and the working and counter electrodes. The reference lead was connected to the platinum wire on the DHE side of the resistor. The DHE works by oxidizing water at one of the platinum wires, thereby generating hydrogen. If the other platinum wire is in close enough proximity, then it will reduce

the generated hydrogen and provide a stable voltage. The current passed is limited by a large resistor within the potentiostat, therefore it does not affect the potential or deplete the hydrogen supply. The reference electrode was always placed on the cathode side of the membrane to minimize interference from methanol.

Recall that the whole cell potential can be determined by subtracting cathode potential from anode potential. This is not possible using the data in this chapter because overpotentials are used instead of potentials. Overpotential is the potential required to overcome kinetic, ohmic, and mass transport losses but it does not include the thermodynamic potential. This is used because DHE electrodes are known to drift slowly. The potential was stable on the time scale of the experiment but was not zero.

Results and Discussion

Figure 12 shows performance of a hydrogen pump cell with hydrogen gas at the anode and cathode. The cell is similar in construction to the methanol fed reactive hydrogen pumps shown later in the chapter. The anode and cathode reactions are the forward and reverse of equation 16. It is noteworthy that cathode polarization is only 6 mV at 250 mA/cm^2, roughly 10% of the whole cell polarization. The whole cell polarization is 60 mV at 250 mA/cm^2. Nearly all the whole cell polarization comes from IR losses. At 250 mA/cm^2 the IR corrected, whole cell polarization is 11 mV, 49 mV lower than the uncorrected value. This experiment shows the viability of the hydrogen cathode both as a reference electrode and when used in

the production of hydrogen. These results also help to confirm that the DHE is functioning as a stable reference electrode.

Minimizing the resistance between reference electrodes and the electrodes to be studied is always of great importance in designing electrochemical experiments. The asymmetry between anode and cathode in Figure 12 can be attributed to the placement of the reference electrode. The DHE was on the cathode side of the membrane, exhibiting significantly lower resistance between the reference – cathode vs reference – anode. The reference electrode was always placed on the cathode side of the membrane to minimize interference from methanol. The whole cell ASR is 0.2 Ohm-cm^2 while the ASR measured from the cathode to the DHE is only 0.04 Ohm-cm^2. The validity of this argument is backed up by modeling data showing nearly identical Tafel slopes for HOR and HER on Pt surfaces.[72]

Figure 13 shows polarization data for the operation of a DMFC based methanol electrolyzer. The overpotential required to accomplish the reactions is far greater than that required in the hydrogen pump cell. The ASR fluctuates but stays within the range of 0.1 to 0.12 Ohm-cm^2, near DOE 2015 estimates for an automotive fuel cell. For reference, DOE estimates 0.072 Ohm-cm^2 as the maximum ASR for an automotive fuel cell in 2015.[73] The significantly lower ASR achievable in fuel cells is due to the use of thinner membranes. The thicker membranes in methanol cells are preferred to help prevent fuel crossover.

The cell stays fully humidified and does not show signs of drying out. Drying out would be noticeable as an increase in ASR. The significant performance

differences between the corrected and uncorrected curves shows the importance of IR correction at these high current densities. Below 200 mA/cm^2, there is little variation between the corrected and uncorrected curves. At 1A/cm^2, there is a 110 mV difference between corrected and uncorrected polarizations.

Both the anode and cathode polarizations are quite significant despite the high loadings of precious metal catalyst. The oxidation of methanol is electrochemically slow. At 1 A/cm^2 it resulted in 430 mV overpotential and 320 mV at 250 mA/cm^2. Interestingly and unexpectedly, the reduction of hydrogen in this environment is far slower than expected. It results in 240 mV at 1 A/cm^2 and 180 mV at 250 mA/cm^2. There is a whole cell polarization of 925 mV at 1 A/cm^2 and 670 mV at 250 mA/cm^2.

Figure 14 shows the effect of changing cathode humidity levels on a cell operating at 80 ºC. There is little sensitivity to changing humidity levels with respect to ASR, whole cell polarization, or individual electrode polarizations. This is believed to be due to full humidification being achieved by the liquid electrode. Although there is little difference in the ASR between the 60 ºC and 100 ºC humidified gasses, there is a small *decrease* in ASR when no cathode gas is flowing. The ASR was approximately 0.01 Ohm-cm^2 lower in that experiment.

The regime with no gas flowing is the closest to what might be encountered in an operational cell. The cell was not operated in this regime at all times due to concerns of flooding and a desire to maintain consistent conditions at the cathode. The IR corrected cell voltage of all 4 curves is similar until about 600 mA/cm^2. After

that point the voltage seems to increase with humidity level. This could be caused by cathode flooding at higher current densities. In a fuel cell, water is produced at the cathode. No water is produced at the cathode of this cell but the movement of hydrogen ions across the membrane drag water or methanol across. This process is known as electroosmotic drag. The presence of additional humidified gasses at the cathode could exacerbate any possible flooding.

Figure 15 shows the effect of changing methanol concentrations at a steady temperature of 100 ºC. Eight molar methanol was chosen at the maximum to explore. 8 molar methanol corresponds to about 22 mole %. 4 and 1 molar methanol correspond to molar ratios of roughly 9% and 2%. These ratios are significantly leaner than the 50% molar ratio of methanol to water expected from the stoichiometry in equation **17**. In DMFCs it's known that increasing methanol concentration leads to decreasing whole cell performance. This performance drop is caused by methanol crossover from the anode to the cathode. One of the central goals of this chapter is understanding how the phenomena of crossover induced performance inhibition translates from a DMFC to a methanol based hydrogen pump cell.

Increasing concentrations of methanol led to improved anode performance but decreased cathode performance. The losses in cathode performance dominated cell performance while whole cell performance was also diminished. The link between cathode polarization and methanol concentration was unexpected. We

have established that just as in DMFC's, performance is enhanced by operation at lower methanol concentrations

Anode operation improved significantly when moving from 1 molar methanol to 4 molar methanol. The improvement from 4 molar to 8 molar methanol was noticeably less significant. This performance improvement begins in the kinetic region but becomes more noticeable as the cell moves into the ohmic regime. Since the data is IR corrected, we attribute this improvement to a combination of.

increasing kinetics at low overvoltages and reduced concentration polarization at higher overvoltages.

Figure 16 shows the effect of several different likely cell operating temperatures on whole cell and half cell polarizations The curves show improving performance

with increasing temperature. This phenomena was expected as the kinetically slow reaction at the anode has been shown to improve with temperature in DMFC's.[3] At 80 ºC and 250 mA/cm^2, the symmetric cell hydrogen cathode polarization was 6 mV. In the DMFC based electrolyzer with 4M methanol feed at the same temperature a cathode polarization of 145 mV was recorded. The cathode polarization had a weak dependence on temperature. At higher current densities, this relationship appears to become stronger. At very low current densities(<100 mA/cm^2), there appears to be almost no relationship between cathode polarization and temperature. Anode onset potential is strongly dependent on temperature as is whole cell polarization.

As for the effect of increasing temperature on the cathode, improved performance must be due to decreased accumulation of methanol and water at the cathode or improved cathode kinetics. Improved cathode kinetics appears unlikely due to the identical onset potential. The position of this change well outside the kinetic region indicates that the change is either mass transport or ohmic related. The curves are IR corrected so mass transport is the more likely possibility. Increased temperatures may improve mass transport at the cathode by speeding evaporation of liquid products and preventing the need for bubble formation.

Conclusions

All tests showed significant polarization of the cathode. Increased concentrations of methanol feed led to increased cathode polarization, decreased anode polarization, and increased whole cell polarization.

 Increasing temperature led to improved performance, mostly due to the anode. Operation with a vapor fed methanol-water system may therefore be preferable by allowing increased operating temperature.

Increased methanol crossover causes increased cathodic overpotential, while changes in temperature do not substantially affect the cathodic overpotential. This likely indicates a mixed potential type mechanism rather than a kinetic explanation. We come to this understanding because increased temperature will tend to improve kinetics.

Overall, the cathode polarization is far greater than expected from the hydrogen symmetric cell cathode. This will limit the utility of such a system when compared with a DMFC. The significant capital cost incurred due to the additional equipment and high catalyst loadings required will also present hurdles to this approach

When compared to a PEM electrolyzer, this system shows promise. The onset potential of a PEM electrolyzer is over 1 V higher than is shown in the methanol electrolysis cell. This significant difference in electrical power consumption means a stationary methanol electrolysis plant could become feasible.

CHAPTER 4

Electrochemistry of Phosphomolybdic Acid

Polyoxometalates Motivation

In the work reported throughout the next three chapters, we will attempt to use polyoxometalate compounds(POM) as redox mediators to in the oxidation of organic compounds. To proceed systematically, we first carry out studies of the electrochemical behavior of POMs and particularly of phosphomolybdic acid. It is important to understand the basic electrochemical behavior of this potential mediator in isolation and in simple electrochemical cells before proceeding to study more complex situations.

Polyoxometalates Background

Berzelius prepared and analyzed the first Keggin ion $(NH_4)_3PMo_{12}O_{40}$ in 1826 and the tungstosilic acid was prepared by Margnac in 1862. The first systematic attempt to understand the nature of heteropoly compounds occurred in 1908 by Miolati.[74] Some of the most significant work was done by Tsigdinos and Wu, who have independently published methods using ether extraction for the synthesis and purification of phosphomolybdic acid.[74,75]

Tsigdinos studied the redox behavior of 12-phosphomolybdic acid which he refers to as dodeca-molybdophosphoric acid. He found multiday stability of polarograms in 0.5 M H_2SO_4, indicating stability in that solvent. He also found that solutions more dilute than 10^{-4} M gave less well defined polarograms. These polarograms showed the presence of multiple waves at increasing oxidation potentials. Reversibility of the first 3 waves was ascertained using cyclic voltammetry at a platinum electrode in water-dioxane solutions. He stated that it is important not to use earlier work due

to an unrecognized hydrolytic instability of polyoxometalates on mercury electrodes and at elevated pH values.[74] Tsigdinos also prepared many of the polyoxometalates including $FePMo_{12}O_{40}$, $PVMo_{12}O_{40}$, $PV_2Mo_{10}O_{40}$, and $PWMo_{11}O_{40}$.[51,74,76,77]

Based upon these reports it became clear that the electrochemistry of Keggin ions varied widely with solvent, necessitating study of the electrochemistry of phosphomolybdic acid in the proposed reaction conditions. In this work, the reaction of phosphomolybdic acid on glassy carbon was studied to determine if a heterogeneous catalyst is necessary. The oxidation of phosphomolybdic acid was then studied using a glassy carbon rotating disk electrode to attempt to elucidate the kinetics of the oxidation reaction. Then a small cell with a hydrogen counter electrode was assembled to test the anode performance of a phosphomolybdic acid based fuel cell/hydrogen pump.

The literature shows several promising examples of fuel cells and hydrogen pumps using phosphomolybdic acid as a mediator but the performance of such devices is hard to ascertain due to the coupling of cell performance and solution reaction.[37,38,42,43] There is significant discussion concerning the current efficiency but little to no discussion of voltage efficiency. We need to understand what are the sources of voltage loss, the kinetic, ohmic, and mass transport overpotential required to reoxidize the phosphomolybdic acid.

One important characteristic which will significantly affect the overpotential required in a flow cell is the degree of reversibility. Based upon the literature we

know that the electrochemical stability and therefore reversibility of phosphomolybdates will vary with solvent. It is highly desirable to use an aqueous solvent because aqueous solvents tend to provide excellent solubility (900+ g/L for phosphomolybdic acid), low cost, and high conductivity.

A reaction can be chemically reversible and simultaneously be electrochemically reversible, quasi-reversible, or irreversible. The nomenclature related to electrochemical reversibility qualitatively describes the rate of electron transfer between the electrode and the molecule. In this work, reversibility will be evaluated using cyclic voltammetry. An electrochemical reaction is said to show reversibility when three criteria are met in the CV experiment: peak height vs square root of the scan rate is linear, $\frac{I_p{}^{OX}}{I_p{}^{RED}} = 1$ and $E_p{}^{OX} - E_p{}^{RED} = \frac{59}{n} mV$, independent of scan rate. Electrochemical reversibility is quantitatively defined by the value of k^0 for the electron transfer reaction $OX + ne^- \underset{\leftrightarrow}{\overset{k0}{}} RED$. The standard heterogeneous rate constant k^0 describes the time required for returning to equilibrium after the application of a potential. We note that the appearance of reversibility is significantly affected by the scan rate used. The scan rate provides an experimentally variable time window for investigation of the reaction. Approximate ranges of k^0 are given below.[78]

Reversible: k^0 > 0.020 cm/s

Quasi-reversible: 0.020 cm/s > k^0 > 5x10^{-5} cm/s

Irreversible: k^0 < 5x10^{-5} cm/s

Materials and Methods

Ex situ cyclic voltammetry experiments were performed using a custom 25 ml H-cell made from Pyrex glass with a NAFION separator. The counter electrode compartment consisted of a Pt wire electrode and 0.5 M H_2SO_4. The working electrode compartment contained either a 1.6 mm diameter platinum disk electrode or a 3-mm diameter glassy carbon disk electrode and an ALS brand single junction Ag/AgCl reference electrode.

The above-mentioned H-cell was also used for quantitative electrolysis with a large area platinum mesh electrode replacing the disk electrode.

Rotating disk experiments were performed using a water jacketed electrochemical RDE cell with an electronic rotator and speed controller (all from Pine Instruments). The counter electrode used was platinum mesh and the reference was the same ALS single junction Ag/AgCl electrode. Where applicable cells were degassed with ultra-high purity nitrogen for 10 minutes and maintained under nitrogen atmosphere. A 3mm diameter glassy carbon Pine Rotating Disk Electrode was used for all experiments. The electrode was jacketed with PEEK plastic.

Diffusion of phosphomolybdic acid across the Nafion 117 membrane was measured using the H cell pictured below (Figure 17). Square wave voltammetry was conducted to track the concentration of active species in the low concentration side. Peak currents were used with a calibration curve to determine the concentration of phosphomolybdic acid which had crossed over. The working

electrode was a Pt disk, the counter electrode was a Pt wire, and the reference was Ag/AgCl. Although the picture shows the electrodes on the yellow POM side, they were on the clear(water) side for the diffusion testing. The high concentration side was 0.25 M POM, the low concentration was 1M Phosphoric Acid. The membrane used was Nafion 117. The surface area available for diffusion was one square inch.

Results and Discussion

The first priority when preparing a new electrochemical system is to understand the electrochemical reactions which may be occurring within the window of operation. Cyclic voltammetry (CV) is an ideal technique by which to do this, providing rapid insight into the locations of relevant reactions. Careful analysis of CV results(including modeling) can provide a wealth of kinetic information as the reaction is better understood.

Figure 18A gives the cyclic voltammograms of phosphomolybdic acid on a glassy carbon electrode. Glassy carbon (GC) is an ideal surface on which to conduct this experiment; it provides an electrochemical surface area near its geometric surface area, resists corrosion well, is conductive, and has comparable electrochemical properties to other carbon materials. However, carbon surfaces can be highly variable and such GC electrodes do not perfectly mimic the behavior of a given graphitized carbon electrode.

In Figure 18A, we see the typical CV of phosphomolybdic acid in water. Three peaks are observed, the approximate half wave potentials of the first two are 0.63 V and 0.36 V vs NHE.

Peaks 1, 2, and 3 are each 2 electron redox reactions.[74] The two electron nature of peak 1 was confirmed by exhaustive electrolys in both H-type and zero gap flow type electrochemical cells. The reactions are listed below.

Peak 1: $H_3PMo_{12}O_{40} + 2e^- + 2H^+ = H_5PMo_{12}O_{40}$

Peak 2: $H_5PMo_{12}O_{40} + 2e^- + 2H^+ = H_7PMo_{12}O_{40}$

Peak 3: $H_7PMo_{12}O_{40} + 2e^- + 2H^+ = H_9PMo_{12}O_{40}{}^{3-}$
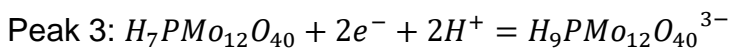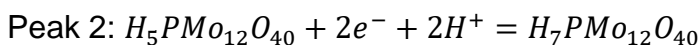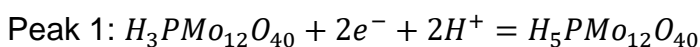
To help elucidate some of the kinetic information contained within Figure 18A, Figure 18B and Figure 18C were constructed. Figure 18B contains the plot of peak separation vs scan rate. An ideally reversible reaction would show no dependence of peak separation on scan rate. Figure 18C is the plot of peak current vs the square root of scan rate. Reversible reactions show a linear relationship between these variables.

Peak 1 has features of both reversible and irreversible waves. The reduction of peak 1 is linear with square root of scan rate, and $\frac{I_p{}^{OX}}{I_p{}^{RED}} = 1$; shown in Figure 18C. The determination of $I_p{}^{OX}$ required the use of a potential hold at 0.4 V to remove the contribution of peak 2 from the resulting signal. Those are 2 of the 3 main criteria for reversibility. The remaining criteria is that the separation between the

two peaks should be 59/n mV, independent of scan rate. The peak separation, as shown in Figure 18B, is almost linearly dependent on square root of scan rate and is always greater than 59/n mV(where n is the number of electrons). Peak separation is relatively unreliable for determining reversibility due to the way it is affected by experimental conditions, including IR loss, current distribution, and extreme scan rates.

Meeting some, but not all of the tests for reversibility is evidence of quasi-reversibility. Peak 1 also shows a shift in the calculated E^0 of 10 mv, linear with square root of scan rate, from 424 mV to 432mV vs Ag/AgCl. To convert an Ag/AgCl reference electrode to NHE, add roughly 205 mV to the potential.

Peak 2 is significantly less well resolved than peak 1 yet still exhibits linearity of I_p^{RED} vs square root of scan rate. Determining an acceptable value for I_p^{OX} was complicated by the proximity to the other waves. The peak separation was strongly dependent on scan rate.

The kinetics of an electrochemical reaction can often be strongly affected by the heterogeneous electrode surface. Metals in general are known to catalyze many electrochemical reactions. Precious metals often exhibit the highest electrochemical activity due to optimum binding strengths with important reactants. Platinum in particular is prized for its activity and stability in a variety of harsh reaction environments. To determine if the phosphomolybdic acid electrochemistry was different on platinum, CVs of phosphomolybdic acid were conducted on a platinum surface (Figure 19).

The voltammograms in Figure 18A and Figure 19 are essentially similar. For peak 1 they share the linearity of peak heights with square root of scan rate, $\frac{I_p{}^{OX}}{I_p{}^{RED}} = 1$, and the dependence of $E_p{}^{Ox} - E_p{}^{Red}$ on scan rate. The peaks are slightly sharper and more resolved but still exhibit the same quasi-reversible features as the glassy carbon voltammograms, indicating that the platinum does not sufficiently catalyze the reaction to achieve reversibility.

Peak Splitting

An unexpected characteristic was noticed when preparing bulk reduced solutions for other experiments; cyclic voltammograms of bulk reduced phosphomolybdic acid are different in appearance from their fully oxidized counterparts. When a cyclic voltammetric scan is performed, the reaction occurs entirely within the boundary layer. This assumption is valid when the ratio of diffusion coefficient to scan rate is sufficiently low. At these scan rates the assumption is valid. This means that the ratio of $PMo_{12}O_{40}{}^{-3}$ Bulk to $PMo_{12}O_{40}{}^{-5}$ Bulk should have no effect on the cyclic voltammetric response after the first cycle.

To better understand this phenomena, solutions of phosphomolybdic acid were bulk reduced by 0 (Figure 18A), 1 (Figure 20) and 2 (Figure 21) electrons. This bulk reduction was conducted using an H-cell and a large area platinum electrode. Cyclic voltammetry was then performed and the results of the 6th cycle were used in the generation of this data. The first CV scan will often depend upon the solution redox state, but by the 6th scan the results will be stable.

72

We can see very little effect on the shape of peaks 2 and 3 from Figure 18A. Peak 1 shows significant changes based on the ratio of $PMo_{12}O_{40}{}^{-3}$ Bulk to $PMo_{12}O_{40}{}^{-5}$ Bulk. $Peak_1{}^{RED}$ gets slightly smaller but shows no change in shape. $Peak_1{}^{OX}$ begins to split into two separate waves at 0.55 V and 0.85 V vs Ag/AgCl. This change indicates the formation of a third species in solution but it must be occurring on a time scale longer than the characteristic time of the CV scans. The third species is likely to be a decomposition product of phosphomolybdic acid, perhaps one or more of the molybdenum oxide compounds.

This type of reaction is known as an ECE reaction in electrochemical notation. E stands for an electron transfer step, C stands for a chemical step. What we believed to be occurring is that an electron is transferred to the POM complex, then a slow chemical step occurs in solution, then the newly formed chemical reacts on the electrode. This is competing with the 3 EE reactions which occur within each individual scan.

One possibility considered for explaining the peak splitting was that it was caused by hydrolysis of the phosphomolybdic acid on the surface of the electrode where it was being reduced. To better distinguish between this possibility and the ECE reaction hypothesis, we conducted cyclic voltammetry in a phosphomolybdic acid solution which was being reduced by glucose (Figure 22).

Figure 22 demonstrates repeat cyclic voltammograms of a 90 ^oC mixture of phosphomolybdic acid, hydrochloric acid, and glucose. The experiment consisted

of heating a single chamber containing the solution, a Pt working and counter electrode, and the reference. The potential was cycled between 0.3 V and 1.0 V vs Ag/AgCl to isolate peak 1 from Figure 20 and Figure 21. The phosphomolybdic acid was reduced chemically by the glucose during this period and experienced no bulk electrochemical reduction as was evidenced by integrating the current over all the cycles. The overall electrochemical charge transferred to the 25 ml solution was a 16 coulomb oxidation in 51 hours.

The 0.4 V reductive peak can be clearly identified in all scans, although the peak height decreases with time and the peak begins to split, showing another peak near 0.5 V. The oxidative peak clearly splits with peak 1 showing a decrease in potential from 0.55 V to 0.45 V and peak 2 increasing in potential from 0.541 V to 0.6 V.

Table 2 below shows the change in peak location as the solution is progressively reduced. Reduction peak 1 does not shift appreciably with the increasing concentration of the reduced species in the bulk. Oxidation peak 1 shifts closer to reduction peak 1 as the concentration of RED_{Bulk} increases, beginning to appear more reversible. Oxidation peak 2 shifts in the other direction, away from both oxidation and reduction peak 1. This makes for a very clear split in the two oxidation peaks. There is a possible reduction peak forming at 0.55 V but it is unclear due to the background current.

It is clear that the phosphomolybdic acid peak splits regardless of whether the solution is reduced chemically(Figure 22 and Table 2) or electrochemically(Figure

21). This peak splitting is further evidence that the reduced form of the phosphomolybdic acid is unstable in these conditions, either succumbing to its known hydrolytic instability or some other solution reaction. [74]

Table 2: Peak Height vs Scan Number

Cycle Number	Starting Time (h)	E_{RED}	E_{OX}-1	E_{OX}-2
2	0.0073	0.405	0.541	N/A
200	2.91	0.398	Not Identifiable	0.557
400	5.84	0.3952	0.459	0.5795
800	11.7	0.3989	0.458	0.5883
3400	51	0.396	0.471	0.597

To further confirm the bulk reaction hypothesis, we conducted the experiment from Figure 22 with no glucose added. This solution maintained its original state of charge throughout the experiment. Figure 23 shows the cyclic voltammograms of phosphomolybdic acid in hydrochloric acid on a platinum electrode. There is almost no change over 4000 cycles. This shows that the reaction causing the peak splitting is occurring in the solution rather than at the electrode since the peak splitting does not occur without bulk reduction.

H-Cell Cycling

During various full scale experiments, the phosphomolybdic acid solution turned dark blue and would not reoxidize (indicated by turning yellow). Single compartment cyclic voltammetry experiments also exhibited unusual behavior, a dark blue compound diffused away from both electrodes during cycling. It became necessary to determine if the cause of this was related to a chemical irreversibility or contamination.

Potentiostatic coulometry (or bulk electrolysis) is a useful technique by which the state of charge of the entire solution can be controlled at will. The state of charge can be tracked by integrating the current(equation 70). The experiments take place on a longer time scale than most electrochemical experiments, enabling access to slower chemical steps. The most common metric for bulk electrolysis experiments in batteries is current efficiency at a given pair of potentials. Current efficiencies less than 1 are indications of irreversible reactions, although not necessarily of the intended compound. Imperfect current efficiency can be caused by side reactions at the electrode, instability of an active compound, solvent breakdown, or crossover of active species.

The afore-mentioned H-cell was used for these experiments with a platinum mesh working electrode and stirring. To minimize the opportunity for contamination, the apparatus was designed such that it is easy to confirm only glass, NAFION, platinum, and the reference electrode were in contact with the solution.

The solution was cycled a total of 60 times(Figure 24) between 0.35 V and 0.8 V, isolating peak 1 from the previous figures. The initial capacity of 35 coulombs corresponds almost perfectly to 2 electron transfer, confirming the literature reports that peak 1 is a 2 electron transfer redox reaction.

The capacity starts at 35 coulombs and drops to 32 coulombs, a loss of 9% capacity over 60 cycles. The capacity fades and recovers several times although there is a general downward trend. After each cycle, the solution recovered its fully oxidized, pale yellow color. No crossover of phosphomolybdic acid was noted on visual inspection of the apparatus. This provided sufficient support to consider 2 electron reduction a safe 100% state of charge for battery experiments. It is possible and advantageous to reduce the solution further, but the stability of further reduction is not examined in this work.

Thin Layer Voltammetry

Figure 25 is a thin layer cyclic voltammogram of phosphomolybdic acid in a flow battery with the pump turned off. This type of experiment is convenient to do for several reasons; bulk electrolysis is performed quickly, the capacitive current gives a measure of the accessible surface area, comparing the peak hysteresis allows inferences concerning activity on the actual electrode surface, and the counter electrode is hydrogen on platinum in acid (0 V by definition). When a reaction is reversible the peaks will be stacked directly above one another since the reaction is exhaustive electrolysis within the thin layer of material that is available. Figure 25 exhibits a feature known as a vertical hysteresis, where the system takes two

different states at a given potential based on the direction of the potential scan. This can be divided into the reversible charge transfer and the hysteresis component of the charge transfer. The hysteresis component is used to quantify the deviation from ideality. [79] This type of hysteresis is called dynamic hysteresis, it is caused by a kinetically slow step which causes the reaction to exhibit irreversible behavior.

36 $Q_{Rev}(E) = \frac{i_B(E)*Q_A(E)-i_A(E)*Q_B(E)}{i_B(E)-i_A(E)}$

37 $H_Y(E) = \frac{Q_A(E)-Q_B(E)}{i_B(E)-i_A(E)}$

38 $H_x(Q) = \frac{E_A(Q)-E_B(Q)}{i_B(E)-i_A(E)}$

The scan rate used in Figure 25 was optimized to the minimum achievable without inducing excessive noise from convection. No fluid was noted to be flowing through the tubing and the results were steady for several cycles.

Peak 1 is centered at 0.646 and peak 2 is centered around 0.431 V. Peak 1 shows a peak separation of 181.5 mV and $\frac{i_{OX}}{i_{RED}}$ of 1.11. Peak 2 shows a peak separation of 207.3 mV and $\frac{i_{OX}}{i_{RED}}$ of 0.75. This significant hysteresis indicates quasi-reversibility with peak 1 being more reversible than peak 2.

Repeated exhaustive electrolysis was performed with reduction at 0.5 V. It is also interesting to note that the peak splitting shown in Figure 18 to Figure 22 do not appear here, despite full oxidation and reduction of the phosphomolybdic acid. This

2

gives more support to the hypothesis that the peak splitting is not caused by the formation of an intermediate but rather a slower following reaction i.e. EEC mechanism instead of ECE.

Figure 26 shows the charge transferred to the solution (Q) vs potential in a thin layer voltammogram. In a fully reversible system this would be a single line as is represented in Figure 27 below. The significant hysteresis present here is more evidence of quasi-reversibility, the electrochemical reaction rate is not sufficient to drive the reaction to completion. It was not feasible to scan at slower scan rates due to noise, faster scan rates failed to reach the conditions of thin layer voltammetry (the ratio of scan rate to solution volume is such that the impact of diffusion and migration can be ignored). This indicates that there is a significant dynamic as opposed to stationary hysteresis, suggesting a kinetic rather than chemical origin for the hysteresis.[79]

The fact that Q returns to zero further suggests that the limitations are kinetics rather than chemical irreversibility. If the reaction was chemically irreversible, the solution and would not return to its original state (Q=0),

The kinetic hysteresis, shown in Figure 28, is isolated through the application of equation 37 to the data in Figure 25 and Figure 26. The peaks at 0.63 V and 0.43 V correspond to peaks 1 and 2 from Figure 25. Peak 2 is larger than peak 1 indicating a greater degree of hysteresis, which follows from the greater deviation of $\frac{i_{Ox}}{i_{Red}}$ from 1 and the increased peak separation of peak 2(Figure 25). Peak 2 is

also highly symmetrical in appearance, indicating that the hysteresis is roughly the same for the forward and backward sweep.

Peak 1 is smaller, commensurate with its decreased deviation of $\frac{i_{Ox}}{i_{Red}}$ from 1 and decreased peak separation. The asymmetry of peak 1 indicates that the hysteresis may not be the same in the forward and reverse potential sweeps.

The presence of an impedance element in series with the electrochemical system will also cause hysteresis due to the current dependence of the apparent potential. Figure 29 represents the ohmic contribution to the hysteresis. The near zero contribution of the ohmic hysteresis for most of the potential range indicates that uncompensated resistance is not the limiting factor in understanding this charge transfer.

Rotating Disk Electrode Voltammetry-Levich Analysis

Convection has the potential to easily disturb the current recorded during an electrochemical experiment; therefore, controlling the influence of convection is critical. Cyclic voltammetry, chronoamperometry, and other electroanalytical techniques rely on a condition of quiescence in the hopes of avoiding the influence of convection. They therefore have to be performed on a relatively short timescale because any solution will experience some thermal convection. This also makes reaction at elevated temperatures difficult since heating the exterior of the vessel will cause significant thermal convection. While these experiments can generate a wealth of kinetic information, it requires a great deal of knowledge to interpret.

Hydrodynamic techniques represent a radically different solution to these problems. By forcing the convection to occur, flowing systems such as rotating disk voltammetry and rotating ring disk voltammetry control the diffusion layer thickness in a manner such that it can be solved analytically. This causes the diffusion layer thickness to be a known function of an independent parameter such as rotation rate. It also decreases the susceptibility to perturbations such as thermal convection or vibrations. Some kinetic information is now apparent from simple observation while more is available through straightforward data processing techniques and graphs. Common metrics are the half wave potential, onset potential, and ¼ and ¾ wave potentials. The diffusion coefficients and kinetic currents can be extracted using the Levich and Koutecky-Levich equations respectively.

Figure 30 shows the results of rotating disk electrode voltammetry. The bulk solution was 50% $H_3PMo_{12}O_{40}$: 50% $H_5PMo_{12}O_{40}$ and the scan rate was 20 mV/sec. The voltammograms show about 200 mV from the onset of oxidation until the curves reach the limiting current, with the overpotential required to reach limiting current increasing with rotation rate. The figure inset shows the perfect linearity and zero intercept of current density vs square root of rotation rate at 1.4 V vs Ag/AgCl. With those conditions met, it is appropriate to use the Levich equation (39) to extract the unknown variable, diffusion coefficient in this case.

Table 3 quantifies the upward apparent shift in potentials with rotation rate. Rotating faster increases the flux of the $H_5PMo_{12}O_{40}$ to the electrode. The upward shift in potential with rotation rate shows that the kinetic current is limiting at the increased rotation rates. This indicates a mixed kinetic and diffusion control for much of the potential regime. In a purely diffusion controlled regime, the current would change with rotation rate but the potentials would not.

The curves in Figure 37 should exhibit a uniform ascent from zero current density to the limiting current. The curves shown do not do this, they exhibit the characteristic plateaus of a stepwise two electron transfer occurring at two different oxidation potentials.[80] This is the same two electron transfer reaction identified previously. It is still possible to use the total limiting current to diagnose the average diffusion coefficient for the two electron transfer using a Levich plot.[81] The Levich equation is

39      $I_L = (0.62)nFAD^{\frac{2}{3}}\omega^{\frac{1}{2}}v^{\frac{-1}{6}}C_{Bulk}$

The Levich plot is a plot of limiting current vs the square root of rotation rate. This should yield a straight line across a wide range of rotation rates, indicating that it is appropriate to treat the reaction as a single step characterized by a large heterogeneous rate constant(k_h). Since this is the case we can use the literature values of v(kinematic viscosity) and the previously determined n=2 to calculate the

Table 3: Redox Metrics vs Rotation Rate

RPM	$E_{1/4}$ (V-Ag/AgCL)	$E_{1/2}0$ (V-Ag/AgCL)	$E_{3/4}$ (V-Ag/AgCL)	$I_{1/4}$ (mA/cm^2)	$I_{1/2}$ (mA/cm^2)	$I_{3/4}$ (mA/cm^2)	I_{lim} (mA/cm^2)
100	0.47	0.55	0.58	5.8	11.6	17.4	23.3
400	0.50	0.57	0.62	11.4	22.9	34.3	45.7
900	0.51	0.59	0.65	17.1	34.1	51.2	68.3
1600	0.52	0.61	0.67	22.6	45.2	67.8	90.4
2500	0.53	0.63	0.72	28.0	56.0	84.1	112.1
3600	0.54	0.64	0.76	33.4	66.8	100.2	133.7
4900	0.54	0.66	0.79	38.8	77.5	116.3	155.1
6400	0.56	0.68	0.81	44.1	88.2	132.3	176.4

diffusion coefficient.[82] The inset on Figure 37 contains the Levich plot, which is linear from 100 RPM to 6400 RPM and intercept 0. The diffusion coefficient of $3.85 * 10^{-6} \frac{cm^2}{Sec}$ @25 ℃ was calculated using the slope of this Levich plot. This diffusion coefficient is lower than other small molecules have a diffusion coefficient on the order of $10^{-5} \frac{cm^2}{Sec}$.[82] This lowered diffusion coefficient will lead to increased mass transport challenges in cell and stack design.

Levich Analysis-Concentration Dependence

The Levich analysis was performed at room temperature and a series of different concentrations(Figure 31). The goal of this experiment was to determine if the limiting current followed the Levich equation at all the degrees of reduction expected in an operating battery. If the Levich equation was not followed, the diffusion coefficient of the active species, the kinematic viscosity, or the C_{Bulk} concentration is not as expected. The Levich analysis would not detect changes in the E^0 unless the redox potential was shifted outside the window scanned.[81,82]

One of the requirements for the use of the Levich equation is that the system is entirely under mass transport control (as confirmed by the zero intercept of the Levich plot). These conditions are perfectly met in the Levich plot shown in Figure 31. The limiting current should rise linearly with the square root of scan rate as shown. The only parameter which changes between the curves is the slope, which derives from the C_{bulk}.

To determine that the state of charge does not affect the operating parameters of the battery, the Levich analysis was performed on the curves shown above (Figure 32). Different states of charge can lead to changing average diffusion coefficients or number of electrons transferred.

The experiment in Figure 32 was performed under inert gas, in 0.4 M phosphomolybdic acid on a glassy carbon electrode with an Ag/AgCl reference and platinum mesh counter. The solution was bulk reduced separately in a stirred, NAFION divided H-Cell with a platinum mesh working electrode. The # of electrons was determined by counting coulombs transferred.

Figure 32 shows a linear trend in Levich slope with increasing the degree of bulk reduction. The high R^2 value confirms that the linear fit is appropriate. The linear nature of this plot confirms that n, D, and v are not changing and C_{Bulk} is changing as expected. This further confirms the validity of the Levich approach here.

Levich Analysis-Temperature Dependence

Temperature changes can lead to changes in electrochemical activity and diffusion coefficients. To better understand the impact of temperature on this system, RDE experiments were performed at several temperatures(Figure 33). The figure shows a steep increase in limiting current with increasing temperature and a large feature around 0.5 V vs Ag/AgCl. The zero intercept is roughly 0.39 V vs Ag/AgCl.

As the temperature is increased in Figure 33, the visible significance of the feature at ~0.5V begins to fade. There is no discernable pattern between $E_{3/4}$-$E_{1/2}$ and $E_{3/4}$-

$E_{1/4}$, indicating that temperature does not significantly affect the overpotential required to reach the limiting current. Table 4 lists the $E_{1/2}$ values for the experiment shown in Figure 33. The $E_{1/2}$ values do decrease with temperature as would be expected based on improved kinetics from the elevated temperature. There is also a trend of increased $E_{1/2}$ with rotation rate, except at 80 ℃. It is possible that the reaction is becoming somewhat more electrochemically facile at elevated temperatures although the change is small.

The Levich analysis was then repeated using the data in Table 5 to determine a temperature dependence. The temperature dependence of the diffusion coefficient was determined to be $D = 2 * 10^{-6} e^{0.0214T(\,℃)} \frac{cm^2}{Sec}$ at $0.01M$. Increased temperature is therefore a useful way to improve the mass transport limitations inherent in the system.

Table 4: $E_{1/2}$ (V vs Ag/AgCl) vs Temperature & Rotation Rate

$E_{1/2}$	400 RPM	900 RPM	1600 RPM	2500 RPM
25 ℃	0.499	0.505	0.50975	0.51625
40 ℃	0.499	0.504	0.50725	0.50943
60 ℃	0.4905	0.485	0.4883	0.4911
80 ℃	0.472	0.4785	0.47835	0.4692

Koutecky Levich Analysis

The rotating disk electrode experiment can also be used to determine the kinetic parameters governing electron transfer (k_h, k_0 and α), using what is known as a Koutecky-Levich analysis. The Koutecky-Levich equation (Equation 40), allows extraction of the kinetic and mass transfer currents from a rotating disk electrode experiment.

Table 5: I_{lim} vs Temperature & rotation Rate

I_{LIM} (mA)	400 RPM	900 RPM	1600 RPM	2500 RPM
25 ℃	2.197613	3.156618	4.182341	5.210101
40 ℃	2.710475	4.062656	5.413819	6.748175
60 ℃	3.815647	5.709211	7.537584	9.309935
80 ℃	4.935081	7.603793	10.19102	13.03289

40 $\quad \dfrac{1}{i} = \dfrac{1}{(0.62)nFAD^{\frac{2}{3}}\omega^{\frac{1}{2}}v^{\frac{-1}{6}}C_{Bulk}} + \dfrac{1}{nFAk_hC_{Bulk}}$

When the disk is rotated at an infinite speed, electron transfer kinetics will govern the current per equation 41 and equation 42.

41 $\quad i = nFAk_hC$

where

42      $k_h = k_0 \exp\frac{-\alpha F \eta}{RT}$

The condition of infinite rotation speed can be simulated by plotting $\frac{1}{i}$ vs $\frac{1}{\omega^{\frac{1}{2}}}$ and finding the intercept of this line. The Koutecky-Levich approach is tempting whenever the plots of $\frac{1}{i}$ vs $\frac{1}{\omega^{\frac{1}{2}}}$ are linear, but it is important to confirm that the slopes of the Koutecky-Levich plots are independent of applied overpotential.[82] To this end, we have prepared a plot of Koutecky-Levich slopes vs applied overpotential (Figure 34). The Koutecky-Levich plots are shown in appendix Figure 73 and Figure 74.

Figure 34 shows the dependence of the Koutecky-Levich slope on applied overpotential in a bulk solution which is 50% $H_3 PMo_{12}O_{40}$: 50% $H_5 PMo_{12}O_{40}$. The Koutecky-Levich slope is the inverse of the Levich equation and has no dependence on η, only the intercept depends on η. This apparent dependence of slope on η is likely due to a changing $n_{apparent}$. That would confirm that only one of the two electrons in the final reaction is participating below the ~150 mV overpotential. It also shows that the Koutecky-Levich approach is only valid above 200 mV.

The point of performing a Koutecky-Levich analysis is to extract the kinetic current(Figure 35). The kinetic current can then be used with equations 41 and 42 to determine the rate constant k_0, which can be used to determine the exchange

current density. The kinetic current is also useful on its own as it describes the reaction in the absence of mass transport limitations.

The green line in Figure 35 is the R^2 value for the linear fit used to determine the data. The red markers show the kinetic current. The fit of $1/i \; vs \; \omega^{\frac{-1}{2}}$ is linear across the entire potential range accessed except for the area around 0 V overpotential.

The kinetic current shows a linear region around -50 to 50 mV where there is no significant activation overpotential required before the current begins to increase. The region between 50 mV and 200 mV overpotential shows very little increase in current indicating that either the redox potential for a second step is higher or it requires significantly more activation energy above its redox potential.

Figure 19 and Figure 22 show that the redox potential for the second redox reaction is approximately 200 mV higher than for the first, indicating good agreement with Figure 35. What this does show is that the round trip efficiency for a time shifted water electrolysis system such as that suggested by Symes and Bloor using phosphomolybdic acid would face an additional 200 mV penalty on the re-oxidation side. [42,43]

The calculated k_h is shown in Figure 75. The curve appears the same as in Figure 35, since they are the same data simply rescaled. Calculation of k_0 and α are performed by fitting equation 42 to this curve. k_0 is 2x10^{-6} cm^2/sec and α is 0.000135. These numbers are not physically reasonable. The K0 value is clearly irreversible yet the kinetics shown are facile. These numbers don't make physical

sense. This probably indicates that our analysis approach is incorrect, most likely because of the simultaneous presence of multiple processes or a complex mechanism. For example, if an ECE mechanism is operating, it could distort the wave shape. If we fit the curve with a simple electron transfer mechanism, such distortion (e.g. peak spreading if the second electron transfer step is slow) would lead to a poor fit of kinetics.

Conclusions

This is one of the first electrochemical studies of phosphomolybdic acid performed in many decades. Much of the original work dates to the 1970s or significantly earlier. The experimental and analytical techniques available have changed notably since then.

In this chapter, we have described the chemical and electrochemical behavior of phosphomolybdic acid. We have shown that on glassy carbon surfaces, the reaction is quasireversible. This will lead to increased overpotentials and associated wasted energy in an operating battery or electrolyzer.

The presence of platinum does not catalyze the reaction which is both good and bad, it lowers device cost by not requiring large quantities of electrocatalyst but it doesn't allow us to lower overpotentials by simply adding platinum.

The reactions proceed in a series of 2 electron steps and the two-electron nature of the first redox peak is confirmed by exhaustive electrolysis, in both the H-cell and the electrochemical flow cell.

The highest potential reoxidation peak splits into two one electron oxidation peaks several hundred millivolts apart following bulk reduction of the solution. This instability is believed to be caused by a solution reaction with the reduced species of phosphomolybdic acid. It is likely due to reaction conditions and needs further investigation. A full study of the reversibility and peak splitting against pH, supporting electrolyte choice, and the potential addition of a stabilizing organic species should be considered.

It had been contemplated that the reversibility in the thin layer voltammetry might be better than in the cyclic voltammetry cell. Some reactions can appear this way due to the massively increased surface area of carbon paper electrodes. This is not the case here as there is significant hysteresis.

The reaction in solution shows acceptable stability over many cycles. This is a fundamental requirement for use in an operating electrolyzer or battery. The lack of crossover is also a telling and positive sign for potential scale up. Nafion is an acceptable divider material.

Diffusion coefficient dependence on concentration and temperature was evaluated from rotating disk experiments. The diffusion coefficients are relatively low, which is to be expected from the size of the molecules. It shows that achieving high current densities will require that attention be paid to the nature of the carbon electrodes used.

A Koutecky-Levich analysis was also performed on the rotating disk electrode data. The analysis was inconclusive, likely due to the change in number of electrons near the open circuit voltage. The apparent change in the number of electrons throughout the 0-200 mV overpotential region is attributed to the instability identified earlier. This means any device operating within this region will only be able to access one electron, leading to further increased flow-rates and losses. It was identified that the entire 2 electrons are able to be accessed above this region.

CHAPTER 5

Zero Gap Cell Electrochemistry of Phosphomolybdic Acid

Introduction

The goal of chapters 4, 5, and 6 is to examine the feasibility of constructing a working electrochemical flow cell, capable of oxidizing a redox mediator to hydrogen in a more cost-effective manner than water oxidation. To analyze the more complex mediated process, we need to understand the heterogeneous electrochemical mediator kinetics, the full cell heterogeneous mediator performance, and the performance of the mediator in oxidizing the substrates. The device architecture used in this chapter is typical of flow reactor systems used in our lab and is the most likely option for scale up, although all materials challenges are not yet solved.

The previous literature tends to show operating curves for fuel cells that utilized phosphomolybdic acid based anodes with different fuels.[38,46,83] Other researchers focused on proving portions of the concept of using POM's as a charge carrier but did not apply it to a full size cell with all the attendant challenges.[42,43,84]

One significant challenge was with mass transport. Keggin ions are extremely large, phosphomolybdic acid for example is one of the smaller anions with a molar mass of 1825 g/mol. While they are extremely soluble on a mass basis, concentrations above 0.5 mol/L begin to reach saturation. This means that it is difficult to achieve the stoich ratios used in fuel cells and other aqueous batteries. Mass transport within the electrode is also more difficult than it would be in a system with smaller anions. The diffusion coefficient, calculated in chapter 4, is on

order of $10^{-6} \frac{cm^2}{Sec}$, an order of magnitude lower than is typical of small molecules in aqueous solutions. One of the possible future solutions to this issue of reduced molar concentration is the ability of these large anions to stabilize multiple degrees of reduction, increasing the number of electrons transferred and with the power density.

The availability of multiple oxidation states opens the opportunity to select which redox couple is optimal for balancing biomass oxidation with electrochemical cell operation. Operation in this regime would provide more power for a fuel cell or require lower potential in an electrolyzer. This is a trade off against the goals of rapid oxidation of biomass. For example, Sarma et al.used the vanadium POM[-5/-7] (2/4 electron) redox couple in their POM based cellulose oxidation process.[39]

Other sources of potential problems lie in the stability of the polyoxometalate to reduction in the aqueous regime. The POM phosphomolybdic acid appears to become unstable in aqueous solutions at greater levels of reduction. For this reason, we have defined 100% state of charge (SOC) as 2-electron reduced $(H_5PMo_{12}O_{40})$ and 0% SOC as fully oxidized$(H_3PMo_{12}O_{40})$.

The electrochemical kinetics of the mediator at the high surface area carbon electrode are also of significant interest. It is known that in vanadium flow battery systems, quasireversible behavior on glassy carbon does not mean that a catalyst will be required on high surface area carbon materials. Systems often behave in different and somewhat unexpected ways as the device architecture is changed.

For the vanadium case, the 3-D nature of the porous electrode provides a high surface area, enhancing the rate of reaction.

We hope to apply what has been learned in vanadium and other aqueous batteries to improving the performance of a phosphomolybdic acid based anode. To this end, we have used hydrophilic, high surface area carbon GDLs, supporting electrolytes, zero gap architecture, and a reference electrode.

To the best of our knowledge, no group has attempted to examine the performance of a POM based fuel cell or electrolyzer in a systematic way. In this chapter, we use a hydrogen cathode to isolate the anode performance. Recall the hydrogen electrode has a potential defined as zero, which will enable comparison with other systems. We explore the effect of states of charge, GDL materials, flow-rates, and temperatures.

Materials and Methods

Phosphomolybdic acid polarization curves were acquired using the Biologic VMP3 B potentiostat with 20A booster. The curves were taken under current control. Current was cycled from reduction to oxidation on each potential step to keep the overall state of charge constant. Each voltage step lasted for one minute (except where otherwise stated) and the potential was sampled at the end. The resistance was measured at the start of each polarization curve using potentiostatic electrochemical impedance spectroscopy (PEIS). The membrane resistance to be corrected was taken to be the zero intercept of the Nyquist plot. Humidified

hydrogen flowed across the cathode at all times to ensure the accuracy of the DHE assumption.

The solution was initially oxidized electrochemically until only a background current was flowing. Then the solution was charged (reduced) while flowing hydrogen across the cathode. The desired state of charge was determined by integrating current in either direction.

A simple pump buffer was constructed to smooth out the periodic noise from the pump. The pump buffer consisted of a sealed beaker with inlet and outlet tubing. Air pressure within the beaker forces electrolyte through the cell at a consistent rate.

The diffusion experiment was conducted in an H-cell. One compartment contained 0.25 M phosphomolybdic acid, the other compartment contained 1 M phosphoric acid as a supporting electrolyte. The phosphoric acid also helped to prevent osmotic pressure from causing crossover. The chambers were controlled at room temperature (25 ℃) and were not degassed. The phosphomolybdic acid chamber was stirred to maintain $C_{Surface} = C_{Bulk}$. A calibration curve was developed to aid in understanding the peak height-concentration relationship. The interconnection between the chambers was a 1 in diameter piece of NAFION. The H-cell used for this experiment had no neck connecting the surface of the membrane to the bulk of the chamber. A platinum working electrode, platinum wire counter electrode, and an Ag/AgCl reference electrode were used. The working and reference

electrode were in the phosphoric acid chamber while the counter electrode was in the phosphomolybdic acid chamber.

All other experiments were conducted in the Fuel Cell Technologies flow battery hardware described in chapter 2.

Results

State of Charge Effects

The first characteristic chosen for study was the effect of state of charge on the operation of a phosphomolybdic acid based electrochemical reactor (Figure 36). The importance of studying the state of charge effects come from a gap in the literature. A common way to study the performance of a biomass-phosphomolybdic acid fuel cell is to show the dependence of polarization curves on charging with different kinds of biomass. When studying the effect of "charging" this sort of cell with different types of biomass, we hypothesized that the authors are studying the effects of state of charge indirectly. To conduct a more rigorous analysis of the effect of state of charge we charged the phosphomolybdic acid solution electrochemically. Precise control over state of charge becomes possible, as does elucidating the difference between state of charge effects and the effect of other solutes on electrochemical performance.

Several things become immediately apparent from the observations of Figure 36. First is that even at relatively low current densities, the lowest states of charge are reaching mass transport limiting currents. The stoich at 40 mA/cm2 for the 10%

SOC curve is almost 3. Stoich is a term which normalizes the flow-rate based on the stoichiometric ratio of reagent input to that demanded by the current. Fuel cells often operate with a stoich between 1 and 3, but stoich close to 1 is preferred on the fuel (anode) side, since this represents the fuel efficiency. The inverse of the stoich is the utilization of reagent in a single pass. The mass transport limited current at 100 % utilization for the 10% SOC curve would be roughly 115 mA/cm^2, as is shown in Table 6. This shows that at lower concentrations it becomes difficult to maintain current due to mass transport limitations. The large stoich required to attain near theoretical performance is likely due to the large size of the ion, the low diffusion coefficient, and low concentration of active species.

Mass transport in a flowing, porous electrode, electrochemical cell can be divided into two aspects: mass transport in the flow stream and mass transport within the porous electrode. Because the stoich ratio is so far above 1, mass transport within the porous electrode is more likely to be the cause of concern. Increasing the flow-rate will improve mass transport characteristics by increasing the tendency towards turbulent mixing. Additional turbulent mixing decreases boundary layer thickness and speeds transport yet flow into the electrode is still a diffusion controlled process. Fuel must diffuse into the electrode and products must diffuse out. Further increasing the flow rate can force the electrolyte through the electrode and under the "lands" on the flow-fields, rather than through the channels. This will tend to promote convective flow within the porous electrode itself.

The mass transport limitation is particularly significant in electrochemical conversion systems due to a phenomenon known as concentration overpotential, the rapid increase in overpotential required as the reactants at the electrode become depleted. Concentration overpotential results from local concentrations at the electrode, which can be vastly different from the bulk concentration. The concentration overpotential will logarithmically increase with conversion of active species at the electrode, as shown in equation 43, which is a form of the Nernst equation (50).[85]

43 $\quad \eta_{conn} = \frac{RT}{nF} ln \frac{C_0}{C_b}$

C_0 is the concentration at the electrode surface, C_b is the concentration in the bulk solution. Fick's first law is then applied to determine the maximum current density.

44 $\quad i = nFD \frac{(C_b - C_0)}{\delta}$

At limiting current densities, equation 44 becomes

45 $\quad i_L = nFD \frac{C_b}{\delta}$

Equation 45 can be written as

46 $\quad i_L = nFK_m C_b$

K_m is a local mass transfer coefficient, it is often approximated as $K_m = V^{0.4} x 1.6 *$ 10^{-4} in aqueous systems.[86] The approximation comes from chromium systems but

is commonly applied to vanadium and other RFB systems. V is the fluid velocity in meters per second squared. Using this approximation with equations 43 and 46 yields equation 47.

47 $\quad \eta_{conn} = \frac{RT}{nF} \ln(1 - \frac{i}{10^{-4}x\frac{nFQ}{A}*C_b})$

Alternatively

48 $\quad \eta_{conn} = \frac{RT}{nF} \ln(\frac{i_L}{i_L - i})$

Which becomes

49 $\quad \eta_{conn} = \frac{RT}{nF} \ln(\frac{nFK_m C_b}{nFK_m C_b - i})$

Where Q is the volumetric flow-rate and A is the cross-sectional area of the porous electrode. Both equations show a rapid increase in η_{conn} as currents increase relative to limiting currents. This effect will become significant at lower current densities in a phosphomolybdic acid cell than in a vanadium battery because C_b for a vanadium battery can be 6 times higher than for a phosphomolybdic acid battery.

Vanadium exhibits a similar diffusion coefficient which is contained within the K_m and i_L values. The vanadium diffusion coefficients vary by oxidation state but are on the order of 10^{-6} cm^2 sec^{-1}.[87] Room temperature diffusion coefficients calculated in chapter 4 for phosphomolybdic acid are also on the order of 10^{-6} cm^2 sec^{-1}. The

similar diffusion coefficients and lowered concentration will require higher flow-rates relative to vanadium systems.

This need for high flow-rates will require significantly increased pumping power. Pumping power is a major concern for battery design, it can consume 3.5% of cell power in some flow battery systems.[88] Decreased flow-rates will result in increased concentration overpotential so this characteristic must be optimized during scale up. Other types of flow-fields may be used such as flow-through or interdigitated which can achieve higher mass transfer rates within the porous electrode than the serpentine (flow-by) flow-fields used in this work.

As the state of charge increases in Figure 36, the OCV (zero current) point begins to decrease. This follows from the Nernst equation (50).

50 $\quad E = E^0 - \frac{RT}{nF} ln \frac{[OX]}{[RED]}$

None of the curves exhibit the logarithmic performance expected when activation overpotential is a major factor. The curves are nearly flat within the kinetic regime. Current begins to flow with even a minimal change in potential, indicating facile kinetics on high surface area carbon electrodes. This is a major beneficial attribute of these cells since there is no need to have a metal electrocatalyst to improve anode performance.

Most of the loss in the higher SOC curves appears to be linear, even though the curves are IR corrected. The IR correction makes ohmic loss an unlikely culprit, although it is possible the IR correction is incomplete.

Reduction performance of the cell appears linear, except the 90% SOC curve. The lower SOC curves appear much less spread out in reduction than in oxidation. As current densities increase, they stay extremely tight. This could be due to the relatively high stoich they are experiencing. Within the current window scanned, the potential stayed above the 4-electron reduction potential. This shows that the system was not mass transport limited. A mass transport limited system would have begun 4 electron reduction once the ability to convert sufficient material with 2 electron reduction was exhausted.

To show the effects of IR loss, Figure 37 shows the IR and non IR corrected curves. The IR corrected curves have a noticeably flatter profile except the 10% SOC curve. There is roughly 100 mV of additional loss at 70 mA/cm^2 due to IR effects. The power loss depends on the overall potential and therefore the SOC but is generally in the area of 20%. This cell is not optimized to prevent IR loss but is characteristic of an early generation design.

To better understand the kinetics of the reaction, we have prepared a plot of only the kinetic portion of the polarization curve (Figure 38). This type of view allows examination of the effect of potential on activation kinetics. The differentiation here is based upon physical understanding of the system. At the extremely low currents shown, mass transport and ohmic losses are unlikely to play a significant role. When the exchange current density is much smaller than the anodic and cathodic currents, the overpotential is mainly due to poor charge transfer.[89]

The oxidation portion of the graph also referred to as anodic or positive, shows decreasing overpotential with increasing states of charge, the same as the general trends in Figure 36. The region with extremely low overpotential allows for the use of the linearized Butler-Volmer (B-V) equation (53), to calculate the exchange current density (i_0). Equation 54 then relates the exchange current density (i_0), the overpotential (η) and the charge transfer resistance. These values help to provide comparisons between systems and can be used for calculations. They are specific to the compound, electrode, and supporting electrolyte.

The Butler-Volmer equation (equation 52) has no dependence on concentration which removes the concentration influence from the state of charge influence. This description of the kinetics is only valid at low current densities, where the reaction is controlled by charge transfer at the electrode rather than transport to and from the electrode. The exchange current density and charge transfer resistances are different in the anodic and cathodic directions, with cathode generally showing more facile kinetics. This is quantified in Table 6.

Both the anodic and cathodic exchange current densities tend to increase with increasing state of charge. One possibility is that this is due to more facile kinetics at increased states of charge. The exchange current density dependence on state of charge is given in equation 51.

$$51 \qquad j_0 = Fk_0(C_{OX}{}^{1-\beta} * C_{RED}{}^{\beta})$$

On the anodic side, there is a clear trend towards decreasing charge transfer resistance with increasing states of charge. This is expected since there is a greater concentration of the active species to be oxidized. The cathodic charge transfer resistances don't show such a clear trend. They improve until 50% SOC and then begin to increase sharply.

The exchange current densities reached here are quite high, this is a strong indicator of facile kinetics. Part of the reason why these exchange current densities are so high is the way they are measured. They are measured as current density per geometric area but the actual surface area of a porous electrode is much higher than the geometric surface area. Hydrogen on platinum in 1 M sulfuric acid, a prototypically "fast" reaction often has exchange current densities around 0.07 mA/cm^2 of actual surface area. [90]

$$52 \qquad j = j_0 * [\exp(\frac{\alpha_a ZF\eta}{RT}) - \exp(-\frac{\alpha_c ZF\eta}{RT})]$$

$$53 \qquad i = -i_0 F \frac{\eta}{RT}$$

$$54 \qquad R_{ct} = -\frac{\eta}{i} = \frac{RT}{i_0 F}$$

$$55 \qquad \eta = \frac{RTi}{nF}(\frac{1}{i_0} + \frac{1}{i_{l,c}} + \frac{1}{i_{l,a}})$$

Table 6: Exchange Current Density Dependence on SOC

SOC	10%	25%	40%	50%	60%	75%	90%
Calculated I_{Lim-OX} (mA)	115.8	289.5	463.1	578	694.7	868.3	1042
+Slope (mA/V)	258.27	440.46	434	446	686	724	686
-Slope (mA/V)	336.73	532	569	632	1163	3088	1032
+I_0 (mA)	6.625	11.298	11.144	11.452	17.615	18.591	17.615
+R_{CT} (V/A)	3.876	2.272	2.304	2.242	1.457	1.381	1.457
-I_0 (mA)	8.628	13.661	14.611	16.229	29.864	79.295	26.5
-R_{CT} (V/A)	2.976	1.879	1.757	1.582	8.598	3.238	9.689

Figure 39 shows the Tafel plot of the various states of charge. Tafel plots are the method commonly used for determining exchange current densities in kinetically slow reactions. To perform this operation the portion of the line where the Tafel plot shows a linear response is used. The plot shown has no linear region within the current densities achieved, this indicates that the reaction is likely kinetically

too fast for Tafel; linearized Butler-Volmer is more appropriate when the reaction is fast.

Effect of Supporting Acid, Temperature, and Flow-rate

It is important to separate the effects of operating conditions, which can have a significant effect on the performance of electrochemical systems. Some of the most important operating parameters of flow-rate, temperature, and supporting acid are examined in the following section. Flow-rate primarily affects the mass transport resistance. Temperature and supporting acids affect the electrode kinetics, mass transport resistance, and resistance.

Increased flow-rates can decrease mass transport resistance by increasing the flux of reactant to and from the active surface of the electrode. This is exemplified by equation 44, where flow-rate can affect the diffusion layer thickness δ. Temperature affects mass transport by changing diffusion coefficients, it affects ASR in some cases by changing membrane hydration or by changing diffusion coefficients. ASR depends on ionic movement through the electrodes and the membrane, therefore decreasing the resistance to ionic movement will decrease the ASR.

Supporting acids are useful for a variety of the properties they provide to the system. They increase the overall ionic concentration, decreasing solution resistance. There is often improvement in the electrochemical rate constants. This improvement comes because solution phase species must be within 10-20

107

angstroms of the electrode surface to allow quantum tunneling of the electrons; the potential drop must also occur within this distance. In insufficiently supported media the potential drop can take place over a longer distance, not allowing all the potential to be used for the electrochemical reaction.[63] Complexation is another important factor, ions tend to cluster and form stable complexes. Providing additional reactants can drive the complex into or out of formation. Polyoxometalates are stabilized at low pH, so increasing acid concentrations will tend to improve stability. Increasing hydrogen ion concentration will also act to stabilize the more reduced forms of polyoxometalates.

Flow-Rate

Figure 40 shows the effect of changing flow-rate on the polarization curves of a phosphomolybdic acid-hydrogen flow cell. Sources of loss in each section of the polarization curve are controlled by kinetics, mass transport, and ohmic losses. The curves below are IR corrected to remove the influence of ohmic losses. The figure presents data with phosphomolybdic acid and water (neat POM), and 1 M HCl with the phosphomolybdic acid and water.

The Neat POM curves show only minimal dependence on flow-rate. This is a strong indicator that the systems represented by those curves are under kinetic, rather than mass transport control. There becomes a slight dependence of potential on flow-rate at extremely high overpotentials, a sign that the system is beginning to influence mass transport effects. The fact that the system stays entirely under kinetic control for over 600 mV shows the severe kinetic limitations

experienced by this system. This data alone shows that phosphomolybdic acid in the absence of supporting electrolyte or surface electrocatalyst is a highly undesirable anode system.

The 6 ml/min voltammogram with 1M HCl show noticeable improvement over the POM only voltammograms. It shows a steep voltage increase around 100-150 mA/cm^2. This cutoff is indicative of mass transport control.

Also of significance is that the 1 M HCL samples begin to experience fuel starvation at about the same stoich numbers. This leads to the question of whether the supply of POM or some other reactive component to the electrode is limiting, rather than diffusion within the electrode.

The mass transport limited current is the maximum current achievable at a given flow-rate if the stoich value is equal to 1. This mass transport control regime begins when the stoich is as low as about 5.

The 1M HCl and 13 ml/min curve show the onset of mass transport control at a higher current density of nearly 200 mA/cm^2, this is a stoich value of about 5 again. The 1M HCl and 30 ml/min curve shows no onset of mass transport control at all within the potential regime that was accessible without damaging equipment. The experiment had to be stopped at 350 mA/cm^2 because the potential on the recharging step was reaching the safety limits of the equipment. For reference a stoich value of 5 at this flow-rate would be about 500 mA/cm^2.

Normalizing Figure 40 using the mass transport limited current yields Figure 41. In Figure 41, the dependence of potential on utilization for the POM only curves is misleading because the current is changing while the potential required is not. This occurs because the system is not under mass transport control. For the 1M HCl + POM samples, the 6 ml/min and 13 ml/min curves are similar in shape with the 6 ml/min sample appearing to have the best performance. It is important to note that the 6 ml/min sample appears the best because the flow-rates are so much lower. The performance of the 13 ml/min sample shows that the mass transport limitations are not yet resolved. The performance of the 30 ml/min sample shows that mass transport is not controlling out to 350 mA/cm^2. The kinetics must therefore be sluggish enough to prevent mass transport from taking over until roughly 400 mV overpotential.

Also of significance is that the 1 M HCL samples begin to experience fuel starvation at about the same stoich numbers. This leads to the question of whether the supply of POM or some other reactive component to the electrode is limiting, rather than diffusion within the electrode.

Mass Transport Limited Current

Flow-rate	6 ml/min	13 ml/min	30 ml/min
I_{max} (mA/cm^2)	482	1045	2412

Temperature Effect

The presence of increased acid and high flow-rates generated improved but still insufficient performance. One of the most trusted ways to increase the rate of any reaction is to increase the temperature, although not all the effects of increased temperature will improve system performance. In the case of a flow battery, it can affect the operation by speeding kinetics, increasing diffusion coefficients, decreasing viscosity, drying membranes, altering solubility, evaporating solvents, and speeding side reactions.

The effect of supporting acid in the previous section led us to try increased acid concentrations as well. The work in chapter 6 suggested that a hydrochloric acid system would be preferable to a sulfuric acid system. Hydrochloric acid is also an excellent choice because it is inexpensive and widely available. Temperatures were varied from 35 ℃ to 80 ℃, higher temperatures were not feasible with the equipment used although they may be beneficial. Further elevating temperatures will require pressurizing the anolyte compartment to prevent excessive moisture loss.

Figure 42 shows the effect of temperature on the operation of a phosphomolybdic acid electrolysis cell at 50% SOC. The parameters varied are temperature and concentration of hydrochloric acid supporting electrolyte. The ideal mass transport limited current is 2500 mA/cm^2. The general trends of decreasing overpotential with increasing acid concentration and temperature are present. The initial addition

of acid from 0->1 M makes the biggest difference in polarization required. There is no temperature where the neat POM outperforms the 1 or 5 M HCl-POM systems.

Operation of a room temperature electrolysis cell in the absence of supporting electrolyte at 100 mA/cm^2 would require over 1000 mV of additional overpotential (nearly 3 times the total energy) relative to the room temperature system with 5 M hydrochloric acid added.

To clarify the results of Figure 42, we have prepared separate plots of each acid concentration (Figure 43, Figure 44, and Figure 45)

Figure 43 shows the effect of temperature on the 1 electron reduced, phosphomolybdic acid only system. The effect of temperature is quite pronounced. A significant difference is noted in the angle of the polarization curves right beginning in the kinetic region, this angle difference is quantified as the exchange current density in c. There is roughly 600 mV additional overpotential required to move the reaction from 80 ℃ down to 35 ℃ at 100 mA/cm^2. The potentials required to reach 100 mA/cm^2 at any temperature below 80 ℃ are within the realm of water oxidation given the proper electrocatalyst. It is unlikely although not impossible that significant water electrolysis is occurring in this system, given that no effective water oxidation catalyst is present on the anode side. The effect of temperature on oxidation potential is not linear and changes with current density.

Figure 44 shows the temperature dependence of the electrolyzer when the anode is supplied with a 1M HCl-POM solution. The electrolyzer performance is

significantly improved versus the neat system. In the neat system, the maximum current density reached was about 130 mA/cm^2. In the 1M HCl system, a maximum current density was reached at 500 mA/cm^2. The dependence on temperature here is much clearer than in the neat system. The 35 ℃ curve still shows significantly worse performance than the other temperatures. The slope is much steeper and it sits at higher potentials by 100 mA/cm^2 than the higher temperatures do at 400 mA/cm^2. At low overpotential, the 50 ℃, 65 ℃, and 80 ℃ curves all show similar slopes but sit roughly 10 mV apart. The polarization curves all track closely to 400 mA/cm^2. The difference between 50 ℃ and 80 ℃ is smaller than the difference between 35 ℃ and 50 ℃. The slopes of the 50 ℃ to 80 ℃ polarization curves continue to improve with temperature within the kinetic region, this is quantified in Figure 46 and Table 9. All of this indicates kinetic limitations that are greatly improved by increasing temperature. The potential decrease in the kinetic region as the temperature increases can be attributed to the falling Nernst potential.

Figure 45 shows the performance of the electrolyzer with an anode feed of 5M HCl and POM. The performance at 35 ℃ slightly improved relative to that with 1M and significantly improved relative to the neat solution. At 50 ℃ and 65 ℃ the 1M and 5M performance is nearly identical. At 80 ℃ the 5 M performance is slightly improved again relative to the 1M. In the 5M HCl solution, all of the curves are much closer together than in any of the other solutions. This indicates decreased kinetic limitations relative to the 1 M HCl and neat solutions. All the kinetic slopes

113

appear flatter in the 5 M HCl solution but that will be quantified in Figure 45 and Table 9.

The subjective analysis above provides a basic understanding of the trends present in the system. We can further characterize the system through the calculation of basic parameters. Understanding the exchange current densities and charge transfer resistances will enable quantitative comparison between various iterations of the designs.

Effect of Temperature and Acid on Exchange Current Density

The anodic exchange current densities are presented in Figure 46 and Table 9. As expected the exchange current densities increase significantly with acid concentration. The temperature dependence is also quite strong and increases with increasing acid concentration. This significant improvement with acid concentration and temperature has the potential to result in large energy savings and increase the viability of these system designs.

The neat phosphomolybdic acid solution displays a linear dependence of i_0 (mA) on temperature (K). The slope for this dependence is roughly 0.0903 mA/K. The 1 M HCl-phosphomolybdic acid solution $\frac{i_0}{k}$ dependence has a slope of 0.746 mA/K. The plot is not linear in this case, it exhibits a steep rise until 338 K and then levels off, showing no more improvement with elevated temperature. The 5 M HCl-phosphomolybdic acid solution $\frac{i_0}{k}$ dependence has an exponential dependence on temperature of $i_0 = 0.0009e^{0.337t}$. This figure shows the immense impacts

114

temperature and acid on the kinetics of phosphomolybdic acid oxidation. The exchange current density can be increased 11,167% by transitioning from 35 ℃, neat solution to 80 ℃, 5M HCl solution (raw data is given in appendix Table 9). The use of room temperature and no supporting acid may explain some of the poor performance of the previously constructed cells in the literature.

Effect of Temperature and Acid on ASR

Recall that the sources of voltage loss in electrochemical system is a sum of resistances, kinetic, ohmic, mass transport, and contact(equation 9). Ohmic resistance often plays a large role in the overall potential loss in an operating electrochemical conversion device, especially at high current densities. Ohmic resistance in the cell is characterized by ASR.

The loss from ASR does not substantially affect the data presented in this chapter because the data is corrected to remove the influence of IR loss. This is done to better isolate the effects of mass transport and kinetic losses. The open circuit ASR dependence on temperature and HCl concentration is presented in Figure 47. The neat phosphomolybdic acid cell exhibited 4-5 times the ASR of the 1 M and 5 M HCl systems at all temperatures. There is a decreasing trend in ASR vs temperature, with 308 K being the exception. The lowest ASR achieved is nearly the same for the 1 M and 5 M HCl samples, at 80 ℃. Resistance in the membrane will tend to decrease with increasing acid concentration. It is also common in flow batteries that much of the resistance is due to conductivity within the electrodes.

Increased solution acid concentration will increase solution conductivity and decrease IR loss through the electrodes.

There are two main strategies commonly used to decrease ASR, increasing the conductivity of the membrane and decrease the total path for the ions to flow though. Conductivity of the membrane is generally increased by increasing the hydration level. Overall ASR is reduced most effectively by decreasing the path length. This can be done using thinner electrodes and thinner membranes. The membrane used in these experiments was NAFION 117, the thickest NAFION membrane sold. It was chosen for stability and ease of handling, rather than optimization of IR loss. Operational batteries are expected to use a membrane $1/7^{th}$ to $2/7^{th}$ the thickness of this membrane. There are some indications in the literature that a size selective membrane rather than a charge selective membrane may be suitable here. That could be a positive development because dialysis membranes are not as dependent on hydration levels and are generally less expensive than PSFA membranes.

Carbon Felt vs Carbon Paper

Kinetic and mass transport properties of electrochemical devices are highly dependent on the environment around the electrode. Electrodes in electrochemical conversion devices work by decreasing the length of the diffusion layer by promoting turbulent flow, while providing a high surface area for the reaction to occur on. Two components of a flow battery are responsible for minimizing the

diffusion length, the liquid-gas diffusion layer (GDL) and the flow-fields. Flow-fields are not addressed in this work.

In a fuel cell, the reaction takes place at the electrode/electrolyte/catalyst interface, directly against the membrane. For this reason, increasing the GDL surface area is unlikely to provide significant benefit. Fuel cells also use a GDL with a microporous layer on the surface to trap catalyst on the surface during deposition. Finally fuel cell GDLs are treated with a hydrophobic coating to prevent flooding.

In the flow battery, it has been found that the reaction can take place throughout the GDL thickness and therefore increased GDL surface area can provide tangible benefits to operational efficiency. Flow battery researchers have also discovered that microporous layers are detrimental to efficiency by hampering diffusion of liquid electrolytes to the membrane. Because flow battery reactions take place on the surface of the GDL instead of on the surface of the catalyst, they require a hydrophilic surface. Wettability is important to maximizing the usable surface area of the GDL for the electrochemical reaction.

We have chosen to explore two common battery GDL materials WOS1002 carbon cloth and SGL 35AA carbon paper. Their properties are described in Table 7. Both are hydrophilic carbon electrode materials with similar thicknesses and through plane resistances. Carbon cloths are expected to have lower mass transport resistance than carbon papers due to their looser weave. This is quantified in the air permeability.

117

Air permeability is calculated using the Gurley method. In this method, two chambers of air are connected by a tube, divided by a piece of GDL. One chamber is pressurized and the other is evacuated. The air permeability is given as the amount of air which can pass through a set area of membrane in a set amount of time.[91] The air permeability of the carbon cloth is 4x higher than the carbon paper.

Table 7: Properties of Electrode Materials

Property	Units	WOS 1002 Carbon Cloth[92]	SGL 35AA Carbon Paper[93]
Thickness	μm	360	300
Weight	g/m^2	125	51
Air Permeability	$cm^3/(cm^2\text{-}sec)$	465	170
TPR	$m\Omega\text{-}cm^2$	<5	<12
Porosity	%	50	90

This difference in permeability may be explained by the noticeable differences in construction. The carbon cloth is a woven material while the carbon paper is a mixture of carbon fibers and binders. SEM images are given in Figure 48. Even at 50X magnification, the carbon cloth looks much more accessible than the carbon paper. Although the rated thicknesses are similar, the carbon cloth looks much thinner in the 20X transverse view. The carbon paper also appears to have a series of sheets with high density while the carbon cloth is more uniform. This likely contributes to the higher air permeability. Electrolyte may become trapped within the layers of the carbon paper and rely on diffusion rather than convection to exchange material with the bulk.

The exchange current densities approximately double with the addition of the second layer. That is expected if the mechanism is increasing surface area. It may not be exactly double due to inconsistencies in compression or other details of cell construction. The exchange current density of the carbon cloth is roughly double that of the carbon paper, again suggesting that increased activity may be playing a large role in differing performances.

In Figure 49, the polarization curves of 2 layer carbon cloth and carbon paper GDLs diverge until about 50 mA/cm^2 and then begin to track together. The low current/overpotential region is known as the kinetic region and represents kinetic losses. The fact that they begin to track together at higher current densities is indicative that the mass transport controlled region has been reached and that the mass transport limitations are similar.

119

Carbon Cloth vs Carbon Paper Exchange Current Densities

	1-layer WOS 1002	2-layer WOS 1002	1-layer SGL 35AA	2-layer SGL 35A
J_0 (mA/cm^2)	11.26	28.12	7.23	12.88

Voltage Stabilization at Each Step

An alternative hypothesis to the surface area one is that the added electrode thickness is retaining more electrolyte. If this were the culprit, the polarization curve would not reach steady state within the step time. Once the current is stepped to a new value, the reactants within the diffusion layer thickness are rapidly consumed. To compensate the diffusion layer thickness grows until it is sufficient to maintain the set current. The driving force required for this increased current is increased overpotential.

The experiment was conducted as galvanic step chronopotentiometry. The maintenance of stable state of charge in a flow battery is essential for characterization as shown in Figure 36. The charge passed in a single polarization curve could affect the state of charge by 10% or more. To maintain a stable state of charge for the anodic portion of the curve, an equal reduction step preceded each oxidation step.

Figure 50 shows the anodic chronopotentiometry of each of the current steps in Figure 49. The two layer carbon paper experiments reached stability faster than

the 1 layer. If electrolyte depletion were causing concern, the potentials would be peaking at the end of each galvanic step. The potential shows a spike at the beginning of each step and begins to decrease. The initial spike may be caused by capacitive charging. The experiment was stopped when the current spiked outside of the safety limits of the equipment. Data was only recorded from steps where the potential appeared stable.

Figure 51 gives the cathodic chronopotentiometry of each current step. At higher current densities neither of the cathodic curves reach stability. The 35AA 2-layer stays stable at higher current densities than the 1-layer does. For this reason, the cathodic portion of the polarization curve in Figure 49 is not shown. The extremely large overpotentials reached are well within the range required for 4 and 6 electron reduction.

Phosphomolybdic Acid Diffusion in Nafion

Most authors proposing polyoxometalate based flow systems state that there will be no crossover issues. They reason that the large size (1800+ g/mol) and negative charge provide sufficient charge and size exclusion for a NAFION membrane.[38,43] The only experimental evidence for this theory utilized UV-Vis spectroscopy to track the crossover concentration. We experienced unexpected crossover levels as evidenced by visual inspection. To better understand the issue of crossover, we turned our attention to developing sensitive methods for detection of crossover species. Initially cyclic voltammetry was used to track the concentration of the crossover POM but the data appeared noisy and unreliable.

Square wave voltammetry was chosen as it is considered to be one of the most sensitive electroanalytical techniques. This sensitivity is owing to the removal of the influence of capacitive contributions to the current.

A diffusion cell was constructed and diffusion was measured across a NAFION membrane. The cell consisted of two chambers, one containing phosphoric acid and the other containing phosphomolybdic acid. The chambers were connected by a NAFION 117 membrane. Phosphoric acid was necessary in the low concentration side to control osmotic crossover of water and to provide sufficient conductivity for the reaction. The concentration of phosphomolybdic acid in the water chamber was tracked using peak currents in square wave voltammetry. Peak currents are described by the Randles-Sevcik equation shown in equation 56.

56 $\quad i_p = 0.4463 nFAC \left(\frac{nFvD}{RT}\right)^{\frac{1}{2}}$

Figure 52 is representative of the square wave voltammetry of the calibration curve. The first peak at roughly 0.179 V was chosen for analysis for its strong correlation to the concentration of phosphomolybdic acid in the system, especially at low concentrations. Figure 53 Shows the peak height-concentration ratio for square wave voltammetry of phosphomolybdic acid in phosphoric acid. There is generally good agreement between the calibration curve and the data, as is evidence by the high R^2 value. Figure 54 gives the crossover vs time as calculated using square wave voltammetry. The slope of the line is plotted as $2x10^{-7} \frac{Mol}{Sec}$.

122

Because crossover is so minimal, the concentration difference stays nearly the same, allowing the use of Ficks first law of diffusion (equation 57). The slope of the crossover is divided by the surface area to give the flux as applied in equation 58. The diffusion coefficient for phosphomolybdic acid across a NAFION membrane is calculated to be D=7.2475x10^{-7} $\frac{cm^2}{Sec}$.

57     $Q = \frac{D}{L}(C_2 - C_1)$

58     $\frac{2x10^{-7}\frac{Mol}{Sec}}{20.2 \; cm^2} = \frac{D}{0.0183 \; cm}\left(0 - 0.25\frac{Mol}{L} * \frac{1L}{1000 \; cm^3}\right)$

This diffusion coefficient is similar to that of other small molecules. For reference the diffusion coefficients of vanadium in NAFION varies, but are on the order of D=10^{-7} $\frac{cm^2}{Sec}$.[94] Vanadium systems are known to have significant issues concerning crossover. This means that crossover could become a concern in phosphomolybdic acid systems too. Diffusion is not the only or even the most important driver of crossover in an electrochemical cell but it is an easy to measure surrogate to describe the expected relative crossover rates. In many systems, electroosmotic drag can have a more significant effect on crossover than diffusion.

Crossover can also be detected by visual examination and UV vis spectrometry but those methods are less sensitive than electrochemical techniques. They are also more susceptible to errors caused by state of charge, since each state of charge is a distinct color. Anecdotally, no crossover was visible using visual examination in H-cell systems. Crossover was clearly occurring during electro-

oxidation of the phosphomolybdic acid in the flow cell systems. A dark blue liquid collected at the cathode during oxidation experiments and had to be washed off. The reduced form of the phosphomolybdic acid is dark blue. It is unclear whether this is entirely electroosmotic drag driven or if the phosphomolybdic acid becomes unstable during oxidation.

This measurement combined with observations of operating cells shows that crossover is a more significant concern in these systems than previously noted in the literature.

Conclusions

In this chapter, we have begun the exploration of the challenges associated with operating an electrochemical flow cell utilizing using phosphomolybdic acid as a model POM feed. We have studied the effect of state of charge, stoich, temperature, supporting acid, and gdl choice. The highest performance design exhibited an exchange current density of 153 mA and an ASR of 0.4 ohm-cm^2. The standard conditions yielded an exchange current density of 1.37 and an ASR of 2.1 ohm-cm^2. Despite this immense improvement, many opportunities are identified to further increase performance.

We have found the effect of supporting acid is profound and not studied in the literature. Some prior authors have used supporting acids such as phosphoric acid to control pH but they did not study the effect of the acid. Many of the reports do not include a supporting acid at all and none have studied hydrochloric acid.

Increasing HCl concentrations is also shown to be beneficial to performance by increasing exchange current density and decreasing cell resistance. Future work could include testing the effect of other acids and further increasing acid concentrations.

The effect of GDL and temperature is expected although untested in the literature. Additional surface area beyond that achieved with one layer of carbon cloth or carbon paper was required to optimize the cell performance. It would be beneficial to test higher surface area carbon materials or still thicker electrodes. The influence of mass transport on the electrodes was determined to be significant. This can be improved by increasing SOC and increasing concentration.

Crossover was another issue identified of unexpected consequence. Crossover issues were dismissed in the literature and considered to be unlikely. Crossover was noticed visually and diffusion coefficients in NAFION were calculated. Crossover was clearly occurring and diffusion coefficients were of the same order as vanadium systems which exhibit significant crossover issues. Crossover POM was removed from the counter electrode by flushing with DI water. This water ran blue (reduced phosphomolybdic acid) and could be turned yellow (oxidized phosphomolybdic acid) with a few drops of hydrogen peroxide. The crossover appears easy to remove and the material could likely be cycled back to the anolyte after flushing although this was not tested.

Long term stability of battery materials and the POM have not been studied but will be important to the functioning of a completed device.

125

CHAPTER 6

Glycerol Oxidation by Polyoxometalates

Introduction and Goals

The overarching goal of this work is the use of organic compounds as a source of protons to decrease the potential required for the electrolytic generation of hydrogen. Chapters 4 and 5 explored the electrochemical stability and reactivity of a polyoxometalate mediated hydrogen production system. Such a system requires a mediator which is not only efficient at reducing the anode potential but is also able to oxidize the biomass model compounds at sufficient rates.

To better understand the rates present, we began by using cyclic voltammetry. The shape of the cyclic voltammograms changes with the reaction rate constant and scan rate in a predictable manner.

Insufficient reaction rates between glucose and POMs made CV an impractical choice. This led to the development of another methodology for tracking the solution redox reaction, repeated bulk electrolysis for changing time periods. This technique was used to search for an acceptable combination of mediator, organic compound, and conditions for the oxidation of organics and reduction of the mediator.

The reagents chosen were selected from literature reports of biomass oxidation using pure polyoxometalate systems, POM mixed with mineral acid, and metallic catalysts. [36–39,52,53,95,96] Iron and copper additives were explored due to their known ability to oxidize glycerol.[57] TiO_2 was chosen for its reported ability to catalyze the oxidation of methanol in energetic conditions. To that end, we undertook the

screening of a variety of polyoxometalates, acidities, and other additives for their reactivity with glycerol.

Materials and Methods

CV experiments: 25 ml solutions of 0.01 M phosphomolybdic acid, with 1 M HCl, and 1 M glucose were prepared. The electrolyte was placed in a 3-electrode cell which was heated from the sides and bottom. A Pt disk working electrode, Pt wire counter electrode, and Ag/AgCl reference electrode were used.

The oxidation screening and kinetic constant experiments were performed using 50 ml solution volume. The solutions were 0.025 M POM with 0.5 M Glycerol and other additives as noted. Solutions were mixed under ice and stored under refrigeration if not used immediately. Solutions were then heated to 90 ℃ and stirred, while flowing into the electrochemical flow cell. The flow cell used was as described in the previous chapter. The flow cell had a steady bleed of nitrogen across the cathode to prevent flooding or back diffusion of hydrogen during OCV periods. The solution was oxidized at 1 V cell potential for 2 hours, then a series of 2, 4, 6, and 8 hour OCV periods were each followed by 2 hours of oxidation at 0.8 V. Current, total charge, and time were all recorded using a Biologic VMP-3 B potentiostat.

Preparation of solutions: The metal catalyst combinations were prepared by mixing the co-catalyst with phosphomolybdic acid, then boiling and stirring for 1 hour, before refrigerating until use. The $FePMo_{12}O_{40}$ was prepared from the $FeNo_3$ salt

and $H_3PMo_{12}O_{40}$. The nitrate salt was chosen because it contains Fe(III) which will not reduce the POM. The $H_3PWMo_{11}O_{40}$ was prepared by mixing stoichiometric amounts of $PW_{12}O_{40}$ with $PMo_{12}O_{40}$. $CuPMo_{12}O_{40}$ was prepared from $H_3PMo_{12}O_{40}$ and $CuSO_4$. The $VPMo_{12}O_{40}$ was prepared from $H_3PMo_{12}O_{40}$ and $VOSO_4$.

UV-vis Spectroscopy was performed on the prepared solutions. Some solutions were immediately reduced upon preparation so 100 µL 30% hydrogen peroxide was added to the 3 mL UV-Vis samples to reoxidize them. The samples were stored for several days in the refrigerator and sonicated for 90 minutes prior to the UV-Vis spectroscopy being performed. A Thorlabs light source and ALS detector were used with a 1 mm path length quartz cuvette. UV-Vis results are shown in the appendix(Figure 85, Figure 86, Figure 87, Figure 88, and Figure 89)

Square wave voltammetry was performed on each of the solutions to help elucidate peak heights. Cyclic voltammetry was performed initially but the scans revealed little. Square wave voltammetry is explained in chapter 4. The scans are given in appendix Figure 90, Figure 91, Figure 92, Figure 93, Figure 94 and Figure 95.

Studying Glucose Oxidation Kinetics Using Cyclic Voltammetry

Cyclic Voltammetry can be used to determine reaction rate constants of coupled chemical and electrochemical reactions. When describing coupled electrochemical and chemical reactions, "E" refers to an electron transfer and "C" refers to any homogeneous elementary chemical reaction step. The order of the letters

describes the order in which the steps take place. For example, an EC reaction (59 and 60) would mean an electron transfer step followed by a chemical step.

59 $\quad Red \leftrightarrow Ox + ne^-$

60 $\quad Ox + A \xrightarrow{K_f} B + C$
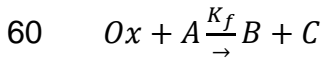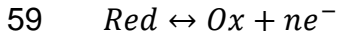
There is a special case of the EC reaction called the EC' reaction whereby the electrochemical reactant is regenerated in the chemical step.

61 $\quad Red \leftrightarrow Ox + ne^-$

62 $\quad Ox + A \xrightarrow{K_f} Red + B$
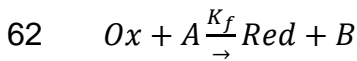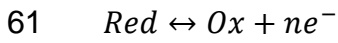
The EC' reaction, also known as the electro-catalytic case, perfectly describes the oxidation of biomass by polyoxometalate in the proposed system. Equations 63 and 64 show the electrocatalytic case applied to the POM-organic system. Equation 65 gives the rate equation for the accumulation of reduced POM in the absence of systemic reoxidation.

63 $\quad H_5PMo_{12}O_{40} \leftrightarrow 2H^+ + H_3PMo_{12}O_{40} + 2e^-$

64 $\quad H_3PMo_{12}O_{40} + \text{Organic} \xrightarrow{K_f} H_5PMo_{12}O_{40} + \text{Oxidized Organic}$
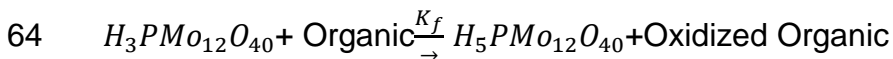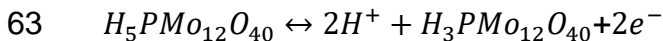
65 $\quad \frac{\partial [H_5PMo_{12}O_{40}]}{\partial t} = k_f [Organic]^x [H_3PMo_{12}O_{40}]^y$

Cyclic voltammetry of the EC' reaction shows a significant change in the recorded voltammograms with scan rate (Figure 55). As the ratio of $\frac{k_f}{v}$ (where v is the scan

130

rate) increases, the reduction peak will shrink relative to the oxidation peak since the substrate is replenishing the reduced POM in the area of the electrode before the reductive sweep can occur. Simple modeling is then required to turn this qualitative data into values of k_f. This technique is a popular option for understanding fast chemical redox reactions.

This technique is fundamentally limited in its ability to understand slow chemical reactions. This limit comes from the necessity of maintaining semi-infinite linear diffusion in a quiescent solution. Extremely low scan rates are not feasible because when scan rates get low enough, other effects will begin to dominate. This will have a similar appearance to increasing K values so it is important to ensure operation above the minimum scan rate. The value P (equation 66), quantifies the validity of the linear diffusion assumption for cyclic voltammetry. The minimum P value for successful cyclic voltammetry experiments is 1.[97] The P value for the studied systems was ranged from over 20 to 4.5.

66      $P = \sqrt{\frac{nvFr_e}{RTD}}$

Glucose was used as the organic substrate in these experiments because it is expected to react with the polyoxometalate readily.[36,38,98] Cyclic voltammetry of the solution is presented in Figure 56, Figure 57, and Figure 58. Upon first examination, the voltammograms appear to show a change similar to what is expected for a coupled reaction. The change in the background curves leads to the belief that a different effect must be occurring.

131

We theorize that the condition of quiescence was disrupted by convection. The container was heated from the bottom and sides to attain the required temperature, this is likely inducing convection. Due to the extremely low value of k_f and the conditions required to increase it, we cannot access scan rates slow enough to determine its value through cyclic voltammetry.

Visual inspection of the solution revealed a change from yellow to blue, indicative of bulk reduction. Figure 58 also shows a reaction is occurring on a slower time scale. The time required to scan at 0.1 mV/sec over a 1400 mV range is nearly 4 hours. By the time multiple scans has occurred, the solution appears to have undergone bulk reduction. The glucose curve contains several of the same features as the bulk reduced, RDE curves did. There is the shoulder at roughly 0.5 V vs Ag/AgCl, and an increase in the diffusion limited current above 0.6 V. This is due to an increased concentration of the reduced species in the bulk.

Screening of Additives and Supporting Acids for Glycerol Reduction

Once it was determined that the kinetics of glucose oxidation by phosphomolybdic acid could not be readily studied with cyclic voltammetry, we turned to bulk oxidation experiments. Glycerol was selected as a model substrate due to its desirable combination of price, availability, and renewable nature. Excess glycerol was placed in a sealed glass reactor with catalyst and thermostatted to 90 ℃. The glass reaction chamber was connected to an electrochemical flow cell. The steady

state current was recorded as R (equation 67). To increase signal, a series of reduction and reoxidation steps were performed.

The batch experiment is expected to be pseudo first order in the mediator, since the experiment has excess substrate (20:1) with the mediator concentration changing. In the continuous experiment, the substrate is supplied in excess(20:1) and the POM is being regenerated. This is a pseudo zeroth order reaction since none of the reagent concentrations are changing. The results of these two experiments are correlated later to help provide confirmation of results and to develop additional parameters.

67    $R = K * [Substrate]^X * [POM_{OX}]^Y [Co - Catalyst]^Z$

The conversion of charge passed to moles is accomplished using the equation 68.

68    $Q = nFN$

Where Q is charge passed in coulombs, n is the number of electrons per equivalent, N is the number of moles reacted, and F is the Faraday constant(96485 C/Mol). For consistency and ease of conversion we work in moles of H^+ or e^-, which directly translates to grams of hydrogen.

Chronocoulometry of Polyoxometalate Based Glycerol Oxidation Catalysts

This section compares the effect of several additives in either water, HCl or H_2SO_4. The presence of sulfuric acid has been shown to increase the rate and alter the

mechanism (PC-ET to ET-OT) for the oxidation of the primary and secondary alcohols by polyoxometalates.[53]

Figure 59: Coulometric Monitoring of the Time Course of Glycerol Oxidation, as Revealed by the POM Re-Oxidation Charge, for Various POM Catalysts in 0.5 M Glycerol shows the chronocoulometry during reoxidation of several catalyst combinations in a solution consisting of catalyst, glycerol, and water. The copper and titanium-dioxide POM solutions show a decrease in activity relative to the base line of the pure phosphomolybdic acid.

They show far lower activity than the pure phosphomolybdic acid for the oxidation of glycerol. The best performing combinations in this system are the iron and vanadium POM complexes. The reoxidation profiles of the iron and vanadium systems are such that they continue to show significant current for their entire reoxidation time. The other combinations undergo rapid reoxidation until they reach a steady state of low constant current. The pure phosphomolybdic acid, vanadium-phosphomolybdic acid, and phosphomolydbdotungstic acid solutions show increasing levels of reduction with each increasing time step of 2, 4, 6, and 8 hours. The iron system approaches its maximum reduction by the second reduction step of 4 hours. The best of these systems still only yield about 70 coulombs or 0.00073 g of hydrogen in 10 hours.

The rates of glycerol oxidation presented in Figure 58 are thoroughly insufficient for the development of a device. It has been suggested that the presence of sulfuric acid can catalyze the oxidation process two separate ways. Several authors

discuss a change in the reaction mechanism from electron transfer to oxygen insertion in the presence of sulfuric acid.[53]

Another possibility is that at higher temperatures(above 50 ℃), the mediators can react with water to produce a variety of oxidizing and super oxidizing compounds. Super oxidizers are species with redox potentials greater than that of the Ce^{3+}/Ce^{4+} redox couple (1.7 V). For example, Fe(III) can be oxidized at the anode of an electrochemical cell to form the super oxidizer Fe(VI) as is shown in equation 69. The Fe(III) to Fe(VI) reaction potential is highly dependent on pH, varying from 2.20 V (acidic medium) to 0.72 V (basic medium).

69      $Fe^{3+} + 4H_2O \leftrightarrow FeO_4{}^{2-} + 8H^+ + 3e^-$
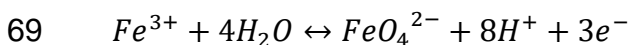
Mediators can also react with anions in the solution such as $SO_4{}^{2-}$ to produce $SO_4{}^-$ radicals which are also powerful oxidizers.[47]

Figure 59 shows the oxidation profile of the catalysts shown in Figure 59: Coulometric Monitoring of the Time Course of Glycerol Oxidation, as Revealed by the POM Re-Oxidation Charge, for Various POM Catalysts in 0.5 M Glycerol when exposed to 5 M sulfuric acid. All combinations tested are significantly less reactive in the sulfuric acid except for the neat phosphomolybdic acid which stayed roughly the same. The iron system was once again the most reactive although far less

reactive than without the acid. It achieved a 10 hour reduction charge of roughly 45 coulombs The extended time period of elevated current for the iron and vanadium systems is no longer present. This could be due to improved electrode

135

kinetics at lowered pH values. It could also be due to lowered reactivity with the glycerol substrate. The titanium dioxide and copper solutions once again provided little activity. The vanadium system was the worst of the remaining combinations. All systems showed continued reduction across the increased time ranges. This indicates that they were not approaching the end of their ability to continue to oxidize the glycerol. This is due to their extremely low reactivity.

In the search for increased reaction rates, hydrochloric acid was also chosen to explore due to its ability to form various chloride radicals, similar to the iron and sulfuric acid systems.

 shows the reoxidation profiles of the selected catalyst combinations in 5 M HCl. It becomes immediately apparent that all the catalyst combinations offer improved performance in the presence of HCl versus neat or with sulfuric acid. Even the titanium dioxide and copper systems showed measurable activity in the presence of hydrochloric acid. In this case the copper showed the lowest activity and vanadium showed the highest. The iron system showed a cutoff at about 60 coulombs, similar to the 70 where it began to cutoff during the neat experiments. Here it reached the cutoff charge in 4 hours instead of 6 hours as in the neat system. The phosphomolydbdotungstic acid combination showed greatly improved performance in the presence of HCl. It rivaled iron within 6 hours and did not show the same type of cutoff as iron, gradually increasing to 82 coulombs in 10 hours.

The vanadium performance in HCl was the most promising with over 112 coulombs or .00116 g hydrogen in 10 hours. One possible explanation for this is that vanadium can form a variety of highly reactive vanadium chloride complexes in acidic conditions.[99]

Understanding the Relationship Between Steady State Current and Total Charge Passed

After examining the above chronocoulometry, it was necessary to understand the influence of the abrupt decrease in current experienced shortly after each reoxidation step occurs. This is shown as the decreasing slope at the beginning of each curve in Figure 59: Coulometric Monitoring of the Time Course of Glycerol Oxidation, as Revealed by the POM Re-Oxidation Charge, for Various POM Catalysts in 0.5 M Glycerol , Figure 59, and

. The charge to current relationship is shown in equation 70. It is desirable to use a simplification of equation 70, shown in equation 71.

70 $\quad q = \int i \, dt$

71 $\quad q = i_{final} * \Delta t$

If this simplification holds, then i_{final} will be shown as a suitable surrogate for R in equation 67.

Figure 61, Figure 62, and Figure 63 show the total charge passed (Y-axis) and the predicted charge from the i_{final} (X-Axis), effectively comparing equations 70 and

71. The final values lie along the red line when they are equivalent and the assumption holds. For reference, 1 electron reduction per Keggin unit corresponds to roughly 120 coulombs, 100% SOC as referenced in chapter 4 and 5 corresponds to 240 coulombs.

Figure 61 shows the comparison of predicted and recorded Q values for the 4-hour time step. That is 2 hours of chemical reduction, followed by 2 hours of concurrent chemical reduction and electrochemical oxidation. The simplification inherent in equation 71 appears valid for all samples except the $FePMo_{12}O_{40}$, $FePMo_{12}O_{40}$ – HCl, and $VPMo_{12}O_{40}$ – HCl. These are the samples showing the highest i_{final}. Interestingly, none of the samples except for the TiO_2-$PMo_{12}O_{40}$ outperformed the Q predicted.

Figure 62 shows the same comparison of the two Q values as before but with 4 hours reduction, followed by 2 hours of chemical reduction and electrochemical reoxidation. As before, the $FePMo_{12}O_{40}$, $FePMo_{12}O_{40}$ – HCl, and $VPMo_{12}O_{40}$ – HCl samples are showing significant differences between the predicted and experienced Q values. Additionally, $PWMo_{11}O_{40}$ – HCl is added to the list of samples which are showing this difference.

Figure 63 further shows this difference at the 8 hour mark, 6 hours of chemical reduction, followed by 2 hours of chemical reduction and electrochemical oxidation. By this point, the top 6 performing catalyst combinations are showing $Q_{predicted}/Q_{actual}$ far less than 1. Those samples are $FePMo_{12}O_{40}$, $FePMo_{12}O_{40}$ – HCl, $PWMo_{11}O_{40}$ – HCl, $PMo_{12}O_{40}$, $VPMo_{12}O_{40}$ – HCl, and $FePMo_{12}O_{40}$ – HCl. It can be

reasonably assumed that all of these samples are now showing sufficient degrees of reduction to require the use of the full equation 67, rather than the simplified version.

We consider three possible reasons for this consistent movement away from the 1:1 ratio of Q to Q-predicted with time. The first is the production of inhibiting products. Inhibiting products could be glycerol oxidation products or compounds formed by the reduction of catalyst complexes. A second is the reduction in the concentration of active catalyst species. The concentration of glycerol is not changing by more than 2.5% based on coulometry. The other plausible explanation is that the electrochemical performance is too low to allow the samples to be fully reoxidized before reaching the end of the 2 hour oxidation period. The latter is unlikely since all samples returned to their initial color, indicating full reoxidation.

We believe that inhibiting glycerol oxidation products are likely not the culprit. The 4, 6, 8 ,and 10 hour steps were all run on the same solution, one after the other. The known glycerol oxidation products are not able to be electrochemically oxidized on carbon felt, so they would still likely be present after the electrooxidation phase. The cell appears to regenerate after each reoxidation step. A chemical study of the products in solution could be used to determine the presence of any inhibiting products and their activity on carbon felts in the presence of POM.

Liu showed the formation of starch-phosphomolybdic acid complexes(Figure 64).[38] Similar complexes with glycerol or glycerol oxidation products and

phosphomolybdic acid may be hindering the reaction progress until they can be oxidized electrochemically. The other likely cause is that the quantity of oxidized phosphomolybdic acid available for reaction is decreasing as it is reduced. This could be due to reduction or due to the formation of the aforementioned glycerol-POM complexes. They may show similar kinetic response, requiring spectroscopy to differentiate.

Catalyst Selection

The purpose of Figure 61, Figure 62, and Figure 63 is to assist in the understanding and selection of catalyst combinations. An ideal biomass oxidation catalyst has both the highest steady state current and the highest Q-transferred. The top performing catalysts in one metric are not necessarily the same as the top performing in the other metric. The choice of which metric to optimize depends on the intended mode of operation.

One proposed mode of operation is pulsed, or semi-batch in response to electricity pricing. The solution reaction occurs in the presence of sunlight or waste heat for many hours, then a hydrogen tank is filled quickly when electrical power is cheap. This mode of operation favors the catalyst with the highest Q-transferred, namely the $VPMo_{12}O_{40}$ – HCl and $VPMo_{12}O_{40}$ based systems.

The continuous process has a higher conversion rate, for this process the higher I_{ss} and associated Q-predicted is preferable. The iron based systems appear to have the highest steady state currents at every time step. Iron has an important

weakness as a catalyst: it is known to be unstable and destructive to NAFION membranes. For this reason iron systems may require a complexing agent to control their activity, such as amino acid complexes.

Reaction Rate vs Conversion Percentage

To better understand the reaction rate, Figure 65, Figure 66, and Figure 67 show the reaction rate vs electrons transferred. The Y axis represents the number of coulombs passed per hour over each time step. The X axis shows the number of electrons transferred. Electrons transferred can also be used as a proxy for time at a constant rate. When read from left to right, each marker represents the time points 4, 6, 8, and 10 hours respectively. This allows a subjective understanding of the effect of changing POM$_{OX}$ concentration when selecting a rate equation. A more rigorous examination of the kinetics will occur in the next section.

Figure 65 shows this for the glycerol-catalyst combination with no supporting acid. As discussed previously, the iron and vanadium systems show the highest activity. The iron data is noisy but no system passes 0.65 electrons per Keggin unit. The dependence of iron reaction rate on conversion appears unclear, unless the first(4hr) data point is erroneous. Iron experiences a sharp reduction in reaction rate around 0.65 electrons per Keggin unit. The phosphomolybdotungstinic acid system is slightly more active than the phosphomolybdic acid only system, showing both a higher rate and a higher conversion. Only the Vanadium system shows an expected dependence of reaction rate on electrons transferred.

Figure 66 shows the reaction rate vs electrons transferred for the polyoxometalate-sulfuric acid systems. All combinations were notably less active when exposed to sulfuric acid. Here the highest activity catalyst by a large margin is the iron phosphomolybdate combination. The last data point was lost, but it outperforms the others in both rate and electrons transferred at every step recorded. The vanadium system underperforms in the presence of sulfuric acid. The pure phosphomolybdic acid-sulfuric acid combination performs quite well. Curiously, the reaction rate appears to increase with conversion. This could be due to sluggish electrode kinetics, causing incomplete reoxidation of the reduced catalyst in the electrochemical step. Once the number of electrons reaches a high enough level, then the reoxidation step may proceed at a higher rate. The vanadium, iron, and tungsten containing systems all appear to follow the expected trend of decreasing reaction rate with decreasing concentration of oxidized mediator.

Figure 67 shows the reaction rate vs electrons transferred plot for the hydrochloric acid-phosphomolybdic acid solution. Hydrochloric acid shows the highest activity of any combination tested. All catalysts showed higher reaction rates than in sulfuric acid or water. Vanadium showed the highest activity and a clear linear trend of decreasing activity vs electrons transferred. Iron showed the highest initial activity, then the activity sharply decreased around 0.5 electrons per Keggin unit. The tungsten system exhibited a rapid but more controlled decrease in activity with electrons transferred. The pure phosphomolybdic acid system showed no clear trend of rate vs electrons transferred.

142

Kinetic Analysis

The experiment performed was designed such that the only reagent changing concentration significantly was the catalyst, the supporting acid and glycerol were supplied in large excess. The reaction rate should only depend on the concentration of catalyst supplied, rolling the effects of the other reagents into the reaction rate k'. This is intended to enable discovery of the reaction order with respect to the catalyst. The experiment can then to be performed at a variety of concentrations for the other reagents. The k' values can then be plotted against concentration to determine k and the reaction orders.

Reaction order is determined by tracking the change in concentration vs time. A zeroth order reaction shows no depenence of reaction rate on concentration, this can occur in systems where there is a limiting factor other than the reagent concentrations. Catalyzed systems where the catalyst surface is saturated with an intermediate or byproduct are the most common example of such zeroth order reactions. It is unlikely that this system is zeroth order because there is no solid catalyst used. First order reactions show a linear relationship between reagent concentration and reaction rate. Vanadium appears to have this relationship in water and hydrochloric acid (Figure 65 and Figure 67). Second order reactions show reaction rates proportional to the square of the concentration. This commonly occurs when two molecuules of the reagent are required to meet in time and space for the reaction to occur. From what is known about the mechanism of biomass oxidation by phosphomolybdic acid, this is unlikely.

Each reaction order will show linear behavior on a different representation of concentration and time. The slope of the appropriate linear plot is then used to determine the value of k'. The reaction rate laws and the appropriate linear plots for different reaction orders are given in Table 8.

The zeroth order plots are given in appendix Figure 76, Figure 77, and Figure 78. The first order plots are given in appendix Figure 79, Figure 80, and Figure 81. The second order plots are given in appendix Figure 82, Figure 83, and Figure 84.

Below is shown the R^2 values of the linear fits. This is done to determine which plot is most appropriate. When multiple reaction orders are linear, it is assumed that the reaction first order. This assumption is made because the reaction mechanism suggests first order kinetics.

Table 8: Reaction Order Equations and Plots

	Zeroth Order	First Order	Second Order
Rate Law	$\dfrac{-d[A]}{dt} = k$	$\dfrac{-d[A]}{dt} = k[A]$	$\dfrac{-d[A]}{dt} = k[A]^2$
Integrated Rate Law	$[A] = [A_0] - kt$	$[A] = [A_0]e^{-kt}$	$\dfrac{1}{[A]} = \dfrac{1}{[A]} + kt$
Linear Plot	[A] vs t	Ln([A]) vs t	$\dfrac{1}{[A]}$ vs t

The reaction is assumed not to be zeroth order. The different rates afforded by the different catalyst molecules chosen suggest a significant involvement in the reaction, making zeroth order kinetics less likely. It is expected that the extremely low reaction rates and corresponding extents of reaction will lead to high degrees of linearity. The degree of conversion may be further complicated by the continuing presence of reduced POM in solution. The 2/4 electron reduced POM couple is used by some similar systems for the oxidation of biomass. This means that the concentration of active species does not decrease linearly. The active species becomes reduced and forms a second active species, albeit likely one of reduced activity relative to the fully oxidized species.

Figure 68 shows the R^2 for the neat solutions, none of the samples show a significant change in linearity with increasing the assumed reaction orders. Vanadium appears linear in all graphs, with the degree of linearity increasing slightly in the 1st order plot. The phosphomolybdic acid and phosphomolybdotungstinic acid systems show slighly decreasing linearity with increasing assumed reaction order, although the correlations are still above 0.95.

Figure 69 shows the R^2 of the sulfuric acid containing solutions. The pure phosphomolybdic acid system appears to be zeroth order, correlation decreases with reaction order. The iron system appears to be first order, The correlation is extremely low for the zeroth order plot(~0.2) and jumps up to almost 1 for first order plot.

Figure 70 gives the R^2 data for the hydrochloric acid containing systems, the highest activity combinations tested. Again, the iron system is clearly first order with an extremely low correlation (~0.2) in the zeroth order plot. The vanadium system exhibits a slight peak in the first order plot. The other systems can all be modeled as zeroth order or first order.

All of this is to suggest that a k' value can be calculated assuming the reactions are first order. Figure 71 gives the k' values for all catalyst combinations tested, note the units are 10^{-3} hr^{-1}. These are extremely low reaction rates. Further experimentation is still required to transform the k' values into k values. k values can be used with the rate equation to determine the size and concentration of reaction chambers necessary for given production rates of hydrogen.

Further optimization is likely possible, especially with respect to the catalyst POM ratios. It may be possible to do away with the expensive POM and use a larger ratio of the relatively inexpensive co-catalyst.

Implications for Scale Up

Construction of hydrogen fueling stations is the definition of eventual success for the ideas presented in this work. The data presented in chapter 5 suggests that phosphomolybdic acid can be reliably oxidized in an electrolysis cell. The current densities shown will allow for reasonable stack sizes.

Stack construction is only half the chemical side of the proposed design (shown in Figure 72). Determining the composition, size, and concentration of the chemical

reduction chamber is essential to understanding scale up feasibility. Hydrogen fuel cell vehicles travel roughly 70 miles per kilogram of hydrogen.[100] According to the Federal Highway Administration, the average American drives roughly 13,500 miles per year.[101] That means the average American vehicle would require 192 kg/yr or 0.022 kg/hr of hydrogen. The electrolytic production of hydrogen fuel will therefore require an average of 590 Amps current at all times per vehicle to be fueled. This is irrespective of what is being electrolyzed. This number creates great challenges and opportunities. Scaling up to the required size will be difficult and costly, but any voltage efficiencies gained will be multiplied over 590 Amps. Assuming 1.6 V for water electrolysis and 0.8 V for POM electrolysis the electrical demand is 944 Watts and 472 Watts respectively.

The highest steady state current achieved was 6.9 mA with POM concentration of 0.025 M, although concentrations of 0.5 M POM are possible. Assuming the reaction is first order in everything, 138mA are possible from a 0.5 M POM solution with 0.5 M glycerol. Much higher glycerol concentrations are also possible, assuming 5M glycerol would yield 1.38 A from a 50 mL reactor. This is based on the assumption that the possibly suspect assumption that the reaction is first order in glycerol. In this ideal situation, a 56 gallon tank containing $3000 worth of molybdenum is required per vehicle. That is based on the molybdenum spot price of $15 per kg.[49]

Conclusions and Future Work

This section is regarded as the most critical for the development of a biomass to hydrogen electrolysis system. The previous chapters 4 and 5 have shown that the Keggin polyoxometalate phosphomolybdic acid can be used as a suitably reversible depolarized anode. The potential is higher than may be desired but still provides a significant benefit over water oxidation.

This chapter has explored relative activities of polyoxometalates and additives, but absolute rates have not been studied. The k' values need to be transformed into k values, to allow further generalization of their results. It is also recommended to examine the reaction rates as the substrate is consumed; do the oxidation products react at the same rate as the glycerol?

While we do not have this portion solved, the reaction rates are quite low. Iron, vanadium, and hydrochloric acid are the most effective promoters studied but they do not push the reaction to sufficient rates for commercialization based on our analysis above. Previous literature had focused on proving the reaction of POM with organics occurred and understanding the mechanism. Most authors did not discuss the rate of reaction. Previous researchers had also conducted their studies in water or sulfuric acid, which we found to be inferior to hydrochloric acid.[38,39,52,53] Note also that the iron system may be significantly more economical than one based on molybdenum. We conclude that while the electrochemical kinetics may be sufficient to run the POM based fuel cell, unless faster reaction rates can be achieved this system is not particularly promising.

CHAPTER 7

Conclusion

This thesis focused on the exploration of systems useful for the anode depolarized, electrochemical production of hydrogen. Methanol was examined as an initial surrogate. The work then shifted to a relatively novel system, polyoxometalate mediated oxidation of biomass. To understand the performance of the polyoxometalate we broke it down into three areas, intrinsic electrochemical properties, zero gap cell performance, and reaction with complex substrate molecules.

The use of methanol as a substrate for the anode depolarized production of hydrogen is a complicated proposition. Over 1 V savings can be achieved vs the water electrolysis system, resulting in lowered electrical demand. Nonetheless the proposed benefit of methanol electrolysis vs DMFCs was mitigation of the challenges posed by crossover. Some of the prior literature had indicated a relative insensitivity to crossover in electrolysis systems. [32] We have shown a significant contribution of cathode polarization to whole cell polarization in methanol electrolysis. We have also shown a sensitivity of cathode polarization to methanol concentration. Taken together, these two attributes show that methanol crossover is contributing to the voltage loss in a methanol electrolyzer. Considering that the crossover issue is not significantly improved, it may make more sense to proceed with DMFC development over methanol electrolysis since liquid methanol is much easier to handle than hydrogen. However, in the context of this effort, the methanol tests simply served as a jumping off point to indicate possible issues.

When we moved to the phosphomolybdic acid system, we noticed that the intrinsic electrochemical properties of phosphomolybdic acid have not been studied since many modern electrochemical techniques were developed. Cyclic voltammetry was performed to understand the locations of relevant redox peaks and their reversibility. Multiple (3) redox peaks were observed in the potential range of interest. The first redox peak of phosphomolybdic acid was determined to be a 2 electron, quasi-reversible reaction in this medium. It was also shown that this peak splits into what is believed to be 2, 1 electron reactions as the solution is bulk reduced. Whether the cause of this bulk reduction is chemical or electrochemical, the separation of the two peaks still occurs. Despite this solution reaction, the anolyte solution was shown to be stable over many cycles, a fundamental requirement for use in an eventual production system.

An average diffusion coefficient was calculated for the 2 electron reduced species of phosphomolybdic acid as $D = 2 * 10^{-6} e^{0.0214T(\text{°C})} \frac{cm^2}{Sec}$. This diffusion coefficient is in the same range as other small molecules such as vanadium yet the solubility is only $1/6^{th}$ that of vanadium, leading to significantly worse mass transport characteristics. However, this is partly offset by the two electron reaction and by the fact that the POM is being used as a mediator, for which the concentration requirements may be less critical than they are in a battery.

Any program to make use of an aqueous phosphomolybdic acid system is expected to require the use of the zero-gap electrochemical cell architecture used in redox flow batteries and fuel cells. We have successfully applied the model of

zero gap cells, employing a NAFION membrane, hydrophilic, high surface area carbon electrodes, and flow-fields to maximize efficiency. We also studied the effect of supporting acids on current density and exchange current densities. In the unsupported phosphomolybdic acid solutions, electrode kinetics was found to be the limiting factor. Unsupported exchange current densities were as low as 1.37 mA/cm^2. The transition to 5 molar HCl supporting electrolyte resulted in 35x increase in exchange current densities. The optimum conditions tested were 80 ℃ and 5M HCl which showed a 110x increase in exchange current density over the unsupported 35 ℃ system. This massive improvement will be beneficial for the variety of biomass oxidation systems and time shifted water electrolysis systems which have been proposed. Further optimization of operating conditions and materials selection are still warranted but it has been shown that the system is feasible for anode oxidation in a flow battery cell.

Most authors describing these systems have noted a lack of crossover of POM species when using a NAFION membrane. They used UV-Vis or visual inspection to determine this. Those authors were using H-cells or different operating conditions. We noted visible crossover during electrochemical cell testing and decided to use an electrochemical detector to track the crossover of these species. The diffusion coefficient of phosphomolybdic acid in NAFION is on the same order as vanadium (D=10^{-7} $\frac{cm^2}{Sec}$) which is known to have significant crossover issues. In this case, the lower concentration will be of substantial benefit in operation. A

better understanding of the issues related to POM crossover will be needed as this system becomes more developed.

The final piece of the puzzle is obtaining sufficient reaction rates with a suitable renewable substrate. Glycerol was chosen for this study as a relatively simple molecule which is available at the appropriate scale and price. Researchers had shown that molecules with similar characteristics may be oxidized by POM based compounds. To the best of our knowledge, no researchers have studied aqueous oxidation of glycerol by POM compounds.

We tested 5 catalyst combinations, dissolved in water, 5 M H_2SO_4 and 5 M HCl for their ability to oxidize glycerol. The iron and vanadium complexes consistently showed the highest reaction rates, as did the HCl electrolyte. The highest performing combination was $V\text{-}PMo_{12}O_{40}$ supported in 5 M HCl. The most optimistic projections require a 211 L tank with 105.5 mol $V\text{-}PMo_{12}O_{40}$, to fuel an average vehicle. That is roughly $3000 worth of molybdenum, $300 of vanadium and a negligible amount of phosphorus. While this adds significant space and capital cost to a hydrogen production system, the greatly decreased electrical requirements may make this system worthy of further investigation. These projections rely on the assumption of first order kinetics in the glycerol oxidation process, an assumption which is only weakly supported at this time.

Future Direction

As an early stage exploration of phosphomolybdic acid based electrolyzers, this work leaves much to future researchers. We have largely established the

electrochemical viability of this system. The key issue remaining to determining viability is the oxidation rates of organic substrates. The reaction rates and k' values calculated are based on an assumed reaction order. K' values are transformed into k values by repeating the experiment across a variety of concentrations for the unchanging constituents. Product characterization should also be performed on the highest activity combinations to better understand the reaction and to track the reaction progress through the depletion of the substrate.

A large number of variations are possible to increase reaction rates in this type of system. Keggin ion based ionic liquids, additional co-catalysts, different or more concentrated acids, different substrates, ultrasonic stirring, and solar activation are all likely methods to further increase reaction rates.

While cell design is already sufficient for basic operation, higher surface area electrodes and thinner membranes are expected to further improve cell performance. Further understanding the relationship between supporting electrolytes and kinetics will also be useful to optimize cell performance. From a cost perspective, the option of uncharged dialysis or porous membranes instead of NAFION may be worthy of investigation. These membranes work on a size exclusion principle rather than a charge exclusion principle but phosphomolybdates are large molecules so this may be viable. Porous membranes have been applied successfully in vanadium systems, for example. Crossover will also need to be understood in both systems to allow for continued

performance over time. One method which was anecdotally successful in mitigation of crossover was periodic flushing of the cathode with DI water.

REFERENCES

1. Climate Change: Vital Signs of the Planet: Effects. Available at: http://climate.nasa.gov/effects/. (Accessed: 26th December 2016)

2. Grid Energy Storage. (2013).

3. Mench, M. M. *Fuel Cell Engines.* (John Wiley & Sons, 2007).

4. Report of the Hydrogen Production Expert Panel: A Subcommittee of the Hydrogen & Fuel Cell Technical Advisory Committee. Available at: http://www.hydrogen.energy.gov/pdfs/hpep_report_2013.pdf.

5. Hydrogen Highways Are Becoming Realities In California | Popular Science. Available at: http://www.popsci.com/hydrogen-highway-becoming-reality-california.

6. Amazon's Fuel-Cell Play Echoes Its Strategy in Cloud Computing | Greentech Media. Available at: https://www.greentechmedia.com/articles/read/Amazons-Fuel-Cell-Play-Echoes-Its-Strategy-in-Cloud-Computing. (Accessed: 18th April 2017)

7. Cheng, X. *et al.* A review of PEM hydrogen fuel cell contamination: Impacts, mechanisms, and mitigation. *J. Power Sources* **165,** 739–756 (2007).

8. Thomas, C. Fuel options for the fuel cell vehicle: hydrogen, methanol or gasoline? *Int. J. Hydrogen Energy* **25,** 551–567 (2000).

9. THOMAS, C. Affordable hydrogen supply pathways for fuel cell vehicles. *Int. J. Hydrogen Energy* **23,** 507–516 (1998).

10. Weber, A. Z. *et al.* Redox flow batteries: a review. *J. Appl. Electrochem.* **41,** 1137–1164 (2011).

11. Grigoriev, S. A., Millet, P., Porembsky, V. I. & Fateev, V. N. Development and preliminary testing of a unitized regenerative fuel cell based on PEM technology. *Int. J. Hydrogen Energy* **36,** 4164–4168 (2011).

12. Bents, D. J. *et al.* Hydrogen-Oxygen PEM Regenerative Fuel Cell Development at the NASA Glenn Research Center. (2005).

13. Mittelsteadt, C. Regenerative Fuel Cells for Energy Storage. (2011).

14. Wang, Y., Leung, D. Y. C., Xuan, J. & Wang, H. A review on unitized regenerative fuel cell technologies, part-A: Unitized regenerative proton exchange membrane fuel cells. *Renew. Sustain. Energy Rev.* **65,** 961–977 (2016).

15. Ursua, A., Gandia, L. M. & Sanchis, P. Hydrogen Production From Water Electrolysis: Current Status and Future Trends. *Proc. IEEE* **100,** 410–426 (2012).

16. Gases - Explosion and Flammability Concentration Limits. Available at: http://www.engineeringtoolbox.com/explosive-concentration-limits-

d_423.html. (Accessed: 5th June 2017)

17. Carmo, M., Fritz, D. L., Mergel, J. & Stolten, D. A comprehensive review on PEM water electrolysis. *Int. J. Hydrogen Energy* **38,** 4901–4934 (2013).

18. Russell, J. H., Nuttall, L. J. & Fickett, A. P. Hydrogen generation by solid polymer electrolyte water electrolysis. *Am. Chem. Soc. Div. …* (1973).

19. Rohland, B., Eberle, K., Ströbel, R., Scholta, J. & Garche, J. Electrochemical hydrogen compressor. *Electrochim. Acta* **43,** 3841–3846 (1998).

20. Inc), L. L. E. Electrochemical Hydrogen Compresso. (2012). Available at: http://www.hydrogen.energy.gov/pdfs/review12/pd048_lipp_2012_o.pdf.

21. Marshall, A. T., Sunde, S., Tsypkin, M. & Tunold, R. Performance of a PEM water electrolysis cell using IrxRuyTazO2 electrocatalysts for the oxygen evolution electrode. *Int. J. Hydrogen Energy* **32,** 2320–2324 (2007).

22. Periodic Table of Elements: Iridium - Ir (EnvironmentalChemistry.com). Available at: http://environmentalchemistry.com/yogi/periodic/Ir.html.

23. *2012 Minerals Yearbook: PLATINUM-GROUP METALS.* (2012).

24. Caravaca, A. *et al.* Electrochemical reforming of ethanol–water solutions for pure H2 production in a PEM electrolysis cell. *Int. J. Hydrogen Energy* **37,** 9504–9513 (2012).

25. Shamsul, N. S., Kamarudin, S. K., Rahman, N. A. & Kofli, N. T. An overview on the production of bio-methanol as potential renewable energy. *Renew. Sustain. Energy Rev.* **33,** 578–588 (2014).

26. Iwasita, T. in *Handbook of Fuel Cells – Fundamentals, Technology and Applications(*ed. Wolf Vielstich Arnold Lamm, H. A. G.) (John Wiley & Sons, 2003).

27. Gasteiger, H. A., Markov&, N., Ross, P. N. & Cairns, E. J. Methanol Electrooxidation on Well-Characterized Pt-Ru Alloys. *J. Phys. Chem* **97,** 12020–12029 (1993).

28. XX55 MADE IN THE USA EXTREME MOBILE POWER FOR DEMANDING APPLICATIONS.

29. FCT - Fuel Cell Technologies - DMFC. Available at: http://www.fuelcelltoday.com/technologies/dmfc. (Accessed: 21st May 2017)

30. Mayyas, A., Wei, M., Chan, S. H. & Lipman, T. Fuel Cell Forklift Deployment in the U.S.

31. Take, T., Tsurutani, K. & Umeda, M. Hydrogen production by methanol–water solution electrolysis. *J. Power Sources* **164,** 9–16 (2007).

32. Cloutier, C. R. & Wilkinson, D. P. Electrolytic production of hydrogen from

aqueous acidic methanol solutions. *Int. J. Hydrogen Energy* **35,** 3967–3984 (2010).

33. Hydrogen generation by electrolysis of aqueous organic solutions. (2002).

34. Ayers, K. E. *et al.* Research Advances Towards Low Cost, High Efficiency PEM Electrolysis. doi:10.1149/1.3484496

35. Song, J., Fan, H., Ma, J. & Han, B. Conversion of glucose and cellulose into value-added products in water and ionic liquids. *Green Chem.* **15,** 2619 (2013).

36. Deng, W., Zhang, Q. & Wang, Y. Polyoxometalates as efficient catalysts for transformations of cellulose into platform chemicals. *Dalton Trans.* **41,** 9817–31 (2012).

37. Liu, W., Mu, W. & Deng, Y. High-Performance Liquid-Catalyst Fuel Cell for Direct Biomass-into-Electricity Conversion. *Angew. Chemie* **126,** 13776–13780 (2014).

38. Liu, W. *et al.* Solar-induced direct biomass-to-electricity hybrid fuel cell using polyoxometalates as photocatalyst and charge carrier. *Nat. Commun.* **5,** 3208 (2014).

39. Sarma, B. B. *et al.* Polyoxometalate-mediated electron transfer-oxygen transfer oxidation of cellulose and hemicellulose to synthesis gas. *Nat.*

Commun. **5,** 4621 (2014).

40. Catalytic formation of carbon monoxide (co) and hydrogen (h2) from biomass. (2014).

41. Sadakane and Eberhard Steckhan., M. 'Electrochemical properties of polyoxometalates as electrocatalysts.' *Chem. Rev.* 219–238 (1998).

42. Symes, M. D. & Cronin, L. Decoupling hydrogen and oxygen evolution during electrolytic water splitting using an electron-coupled-proton buffer. *Nature chemistry* **5,** 403–409 (2013).

43. Bloor, L. G. *et al.* Solar-Driven Water Oxidation and Decoupled Hydrogen Production Mediated by an Electron-Coupled-Proton Buffer. *J. Am. Chem. Soc.* **138,** 6707–6710 (2016).

44. Gu, C. & Shannon, C. Investigation of the photocatalytic activity of TiO2–polyoxometalate systems for the oxidation of methanol. *J. Mol. Catal. A Chem.* **262,** 185–189 (2007).

45. Ozer, R. R. & Ferry, J. L. Investigation of the Photocatalytic Activity of TiO 2 −Polyoxometalate Systems. *Environ. Sci. Technol.* **35,** 3242–3246 (2001).

46. Kim, W. B., Voitl, T., Rodriguez-Rivera, G. J. & Dumesic, J. A. Powering fuel cells with CO via aqueous polyoxometalates and gold catalysts.

Science **305,** 1280–1283 (2004).

47. Carson, R. & Bremer, B. Mediated electrochemical oxidation process used as a hydrogen fuel generator. (2003).

48. *U.S. Geological Survey, Mineral Commodity Summaries, January 2015.* (2015).

49. Molybdenum Prices and Molybdenum Price Charts - InvestmentMine. Available at: http://www.infomine.com/investment/metal-prices/molybdenum-oxide/. (Accessed: 18th June 2017)

50. 85% Phosphoric Acid Food Grade - Buy 85% Phosphoric Acid,Phosphoric Acid,Phosphoric Acid Food Grade Product on Alibaba.com. Available at: https://www.alibaba.com/product-detail/85-phosphoric-acid-food-grade_60630571994.html?s=p. (Accessed: 19th June 2017)

51. Tsigdinos, G. A. & Hallada, C. J. Molybdovanadophosphoric acids and their salts. I. Investigation of methods of preparation and characterization. *Inorg. Chem.* **7,** 437–441 (1968).

52. Neumann, R. Activation of Molecular Oxygen, Polyoxometalates, and Liquid-Phase Catalytic Oxidation. *Inorg. Chem.* **49,** 3594–3601 (2010).

53. Khenkin, A. M. & Neumann, R. Oxidative C−C Bond Cleavage of Primary Alcohols and Vicinal Diols Catalyzed by $H_5PV_2Mo_{10}O_{40}$ by an Electron

Transfer and Oxygen Transfer Reaction Mechanism. *J. Am. Chem. Soc.*
130, 14474–14476 (2008).

54.   Yang, Z. *et al.* Electrochemical Energy Storage for Green Grid.
doi:10.1021/cr100290v

55.   Condon, N., Klemick, H. & Wolverton, A. Working Paper Series Impacts of
Ethanol Policy on Corn Prices: A Review and Meta-Analysis of Recent
Evidence. (2008).

56.   How much gasoline does the United States consume? - FAQ - U.S. Energy
Information Administration (EIA). Available at:
https://www.eia.gov/tools/faqs/faq.cfm?id=23&t=10. (Accessed: 30th
December 2016)

57.   Quispe, C. A. G., Coronado, C. J. R. & Carvalho Jr., J. A. Glycerol:
Production, consumption, prices, characterization and new trends in
combustion. *Renew. Sustain. Energy Rev.* **27,** 475–493 (2013).

58.   Pagliaro, M., Ciriminna, R., Kimura, H., Rossi, M. & Della Pina, C. From
Glycerol to Value-Added Products. *Angew. Chemie Int. Ed.* **46,** 4434–4440
(2007).

59.   Soares, R. R., Simonetti, D. A. & Dumesic, J. A. Glycerol as a Source for
Fuels and Chemicals by Low-Temperature Catalytic Processing. *Angew.
Chemie Int. Ed.* **45,** 3982–3985 (2006).

60. The Soap and Detergent Association. Glycerine: an overview.

61. Colella, W. G., James, B. D., Moton Nrel, J. M., Saur, G. & Ramsden, T. Techno-economic Analysis of PEM Electrolysis for Hydrogen Production. (2014).

62. Anderson, E. Cost Reduction Strategies for PEM Electrolysis.

63. Compton, Richard G., Banks, C. E. *Understanding Voltammetry*. (Imperial College Press, 2010).

64. Amanda Quiroga. Cyclic Voltammetry - Chemistry LibreTexts. Available at: https://chem.libretexts.org/Core/Analytical_Chemistry/Instrumental_Analysis/Cyclic_Voltammetry. (Accessed: 26th June 2017)

65. Subject: Square Wave Voltammetry.

66. Aaron, D., Tang, Z., Papandrew, A. B. & Zawodzinski, T. A. Polarization curve analysis of all-vanadium redox flow batteries. *J. Appl. Electrochem.* **41,** 1175–1182 (2011).

67. Duffy, M. Fuel Cell System Cost for Transportation-2008 Cost Estimate (Revised), Independent Review, Published for the U.S. Department of Energy Hydrogen Program (Book). (2009).

68. Chong, L. *et al.* Investigation of Oxygen Reduction Activity of Catalysts Derived from Co and Co/Zn Methyl-Imidazolate Frameworks in Proton

Exchange Membrane Fuel Cells. *ChemElectroChem* **3,** 1541–1545 (2016).

69. Gogel, V. *et al.* Performance and methanol permeation of direct methanol fuel cells: dependence on operating conditions and on electrode structure. *J. Power Sources* **127,** 172–180 (2004).

70. Wilson, M. S. & Gottesfeld, S. Thin-film catalyst layers for polymer electrolyte fuel cell electrodes. *J. Appl. Electrochem.* **22,** 1–7 (1992).

71. Li, G. & Pickup, P. G. Measurement of single electrode potentials and impedances in hydrogen and direct methanol PEM fuel cells. *Electrochim. Acta* **49,** 4119–4126 (2004).

72. Skúlason, E. *et al.* Modeling the Electrochemical Hydrogen Oxidation and Evolution Reactions on the Basis of Density Functional Theory Calculations. *J. Phys. Chem. C* **114,** 18182–18197 (2010).

73. DOE Technical Targets for Polymer Electrolyte Membrane Fuel Cell Components | Department of Energy. Available at: https://energy.gov/eere/fuelcells/doe-technical-targets-polymer-electrolyte-membrane-fuel-cell-components. (Accessed: 27th May 2017)

74. Tsigdinos, G. A. & Hallada, C. J. Synthesis and electrochemical properties of heteropolymolybdates. *Journal of the Less Common Metals* **36,** 79–93 (1974).

75. CONTRIBUTION TO THE CHEMISTRY OF PHOSPHOMOLYBDIC ACIDS, PHOSPHOTUNGSTIC ACIDS, AND ALLIED SUBSTANCES. BY HSEIN WU. (Prom the Biochemical Laboratory oj Harvard Medical School, Boston.) (Received for publication, June 10, 1920.) . Available at: http://www.jbc.org/content/43/1/189.full.pdf. (Accessed: 2nd February 2016)

76. Hallada, C. J., Tsigdinos, G. A. & Hudson, B. S. Molybdovanadophosphoric acids and their salts. II. Investigation of solution properties. *J. Phys. Chem.* **72,** 4304–4307 (1968).

77. Tsigdinos, G. a. Heteropoly compounds of molybdenum and tungsten. *Topics in Current Chemistry* **76,** 1–64 (1978).

78. Kelly, R. Analytical electrochemistry, basic concepts. Available at: http://www.asdlib.org/onlineArticles/ecourseware/Kelly_Potentiometry/EC_CONCEPTS1.HTM. (Accessed: 6th February 2017)

79. Matencio, T., Pernaut, J. M. & Vieil, E. Analysis of hysteresis phenomenon as observed from voltammetric data of conducting polymers: part I. *J. Braz. Chem. Soc.* **14,** 90–96 (2003).

80. Rongfeng, Z. & Evans, D. H. The current for a two-electron reaction is not necessarily twice that of a one-electron reaction. *J. Electroanal. Chem.* **385,** 201–207 (1995).

81. Sakai, M. & Ohnaka, N. Kinetics of the Second Charge Transfer Step in an EE Mechanism by Rotating Ring-Disk Electrode Voltammetry. *J. Electrochem. Soc.* **137,** 576 (1990).

82. Treimer, S., Tang, A. & Johnson, D. C. A Consideration of the Application of Koutecký-Levich Plots in the Diagnoses of Charge-Transfer Mechanisms at Rotated Disk Electrodes. *Electroanalysis* **14,** 165 (2002).

83. Zhao, X. & Zhu, J. Y. Efficient Conversion of Lignin to Electricity Using a Novel Direct Biomass Fuel Cell Mediated by Polyoxometalates at Low Temperatures. *ChemSusChem* **9,** 197–207 (2016).

84. Rausch, B., Symes, M. D., Chisholm, G. & Cronin, L. Decoupled catalytic hydrogen evolution from a molecular metal oxide redox mediator in water splitting. *Science* **345,** 1326–30 (2014).

85. Tang, A., Bao, J. & Skyllas-Kazacos, M. Studies on pressure losses and flow rate optimization in vanadium redox flow battery. *J. Power Sources* **248,** 154–162 (2014).

86. Ma, X., Zhang, H. & Xing, F. A three-dimensional model for negative half cell of the vanadium redox flow battery. *Electrochim. Acta* **58,** 238–246 (2011).

87. Yamamura, T., Watanabe, N., Yano, T. & Shiokawa, Y. Electron-Transfer Kinetics of Np[sup 3+]?Np[sup 4+], NpO[sub 2][sup +]?NpO[sub 2][sup 2+],

V[sup 2+]?V[sup 3+], and VO[sup 2+]?VO[sub 2][sup +] at Carbon Electrodes. *J. Electrochem. Soc.* **152,** A830 (2005).

88. Viswanathan, V. *et al.* Cost and performance model for redox flow batteries. *J. Power Sources* **247,** 1040–1051 (2014).

89. Electrode Kinetics 2 Background.

90. Pletcher, D. & Royal Society of Chemistry (Great Britain). *A first course in electrode processes.* (Royal Society of Chemistry, 2009).

91. JW Walkinshaw. *Air resistance of paper (Gurley method) (Revision of T 460 om-02).* (2006).

92. Plain Carbon Cloth - 1071 HCB. Available at: http://www.fuelcellstore.com/fuel-cell-components/gas-diffusion-layers/carbon-cloth/avcarb-1071-hcb. (Accessed: 18th May 2017)

93. Properties of SIGRACET ® GDL 34/35.

94. Sun, C., Chen, J., Zhang, H., Han, X. & Luo, Q. Investigations on transfer of water and vanadium ions across Nafion membrane in an operating vanadium redox flow battery. *J. Power Sources* **195,** 890–897 (2010).

95. Mylonas, A. & Papaconstantinou, E. Photocatalytic degradation of chlorophenols to CO2 and HCl with polyoxotungstates in aqueous solution. *J. Mol. Catal.* **92,** 261–267 (1994).

96. Reichert, J., Brunner, B., Jess, A., Wasserscheid, P. & Albert, J. Biomass oxidation to formic acid in aqueous media using polyoxometalate catalysts – boosting FA selectivity by in-situ extraction. *Energy Environ. Sci.* **8,** 2985–2990 (2015).

97. Zoski, C. G., Bond, A. M., Colyer, C. L., Myland, J. C. & Oldham, K. B. Near-steady-state cyclic voltammetry at microelectrodes. *J. Electroanal. Chem. Interfacial Electrochem.* **263,** 1–21 (1989).

98. Muradov, N. & T-Raissi, A. Solar Production of Hydrogen Using 'Self-Assembled' Polyoxometalate Photocatalysts. *J. Sol. Energy Eng.* **128,** 326 (2006).

99. Carrick, W. L., Reichle, W. T., Pennella, F. & Smith, J. J. Transition Metal Catalysts. II. Formation and Catalytic Activity of Organovanadium Compounds Formed by Interaction of Diphenylmercury and Vanadium Halides [1]. *J. Am. Chem. Soc.* **82,** 3887–3892 (1960).

100. 8 Things You Need To Know About Hydrogen Fuel-Cell Cars | Edmunds. Available at: https://www.edmunds.com/fuel-economy/8-things-you-need-to-know-about-hydrogen-fuel-cell-cars.html. (Accessed: 18th June 2017)

101. Average Annual Miles per Driver by Age Group. Available at: https://www.fhwa.dot.gov/ohim/onh00/bar8.htm. (Accessed: 18th June 2017)

APPENDIX
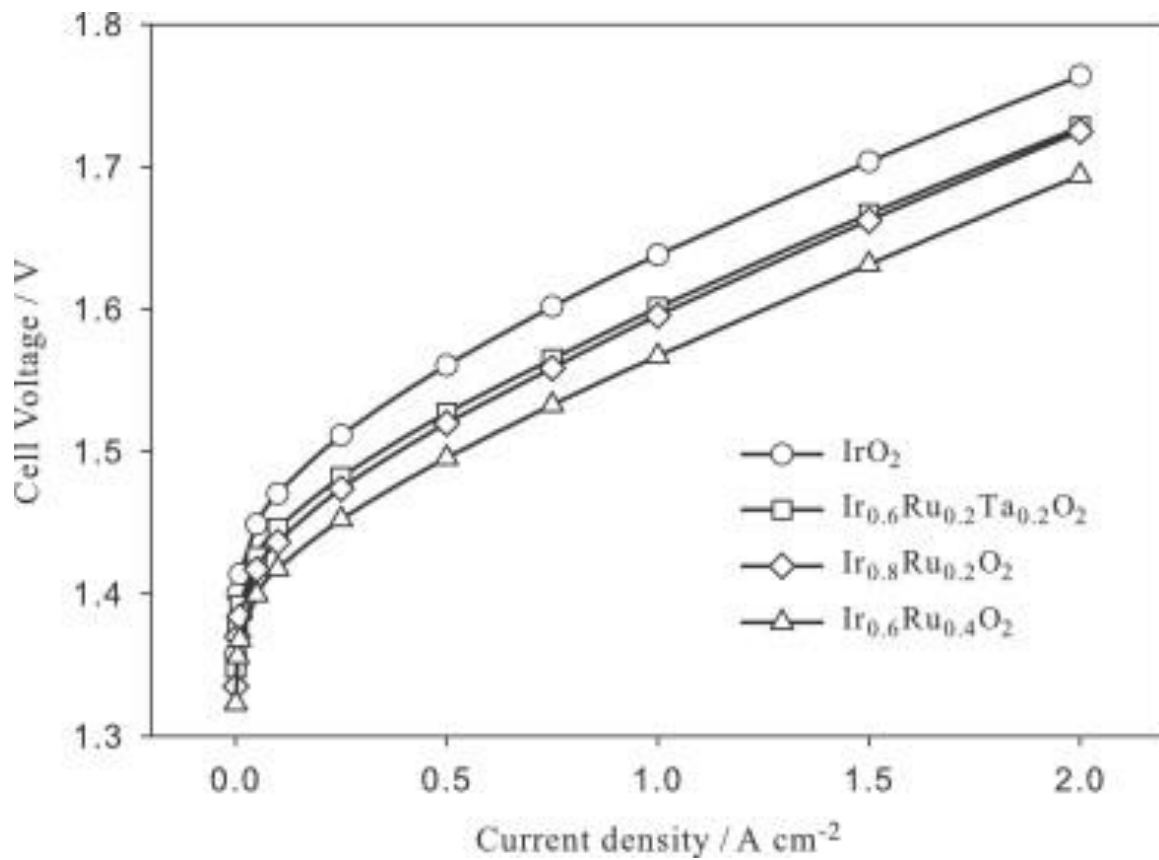
Figure 1: Performance of a PEM Water Electrolyzer With State of the Art Anodes

at 80 ℃ (Reproduced from Reference 21)
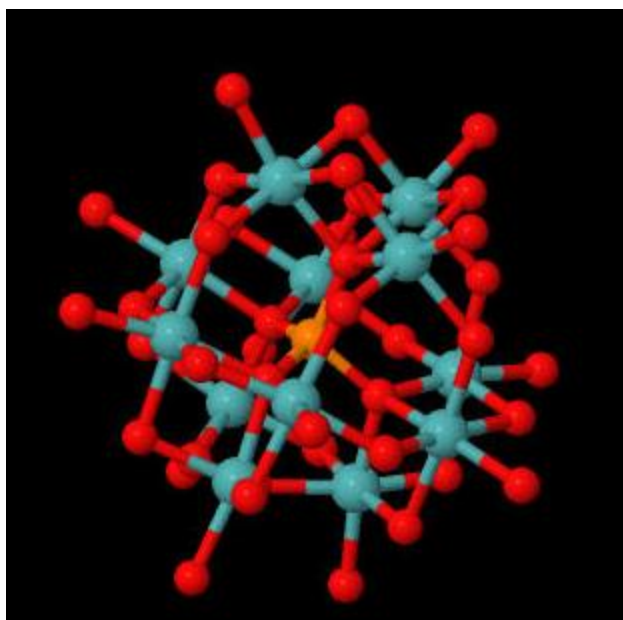
Figure 2: Keggin Ion
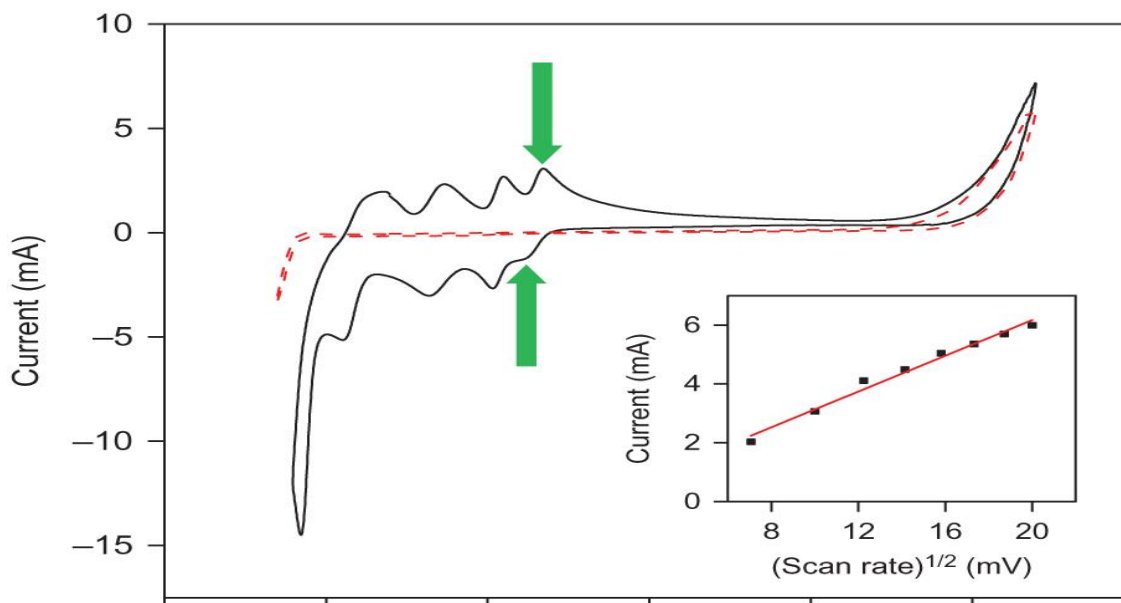
Figure 3: Cyclic Voltammetry (CV) of 0.5 M Phosphomolybdic Acid on a Pt

Electrode. (Reproduced from Reference 42)
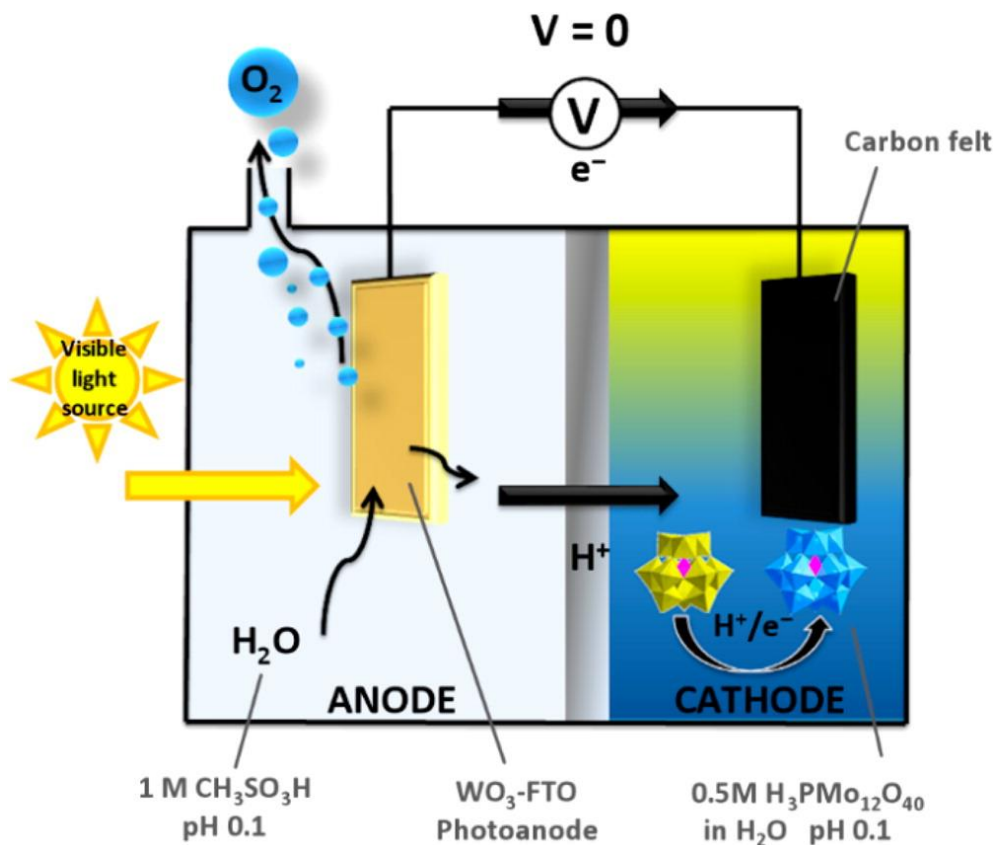
Figure 4: The system proposed by Bloor and Cronin whereby water is oxidized at the photoanode and the resulting hydrogen is stored in the polyoxometalate cathode. The polyoxometalate is then reoxidized electrochemically after the oxygen is no longer present. (Reproduced from Reference 43)
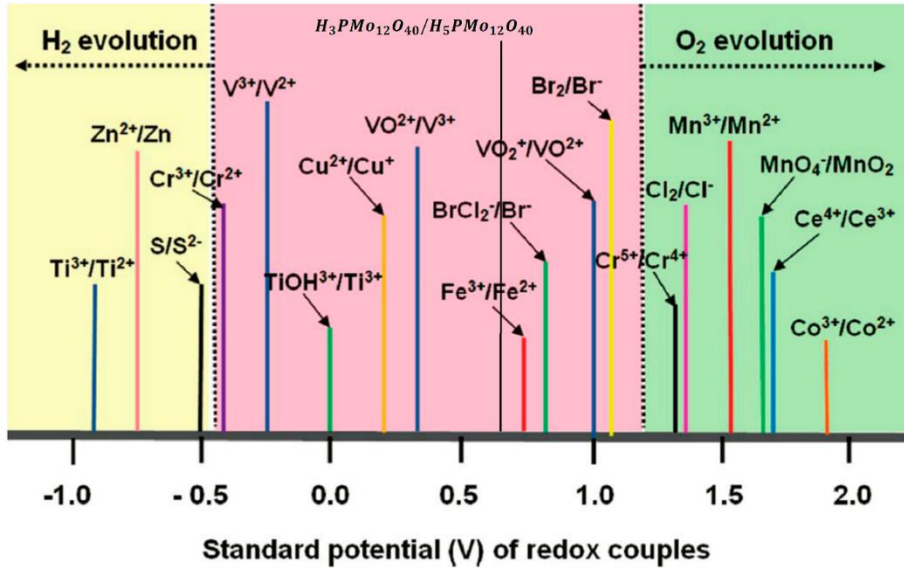
Figure 5: Table of Selected Redox Potentials(Reproduced from Reference 54)
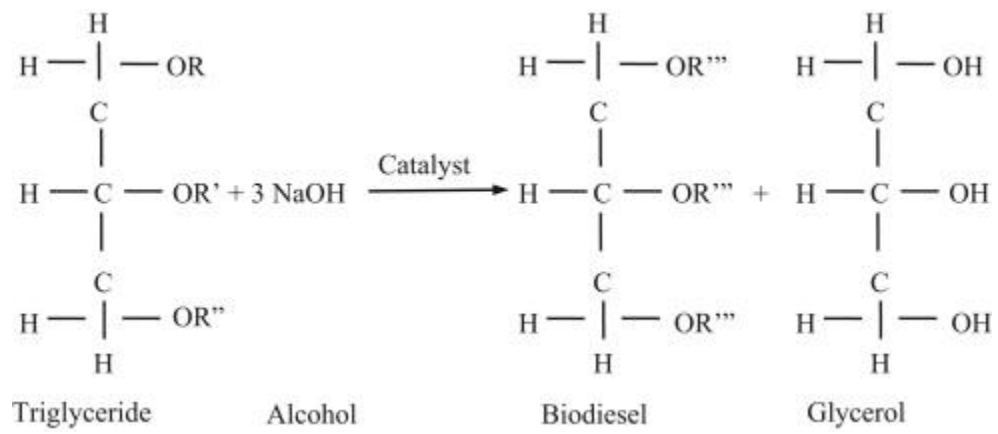
Figure 6: Production of Glycerol (Reproduced from Reference 57)
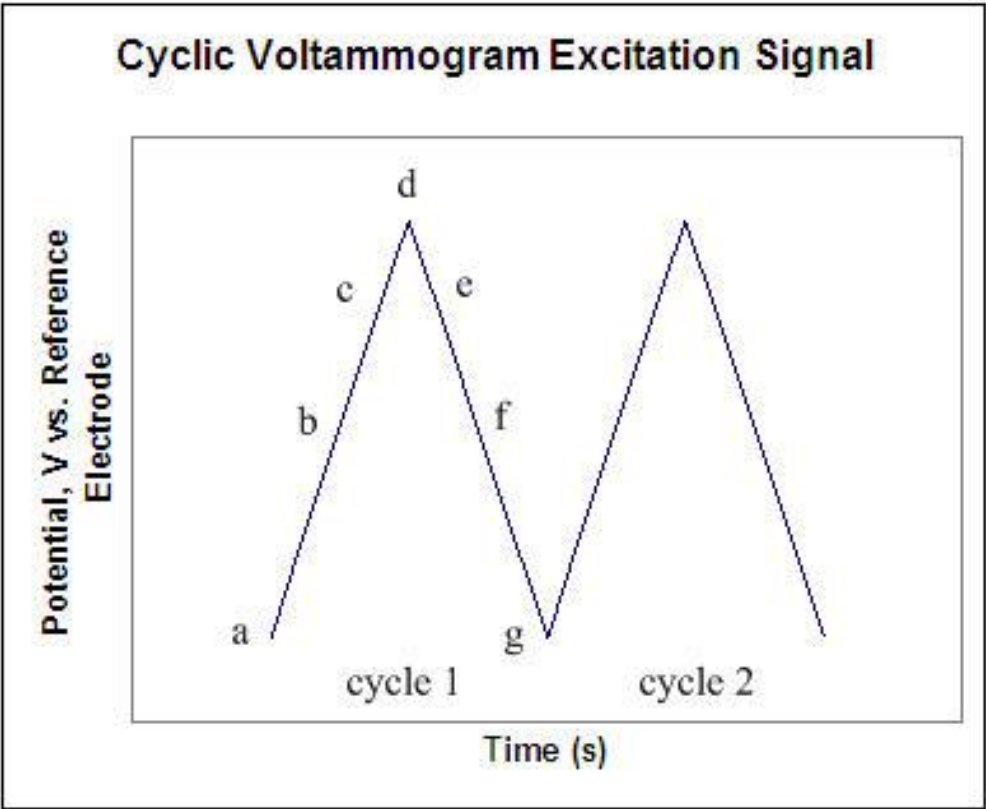
Figure 7: CV Potential Waveform (Reproduced from Reference 64)
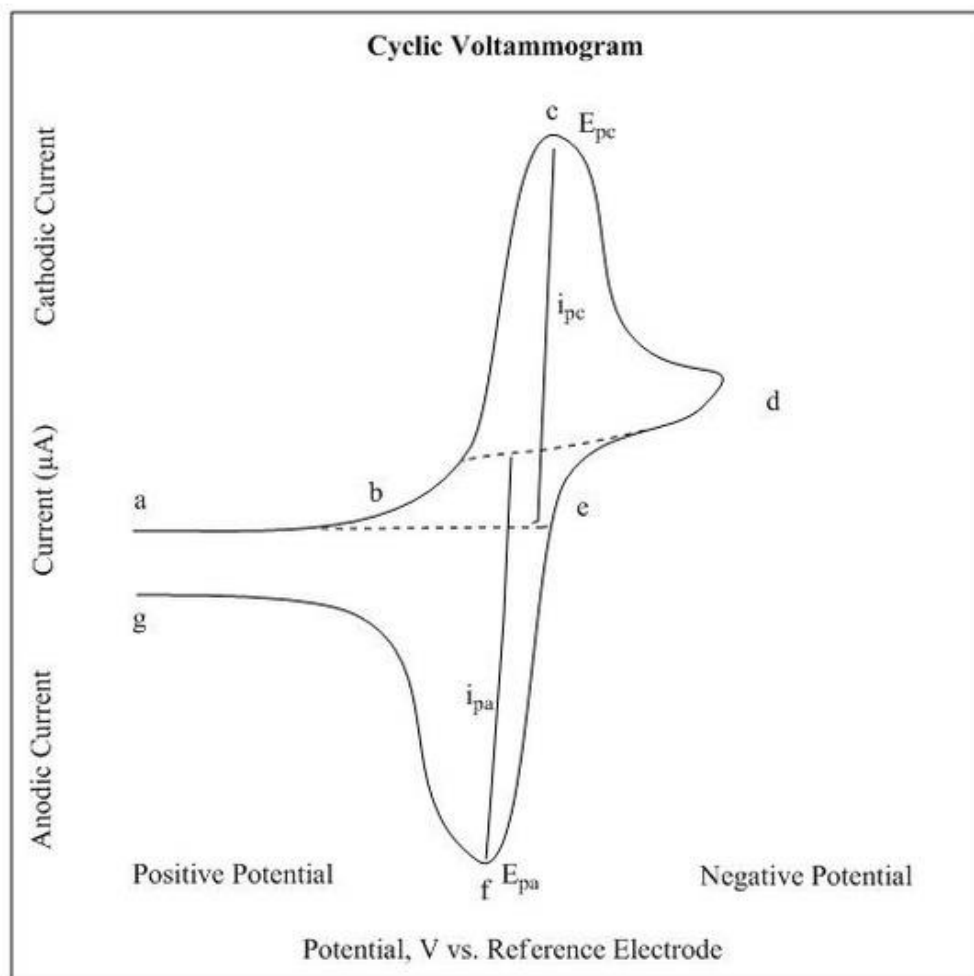
Figure 8: CV of a Single Electron Reduction-Oxidation (Reproduced from

Reference 64)
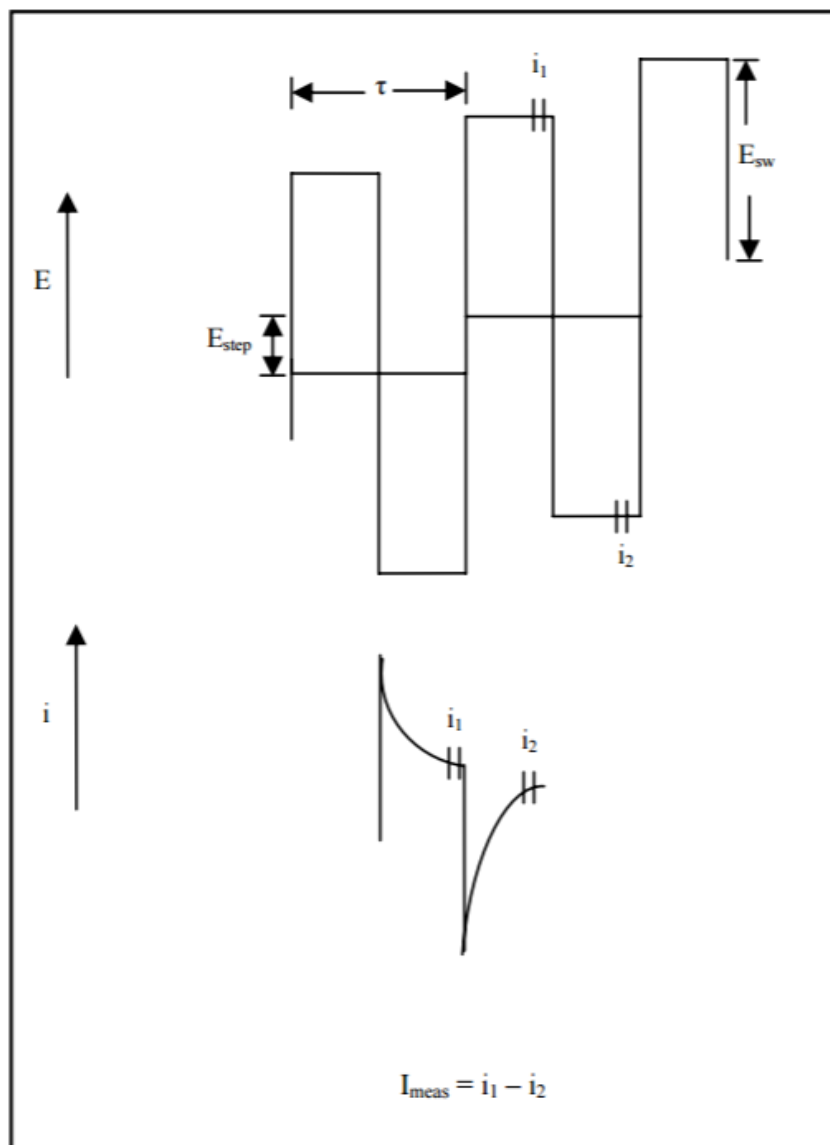
Figure 9: Square Wave Voltammetry Potential and Current Waveform

(Reproduced from Reference 65)
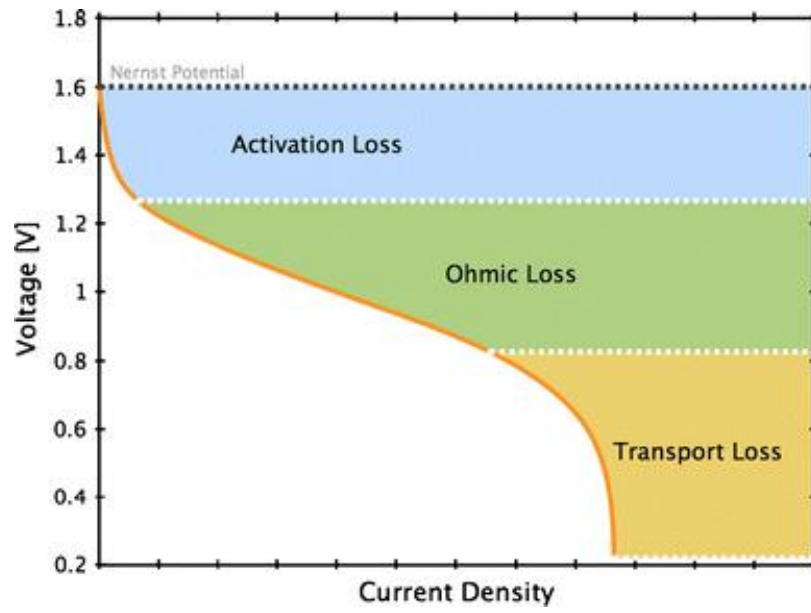
Figure 10: Generalized Polarization Curve (Reproduced from Reference 66)
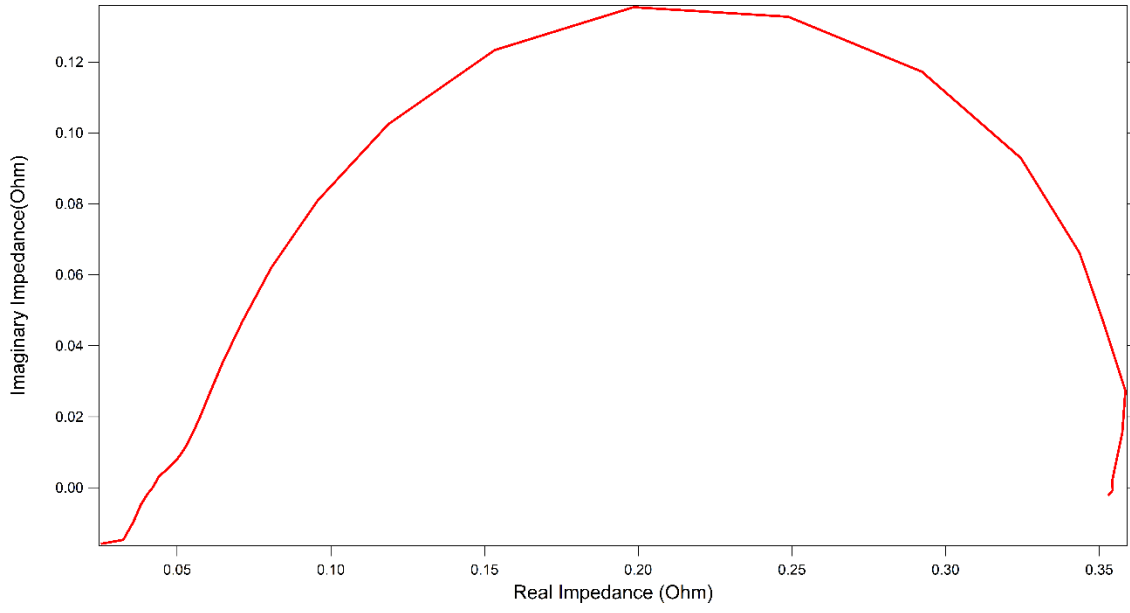
Figure 11: Nyquist Plot for a Fuel Cell
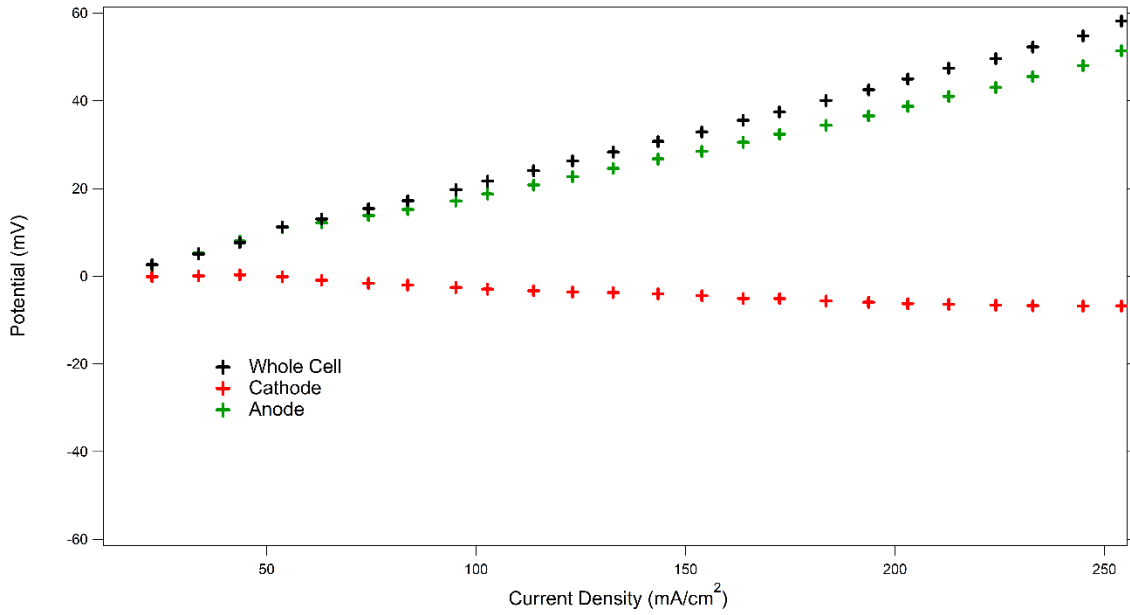
Figure 12: Hydrogen/Hydrogen Symmetric Cell, Anode: Pt/Ru 5.3 mg/cm^2,

Cathode: Pt 5.4 mg/cm2, Anode/Cathode Gas: Hydrogen, Flow-rate: 100 sccm,

Back pressure: 15 PSI, NAFION 117 Membrane, 80 ºC, Curves are not IR

Corrected, ASR 0.2 Ohm-cm^2
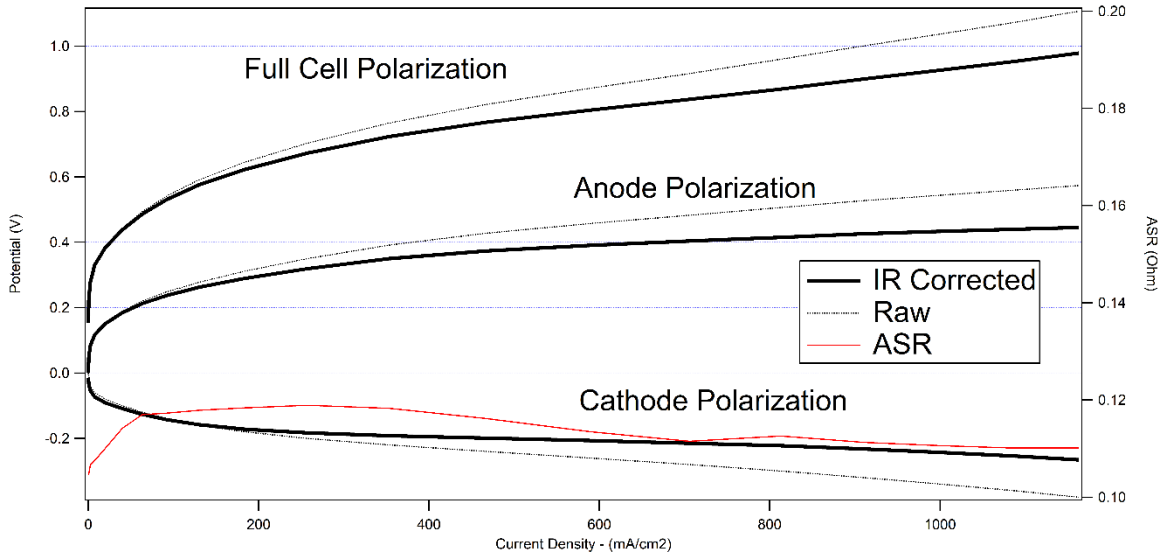
Figure 13: Effect of IR Compensation: Fuel 8M Methanol, Anode: Pt/Ru 2.9

mg/cm^2, Cathode: Pt 2.9 mg/cm^2, Cathode Gas: Argon, Flow-rate: 100 sccm,

Back pressure: 15 PSI, NAFION 117 Membrane, Curves are IR Corrected, 60 ºC,
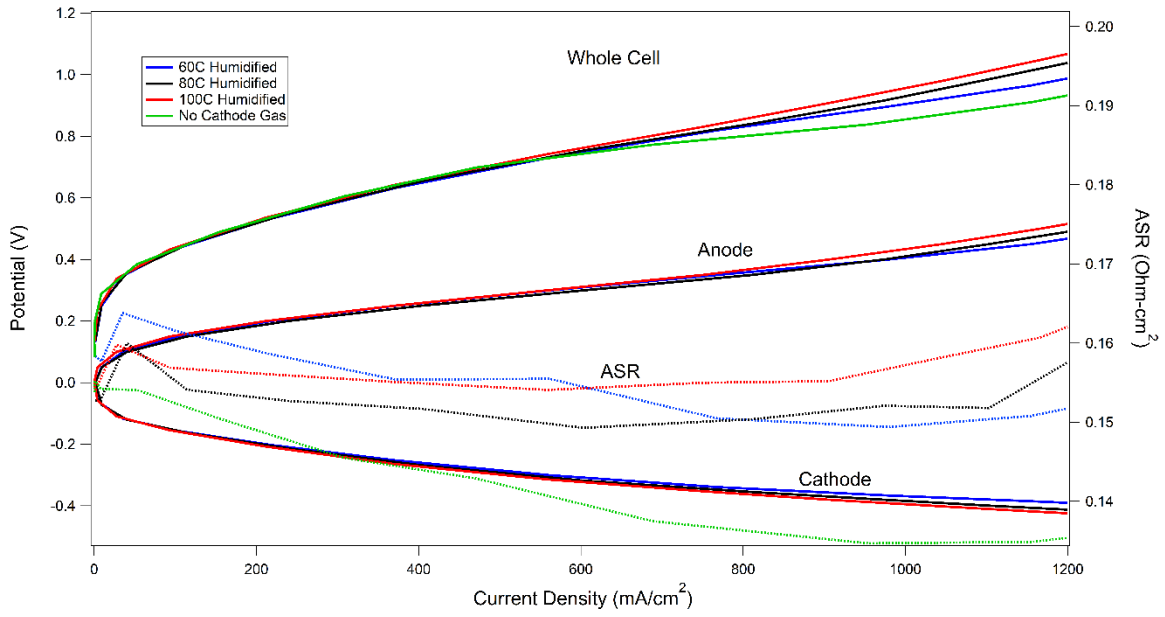
Figure 14: Fuel: 4 Molar MeOH, Anode: Pt/Ru 4.6 mg/cm2, Cathode: Pt 4.5 mg/cm2, Cathode Gas: Argon, Flow-rate: 100 sccm, Back pressure: 15 PSI, Temperature: 80 ⁰C, NAFION 117 Membrane, Curves are IR Corrected
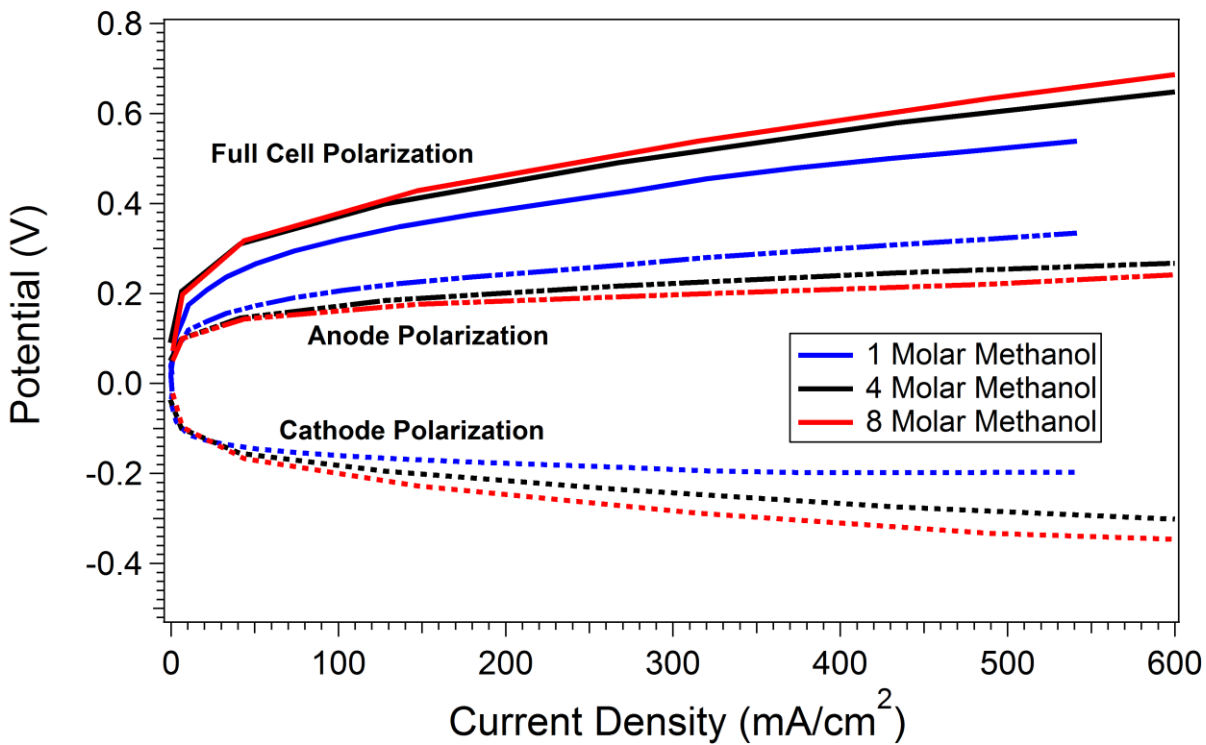
Figure 15: Fuel: MeOH, Anode: Pt/Ru 4.6 mg/cm^2, Cathode: Pt 4.5 mg/cm^2,

Cathode Gas: Argon, Flow-rate: 100 sccm, Back Pressure: 15 PSI, Temperature:

100 ºC, NAFION 117 Membrane, Curves are IR Corrected
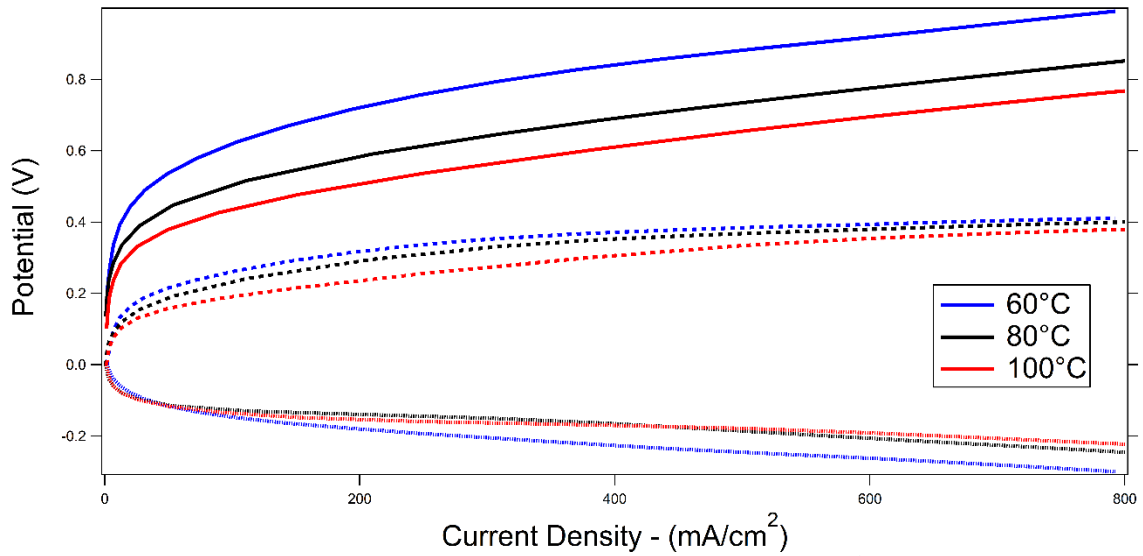
Figure 16: Fuel: 4 M Methanol, Anode: Pt/Ru 2.9 mg/cm^2, Cathode: Pt 2.9

mg/cm^2, Cathode Gas: Argon, Flow-rate: 100 sccm, Back pressure: 15 PSI,

NAFION 117 Membrane, Curves are IR Corrected, ASR < 0.2 Ohm-cm^2
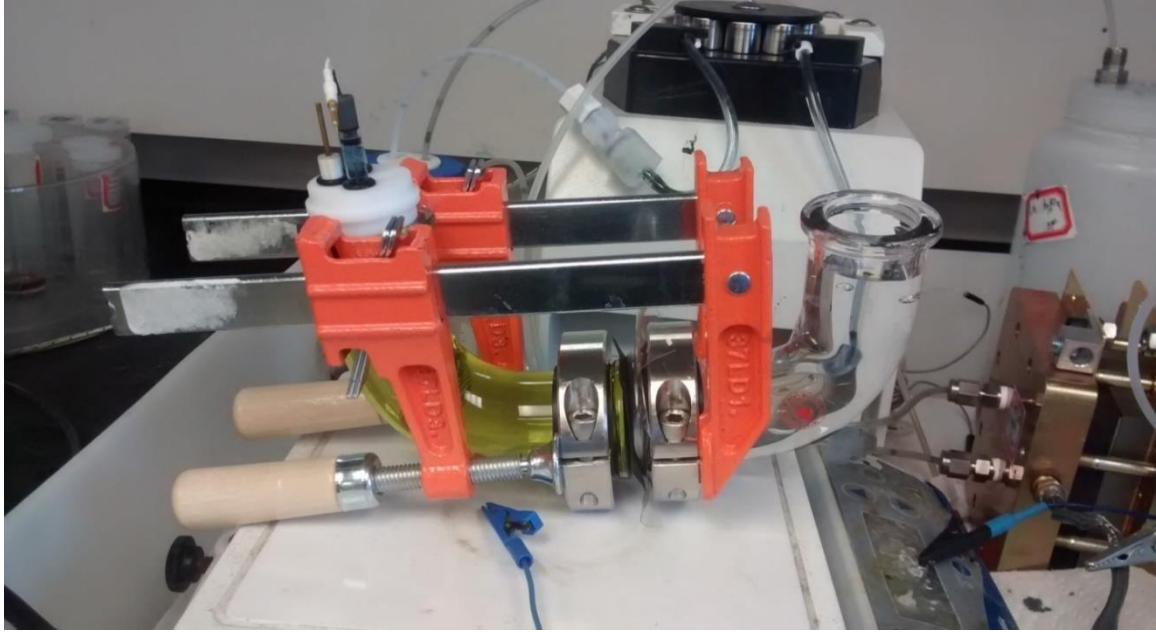
Figure 17: H-cell used for diffusion experiments with NAFION separator.
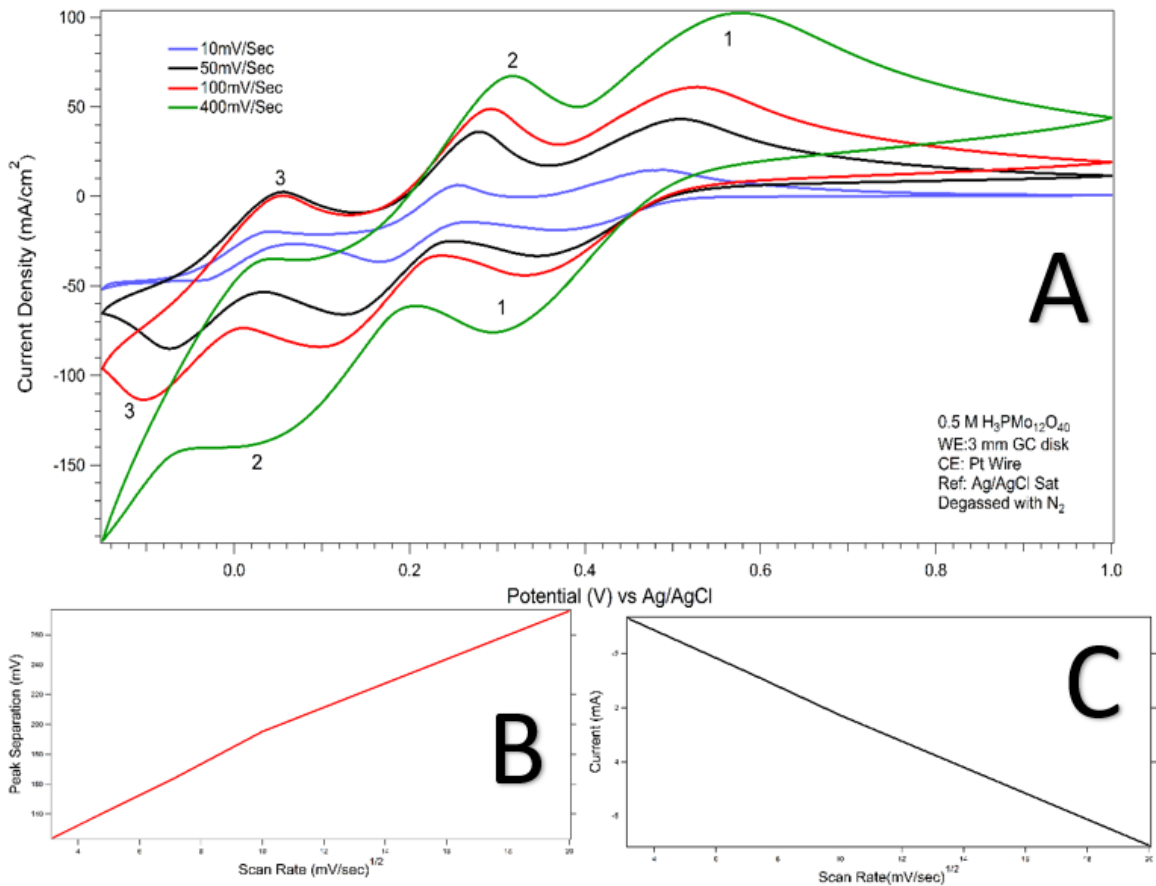
Figure 18: A: Cyclic Voltammetry of Phosphomolybdic Acid on Glassy Carbon. 0.5 M $H_3PMo_{12}O_{40}$, We: 3mm GC disk, Ce: Pt wire, Ref: Ag/AgCl (0.205 V vs NHE), T = 25 °C; B: Scan Rate vs E_p^{OX}-E_p^{RED} for Peak 1; C: Scan Rate vs Peak Current for Peak 1
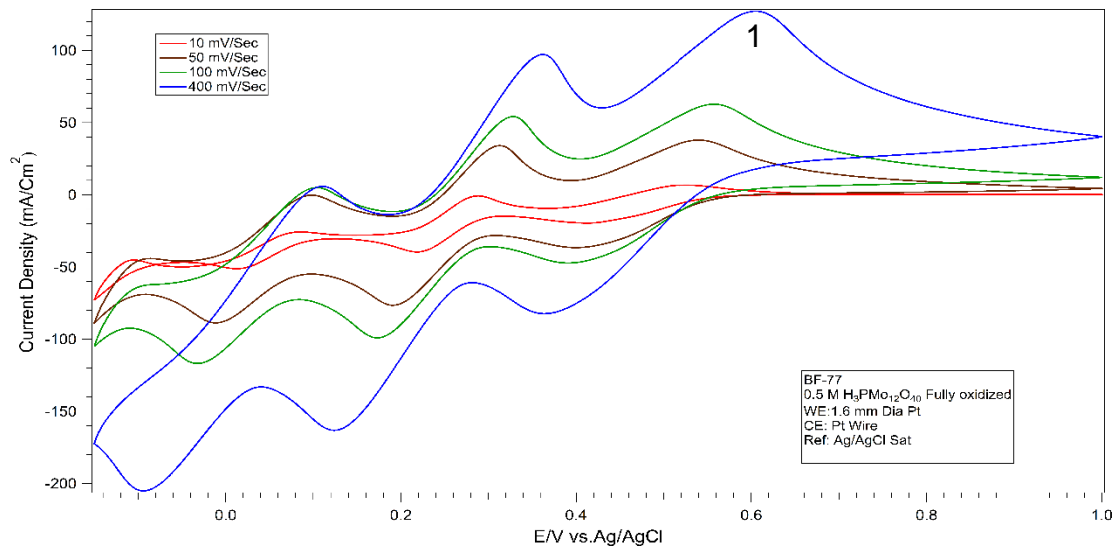
Figure 19: Cyclic Voltammetry of Phosphomolybdic Acid on Platinum. 0.5 M

H3PMo12O40, We: 1.6 mm Pt disk, Ce: Pt wire, Ref: Ag/AgCl (0.205 V vs NHE)
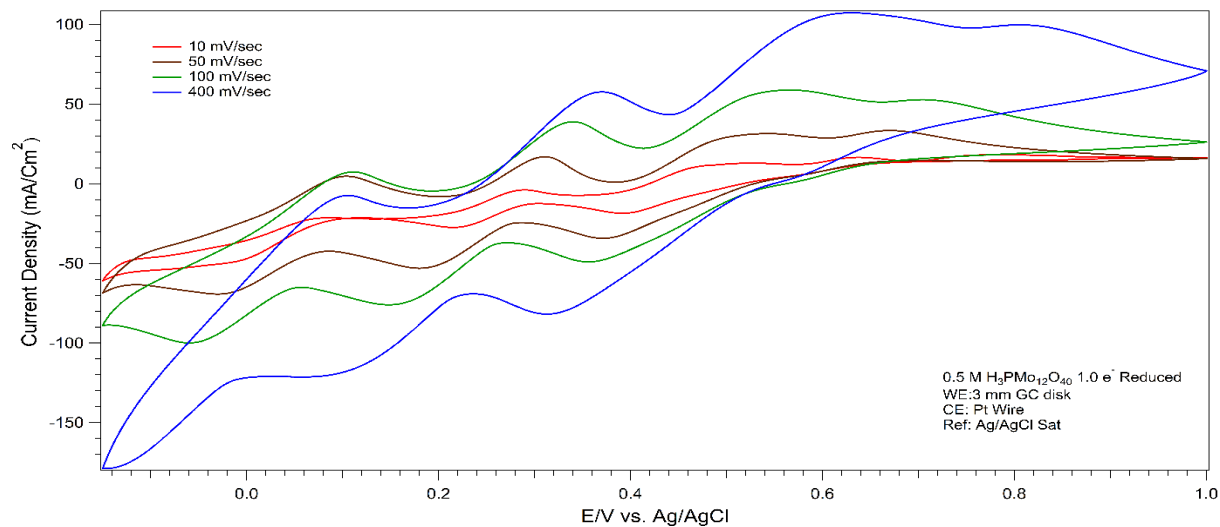
Figure 20: Cyclic Voltammetry of Phosphomolybdic Acid Bulk Reduced One

Electron. 0.25 M $H_3PMo_{12}O_{40}$/0.25 M $H_5PMo_{12}O_{40}$, We: 3mm GC disk, Ce: Pt

wire, Ref: Ag/AgCl (0.205 V vs NHE)
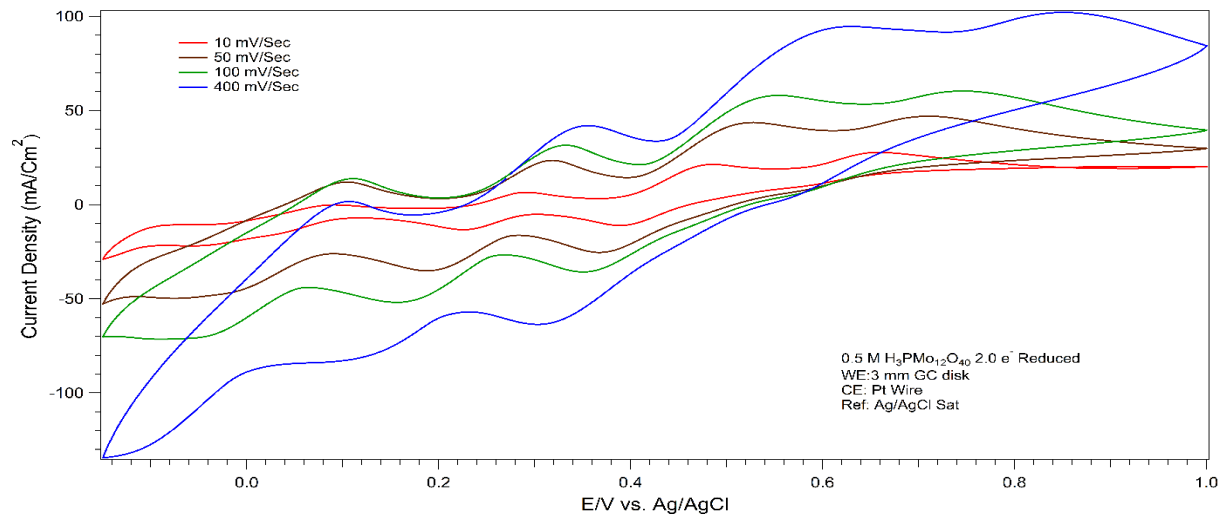
Figure 21: Cyclic Voltammetry of Phosphomolybdic Acid Bulk Reduced Two Electrons. 0.5 M $H_5PMo_{12}O_{40}$, We: 3mm GC disk, Ce: Pt wire, Ref: Ag/AgCl (0.205 V vs NHE)
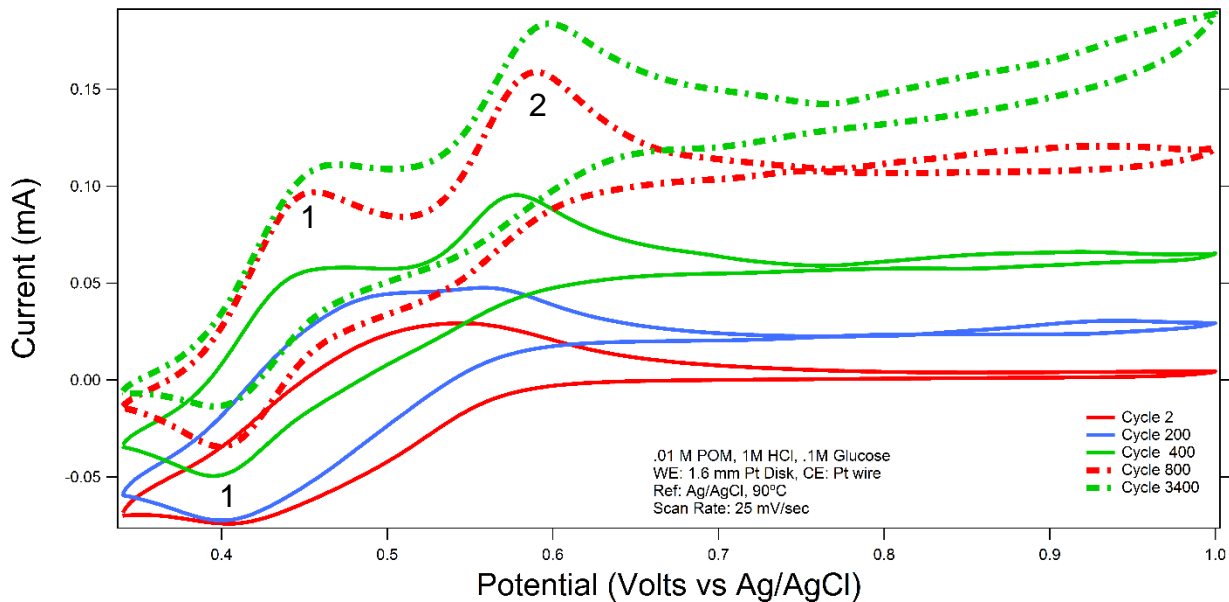
Figure 22: Repeated CV of Phosphomolybdic Acid During Bulk Reduction by
Glucose. 0.01 M $H_3PMo_{12}O_{40}$, 1M HCl, We: 1.6mm Pt disk, Ce: Pt wire, Ref:
Ag/AgCl (0.205 V vs NHE), 90℃, v = 25 mV/sec
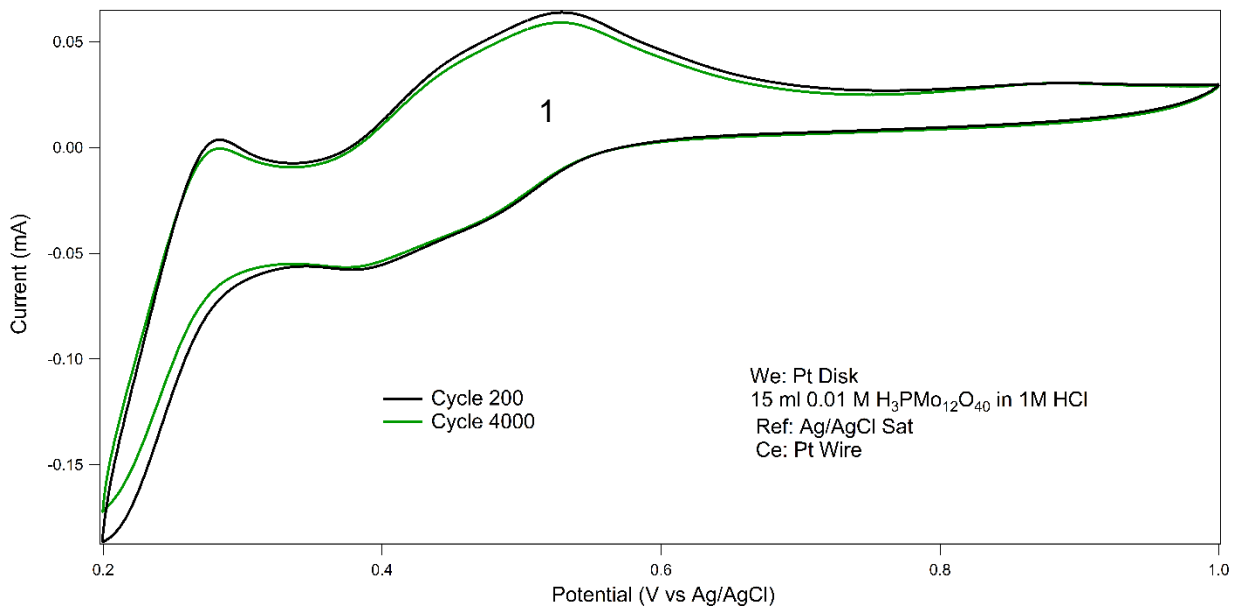
Figure 23: Repeated CV of Phosphomolybdic Acid. 0.01 M $H_3PMo_{12}O_{40}$, 1M HCl,

We: 1.6mm Pt disk, Ce: Pt wire, Ref: Ag/AgCl (0.205 V vs NHE), 90°C, v = 25

mV/sec
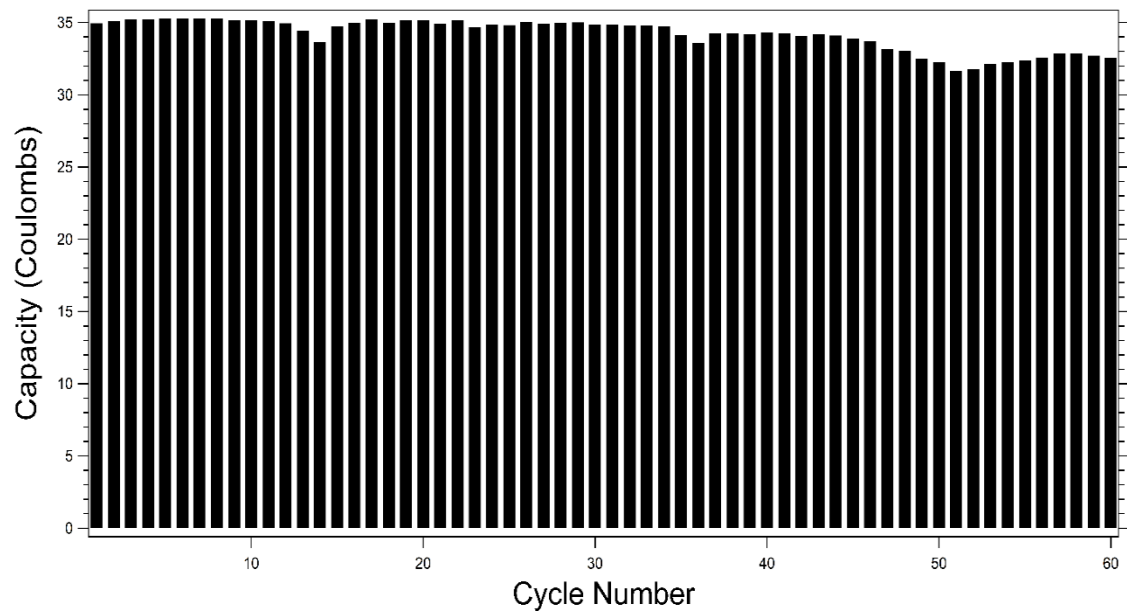
Figure 24: 2 Electron Potentiostatic Coulometry, 0.015 M $H_3PMo_{12}O_{40}$ in 1 M HCl.

An H-Cell with a NAFION divider was used. We: Pt mesh, Ce: Pt wire in 0.5 M

0.5 M H_2SO_4, Ref: Ag/AgCl. The voltage window was 0.35 to 0.8 V Vs Ag/AgCl
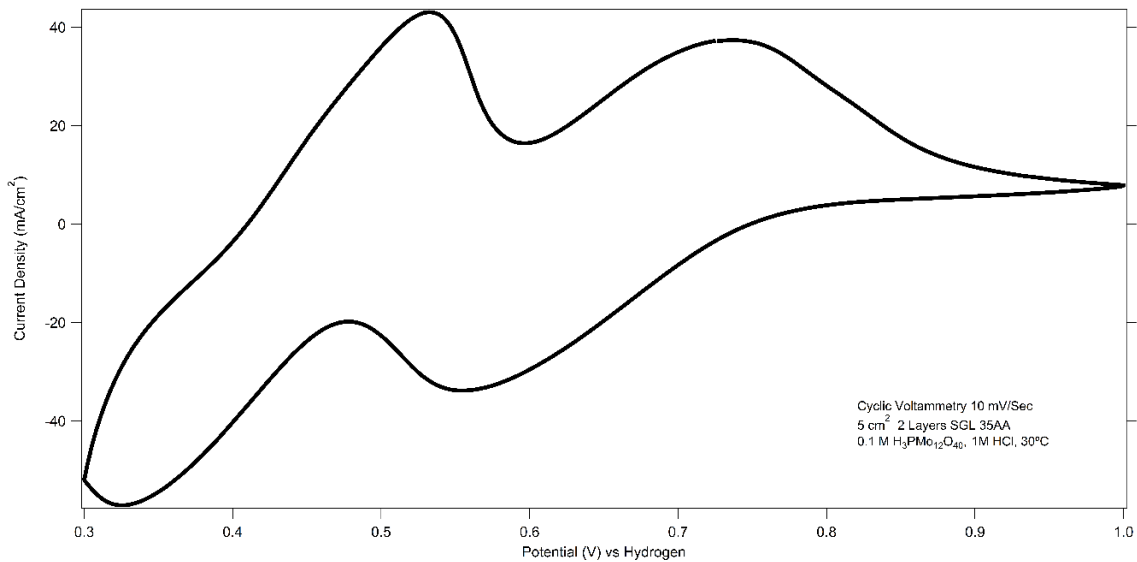
Figure 25: Thin layer voltammogram of phosphomolybdic acid supported in hydrochloric acid. This scan was performed in a flow battery type cell with the pump stopped and a hydrogen-Pt cathode. v:10 mV/Sec, We: 5 cm^2 SGL 35AA, Ce: H_2 on Pt, Anolyte: 0.1 M $H_3PMo_{12}O_{40}$ in 1M HCl, T: 30 ℃
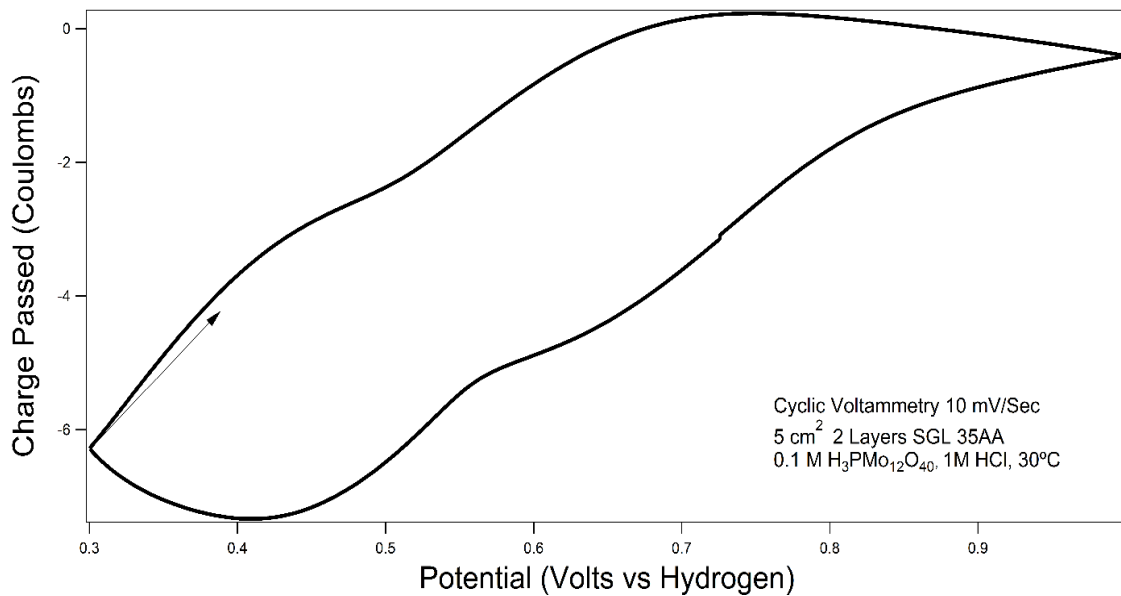
Figure 26: Charge Transferred in Thin layer voltammogram of phosphomolybdic acid supported in hydrochloric acid. This scan was performed in a flow battery type cell with the pump stopped and a hydrogen-Pt cathode. v:10 mV/Sec, We: 5 cm^2 SGL 35AA, Ce: H$_2$ on Pt, Anolyte: 0.1 M H$_3$PMo$_{12}$O$_{40}$ in 1M HCl, T: 30 ℃

Cyclic Voltammetry 10 mV/Sec
5 cm^2 2 Layers SGL 35AA
0.1 M H$_3$PMo$_{12}$O$_{40}$, 1M HCl, 30ºC
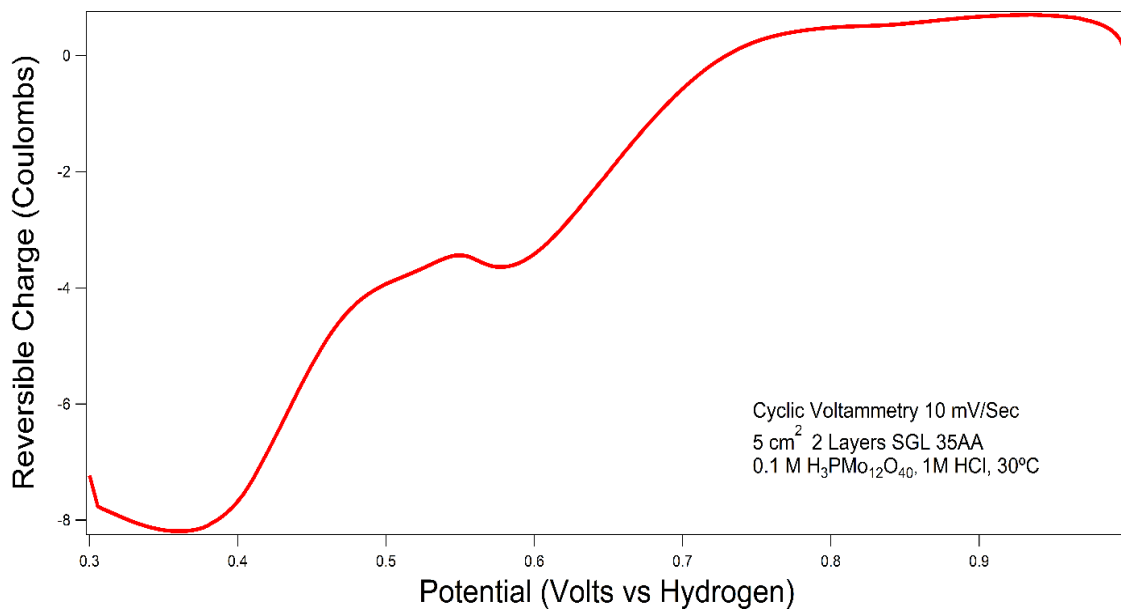
Figure 27: Reversible Component of Charge Transfer in a Thin layer

voltammogram of phosphomolybdic acid supported in hydrochloric acid. This

scan was performed in a flow battery type cell with the pump stopped and a

hydrogen-Pt cathode. v:10 mV/Sec, We: 5 cm^2 SGL 35AA, Ce: H$_2$ on Pt, Anolyte:

0.1 M H$_3$PMo$_{12}$O$_{40}$ in 1M HCl, T: 30 ℃
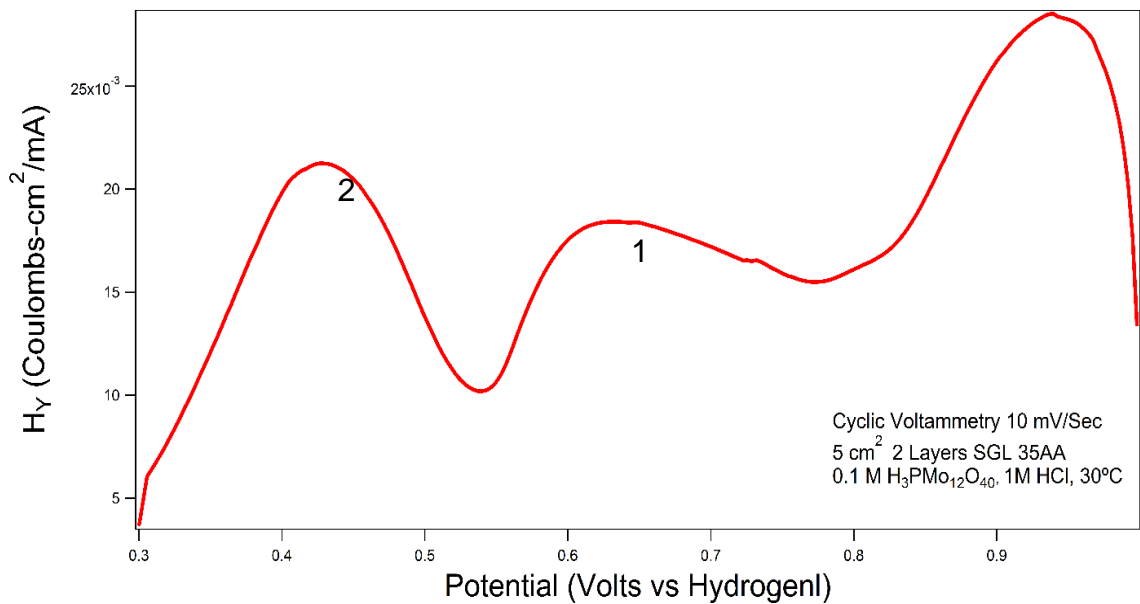
Figure 28: Kinetic Hysteresis in a Thin layer voltammogram of phosphomolybdic acid supported in hydrochloric acid. This scan was performed in a flow battery type cell with the pump stopped and a hydrogen-Pt cathode. v:10 mV/Sec, We: 5 cm^2 SGL 35AA, Ce: H$_2$ on Pt, Anolyte: 0.1 M H$_3$PMo$_{12}$O$_{40}$ in 1M HCl, T: 30 ℃
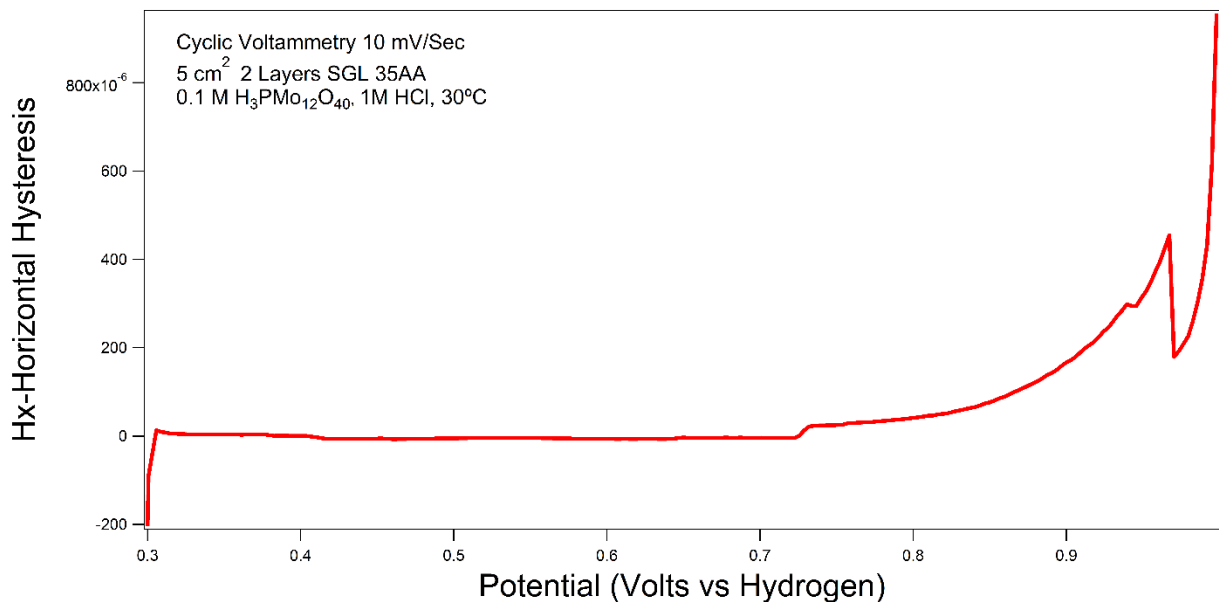
Figure 29: Impedance Contribution to the Hysteresis in a Thin layer voltammogram of phosphomolybdic acid supported in hydrochloric acid. This scan was performed in a flow battery type cell with the pump stopped and a hydrogen-Pt cathode. v:10 mV/Sec, We: 5 cm^2 SGL 35AA, Ce: H$_2$ on Pt, Anolyte: 0.1 M H$_3$PMo$_{12}$O$_{40}$ in 1M HCl, T: 30 ℃
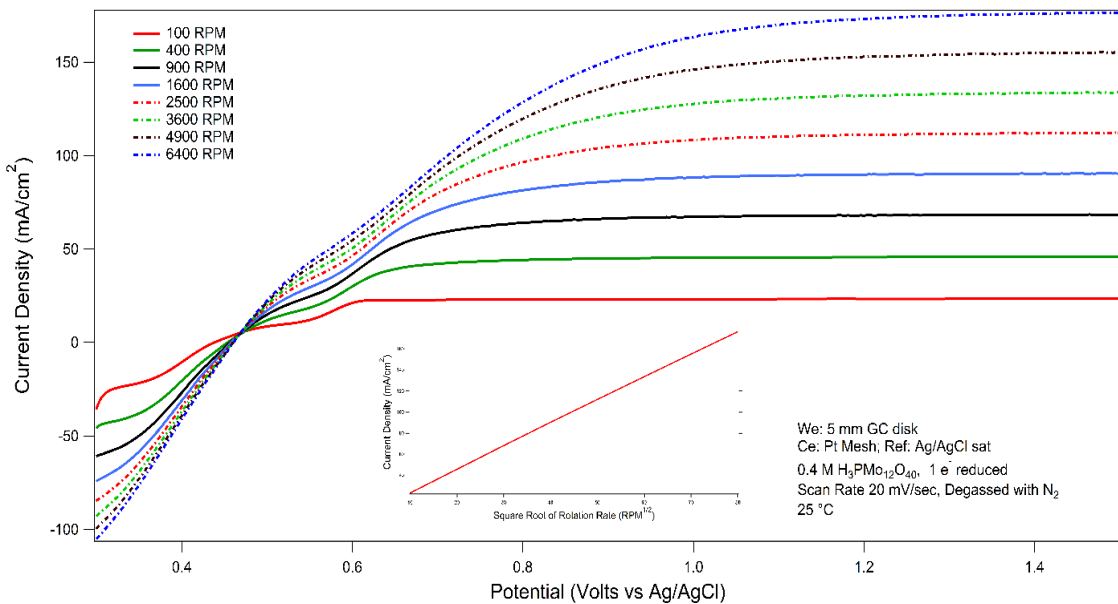
Figure 30: Effect of Rotation Rate on Rotating Disk Electrode Voltammograms.

0.2 M H$_3$PMo$_{12}$O$_{40}$/ 0.2 M H$_5$PMo$_{12}$O$_{40}$, v=20 mV/sec, We: 5mm GC disk, Ce: Pt

mesh, Ref Ag/AgCl (0.205 V vs NHE), T=25℃, Levich Plot at 1.5 V vs Ag/AgCl
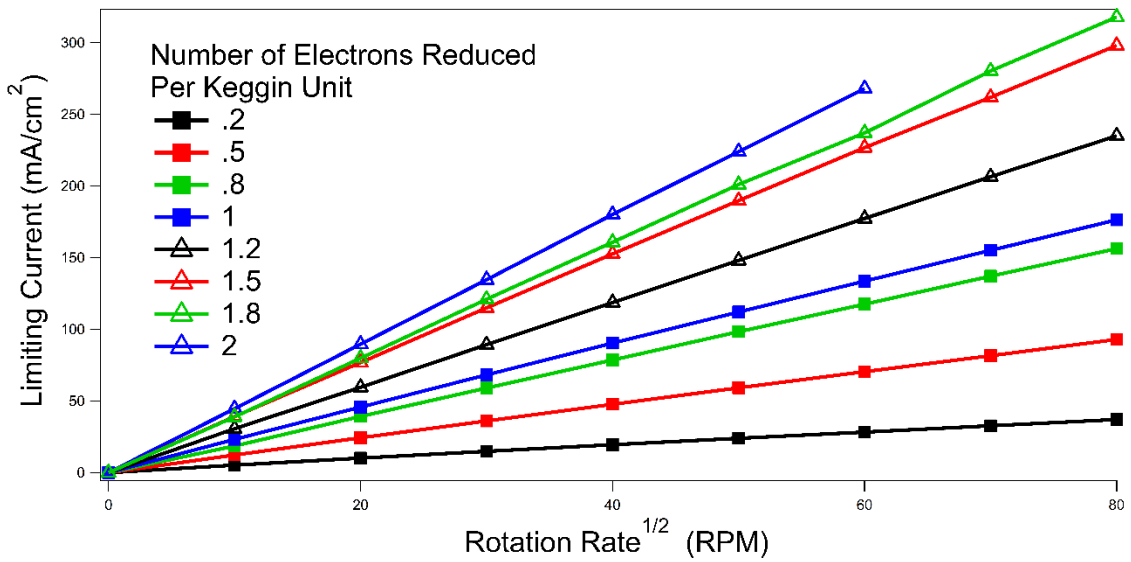
Figure 31: Levich Plot of Phosphomolybdic Acid, V = 1.5 V vs Ag/AgCl, We: GC

disk, Ce: Pt mesh, REF: Ag/AgCl (0.205 V vs NHE)
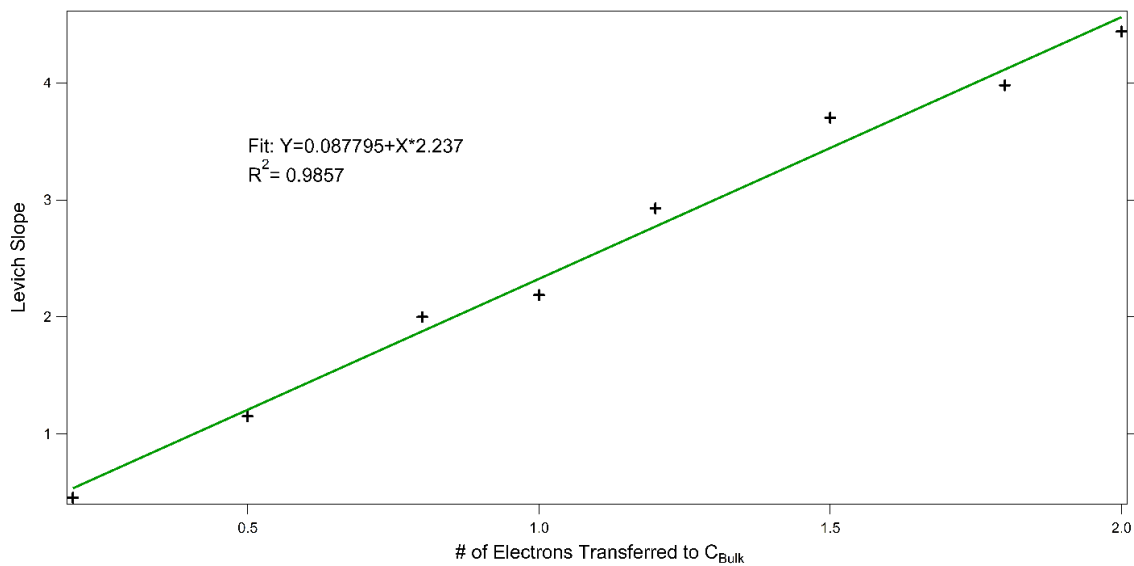
Figure 32: Effect of $H_3PMo_{12}O_{40}/H_5PMo_{12}O_{40}$ Ratio on the Levich Slope

Within the figure:

Fit: Y=0.087795+X*2.237
R^2= 0.9857

Levich Slope (y-axis)

# of Electrons Transferred to C_{Bulk} (x-axis)
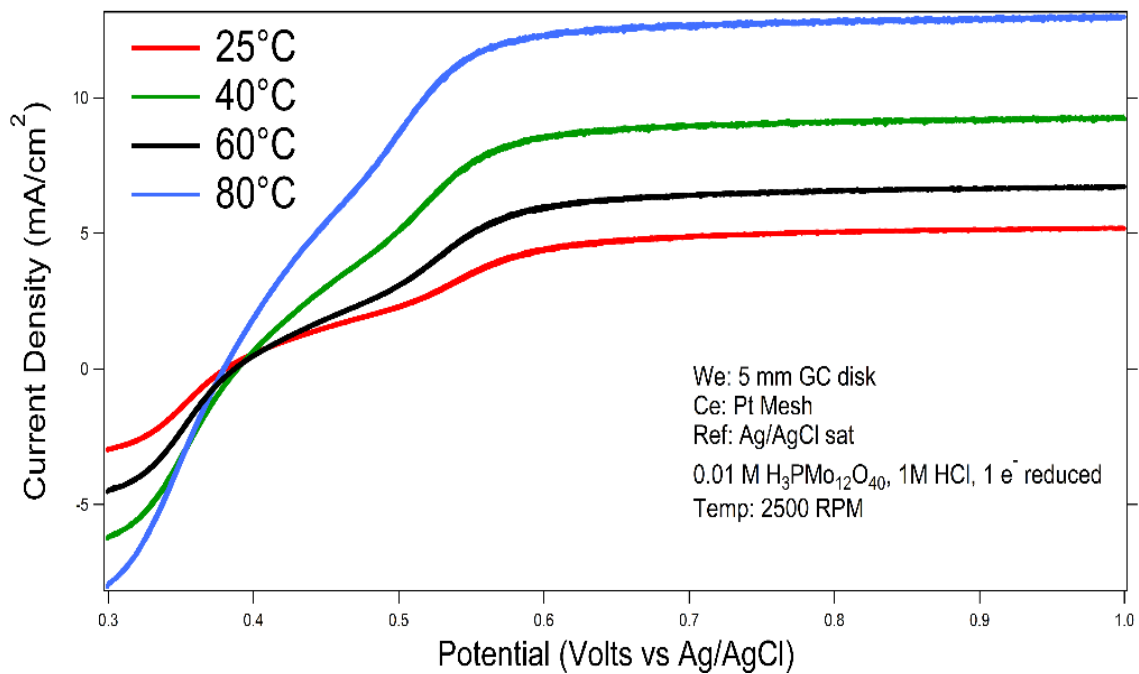
Figure 33: 0.2 M $H_3PMo_{12}O_{40}$/ 0.2 M $H_5PMo_{12}O_{40}$, v=20 mV/sec, We: 5mm GC

disk, Ce: Pt mesh, Ref Ag/AgCl (0.205 V vs NHE), ω: 2500 RPM;
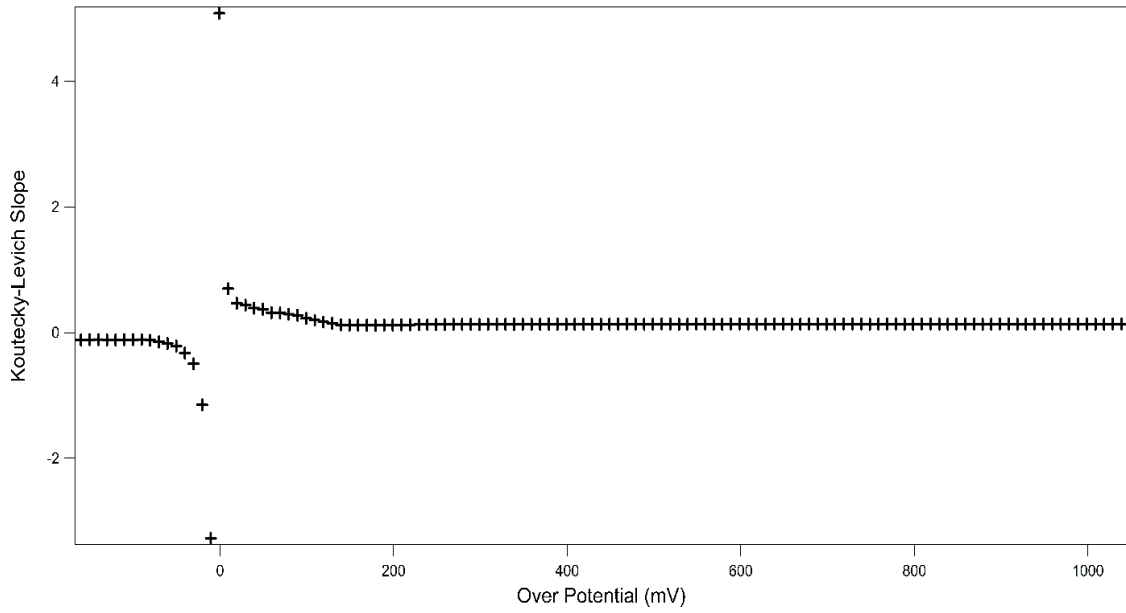
Figure 34: Effect of Overpotential on the Koutecky-Levich Slope. The data was

extracted from Figure 30
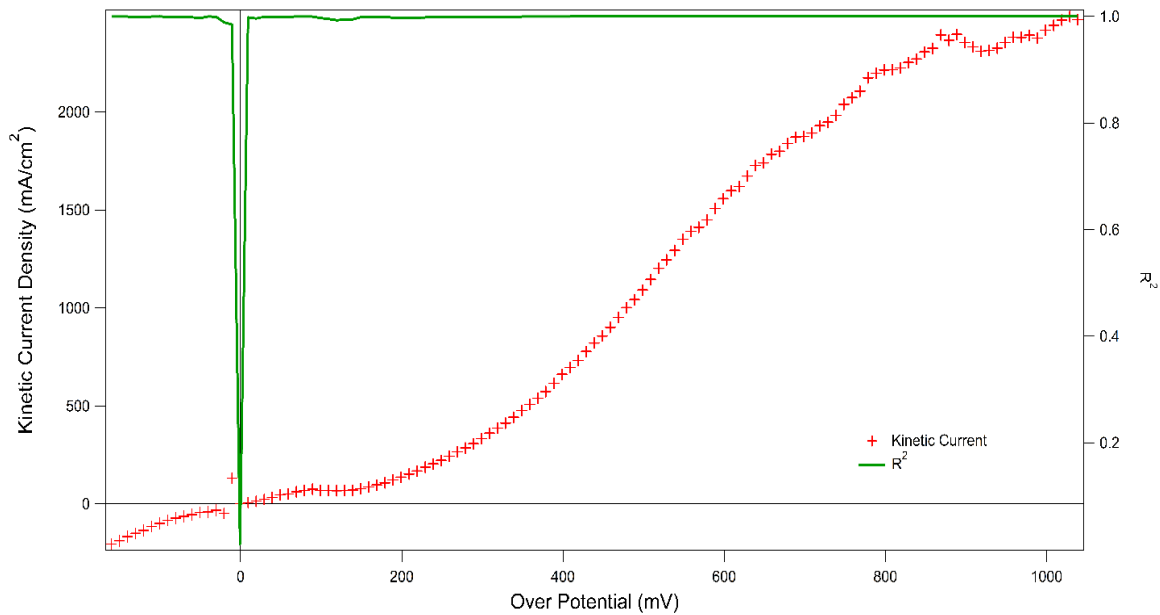
Figure 35: Kinetic current extracted from Figure 30
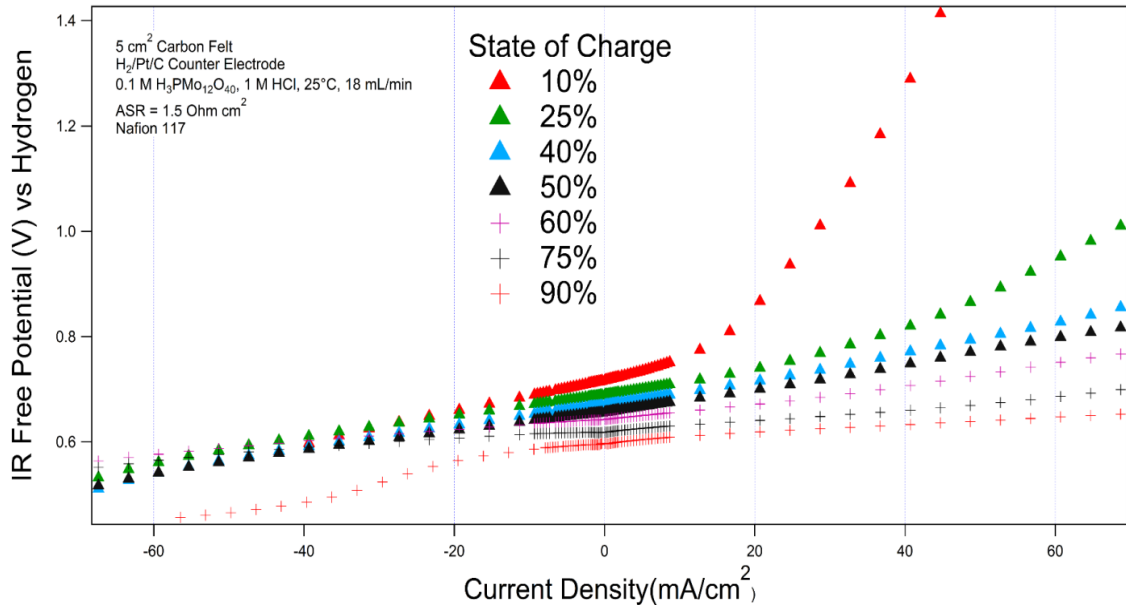
Figure 36: The voltammogram of several different states of charge. 0.1 M

Phosphomolybdic Acid, NAFION 117 Membrane, 2-layer WOS 1002 Anode

GDL. Curves are IR Corrected ASR = 1.5 Ohm-cm^2
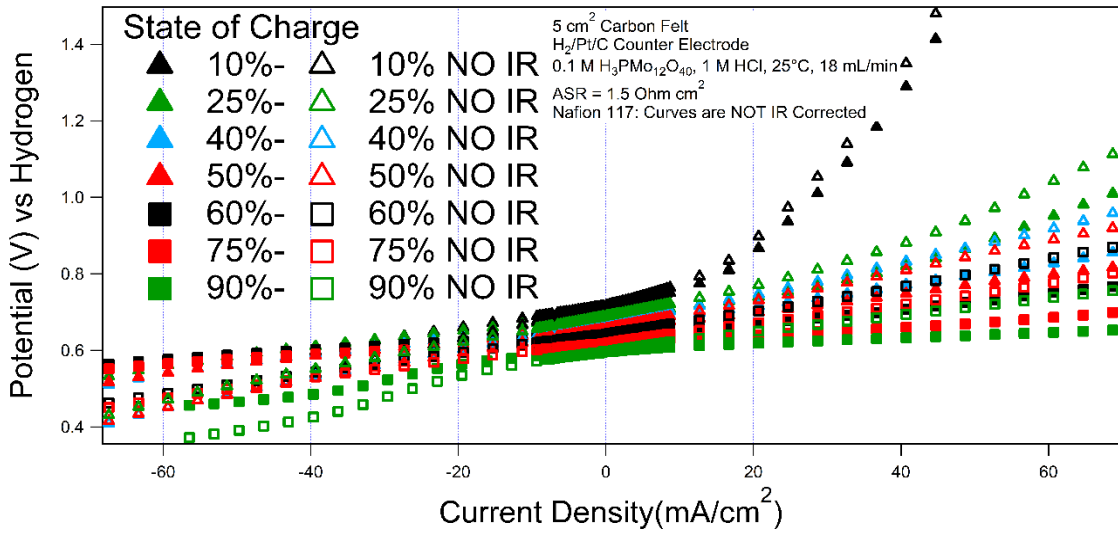
Figure 37: The voltammogram of several different states of charge. 0.1 M
Phosphomolybdic Acid, NAFION 117 Membrane, 2-layer WOS 1002 Anode
GDL. No IR correction, ASR = 1.5 Ohm-cm^2
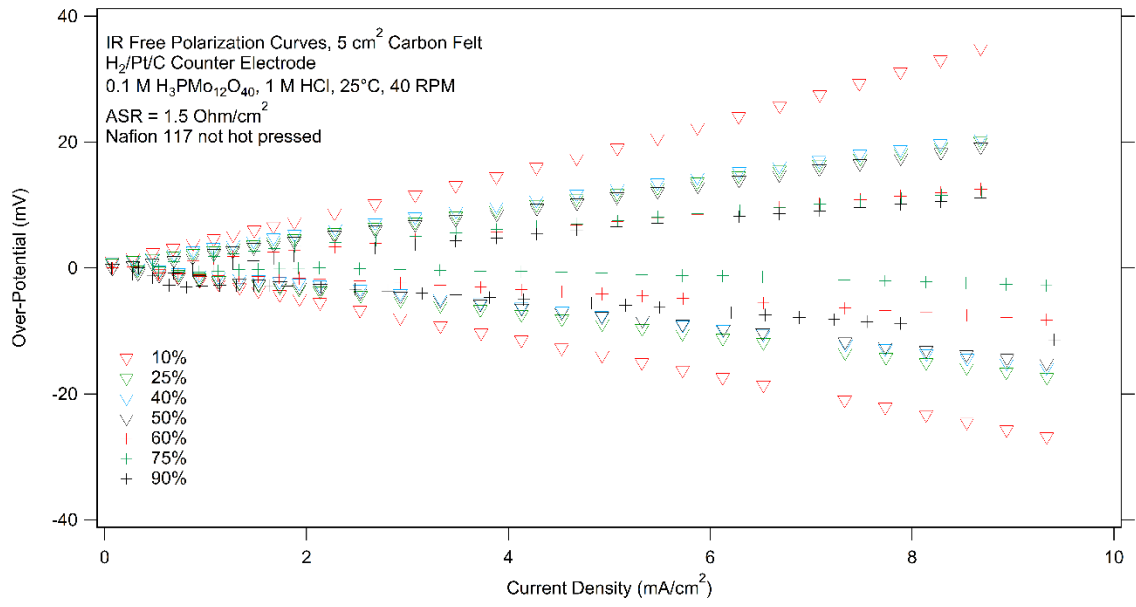
Figure 38: Linear Representation of Overpotential vs SOC in the Kinetic Region
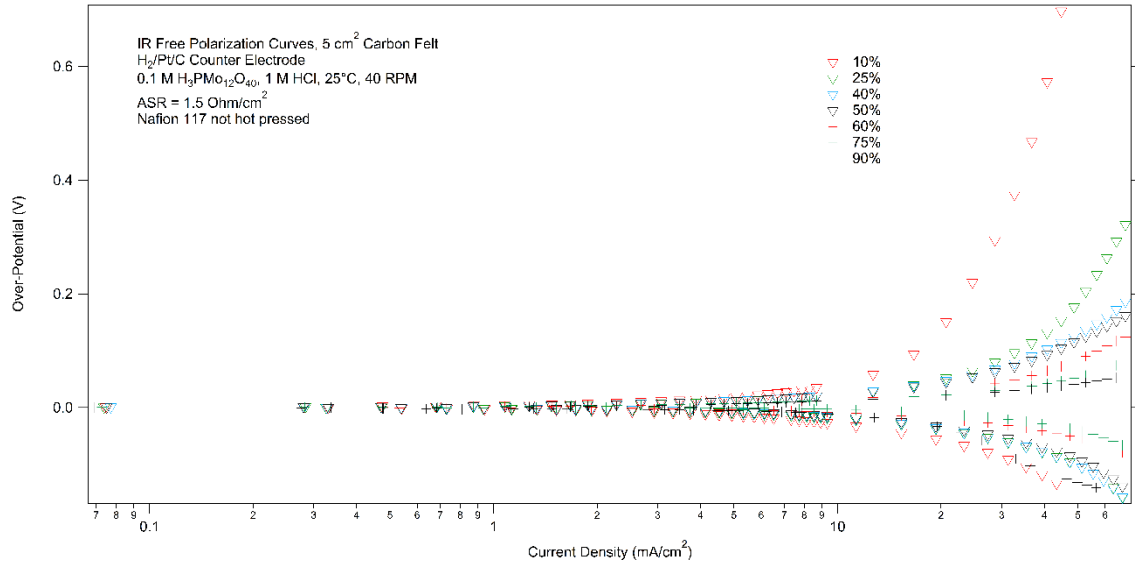
Figure 39: The Tafel plot of several different states of charge. 0.1 M

Phosphomolybdic Acid, NAFION 117 Membrane, 2-layer WOS 1002 Anode

GDL. Curves are IR Corrected ASR = 1.5 Ohm-cm2
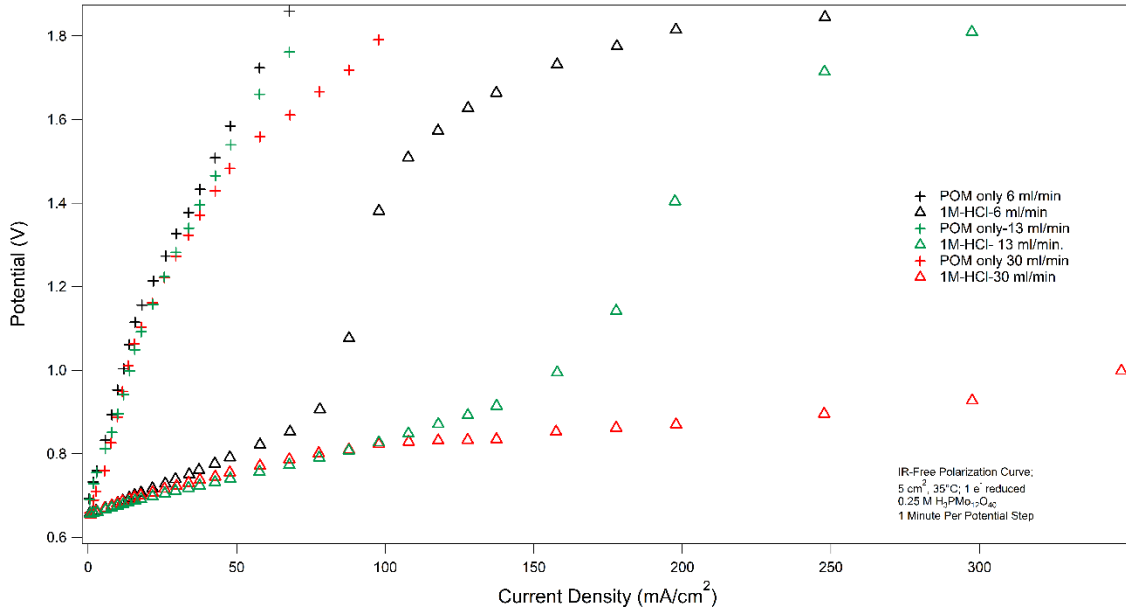
Figure 40: Flow-rates and Supporting Acids, 0.25 M Phosphomolybdic Acid,

NAFION 117 Membrane, 2-layer WOS 1002 Anode GDL.
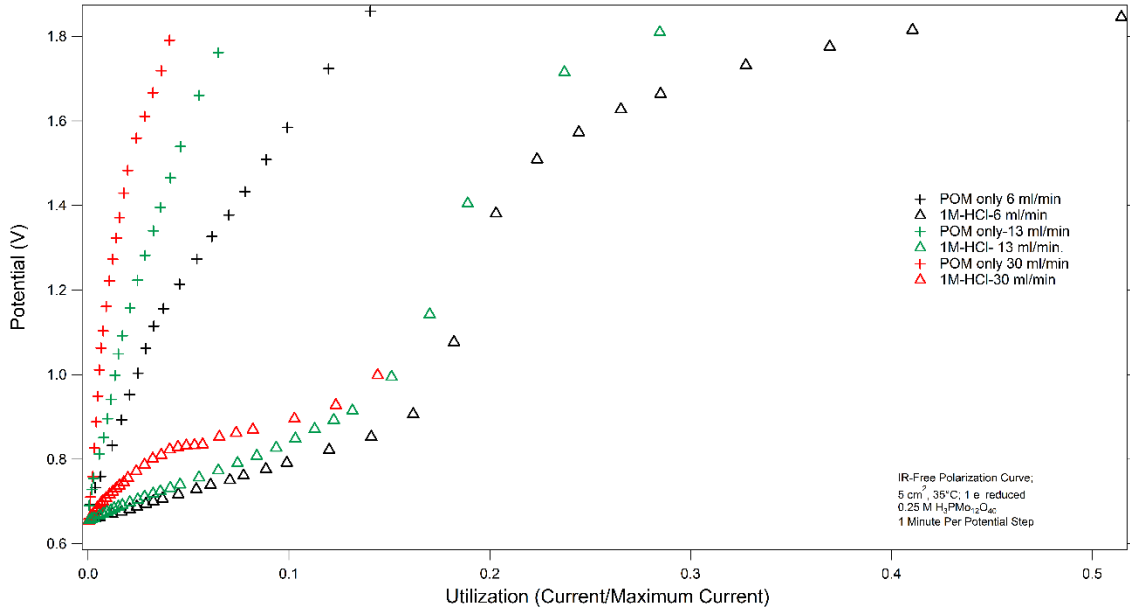
Figure 41: Utilization Normalized Polarization Curves, 0.25 M Phosphomolybdic

Acid, , NAFION 117 Membrane, 2-layer WOS 1002 Anode GDL.
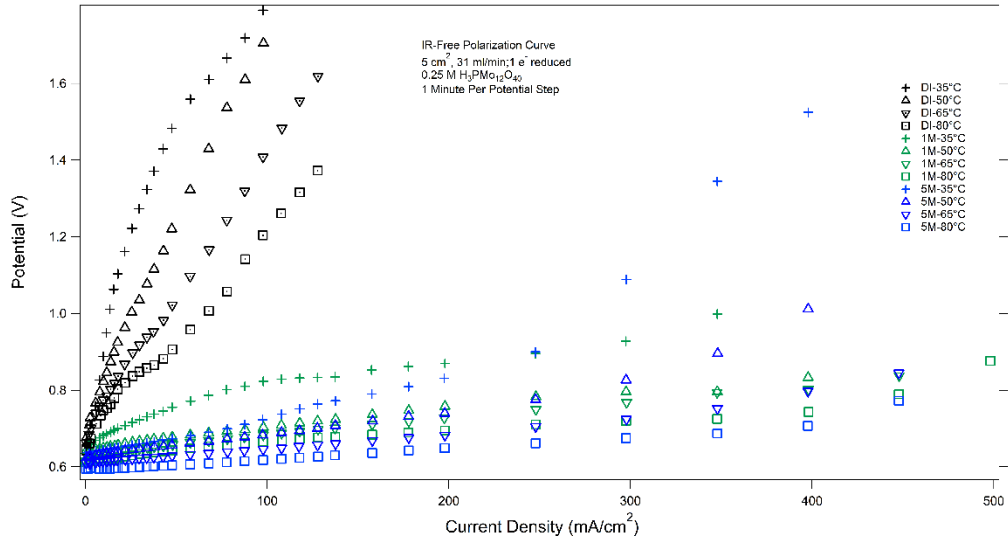
Figure 42: Effect of Temperature on Polarization Curves of 0.25 M

Phosphomolybdic Acid, NAFION 117 Membrane, 2-layer WOS 1002 Anode

GDL.
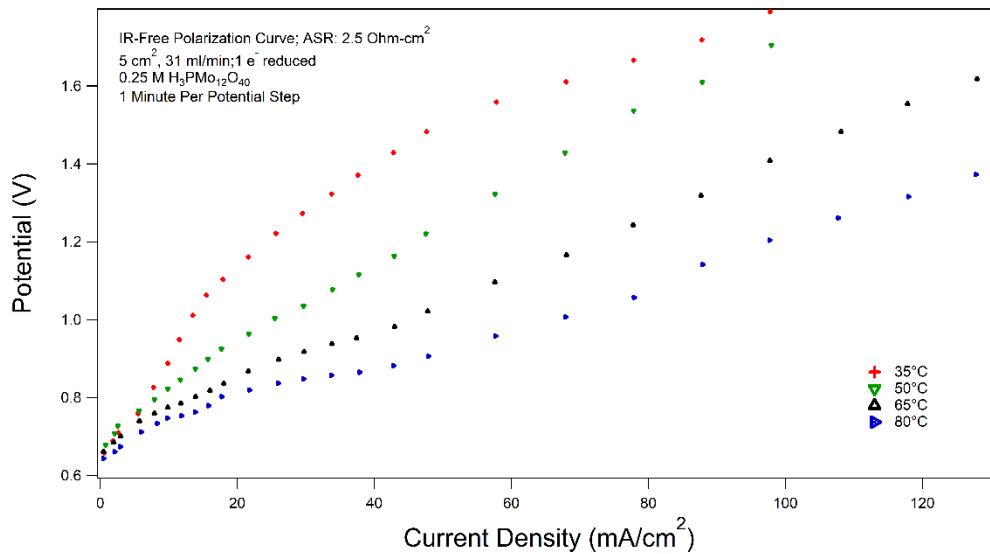
Figure 43: Effect of Temperature on Oxidation Polarization Curves of Neat

Phosphomolybdic Acid, NAFION 117 Membrane, 2-layer WOS 1002 Anode

GDL.
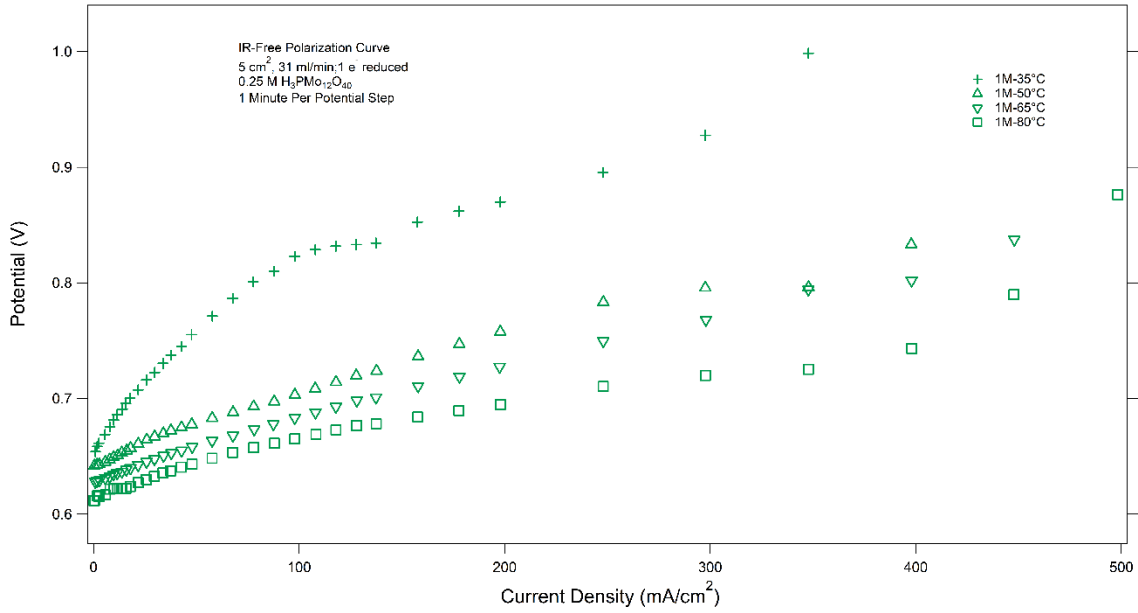
Figure 44: Effect of Temperature on Oxidation Polarization Curves of 0.25 M

Phosphomolybdic Acid in 1M HCl, NAFION 117 Membrane, 2-layer WOS 1002
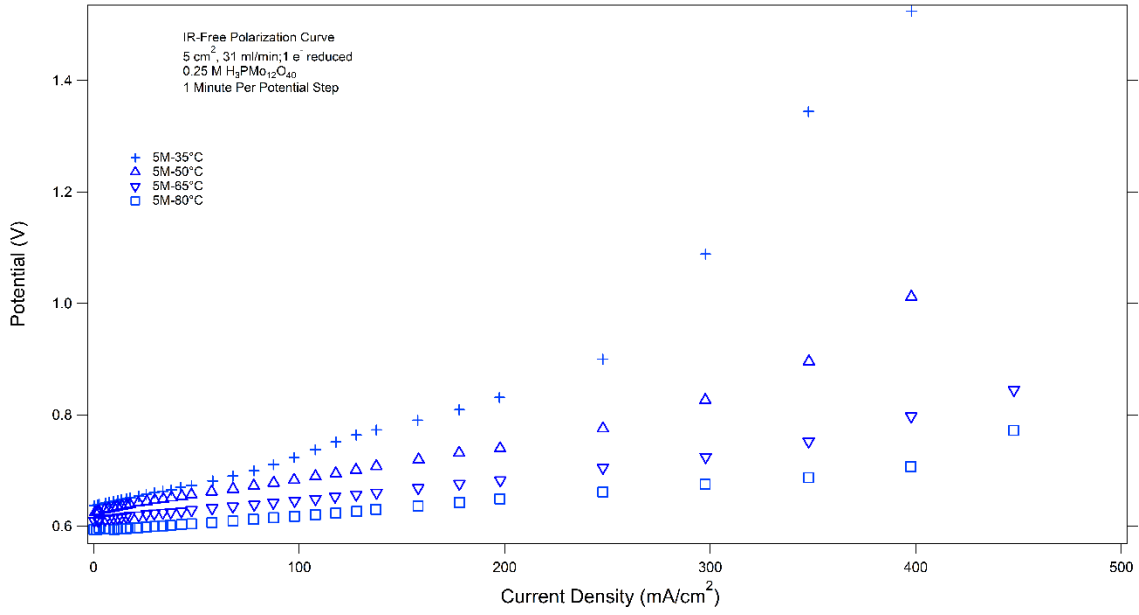
Anode GDL.

Figure 45: Effect of Temperature on Oxidation Polarization curves of 0.25 M

Phosphomolybdic Acid in 5M HCl, NAFION 117 Membrane, 2-layer WOS 1002

Anode GDL.
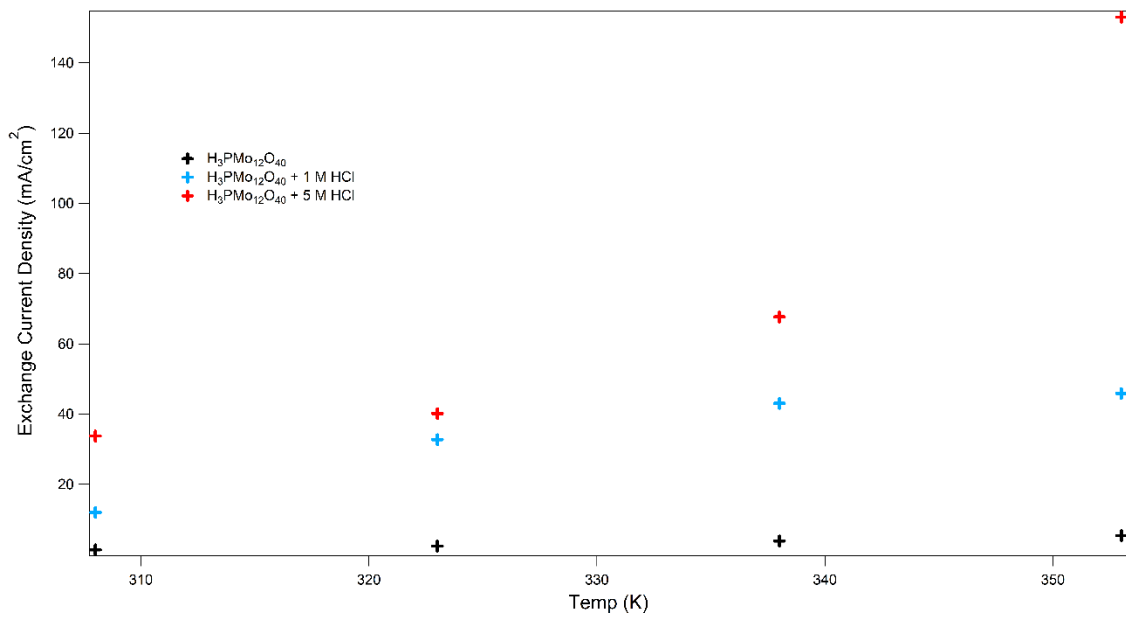
Figure 46: Exchange Current Densities Dependence on Temperature and

Supporting Acid
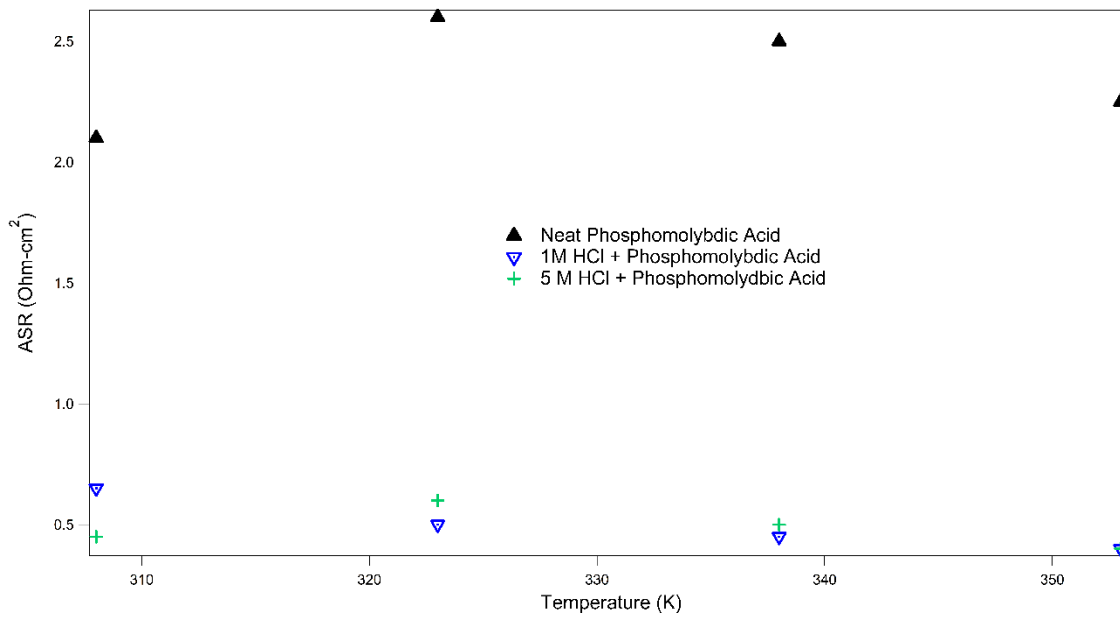
Figure 47: ASR vs Temperature and HCl Concentration
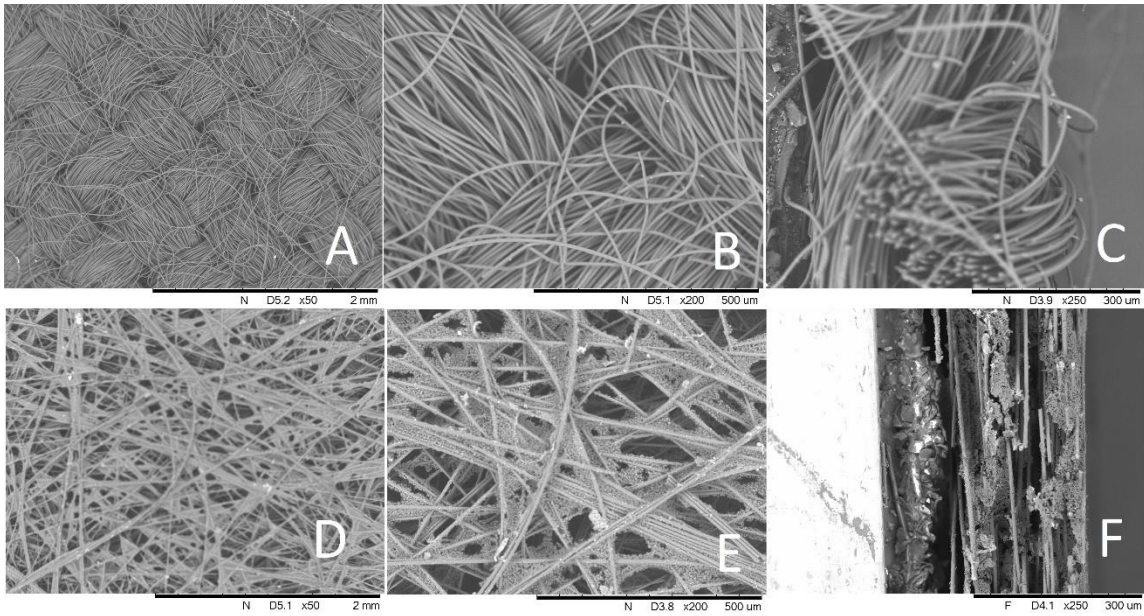
Figure 48: SEM Images of WOS 1002 Carbon Cloth A (50x), B (200x), C (250x Transverse), and Carbon Paper D (50x), E (2c00x), F (250x Transverse)
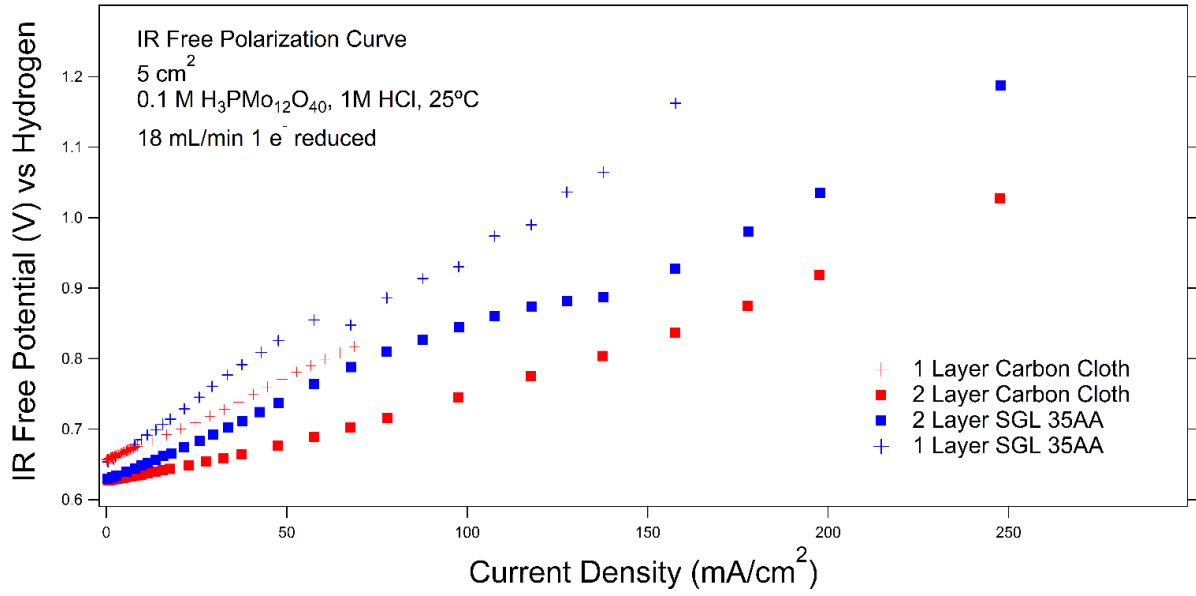
Figure 49: CE Tech WOS1002 Carbon Cloth Vs SGL 35AA Carbon Paper, Step

Time 30 Seconds
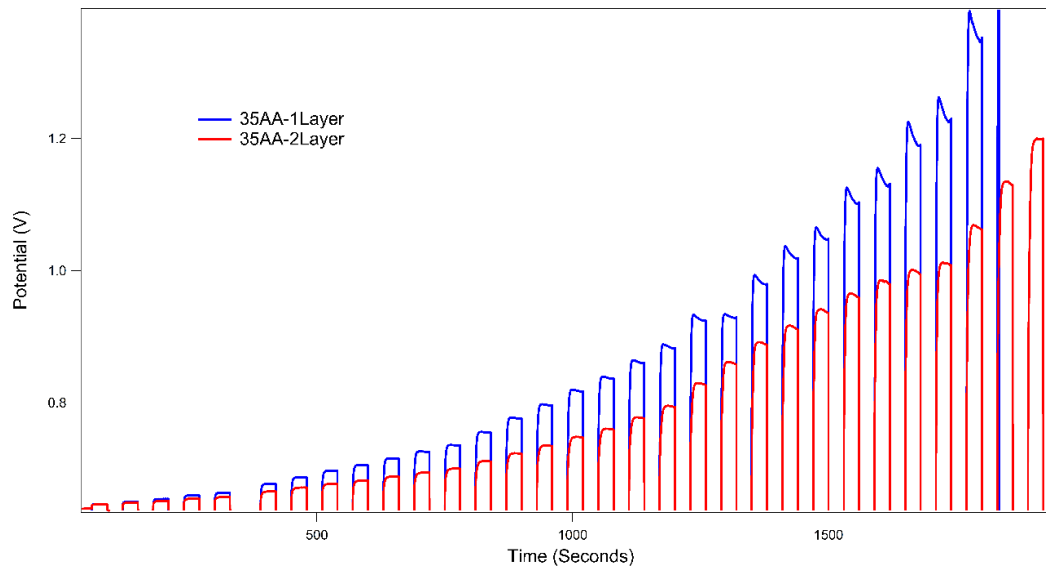
Figure 50: Anodic Chronopotentiometry
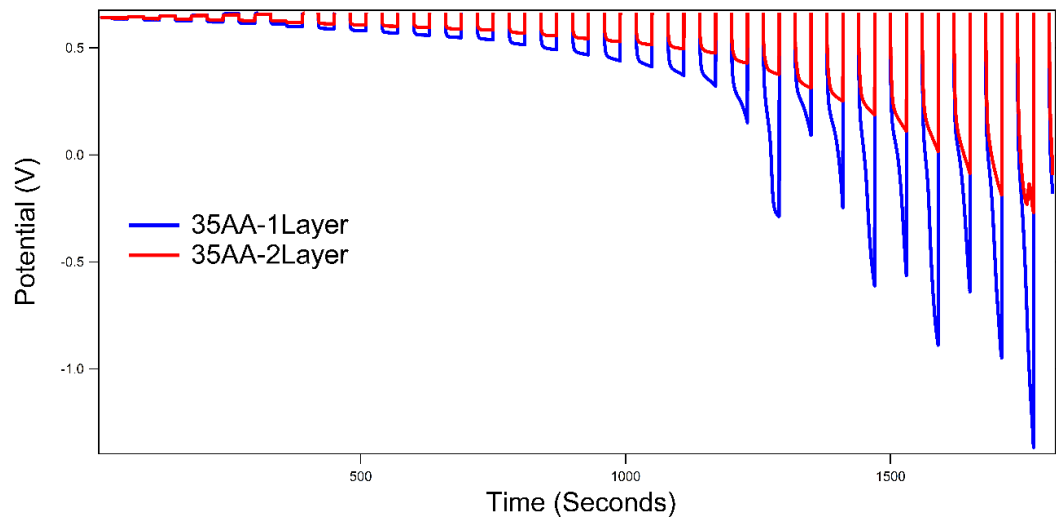
Figure 51: Cathodic Chronopotentiometry
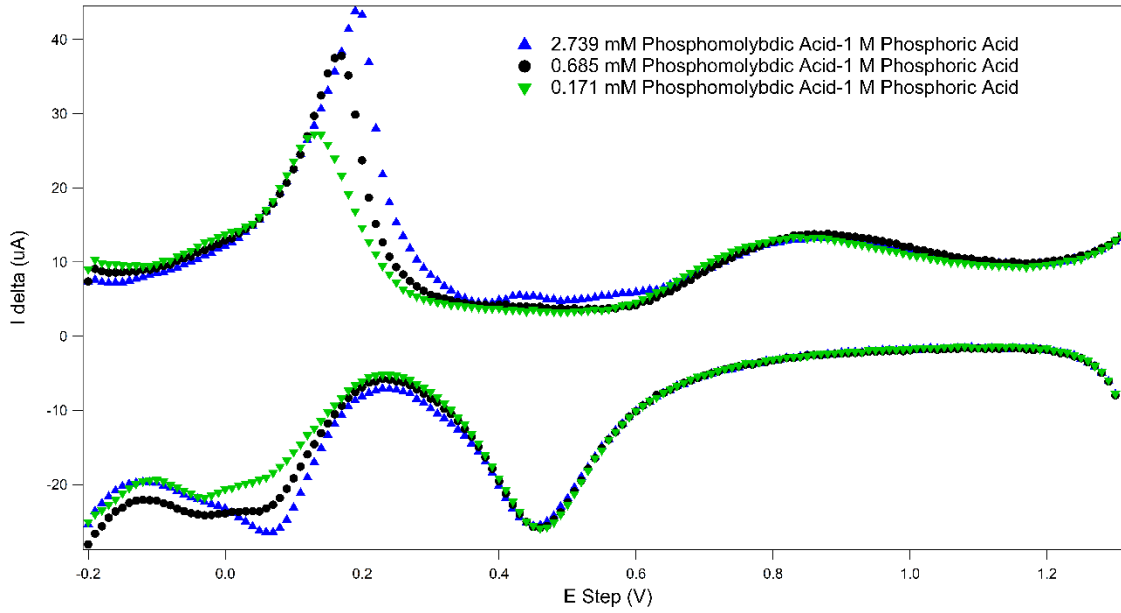
Figure 52: Calibration Curve Square Wave Voltammetry of Phosphomolybdic Acid in Phosphoric Acid. We: Pt disk, Ce: Pt wire, Ref: Ag/AgCl. E_Step: 10 mV,Pulse Height:25 mV, τ:100ms
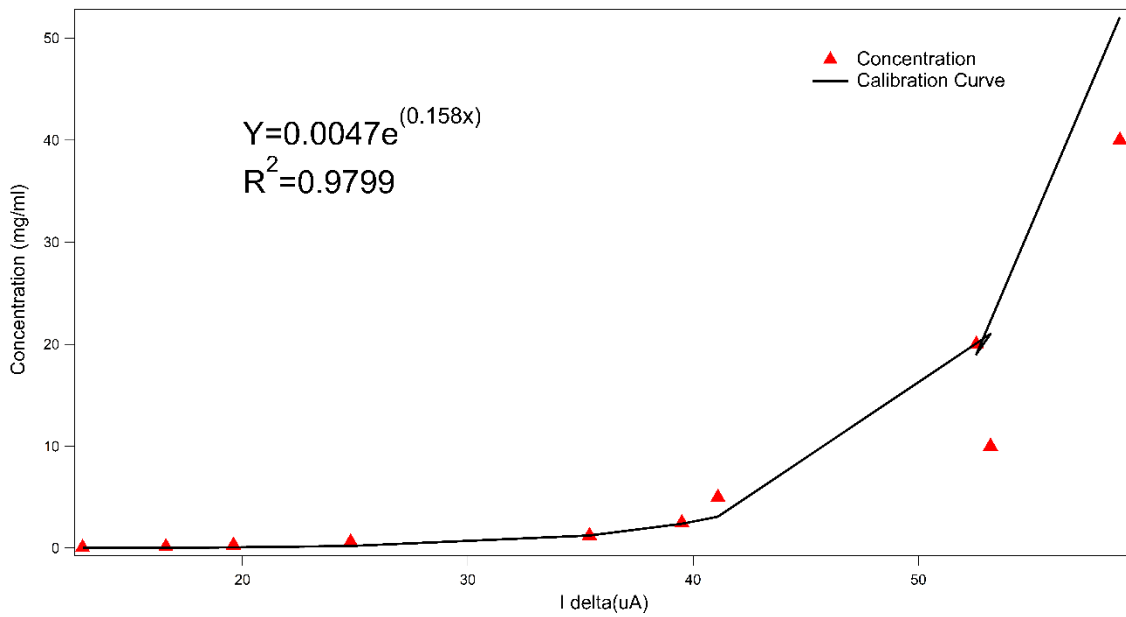
Figure 53: Calibration Curve of Peak Heights to Concentration
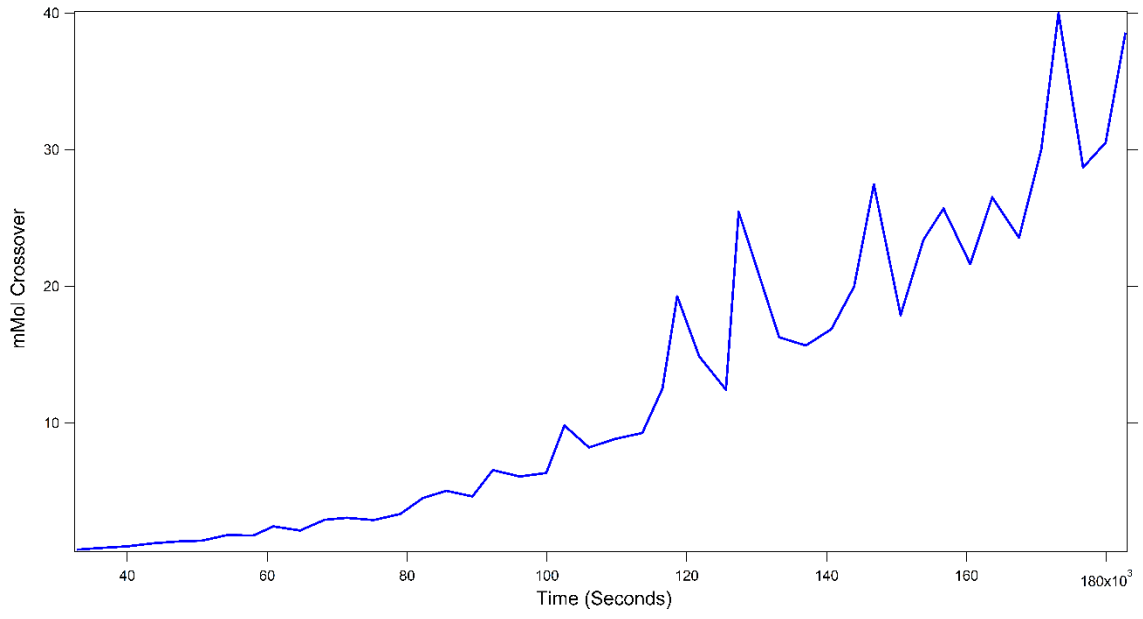
Figure 54: Phosphomolybdic Acid Crossover vs Time
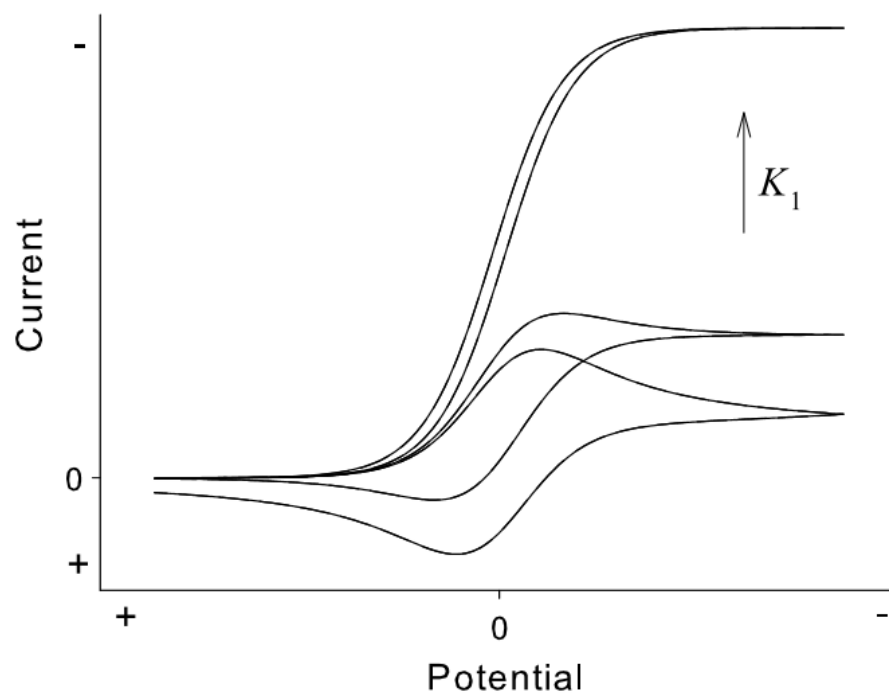
Figure 55: Effect of chemical kinetics on the cyclic voltammetry of the catalytic

mechanism at a macroelectrode (Reproduced from Reference [63])
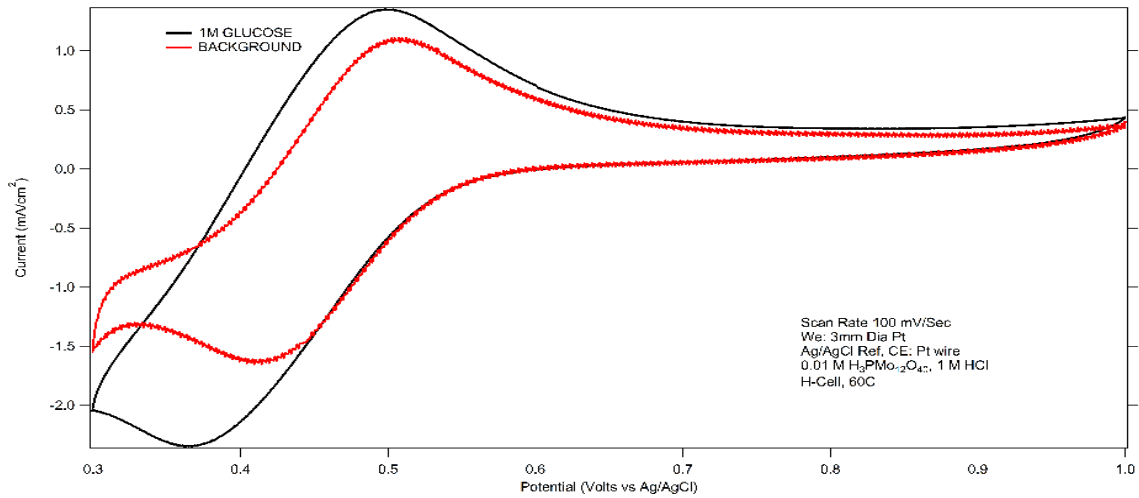
Figure 56: Glucose Cyclic Voltammetry,v=100 mV/sec, 0.01 M $H_3PMo_{12}O_{40}$, 1 M

HCl, 1 M glucose T= 60 ℃, We: 3mm Pt disk, Ce: Pt wire, Ref: Ag/AgCl.
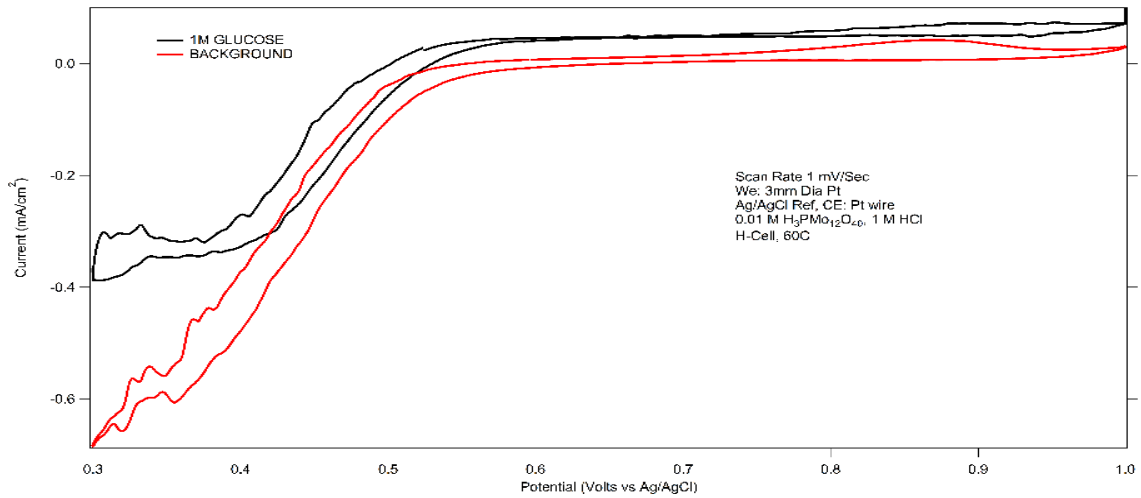
Figure 57: Glucose Cyclic Voltammetry. v=1 mV/sec, 0.01 M H₃PMo₁₂O₄₀, 1 M

HCl, 1 M glucose T= 60 ℃, We: 3mm Pt disk, Ce: Pt wire, Ref: Ag/AgCl.
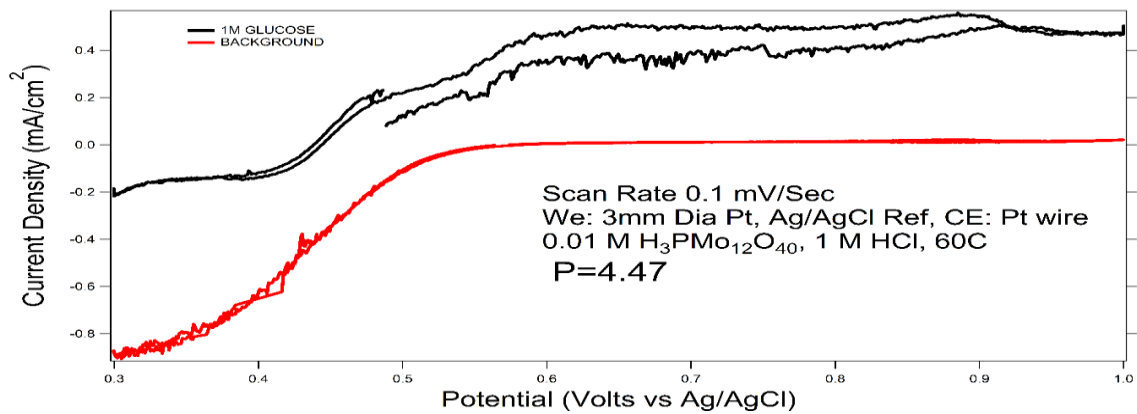
Figure 58: Glucose Cyclic Voltammetry. v=0.1 mV/sec, 0.01 M $H_3PMo_{12}O_{40}$, 1 M
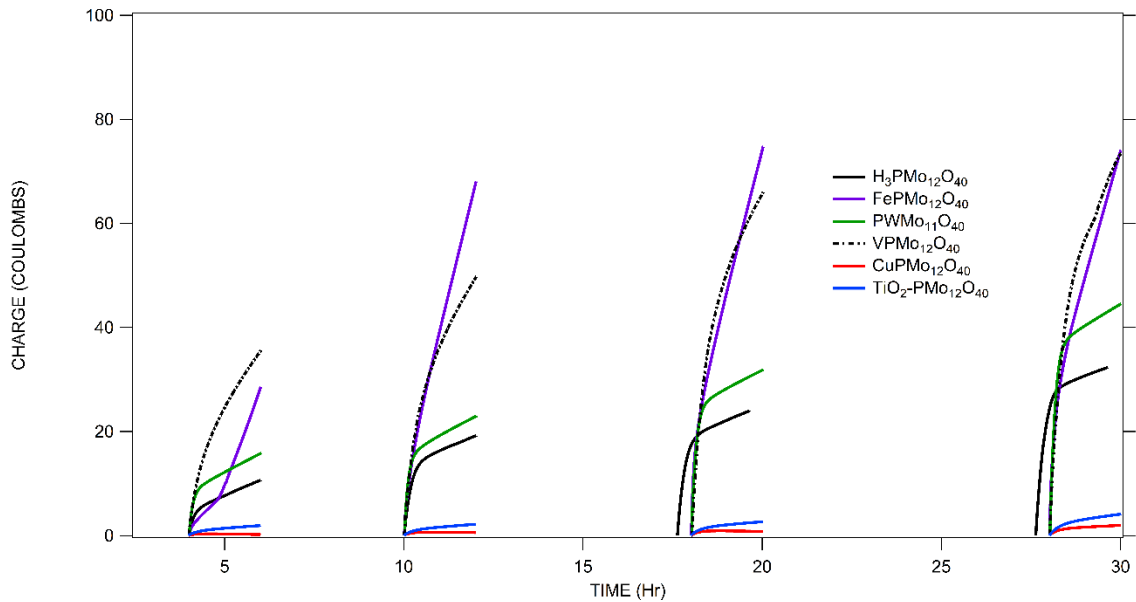
HCl, 1 M glucose T= 60 ℃, We: 3mm Pt disk, Ce: Pt wire, Ref: Ag/AgCl.

Figure 59: Coulometric Monitoring of the Time Course of Glycerol Oxidation, as

Revealed by the POM Re-Oxidation Charge, for Various POM Catalysts in 0.5 M
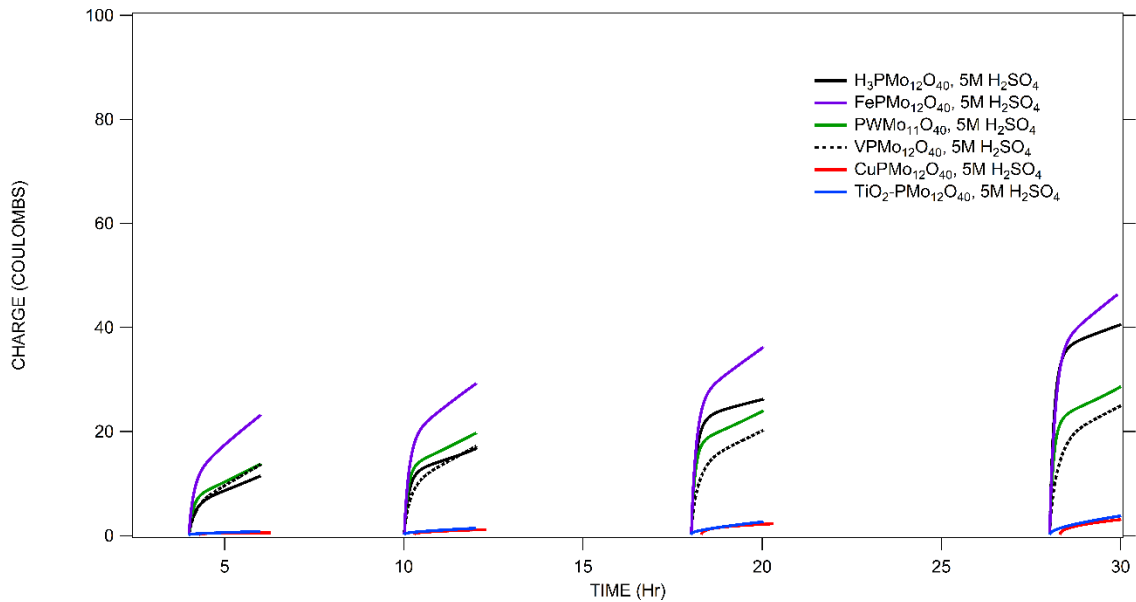
Glycerol

Figure 59: Coulometric Monitoring of the Time Course of Glycerol Oxidation, as Revealed by the POM Re-Oxidation Charge, for Various POM Catalysts in 0.5 M Glycerol + 5M H_2SO_4
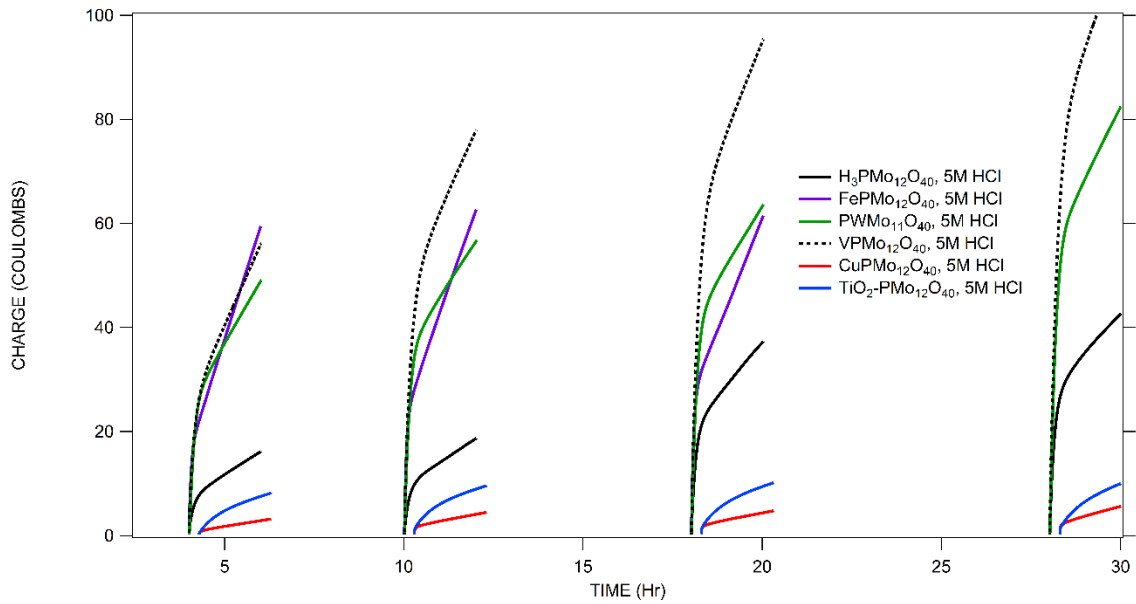
Figure 60: Coulometric Monitoring of the Time Course of Glycerol Oxidation, as

Revealed by the POM Re-Oxidation Charge, for Various POM Catalysts in 0.5 M

Glycerol + 5M HCl
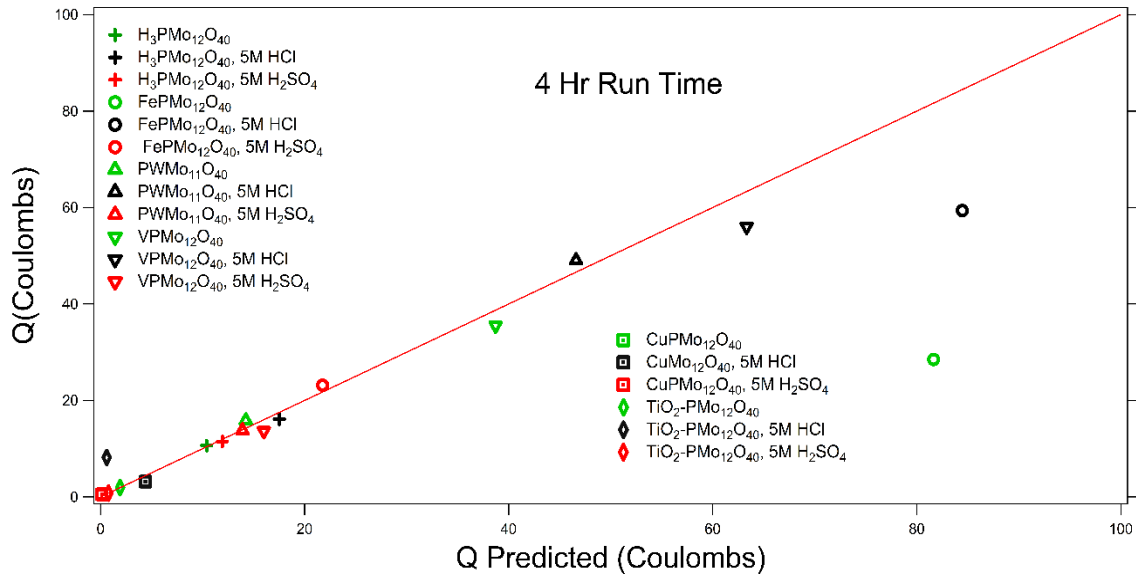
Figure 61: 4 Hour, Q Measured vs Q Predicted
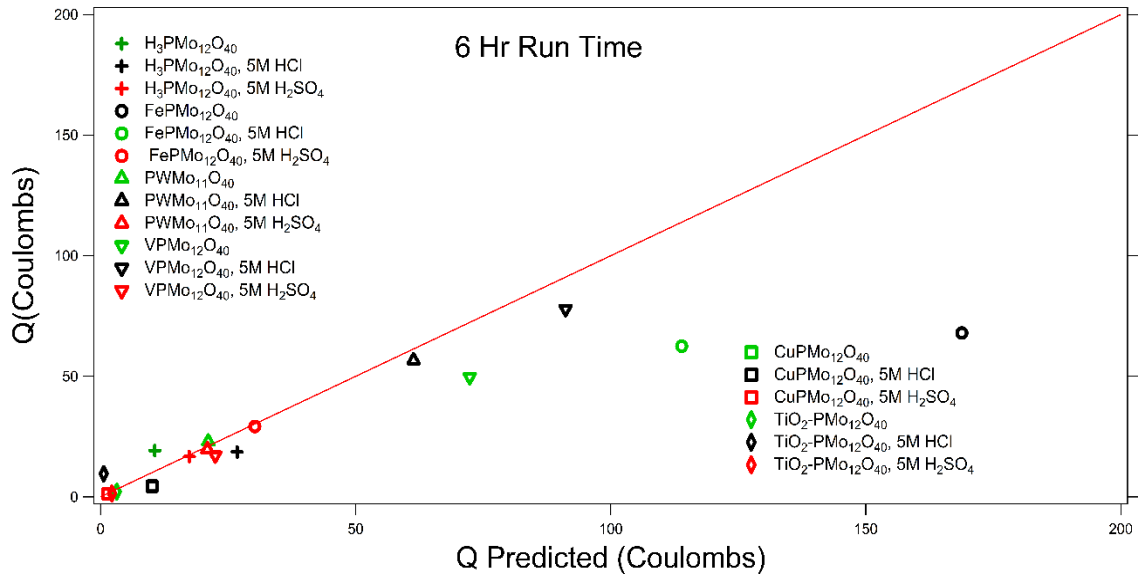
Figure 62: 6 Hour, Q Measured vs Q Predicted
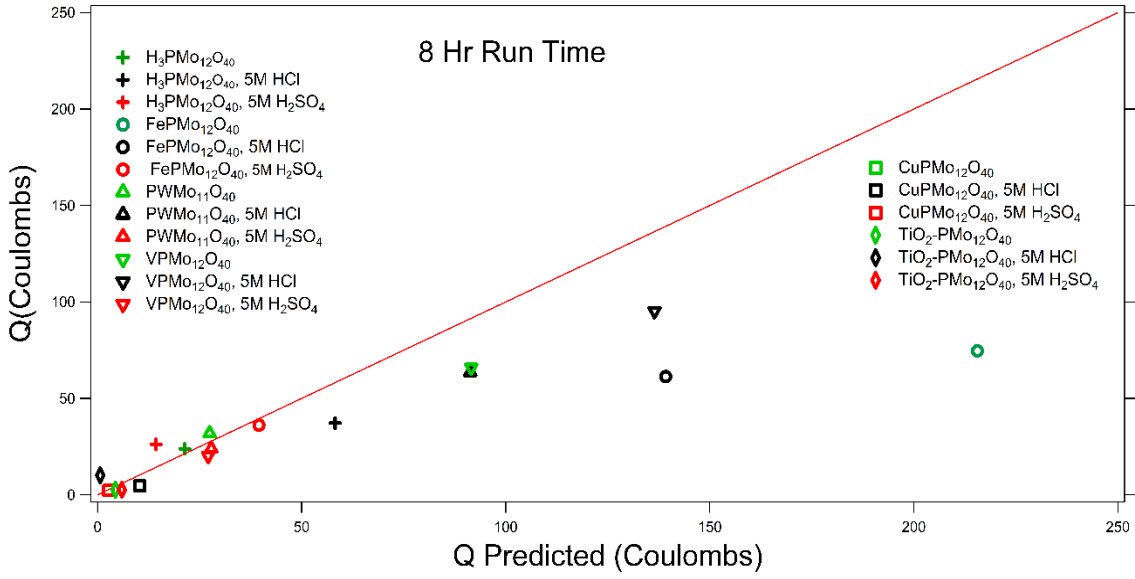
Figure 63: 8 Hour, Q Measured vs Q Predicted
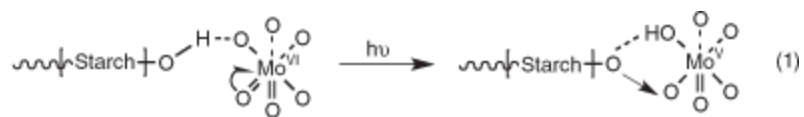
Figure 64: Formation of Starch-POM Complexes(Reproduced from Reference 38)
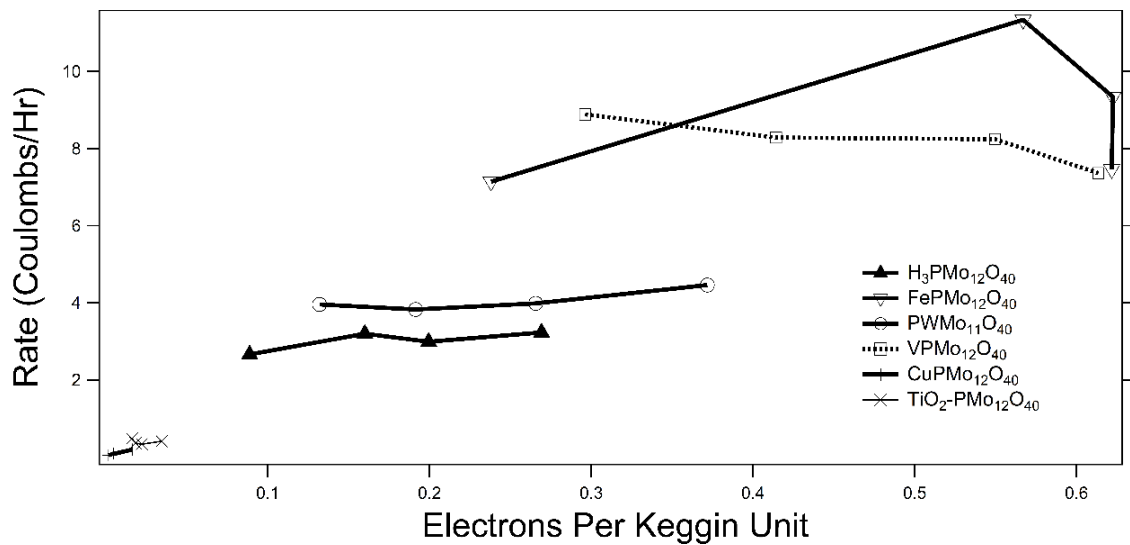
Figure 65: Reaction Rate vs Electrons Transferred, Neat Solution
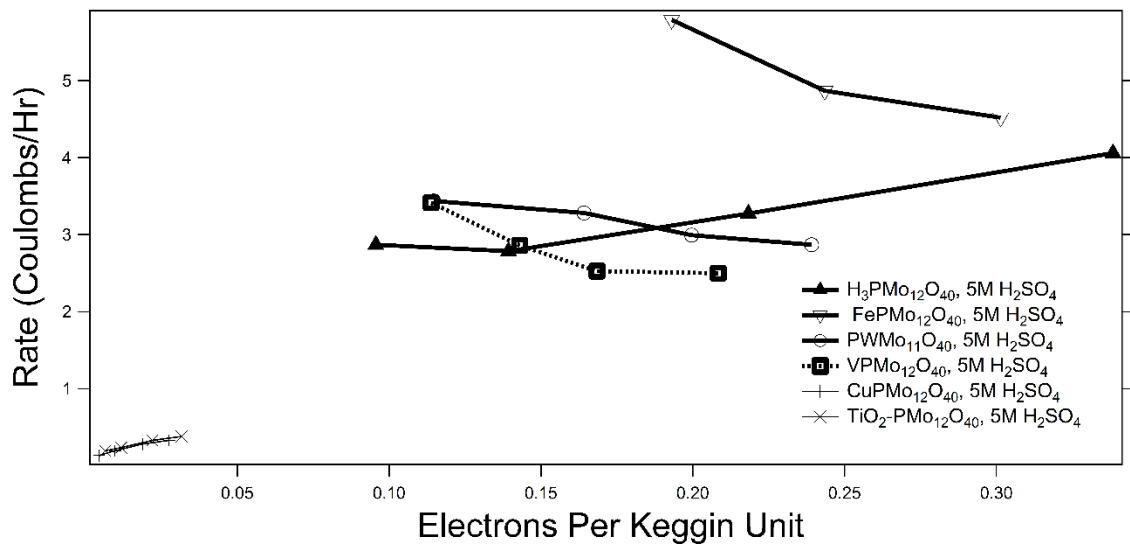
Figure 66: Reaction Rate vs Electrons Transferred, H_2SO_4 Solution
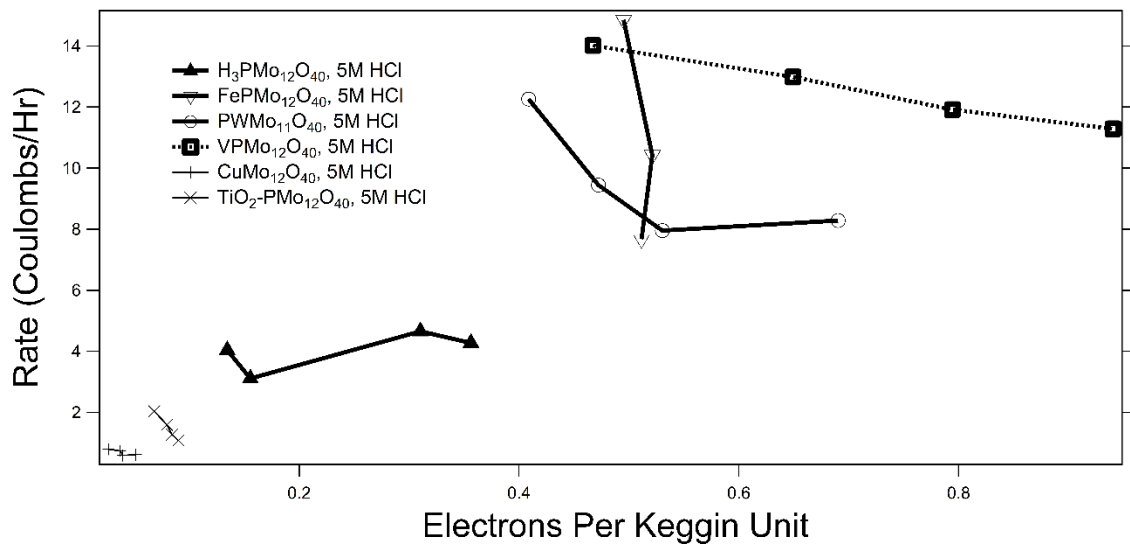
Figure 67: Reaction Rate vs Electrons Transferred, HCl Solution
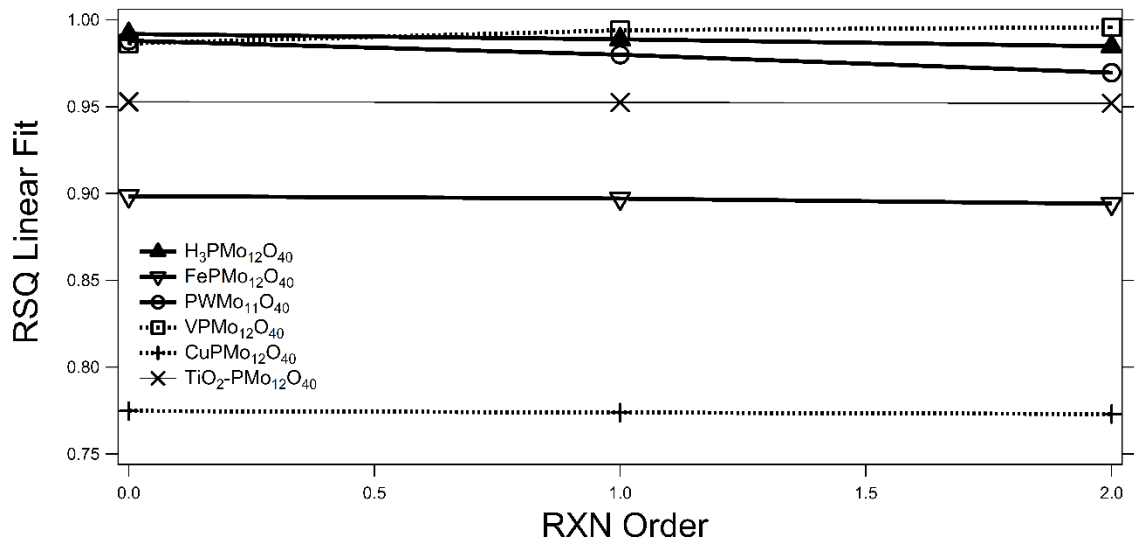
Figure 68: R^2 for Linear Fit vs Reaction Order Plot-Neat
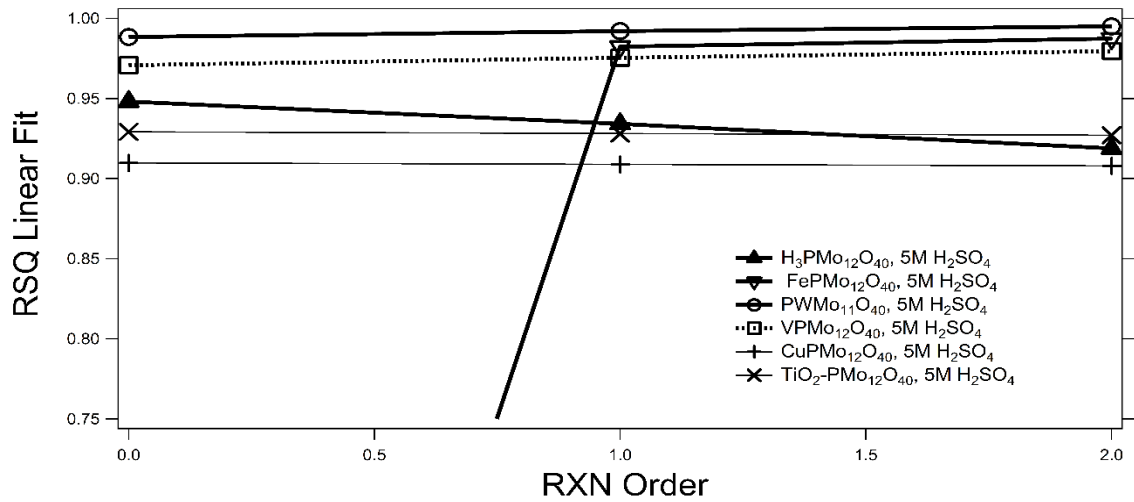
Figure 69: R^2 for Linear Fit vs Reaction Order Plot-H_2SO_4
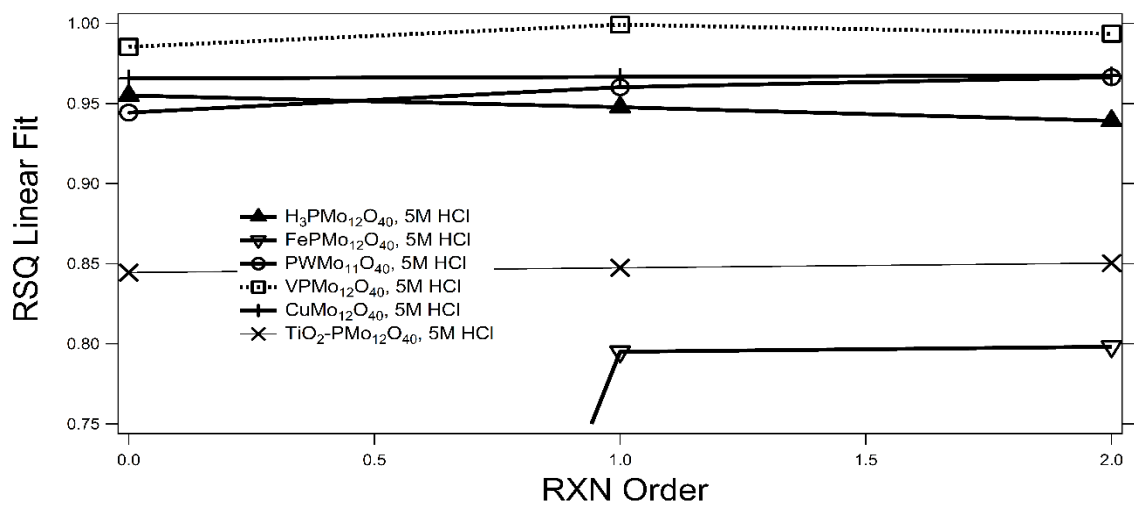
Figure 70: R^2 for Linear Fit vs Reaction Order Plot-HCl
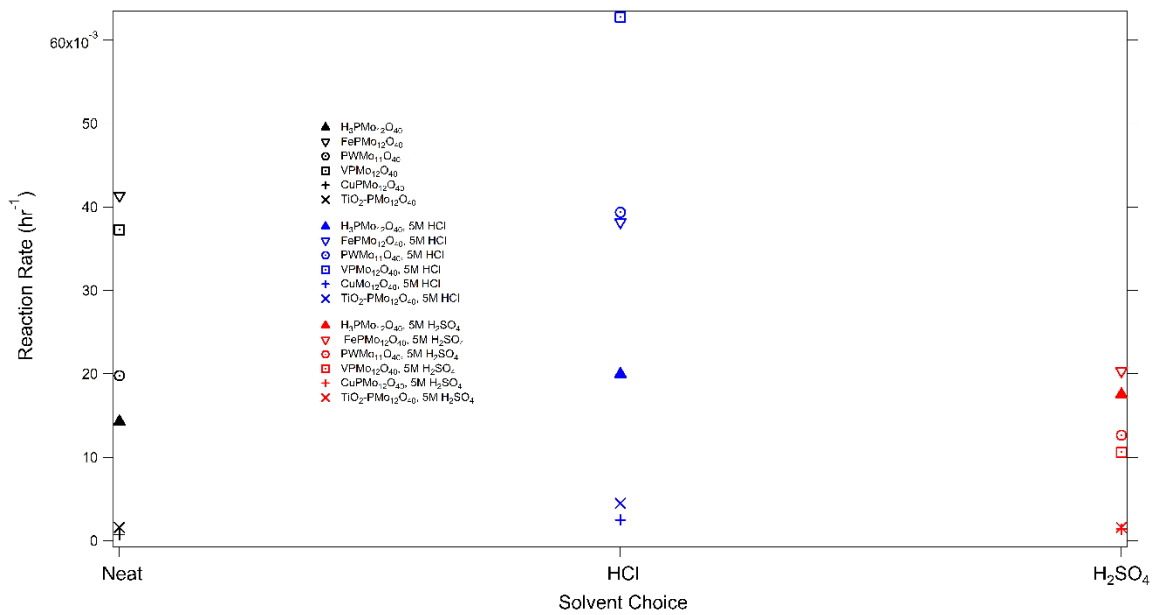
Figure 71: k' Values for all solvent and catalyst combinations
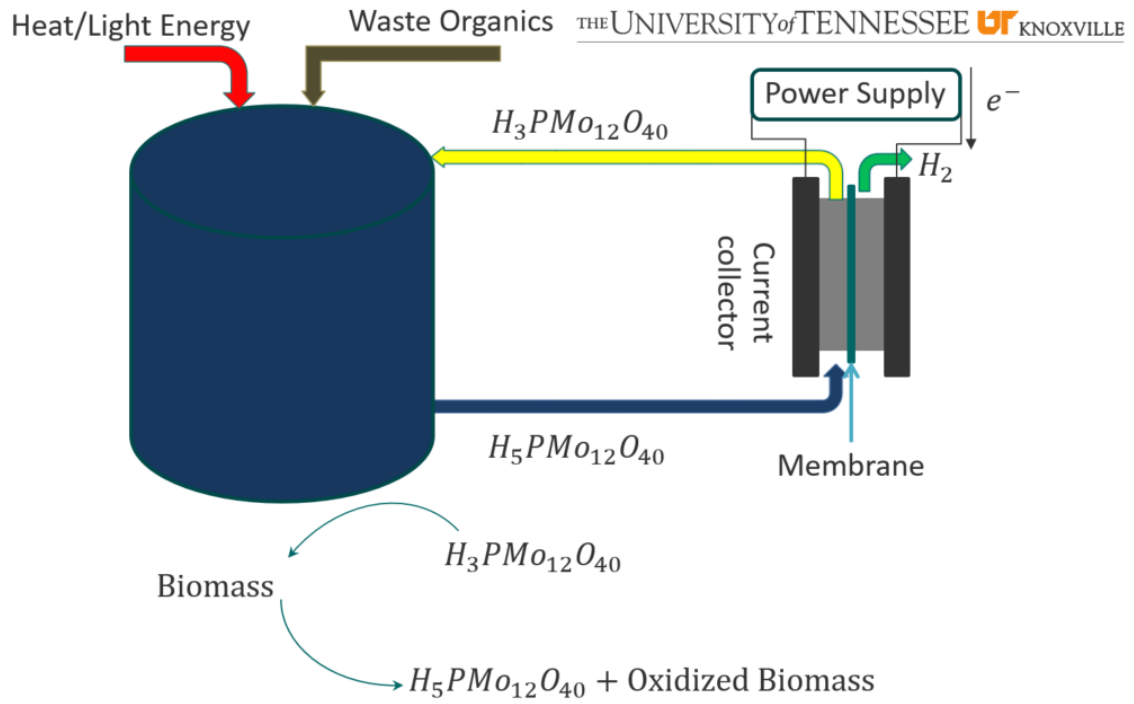
Figure 72: Schematic of Proposed System Design
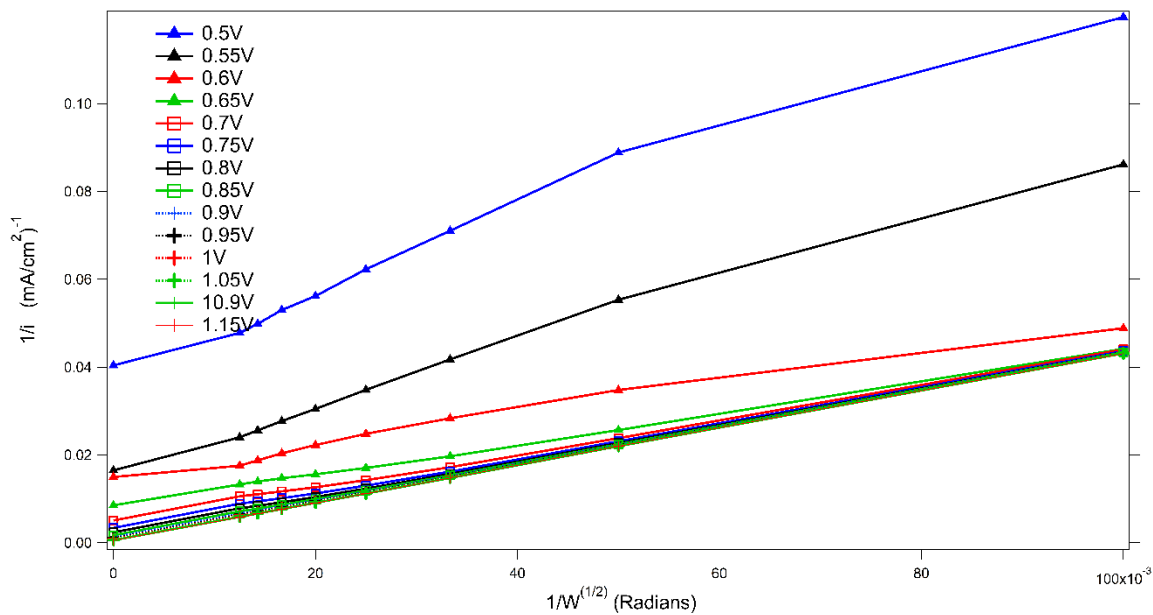
Figure 73: Koutecky-Levich Plot, Rotating Disk Electrode, 0.2 M H₃PMo₁₂O₄₀/ 0.2

M H₅PMo₁₂O₄₀, v=20 mV/sec, We: 5mm GC disk, Ce: Pt mesh, Ref Ag/AgCl

(0.205 V vs NHE), T=25°C, Levich Plot at 1.5 V vs Ag/AgCl
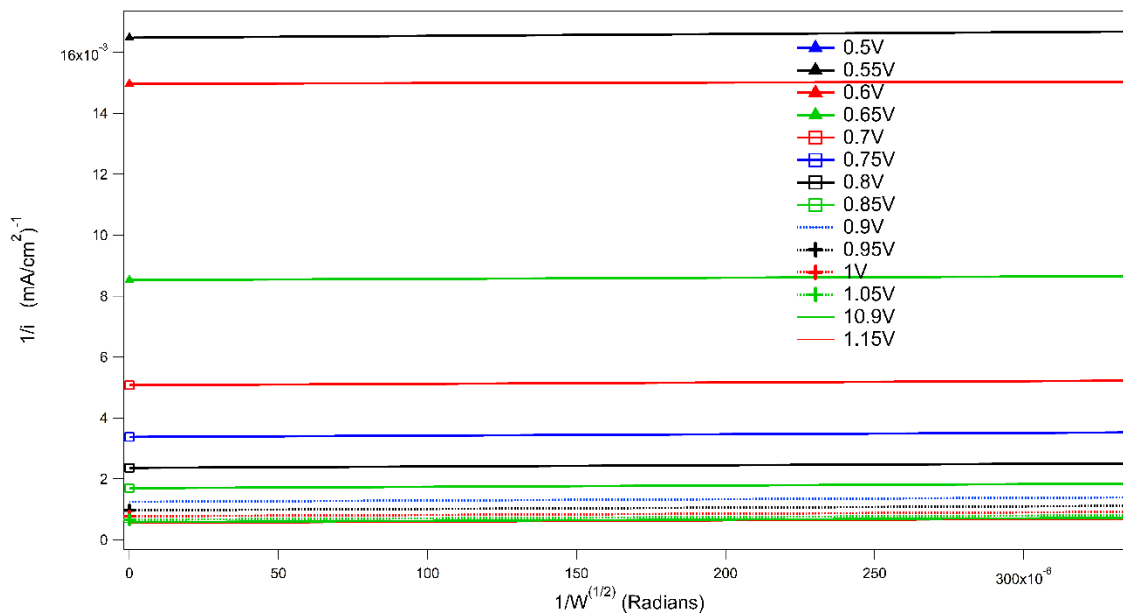
Figure 74: Koutecky-Levich Plot, Rotating Disk Electrode, 0.2 M H3PMo12O40/ 0.2 M H5PMo12O40, v=20 mV/sec, We: 5mm GC disk, Ce: Pt mesh, Ref Ag/AgCl (0.205 V vs NHE), T=25°C, Levich Plot at 1.5 V vs Ag/AgCl
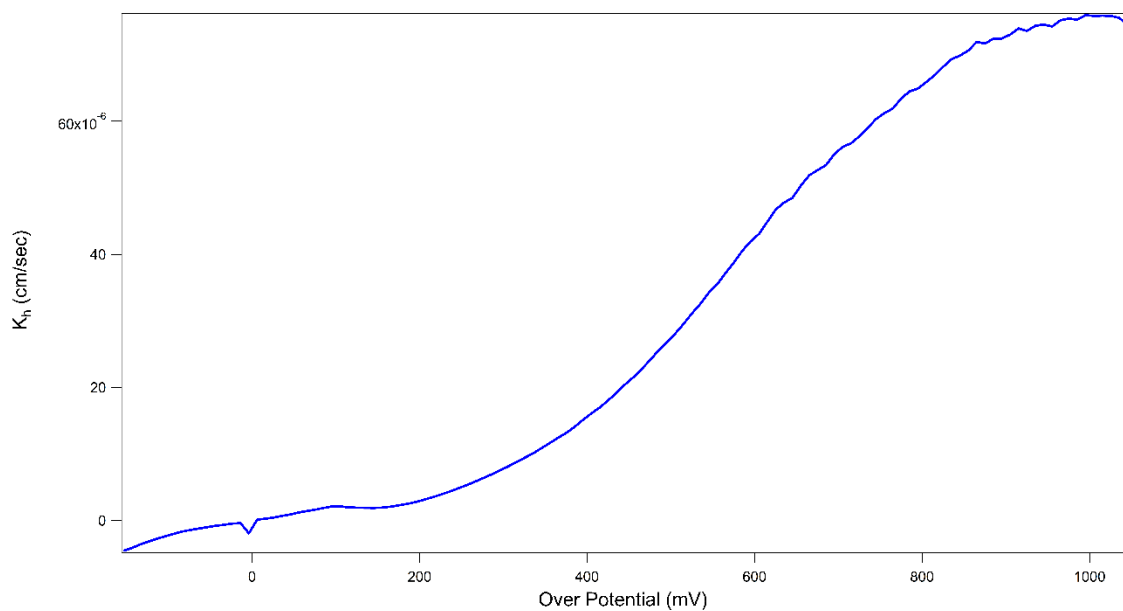
Figure 75: k_h vs Overpotential

Table 9: Kinetic Parameters Dependence on Temperature and Acid

Acid(M)	Temp ℃	mA/mV	Rct (V/A)	i_0 (mA)	ASR (Ohm-cm2)
0.00	35.00	52.87	19.33	1.37	2.10
0.00	50.00	89.21	11.46	2.43	2.60
0.00	65.00	135.29	7.56	3.85	2.50
0.00	80.00	181.64	5.63	5.41	2.25
1.00	35.00	463.25	2.21	12.03	0.65
1.00	50.00	1201.68	0.85	32.72	0.50
1.00	65.00	1511.46	0.68	43.07	0.45
1.00	80.00	1541.90	0.66	45.89	0.40
5.00	35.00	1300.55	0.79	33.77	0.45
5.00	50.00	1474.99	0.69	40.16	0.60
5.00	65.00	2375.21	0.43	67.68	0.50
5.00	80.00	5141.63	0.20	153.01	0.40
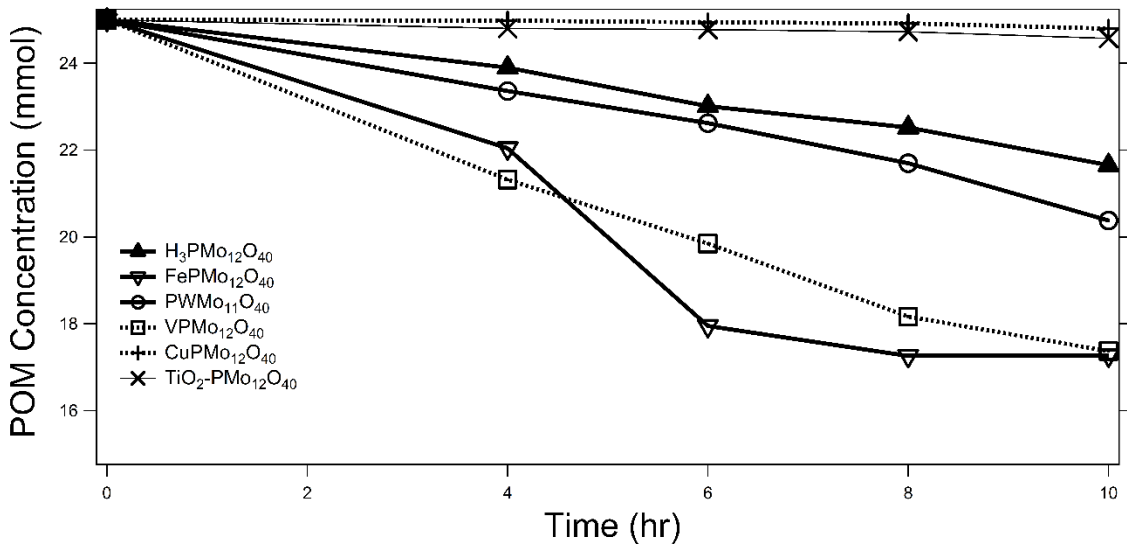
Figure 76: Zeroth Order POM Concentration vs Time-Neat
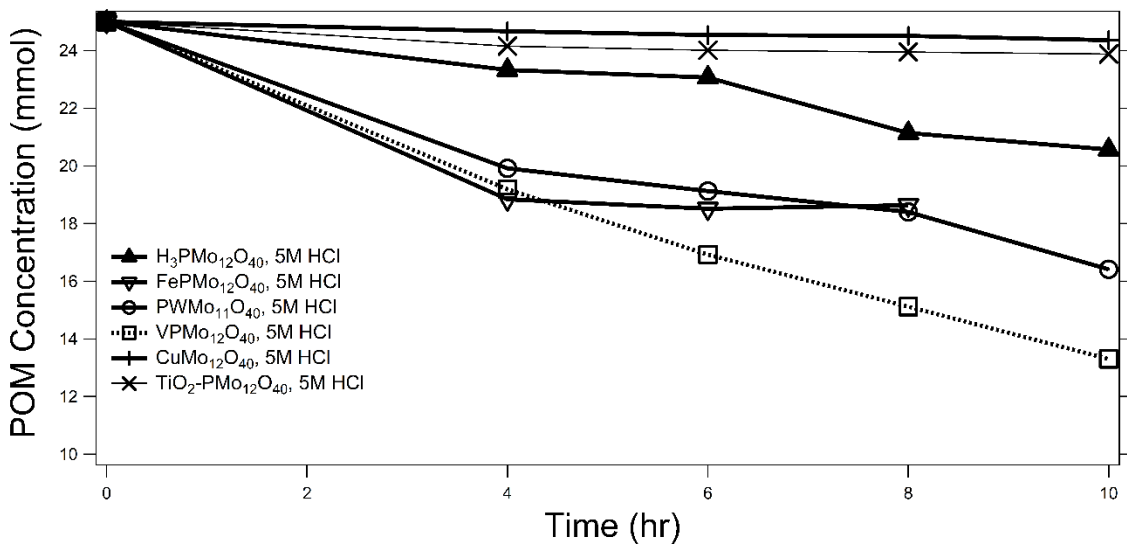
Figure 77: Zeroth Order POM Concentration vs Time-HCl
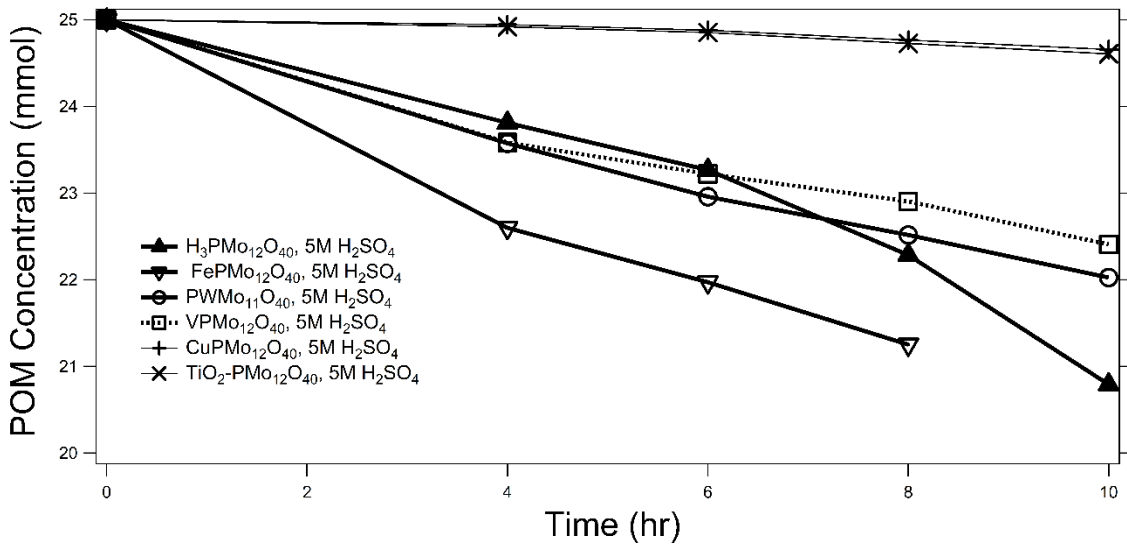
Figure 78: Zeroth Order POM Concentration vs Time-H$_2$SO$_4$
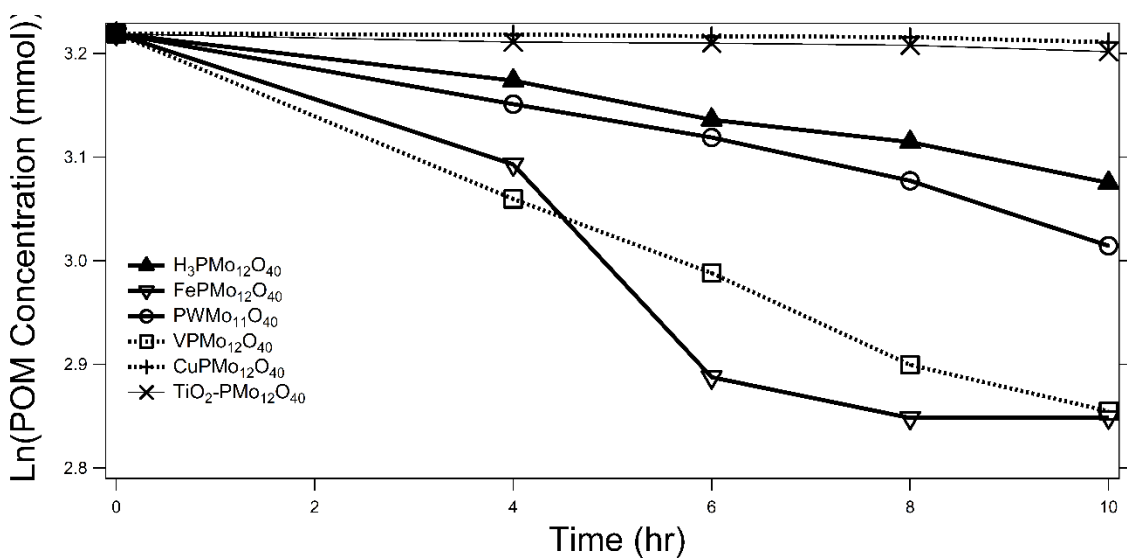
Figure 79: First Order POM Concentration vs Time-Neat
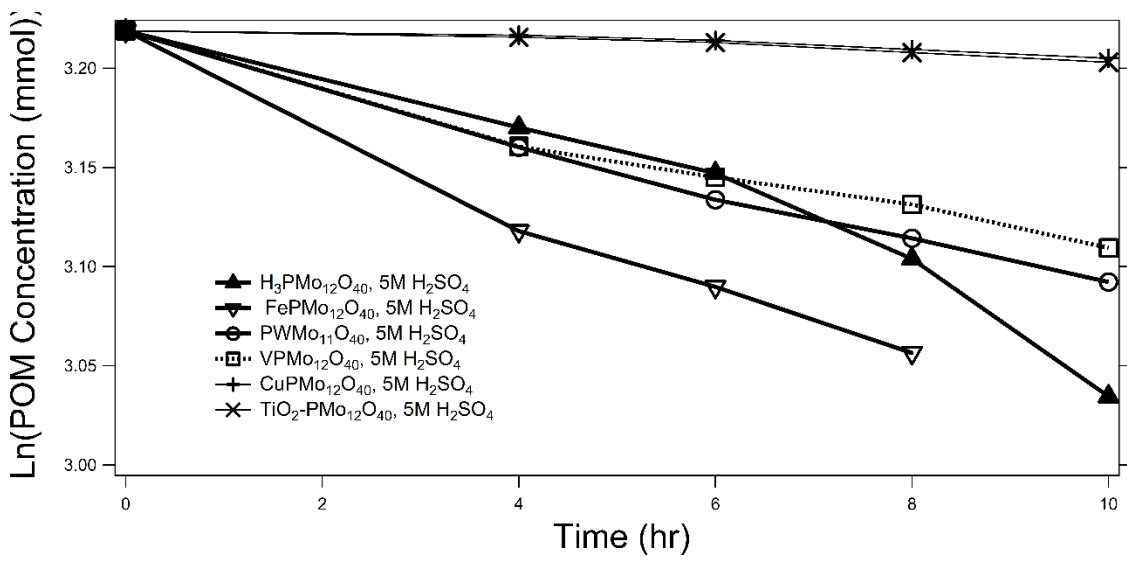
Figure 80: First Order POM Concentration vs Time-H₂SO₄
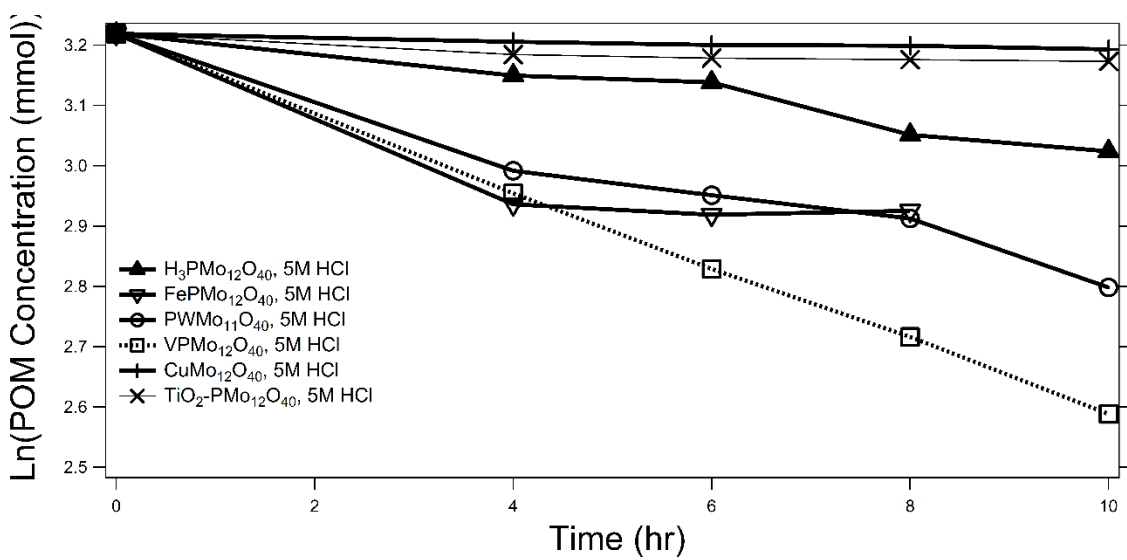
Figure 81: First Order POM Concentration vs Time-HCl
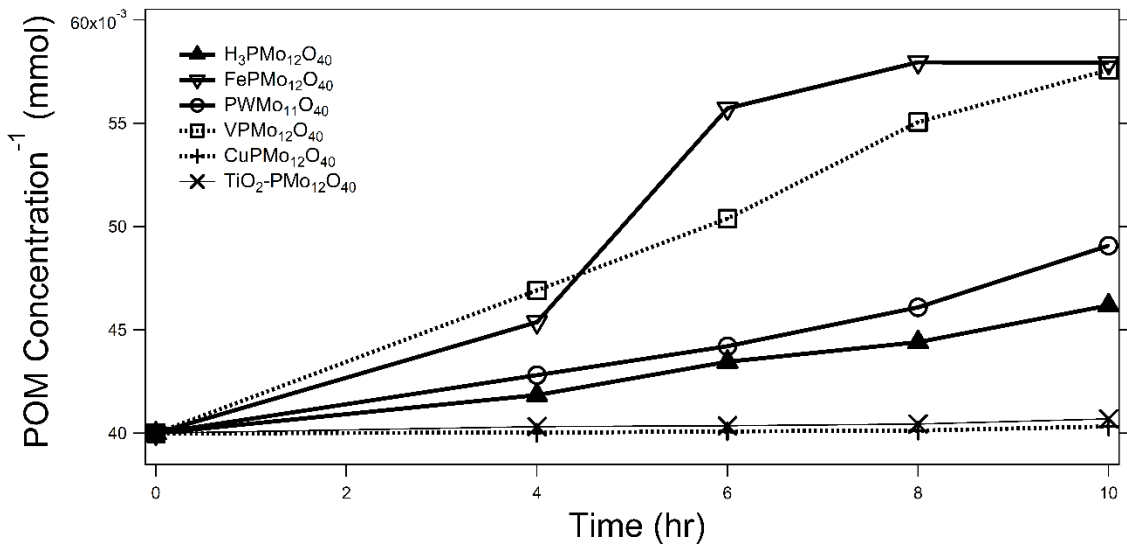
Figure 82: Second Order POM Concentration vs Time-Neat
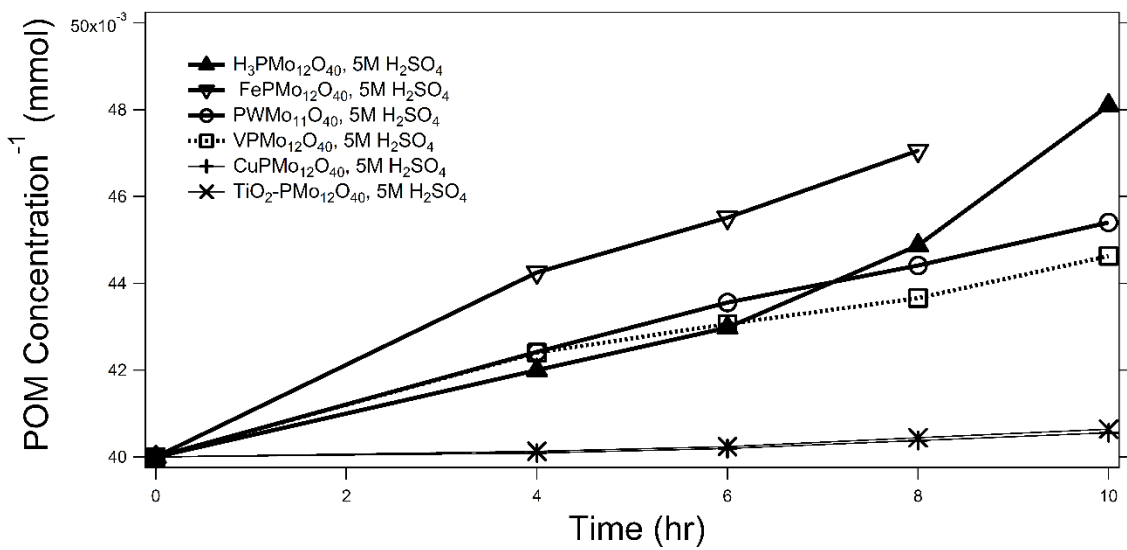
Figure 83: Second Order POM Concentration vs Time-H_2SO_4
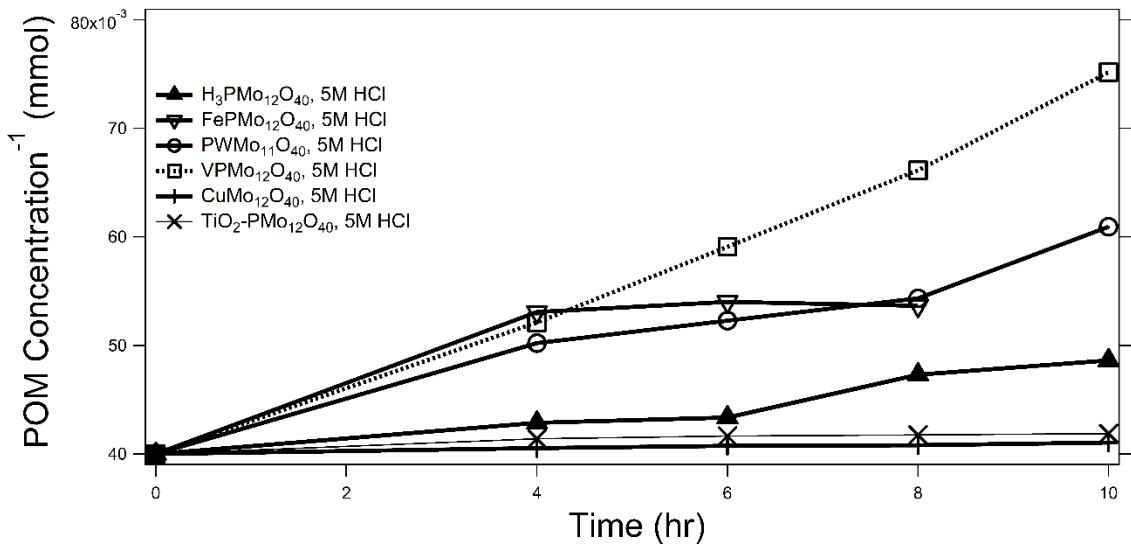
Figure 84: Second Order POM Concentration vs Time-HCl
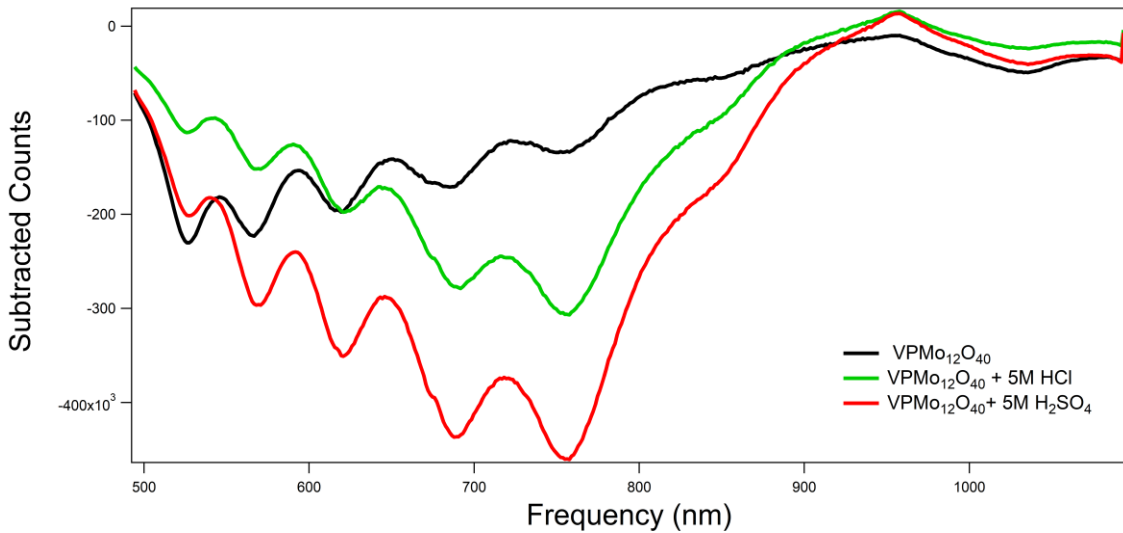
Figure 85: UV-VIS Absorption Spectra of V- Phosphomolybdic Acid in Various
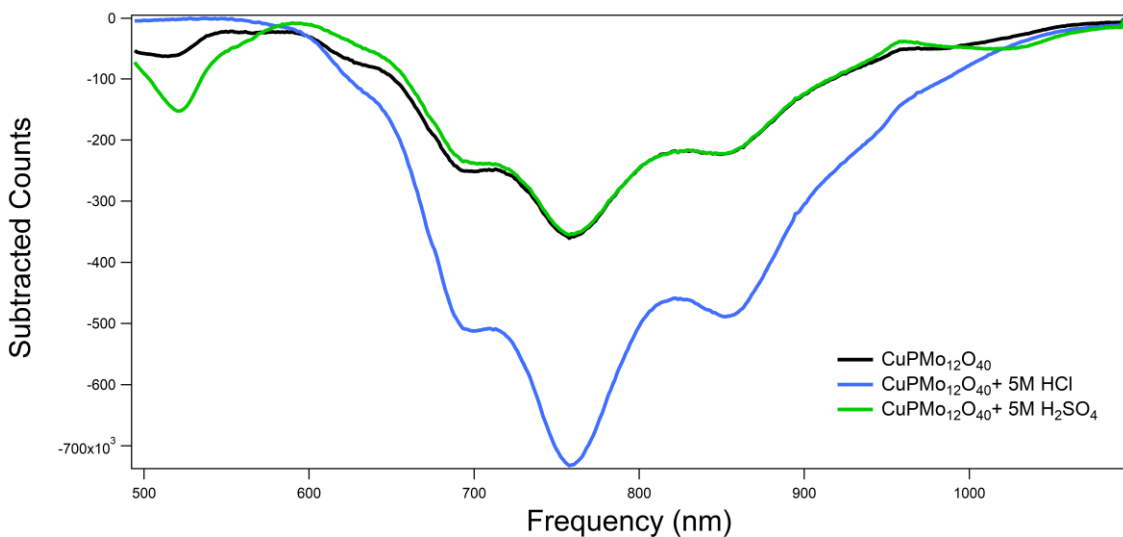
Media

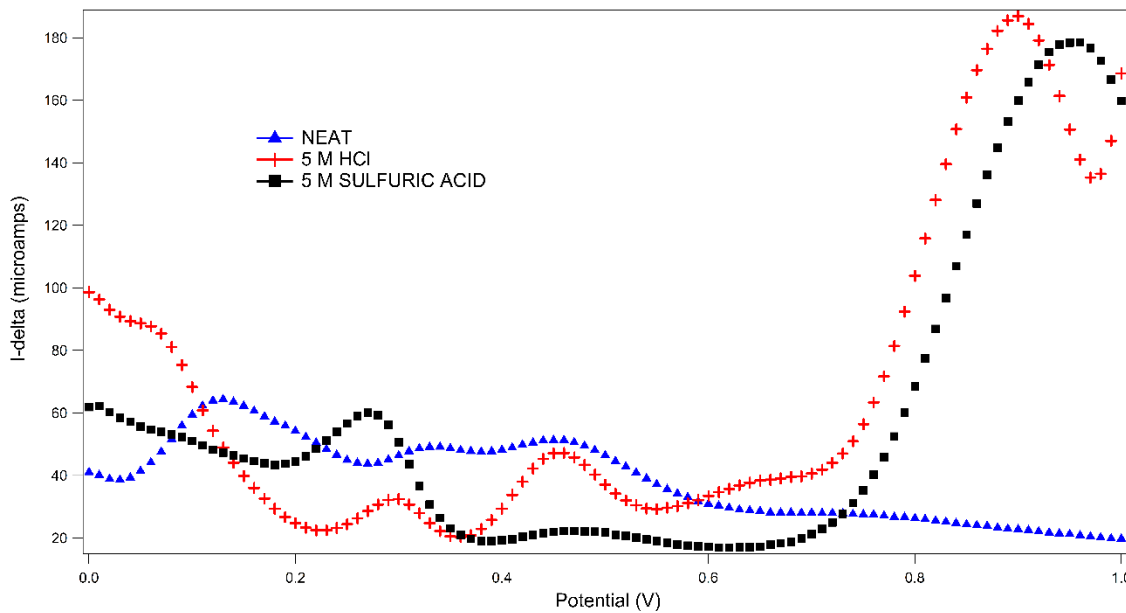Figure 86: UV-VIS Absorption Spectra of Cu-Phosphomolybdic Acid in Various
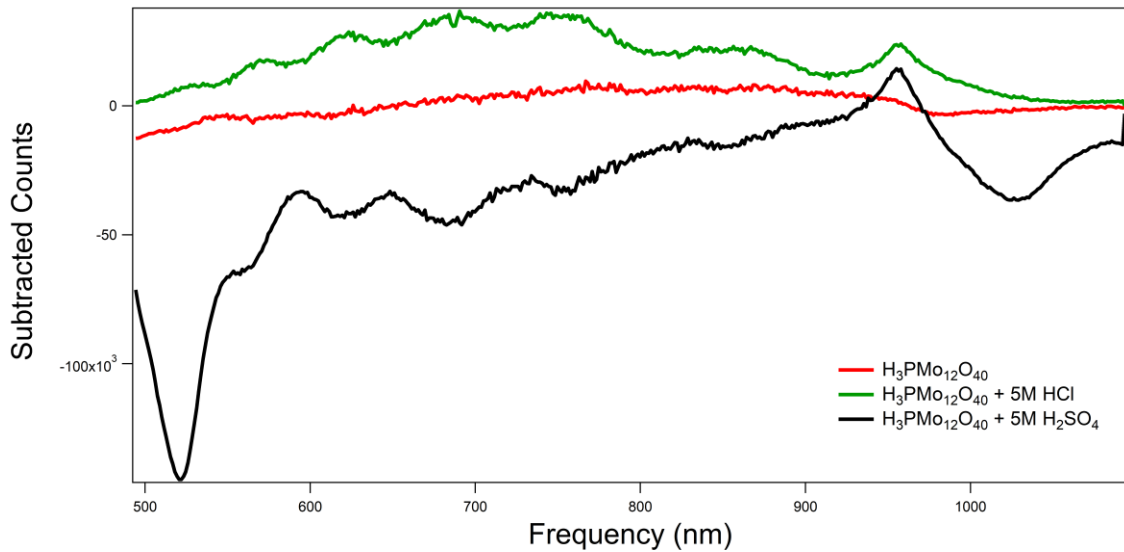
Media

Figure 87: UV-VIS Absorption Spectra of Phosphomolybdic Acid in Various
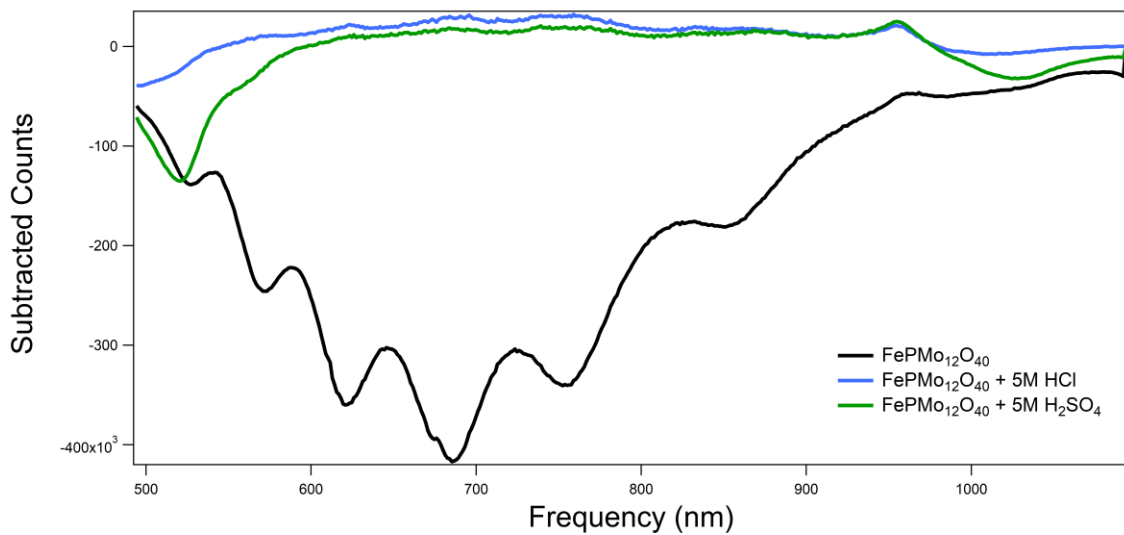
Media

Figure 88: UV-VIS Absorption Spectra of Fe-Phosphomolybdic Acid in Various
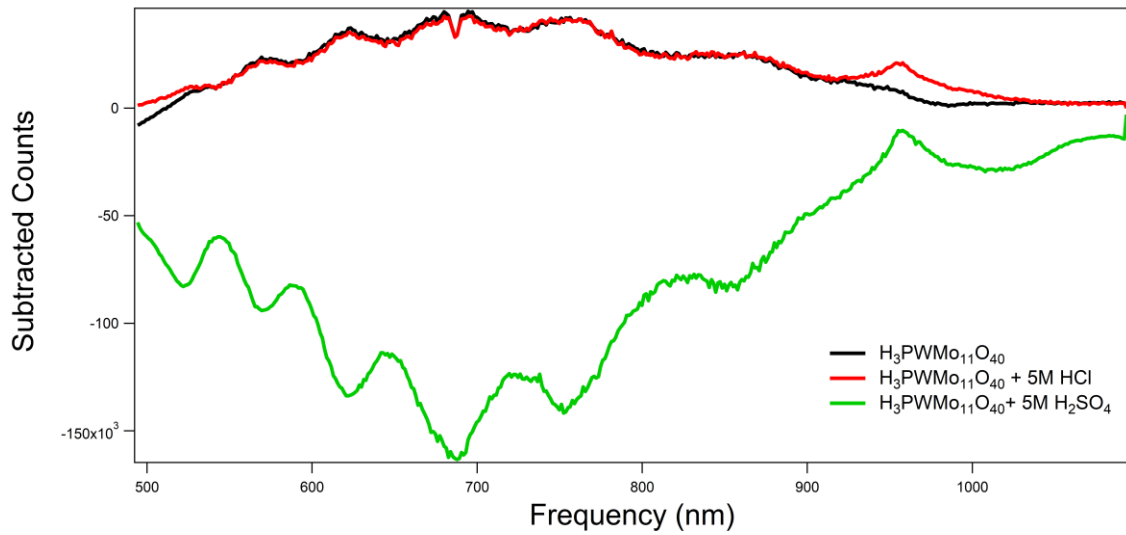
Media

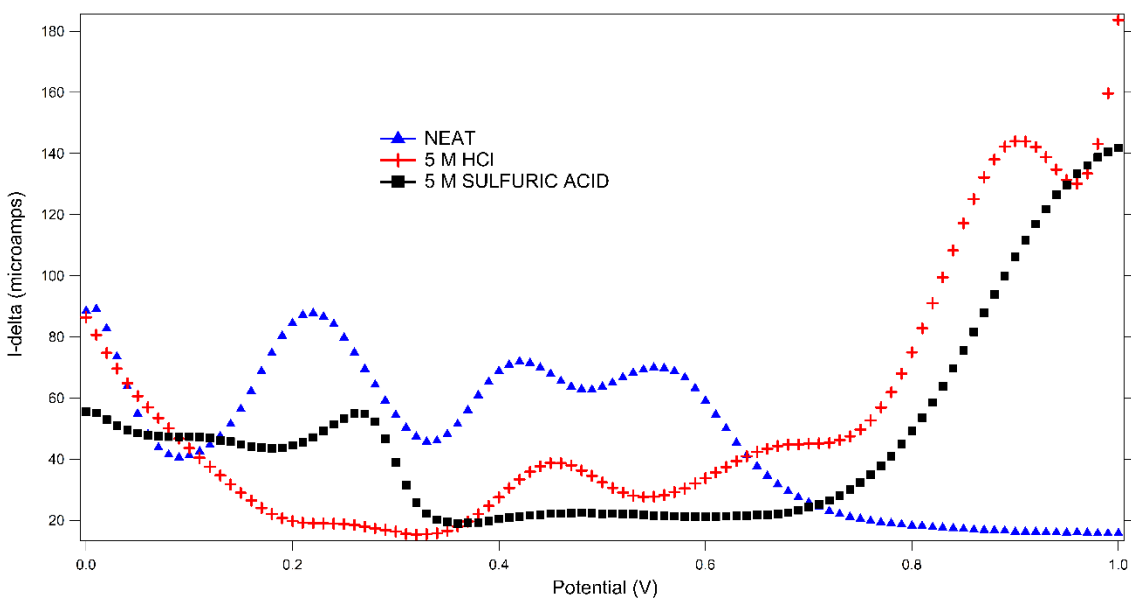Figure 89: UV-VIS Absorption Spectra of Phosphomolydbotunsgtinic Acid in

Various Media

Figure 90: Square Wave Voltammetry of 0.01 M $H_3PMo_{12}O_{40}$. We: Pt disk, Ce:

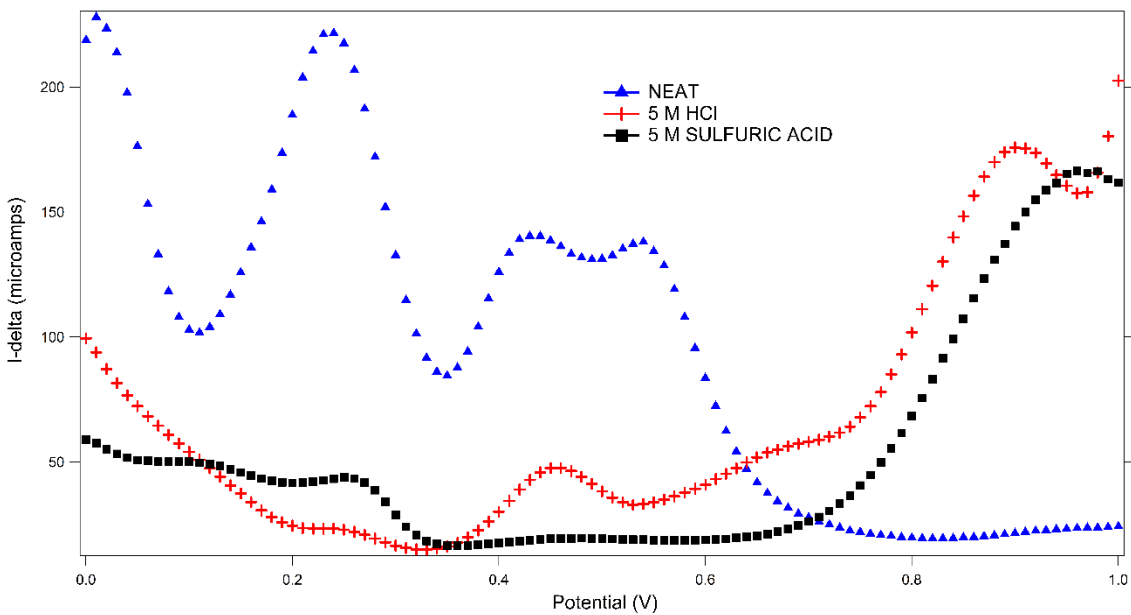Pt wire, Ref: Ag/AgCl. E_Step: 10 mV,Pulse Height:25 mV, τ:100ms
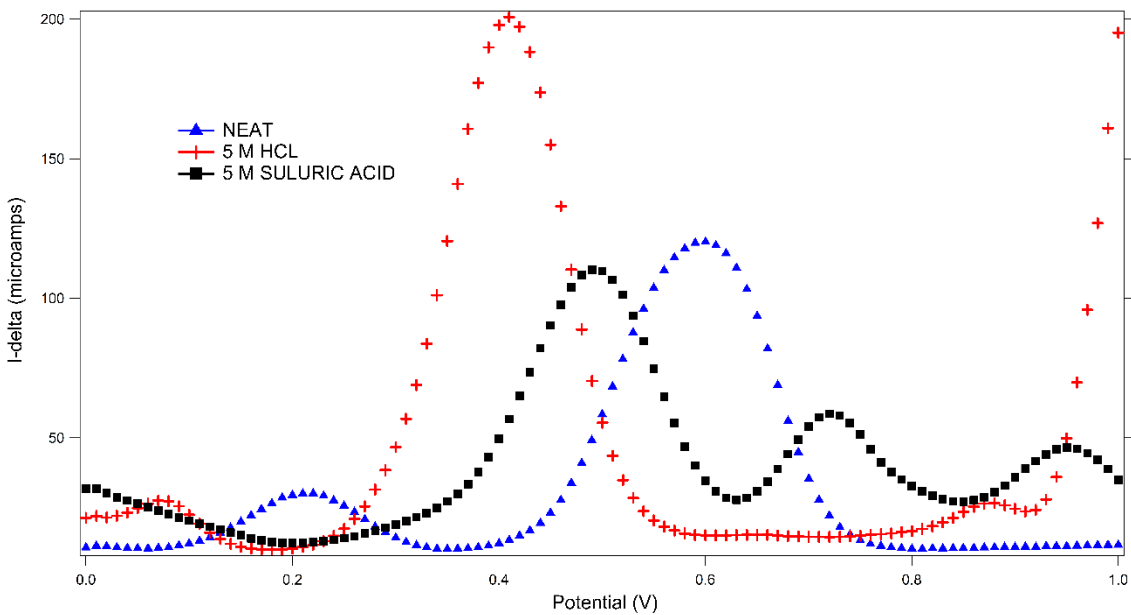
Figure 91: Square Wave Voltammetry of 0.01 M Fe-H$_3$PMo$_{12}$O$_{40}$. We: Pt disk,

Ce: Pt wire, Ref: Ag/AgCl. E_Step: 10 mV,Pulse Height:25 mV, τ:100ms

Figure 92: Square Wave Voltammetry of 0.01 M H$_3$PWMo$_{11}$O$_{40}$. We: Pt disk,

Ce: Pt wire, Ref: Ag/AgCl. E_Step: 10 mV,Pulse Height:25 mV, τ:100ms

Figure 93: Square Wave Voltammetry of 0.01 M $VOSO_4$-$H_3PMo_{12}O_{40}$. We: Pt

disk, Ce: Pt wire, Ref: Ag/AgCl. E_Step: 10 mV,Pulse Height:25 mV, τ:100ms

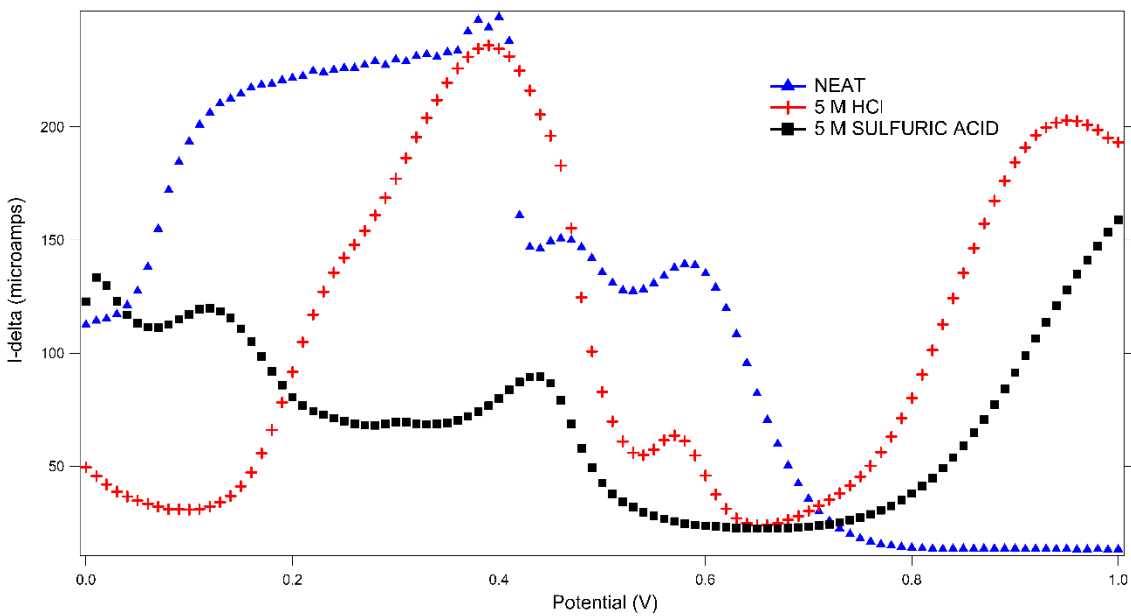Figure 94: Square Wave Voltammetry of 0.01 M $CuSO_4$-H3PMo12O40 . We: Pt
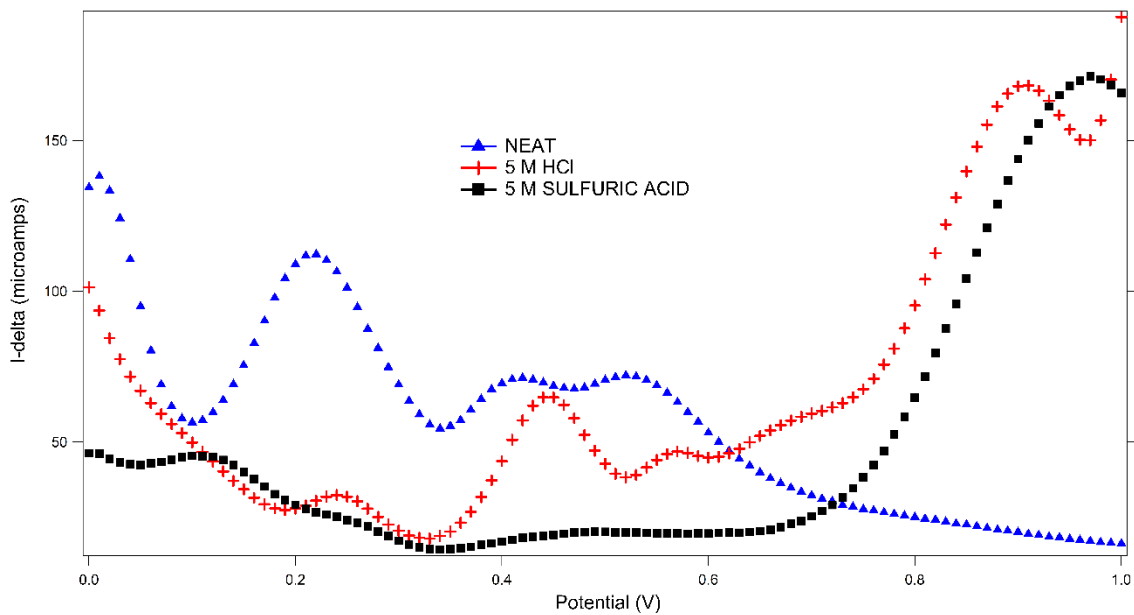
disk, Ce: Pt wire, Ref: Ag/AgCl. E_Step: 10 mV,Pulse Height:25 mV, τ:100ms

Figure 95: Square Wave Voltammetry of 0.01 M TiO_2-$H_3PMo_{12}O_{40}$. We: Pt disk,

Ce: Pt wire, Ref: Ag/AgCl. E_Step: 10 mV,Pulse Height:25 mV, τ:100ms

VITA

Brian M. Fane grew up in Miami, Florida. He enrolled at University of Florida in Gainesville, Fl in 2005. As an undergraduate student, Brian interned at nuclear power plants and raced mountain bikes before graduating with a Bachelor of Science degree in Chemical Engineering in 2010. That year Brian went to work on nonproliferation studies at Los Alamos National Laboratory. In 2011 he joined the Department of Chemical and Biomolecular Engineering at The University of Tennessee, Knoxville as a graduate student. He worked in the research group of Governor's Chair Professor Thomas Zawodzinski. During graduate school, he worked at the University of Tennessee Research Foundation examining intellectual property and commercialization of UT inventions.